Mechanisms underlying TSC-associated neuropsychiatric disorders in the zebrafish model

by

Olga Katarzyna Doszyń

Doctoral dissertation

Laboratory of Developmental Neurobiology

International Institute of Molecular Mechanisms and Machines

Polish Academy of Sciences

Laboratory of Molecular and Cellular Neurobiology

International Institute of Molecular and Cell Biology in Warsaw

Warsaw PhD School in Natural and BioMedical Sciences

Supervisor: Justyna Zmorzyńska, Ph.D, DSc habil.

Warsaw, June 2025

Table of contents

List of abbreviations

ADHD – attention deficit hyperactivity disorder
AG – (D, L)-allylglycine
Akt (PKB) – protein kinase B
AMPA – α-amino-3-hydroxy-5-methyl-4-isoxazolepropionic acid
ASD – autism spectrum disorder
BDNF – brain-derived neurotrophic factor
BLA – basolateral amygdala
BNST – bed nucleus stria terminalis
BNSTa – anterior division of BNST
CaM – calmodulin
CBD – cannabidiol
CeA – central amygdala
ChAT – choline acetyltransferase
ChR – channelrhodopsin
CNS – central nervous system
cpGFP – circularly permuted green fluorescent protein
CRISPR – clustered regularly interspaced short palindromic repeats
D – dorsal telencephalon
Deptor – DEP domain-containing mTOR-interacting protein
dHb – dorsal habenula
DIFF – differential illumination focal filtering
dpf – days post-fertilization
Dox – doxycycline
DS – Dravet syndrome
EEG – electroencephalography
EmT – eminentia thalami
ERK – extracellular signal-regulated kinase
FingR – fibronectin intrabody generated by mRNA
FRET – fluorescence resonance energy transfer
GABA – γ-Aminobutyric acid
Gal4-UAS – galactose transcription factor – upstream activating sequence system
GAP – GTPase-activating protein
GECI – genetically encoded calcium indicator
GEVI – genetically encoded voltage indicator
GFP – green fluorescent protein
GPCR – G-protein-coupled receptor
GPHN – gephyrin
$GRAB_{DA}$ – G-protein-coupled receptor-based dopamine sensor
Grb10 – growth factor receptor-bound protein 10
GtACR – anion conducting channelrhodopsin
HC – habenula commissure
hpf – hours post-fertilization
HRM – high resolution melting

ID – intellectual disability
IRS-1 – insulin receptor substrate-1
KA – kainic acid
LdHb – left dorsal habenula
LFP – local field potential
LS – lateral septum
MAPK – mitogen-activated protein kinase
MeA – medial amygdala
MeAp – posterior division of MeA
MGE – medial ganglionic eminence
mLST8 – mammalian lethal with Sec13 protein 8
MO – morpholino
MS – medial septum
mSin1 – mammalian SAPK interacting protein 1
mTOR – mammalian/mechanistic target of rapamycin
mTORC1 – mammalian/mechanistic target of rapamycin complex 1
mTORC2 – mammalian/mechanistic target of rapamycin complex 2
NMI – no mutations identified
PA – pallidum
PAC – photoactivated adenylyl cyclase
PA-GFP – photoactivatable green fluorescent protein
pAmy - pallial amygdala
PCR – polymerase chain reaction
PI3K – phosphoinositide 3-kinase
pIGLET – phiC31 Integrase Genomic Loci Engineered for Transgenesis
PiVR – Raspberry Pi Virtual Reality
PKC – protein Kinase C
PLCγ – phospholipaseCγ
PRAS40 – proline-rich Akt substrate of 40 kDa
PTU – 1-phenyl-2-thiourea
PTZ – pentylenetetrazol
Raptor – regulatory protein associated with mTOR
RDX – 1,3,5-trinitroperhydro-1,3,5-triazine
RFP – red fluorescent protein
Rheb – Ras homolog enriched in brain protein
Rictor – rapamycin insensitive companion of mTOR
Rps6 – ribosomal S6 protein
ROI – region of interest
Se – septum
SEGA – subependymal giant cell astrocytoma
SEN – subependymal nodule
SGK – serum- and glucocorticoid-induced protein kinase
SM – stria medullaris
Str – striatum
SV2A – synaptic vesicle glycoprotein 2A
TALENs – transcription activator-like effector nucleases

TAND – TSC-associated neuropsychiatric disorder
TBC1D7 – TBC1 domain family member 7
Tel2 – telomere length regulation protein TEL2 homolog
Tet – tetracycline
TH – tyrosine hydroxylase
TOSCA – Tuberous Sclerosis Registry to Increase Disease Awareness
TS – posterior tail of the striatum
TSC – tuberous sclerosis complex
TSC1 – tuberous sclerosis protein 1 (hamartin)
TSC2 – tuberous sclerosis protein 2 (tuberin)
Tti1 – TELO2 Interacting Protein 1
VGB – vigabatrin
vHb – ventral habenula
VR – virtual reality
WM – white matter
Wt – wild-type
ZBB – Zebrafish Brain Browser
ZFNs – zinc finger nucleases

Chapter 1. General introduction

1.1 Tuberous Sclerosis Complex

Tuberous Sclerosis Complex (TSC) is a multisystem genetic disorder with prominent neurological manifestations, and a prevalence estimated at between 1:6 000 and 1:10 000 live births. Beyond the brain, it also commonly affects skin, kidneys, heart, lungs and eyes (Northrup et al., 2024). In particular, lung or kidney dysfunctions are the leading cause of a shortened life span of TSC patients (Caban et al., 2016). While age of diagnosis can vary greatly, the majority of TSC patients are identified in their infancy or childhood, due to outwardly visible early onset symptoms such as skin lesions and epileptic seizures, or are diagnosed prenatally based on the presence of benign tumors of the heart, cardiac rhabdomyoma (Kingswood et al., 2017; Northrup et al., 2024).

TSC is caused by an inactivating mutations in either the *TSC1* or *TSC2* gene, encoding the proteins Hamartin and Tuberin respectively (Crino et al., 2006). It is inherited in an autosomal dominant manner; however, familial inheritance accounts for approximately one third of cases, while the remaining two thirds are born with *de novo* mutations (Rosengren et al., 2020). According to the Leiden Open Variation Database (version 3), 984 unique pathogenic or likely pathogenic variants in *TSC1* and 2832 in *TSC2* have been reported up to date (Fokkema et al., 2021). For *TSC1*, small indels make up over half of pathogenic variants, and recurring regions of exons 4-9, 15 and 18 are the most critical for Hamartin function and stability. For *TSC2*, small indels are still common (38% variants), but pathogenic missense variants occur more frequently than in *TSC1* (approx. 26% variants), and are frequently located within the C-terminal domain encoding region (Man et al., 2024). Moreover, 10-15% of TSC patients are diagnosed based on clinical criteria, but have had no mutations identified (NMI) (Man et al., 2024). While this could point to a third, unknown TSC gene, most studies do not support this hypothesis, as mutations in other components of the mTOR pathway are not associated with the TSC phenotype (Man et al., 2024). A case study has been published of a child presenting with some TSC-associated symptoms, who had a pathogenic somatic variant in *RHEB*, but not in *TSC1* or *TSC2* (Lee et al., 2023). Still, their symptoms could potentially be attributed to an undetected mutation in a deep intronic region of *TSC1* or *TSC2*, as has been previously the case in some TSC patients with NMI who have been re-genotyped with newer sequencing techniques (West et al., 2023). In the majority of TSC individuals with NMI by initial screening, however, mosaicism in either somatic or germline cells has been identified (Tyburczy et al., 2015).

Based on patient data, *TSC2* mutations are generally associated with more severe phenotypes (Salussolia et al., 2019). Expectedly, mutations in regions coding for more functionally critical protein domains also result in greater disease severity. Conversely, TSC patients with NMI, including those later re-diagnosed with mosaic or deep intronic variants, tend to present with milder symptoms (Man et al., 2024). Additionally, the variability in symptom severity between TSC patients can be partly explained by the two-hit hypothesis, where a pathogenic variant is inherited in one allele, and the second allele becomes affected by a somatic mutation. Such double hit variants have been identified in multiple patient samples (Man et al., 2024).

The TSC proteins are widely expressed across cell types and tissues. Commonly, the brain, heart, lungs, eyes, and kidneys are affected with tumors known as hamartomas (Orlova & Crino, 2010).

Hamartomas are benign, but they negatively affect organ development and function through structural disruptions, compression of surrounding tissues and displacement of cells. Hamartomas include subependymal nodules (SENs) and subependymal giant cell astrocytomas (SEGAs). SENs are small lesions lining the lateral and third ventricles of the brain (Crino et al., 2006; Salussolia et al., 2019). SEGAs are glial tumors which in some patients may lead to hydrocephalus, increased intracranial pressure, and death (Caban et al., 2016). Another type of brain tumor found in TSC patients are cortical tubers, a feature similar to type IIb focal cortical dysplasia (House et al., 2015). Cortical tubers have been linked to other neurological manifestations of TSC, such as epilepsy or intellectual disability (Jansen et al., 2008). However, some studies suggest that the tuber burden is not necessarily a sole cause of epileptic seizures, and that dysregulated mTOR activity in itself, present also in perituberal tissue, might lead to epileptogenesis (Ruppe et al., 2014). Broadly, the types and onset of seizures also vary greatly between TSC patients. They can present with focal, generalized or mixed seizures, and over 80% of TSC patients experience at least one seizure episode in their life. Approximately 37% of patients have infantile spasms, and in general, seizures usually begin in early childhood (within the first year of age), but some patients might not develop epilepsy until adolescence, or even early adulthood (Salussolia et al., 2019). Early onset epilepsy, in turn, has been linked to cognitive deficits, with TSC patients who experienced infantile spasms performing worse in tests of cognitive function and fine motor skills. Additionally, the timing and frequency of seizures in later periods of childhood development were correlated with Autism spectrum disorders (ASD)-associated behaviors, with the age of onset having a particularly significant impact on developmental outcomes (Capal et al., 2017). However, the pathogenesis, severity and variability of developmental disorders present in TSC patients are a complex issue, and cannot be reduced to a simple, direct relationship between the tumor or seizure burden, and the observed cognitive, behavioral or psychiatric disorders.

1.2 TSC-associated neuropsychiatric disorders

A range of neurodevelopmental, behavioral and psychiatric conditions, collectively termed TSC-associated neuropsychiatric disorders (TANDs), occurs in approximately 90% of TSC patients (Henske et al., 2016). They can co-occur with any TSC mutation, but are more frequent in *TSC2* variants (Curatolo et al, 2015; Numis et al., 2011). The classification of TANDs encompasses a wide umbrella of symptoms (Curatolo et al., 2015b; de Vries et al., 2015). ASD and attention deficit hyperactivity disorder (ADHD) are each diagnosed in around 40% of TSC patients. About 50% of TSC patients present with varying levels of intellectual disability (ID), and even among those with no ID, learning disorders, attention deficits and memory deficits have been reported, impacting their academic capabilities. Anxiety and mood disorders are also often found in individuals with TSC (Curatolo et al., 2015b).

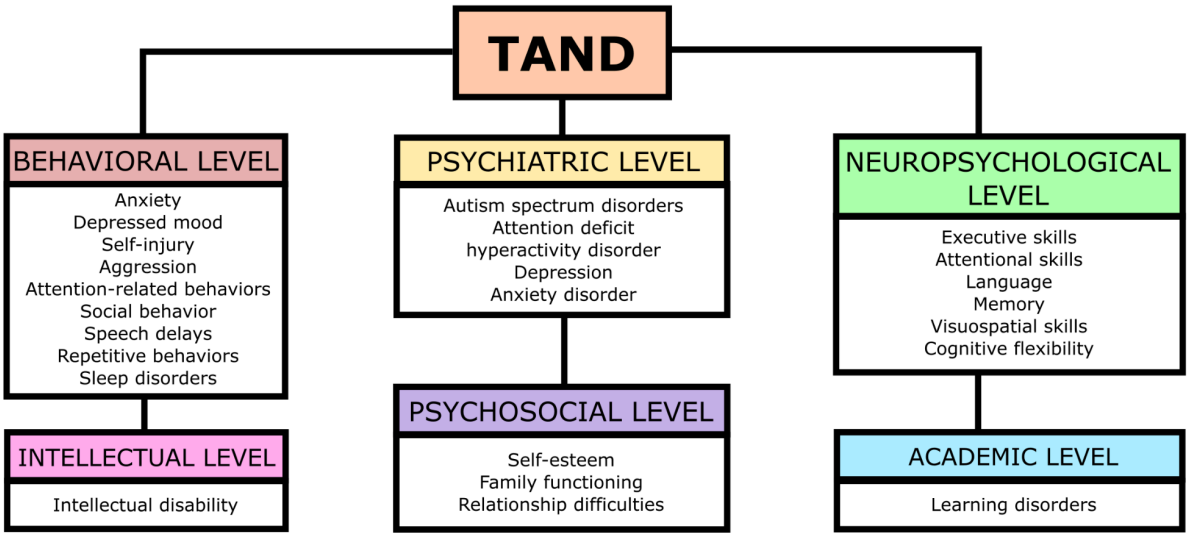

Figure 1. Chart representing examples of neuropsychiatric disorders and symptoms most commonly associated with TSC (based on Curatolo et al., 2015b).

According to the international Tuberous Sclerosis Registry to Increase Disease Awareness (TOSCA) report, TANDs such as ID, ASD and ADHD tend to be diagnosed later (around 7-8 years of age on average) than the same disorders in children without TSC (around 3-4 years of age) (Kingswood et al., 2017). Additionally, while the aforementioned conditions are frequently associated with TSC, mood disorders such as anxiety or depression might be underdiagnosed (de Vries et al., 2018).

1.3 Mechanisms underlying TSC

TSC is considered representative to a group of diseases termed mTORopathies, i.e., stemming from the hyperactivation of mammalian/mechanistic target of rapamycin (mTOR) signaling (Man et al., 2024). The mTOR protein forms two distinct complexes, mTORC1, comprised of proteins mTOR, mLST8, PRAS40, Tti1, Tel2, Deptor and Raptor, and mTORC2, comprised of mTOR, mLST8, mSin1, Protor, Tti1, Tel2, Deptor and Rictor. mTORC1 is regulated by many intra- and extracellular factors, such as cellular stress, nutrient availability, hormones, trophic factors, amino acids, cell adhesion molecules, and, in the CNS, neurotransmitters. In response, it regulates multiple cellular processes, including cell cycle, proliferation and growth, as well as protein synthesis and translation, lipid synthesis, and autophagy (Salussolia et al., 2019; Switon et al., 2017). In the brain, dysregulated mTORC1 activation can disrupt key developmental processes such as axon genesis, guidance and specification, dendritogenesis and dendritic spine formation; mTORC1 is also involved in the processes of neuronal and synaptic plasticity, learning and memory (Switon et al., 2017). mTORC2 is activated by growth factors and hormones acting through phosphoinositide 3-kinase (PI3K), neurotrophins, and is involved in cell cycle progression, cellular metabolism, actin cytoskeleton remodeling, protein degradation, and maintaining the integrity of mitochondrion-associated membranes. It has also been shown to regulate dendritogenesis and synaptic transmission (Switon et al., 2017). Additionally, dysregulation of mTOR signaling can

alter the balance between neuronal excitation and inhibition, contributing to epileptogenesis (Specchio et al., 2023).

In the canonical pathway, mTORC1 is directly activated by RHEB, which in turn is regulated by the TSC complex, comprised of the proteins TSC1, TSC2 and TBC1D7 (Fig.2). Therefore, a loss of either of the TSC proteins interferes with this regulation mechanism, resulting in sustained hyperactivation of mTORC1 (Salussolia et al., 2019). Notably, mutations in TBC1D7 do not result in TSC symptoms (Switon et al., 2017). At the same time, some data suggest positive regulation of mTORC2 by the TSC complex (Huang et al., 2008). Additionally, as mTORC1 and mTORC2 share some upstream regulators, there is documented cross-talk between the two complexes. For instance, mTORC1 can inhibit mTORC2 via insulin receptor substrate-1 (IRS-1) growth factor receptor-bound protein 10 (Grb10), while mTORC2 can deactivate TSC2 (and thus activate mTORC1) through Akt, PKC or SGK signaling (Ragupathi et al., 2024). While there has been little research on potential TSC complex action outside of mTOR, there is some evidence for non-canonical role of TSC1/2 and RHEB in signaling, transport and secretion across the plasma membrane, and actin cytoskeleton regulation (Neuman & Henske, 2011). These have been speculated to potentially contribute to the pathogenesis of TSC, however, this has not been fully explored up to date, and the majority of studies focus on the TSC1/2-mTORC1 pathway.

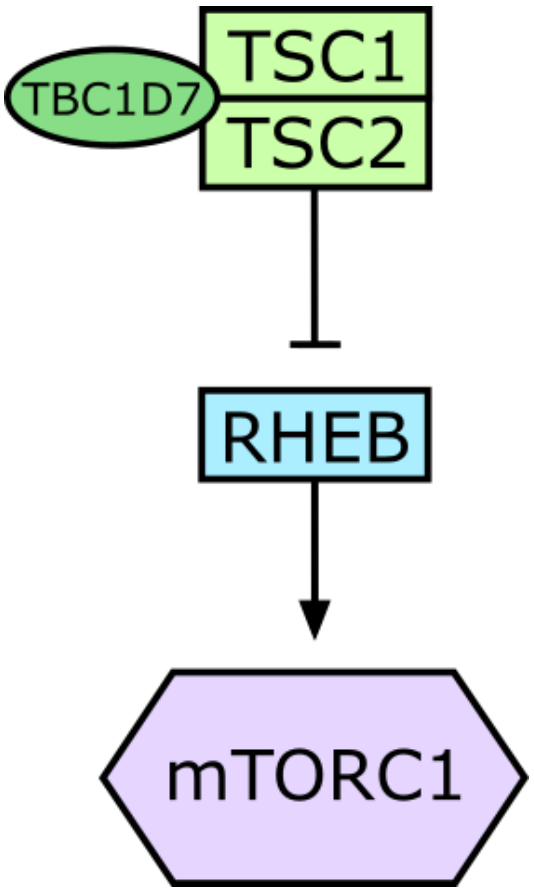

Figure 2. Regulation of mTORC1 by the TSC complex.

In TSC, disruption of white matter (WM) was also linked to neurodevelopmental deficits. Altered neurite density in WM was correlated with greater disease severity with regards to seizures and cognitive impairments (Anaby et al., 2022). An analysis of global WM connectivity in TSC patients revealed reduced connectivity between hemispheres, which was most significantly impaired in individuals with ASD or intellectual disability (Im et al., 2016), and WM dysconnectivity in infants with TSC has been linked to the development of ASD symptoms later in life (Prohl et al., 2019). A recent study also linked TANDs with abnormalities in WM in the limbic system, which is involved in behavior, memory and emotional responses (Sato et al., 2022; Mori & Aggarwal, 2014). Sato et al. showed an association between disrupted WM integrity in the limbic system and intellectual disability, autistic features and behavioral problems (Sato et al., 2022). We have also found impaired brain connectivity in our zebrafish TSC model (Kedra et al., 2020), recapitulating patients data. In zebrafish, cells with mTorC1 hyperactivation were found to migrate into the WM regions (Kedra et al., 2020; Kim et al., 2011; Prentzell et al., 2021), coinciding with neuronal hyperactivity in the WM (Prentzell et al., 2021), suggesting that these mislocalized cells might act as epileptogenic foci. In turn, it is known

that alterations of WM integrity can be caused by seizures (Moavero et al., 2016). Both mTORC1 hyperactivation by deletion of *Tsc1* and hypoactivation by an oligodendrocyte-specific deletion of *Rptor* were shown to affect myelination in a mouse model (Lebrun-Julien et al., 2014), disrupting WM structure. However, while we know that mTORC1 hyperactivity itself, as well as seizures and impairments in brain connectivity all contribute to neuropsychiatric and neurodevelopmental disorders, there is still a need for additional data regarding the developmental perspective of how the TANDs arise and its mechanistic understanding, in order to provide patients with accurate and timely diagnosis and treatment.

1.4 Treatment of TSC and TANDs

Management of TSC focuses in the first place on the most life-threatening conditions, such as enlarging SEGAs, epilepsy and renal tumors, all of which can be treated with surgery – in case of epilepsy, by removal of tubers (Northrup et al., 2024). However, due to associated risks or comorbid conditions, not all patients qualify for SEGA resection (Ebrahimi-Fakhari & Franz, 2020); and although surgical removal of epileptogenic tubers can be successful in many patients, the presence of multiple tubers can make it challenging (Specchio et al., 2023). Therefore, there is a continued search for pharmacological treatments of TSC. Since mutations in the TSC genes result in hyperactivation of mTORC1, mTOR inhibitors have been an obvious avenue of exploration. Clinically available mTORC1 inhibitors used in patients with TSC include rapamycin, also known as sirolimus, and its derivatives such as everolimus. They function by dissociating the binding of Raptor, a crucial component of the complex, from mTORC1. Treatment with everolimus has been shown to reduce the volume of SEGAs, as well as kidney tumors and skin lesions (Caban et al., 2016; Franz et al., 2016). Additionally, everolimus treatment decreases seizure frequency in TSC patients, especially in children under six years old (Curatolo et al., 2018). Pharmacological inhibition of mTORC1 in children with TSC was also demonstrated to improve WM integrity (Peters et al., 2018). When it comes to TANDs, however, treatment with everolimus has failed to significantly improve cognitive functioning, social and behavioral impairments, neuropsychological deficits, and motor function in children and adolescents with TSC (Kadish et al., 2020; Overwater et al., 2019). Additionally, both the EXIST-1 and EXIST-3 trials have provided evidence that, while everolimus treatment is considered safe, it can have some systemic side effects, including stomatitis and increased risk of infection (Curatolo et al, 2018; Franz et al, 2016). Everolimus has also been found to increase pre-dose concentrations of such anti-seizure medications as carbamazepine and clobazam, which should be taken into account if those drugs were to be administered together (Schubert-Bast & Strzelczyk, 2021). In USA and Europe, everolimus has been approved for treatment of kidney tumors in patients above the age of 18, and for treatment of SEGAs in patients of all ages who cannot be effectively treated with surgery (Józwiak et al., 2020).

Alternatively, in TSC patients presenting with infantile spasms, the first-line treatment to prevent epileptic seizures is vigabatrin (VGB). It functions as an inhibitor of γ-Aminobutyric acid (GABA) transaminase, increasing inhibitory neurotransmission by stopping the breakdown of GABA. Vigabatrin is highly effective, preventing further occurrence of infantile spasms in 95% of patients (Hancock & Osborne, 1999). In patients with refractory focal seizures, it can also be administered in conjunction with other anti-epileptic drugs, acting on GABA receptors (clobazam), AMPA glutamate receptors (perampanel, topiramate), synaptic vesicle protein SV2A (levetiracetam, brivaracetam) and voltage-gated or voltage-sensitive sodium channels (valproate, lamotrigine,

oxcarbazepine, carbamazepine, topiramate, lacosamide) (Schubert-Bast & Strzelczyk, 2021). Some clinicians have been reluctant to prescribe vigabatrin due to reported side effects, particularly visual defects. Indeed, the drug was introduced with a black-box warning that vision loss can occur in 30% of cases, and a recommendation to closely monitor patients for vision impairments during and after treatment (Cruz 2010). However, a more recent study has concluded that this risk had been exaggerated, and is outweighed by the benefits of seizure prevention (Foroozan 2018). The EPISTOP trial, evaluating the potential of preventative epilepsy treatment in infants with TSC, has concluded that vigabatrin was safe at the anti-epileptic dosage. Administration of vigabatrin upon the diagnosis of epileptiform activity during EEG monitoring successfully delayed the onset of seizures and reduced seizure severity (Kotulska et al., 2021). While earlier age of onset and higher frequency of seizures are associated with stronger cognitive and behavioral impairments, conventional epilepsy treatment with vigabatrin did not improve IQ outcomes or behavioral problem scores, including ASD-related behaviors (Uematsu et al., 2020). This suggests that while the severity of some TANDs can be worsened by epilepsy, they do arise independently. In the EPISTOP trial, the percentage of patients with neurodevelopmental delay was lower following the novel preventative treatment than in the conventionally treated group. Furthermore, none of the preventatively treated patients had severe learning disability, although this particular finding was not deemed significant due to the low sample size and the follow-up monitoring up to only 2 years of age. Nevertheless, the results implied that prevention of seizures with vigabatrin could improve cognitive outcomes (Kotulska et al., 2021).

Cannabidiol (CBD) has also been approved for treatment of TSC-associated seizures, due to its anti-epileptic action demonstrated in the GWPCARE6 trial (Thiele et al., 2021). However, it is notable that CBD might interact with multiple other anti-epileptic drugs, including valproate, clobazam and everolimus/sirolimus (Schubert-Bast & Strzelczyk, 2021). It also does not decrease the volume of SEGAs (Barnett et al., 2020), and its effect on overall mTORC1 signaling is not yet clear (Schubert-Bast & Strzelczyk, 2021).

When it comes to TANDs, patients are referred to a neurodevelopmental specialist or psychiatrist, and treated with behavioral or psychological therapy and/or medication according to their diagnosed disorder (Northrup et al., 2024). However, it is important to note that the incidence and clinical presentation of TANDs do not always entirely correlate with the tumor or seizure burden (Wong 2019), and the precise molecular mechanisms underpinning the observed behavioral and developmental conditions are not yet fully understood. Therefore, there is still need for both more research on the effects of established anti-epileptic drugs on TANDs, and for novel therapeutic targets aimed specifically at treating TANDs.

1.5 TSC and TANDs in animal models

Full homozygous *Tsc1* or *Tsc2* rodent knockouts are lethal during early embryonic development (Kobayashi et al., 2001; Onda et al., 1999). Heterozygous mice are most commonly used as models of TSC, alongside full knockouts of either TSC gene in specific cells (Santos et al., 2025). This recapitulates the autosomal dominant or mosaic pattern of mutation in TSC patients. Similarly to patients data (Henske et al., 2016), a comparison between *Tsc1*- and *Tsc2*-deficient mice has shown a greater hyperactivation of mTORC1 and a more severe seizure phenotype with the latter, although with conditional knockouts, the timing of the deletion also had a significant impact on disease

severity (Magri et al, 2013). In addition to epilepsy, mouse models of TSC also recapitulated various behavioral symptoms that align with TANDs.

Various rodent TSC models have shown deficits in cognition and learning, measured by tests of novel object recognition, or spatial memory in the Morris Water Maze or Radial Arm Maze (reviewed in Santos et al., 2025). *Tsc1*$^{+/-}$ and *Tsc2*$^{+/-}$ mice displayed learning and social deficits even in the absence of seizures or brain tumors (Ehninger et al., 2008; Goorden et al., 2007). Studies conducted on *Tsc1*-deficient mice have shown the potential of rapamycin to rescue some ASD-related symptoms such as social deficits (Sato et al., 2012; Tsai et al., 2018), or structural and electrophysiological changes in the cerebellum (Tsai et al., 2018). However, the efficacy of this treatment depended significantly on the timing of the intervention with regards to the animals' age, and repetitive behaviors could not be rescued within the time window of the study (Tsai et al., 2018). Additionally, in both *Tsc1*$^{+/-}$ and *Tsc2*$^{+/-}$ mice, rapamycin lowered the increased rearing behavior, which can be induced by environmental stress (Sato et al., 2012). When it comes to anxiety, it was found to be much more prevalent in *Tsc2*- rather than *Tsc1*-deficient rodents, although the results were also varied depending on the behavioral test used (Santos et al., 2025).

Tsc1 or *Tsc2* deletions in cerebellar Purkinje cells resulted in motor impairments, as well as autistic-like phenotypes, such as social deficits and repetitive behaviors, that could be rescued by rapamycin treatment (Reith et al., 2013; Tsai et al., 2012). A conditional heterozygous knockout of *Tsc1* in inhibitory neurons derived from medial ganglionic eminence (MGE) affected hippocampal function in mice, resulting in impaired contextual fear discrimination and working spatial memory (Haji et al., 2020). In a study by Normand et al., a mosaic *Tsc1* deletion in the thalamic precursors at embryonic day (E) 12.5 resulted in repetitive grooming behavior seizures and abnormal neuronal activity with epileptiform features in adult mice. Conversely, only some mice with Tsc1 inactivation at E18.5 experienced seizures later in life. These results have demonstrated that the spatial distribution of affected cells and the developmental timing of *Tsc1* inactivation strongly influence the phenotype of individuals with a mosaic TSC mutation (Normand et al., 2013).

Mice expressing a dominant-negative *Tsc2* transgene, which has a mutation affecting its GAP domain and the capacity to inhibit RHEB, displayed social deficits and impaired rotarod motor learning (Chévere-Torres et al., 2012), as well as anxiety-like behavior (decreased time spent in the open arms) in the elevated plus maze test (Ehninger & Silva, 2011). A study on a conditional hypomorphic *Tsc2* mouse mutant demonstrated a gradation of cellular and behavioral effects such as neuron enlargement, anxiety, social deficits and learning impairments, negatively correlated with TSC2 protein levels. These findings were consistent with prior studies showing that the severity of neurological TSC symptoms was correlated with tuberin levels: namely, mutations in *TSC2* result in more severe phenotypes than mutations in *TSC1*, truncating mutations in *TSC2* lead to worse outcomes than missense mutations, and in patients with mosaicism, the severity of symptoms depends on the proportion of affected cells to those with two normal alleles. (Yuan et al., 2012).

The Eker rat, which carries a spontaneous mutation in the *Tsc2* gene, is free of cerebral hamartomas and spontaneous seizures, although it is vulnerable to progressive induction of seizure susceptibility through a chemically-induced process termed kindling (Waltereit et al., 2006). Naive *Tsc2*$^{+/-}$ rats show reduced novel object and social exploration, and increased anxiety; an induction of status epilepticus by kainic acid results in anxiety and social evade, suggesting that although behavioral

impairments in TSC arise independently of epilepsy, they can be aggravated by seizures (Waltereit et al., 2011).

Overall, various rodent models have managed to recapitulate many of the TANDs-related symptoms experienced by TSC patients. In many aspects, however, zebrafish (*Danio rerio*) are more advantageous than the popular mouse models: zebrafish are small in size, quick to mature, characterized by high fecundity and ease of maintenance (Bradford et al., 2017; Hortopan et al., 2010). Additionally, in contrast to mammals, their extrauterine development allows for observation of live embryos, including homozygous *tsc1* or *tsc2* gene knockouts. It is also worth noting that $tsc2^{-/-}$ homozygous zebrafish are accepted as TSC model, recapitulating disease symptoms more accurately than the heterozygous $tsc2^{+/-}$ fish (Kim et al., 2011; Scheldeman et al., 2017; Kedra et al., 2020).

Belonging to the teleosts, zebrafish underwent a genome duplication in the Devonian period, and in the time since, some of those duplicated genes have diversified, acquiring new functions (Ravi & Venkatesh, 2008). As a result, zebrafish possess two distinct homologs of the mammalian *tsc1* gene, named *tsc1a* and *tsc1b*. DiBella et al. have used antisense morpholino oligonucleotides in order to knock down the *tsc1a* gene; and while this impacted kidney development, the authors did not address the impact of *tsc1a* loss on the brain (DiBella et al., 2009). It is also worth noting that the zebrafish Tsc1a and Tsc1b proteins share respectively 36 and 44% sequence identity with the human TSC1 (DiBella et al., 2009), while the zebrafish Tsc2 protein shares 73% sequence identity with the human TSC2 (Kim et al., 2011).

In 2011, Kim et al. created the $tsc2^{vu242}$ zebrafish line with a missense mutation leading to a premature STOP codon in the *tsc2* gene. The version of the Tuberin protein encoded by the mutant allele lacks the GTPase-activating protein (GAP) domain necessary for Rheb inactivation and, consequently, mTORC1 inhibition (Kim et al., 2011). While heterozygous $tsc2^{vu242/+}$ zebrafish show some increase in mTORC1 activation, they are viable; in contrast, $tsc2^{vu242/vu242}$ mutants die within the first two weeks of development, and display a more severe phenotype while alive. Studies have confirmed mTorC1 hyperactivation, increased cell size and disruptions of gray and white matter organization (Kim et al., 2011; Kedra et al., 2020), seizures and impaired locomotion (Scheldeman et al., 2017; Kedra et al., 2020) and abnormalities in axon guidance, as well as anxiety-like behaviors (Kedra et al., 2020) in the $tsc2^{vu242/vu242}$ mutant. Therefore, the $tsc2^{vu242/vu242}$ fish can be considered a valid model of TSC, as it recapitulates many changes seen in TSC patients.

Chapter 2. Aims and scope of the thesis

This thesis, using the zebrafish model of TSC, aims to explore the mechanisms leading to selected TANDs, with the goal of identifying potential future targets of treatment. In Chapter 3, I introduce the zebrafish as a model for studying seizure disorders, such as TSC, and explain its value for translational research. In Chapter 4, I present an overview of state-of-the-art methods to study brain development and function in zebrafish, including brain imaging techniques used in our laboratory. In Chapter 5, I analyze light preference in larval $tsc2^{vu242}$ fish, and aim to uncover the molecular and cellular mechanisms underlying this behavior. Using immunofluorescence stainings and live calcium imaging, I show how mTorC1 hyperactivity in the left habenula dysregulates neuronal activity, impairs sensory integration and leads to aberrant responses to light stimuli in the

tsc2$^{vu242/vu242}$ mutant. I also demonstrate that preventative treatment with the mTorC1 inhibitor rapamycin, either delivered into bathing medium or injected directly into the left habenula, results in normalized light response. Chapters 6 and 7 provide a detailed description of two protocols developed for the study described in Chapter 5: immunofluorescence in whole zebrafish larval brains, and injections of rapamycin into the zebrafish habenula. In Chapter 8, based on prior findings of our laboratory, I aim to discover the role of TrkB signaling in anxiety, and I map the amygdaloid complex in larval zebrafish based on brain topology and the expression of marker proteins. Using behavioral testing, and molecular analysis by ELISA assay, Western blot and immunofluorescence, I demonstrate that TrkB signaling is involved in regulation of anxiety-like behavior in *tsc2*^{vu242} fish independently of mTorC1. I also show the effect of TrkB inhibition on brain activity in the habenula, pallium and subpallium of *tsc2*^{vu242} larvae, and identify selected amygdaloid territories in the developing zebrafish brain. The findings of this thesis and the potential future research directions are summarized and discussed in Chapter 9.

References

Anaby D, Shrot S, Belenky E, Ben-Zeev B, Tzadok M, 2022. ***Neurite density of white matter significantly correlates with tuberous sclerosis complex disease severity.*** Neuroimage Clin, 35:103085.

Barnett JR, Grinspoon RA, Harisinghani M, Caruso PA, Thiele EA, 2020. ***The efficacy of cannabidiol on renal angiomyolipoma and subependymal giant cell tumor volume in tuberous sclerosis complex.*** J Clin Neurosci, 77:85-88.

Bradford YM, Toro S, Ramachandran S, Ruzicka L, Howe DG, Eagle A, Kalita P, Martin R, Taylor Moxon SA, Schaper K, Westerfield M, 2017. ***Zebrafish Models of Human Disease: Gaining Insight into Human Disease at ZFIN.*** ILAR J, 58(1):4-16.

Caban C, Khan N, Hasbani DM, Crino PB, 2016. ***Genetics of tuberous sclerosis complex: implications for clinical practice.*** Appl Clin Genet, 10:1-8.

Capal JK, Bernardino-Cuesta B, Horn PS, Murray D, Byars AW, Bing NM, Kent B, Pearson DA, Sahin M, Krueger DA; TACERN Study Group, 2017. ***Influence of seizures on early development in tuberous sclerosis complex.*** Epilepsy Behav, 70(Pt A):245-252.

Chévere-Torres I, Maki JM, Santini E, Klann E, 2012. ***Impaired social interactions and motor learning skills in tuberous sclerosis complex model mice expressing a dominant/negative form of tuberin.*** Neurobiol Dis, 45(1):156-64.

Crino PB, Nathanson KL, Henske EP, 2006. ***The tuberous sclerosis complex.*** N Engl J Med, 355(13):1345-56.

Cruz MP, 2010. ***Vigabatrin (Sabril), a Gamma-Aminobutyric Acid Transaminase Inhibitor for the Treatment of Two Catastrophic Seizure Disorders.*** P T, 35(1):20–3.

Curatolo P, Moavero R, Roberto D, Graziola F, 2015. ***Genotype/Phenotype Correlations in Tuberous Sclerosis Complex.*** Semin Pediatr Neurol, 22(4):259-73.

Curatolo P, Moavero R, de Vries PJ, 2015b. ***Neurological and neuropsychiatric aspects of tuberous sclerosis complex.*** Lancet Neurol, 14(7):733-45.

Curatolo P, Franz DN, Lawson JA, Yapici Z, Ikeda H, Polster T, Nabbout R, de Vries PJ, Dlugos DJ, Fan J, Ridolfi A, Pelov D, Voi M, French JA, 2018. ***Adjunctive everolimus for children and adolescents with treatment-refractory seizures associated with tuberous sclerosis complex: post-hoc analysis of the phase 3 EXIST-3 trial.*** Lancet Child Adolesc Health, 2(7):495-504.

DiBella LM, Park A, Sun Z, 2009. ***Zebrafish Tsc1 reveals functional interactions between the cilium and the TOR pathway.*** Hum Mol Genet, 18(4):595-606.

Ebrahimi-Fakhari D & Franz DN, 2020. ***Pharmacological treatment strategies for subependymal giant cell astrocytoma (SEGA).*** Expert Opin Pharmacother, 21(11):1329-1336.

Ehninger D, Han S, Shilyansky C, Zhou Y, Li W, Kwiatkowski DJ, Ramesh V, Silva AJ, 2008. ***Reversal of learning deficits in a Tsc2+/- mouse model of tuberous sclerosis.*** Nat Med, 14(8):843-8.

Ehninger D & Silva AJ, 2011. ***Increased levels of anxiety-related behaviors in a Tsc2 dominant negative transgenic mouse model of tuberous sclerosis.*** Behav Genet, 41(3):357-63.

Fokkema IFAC, Kroon M, López Hernández JA, Asscheman D, Lugtenburg I, Hoogenboom J, den Dunnen JT, 2021. ***The LOVD3 platform: efficient genome-wide sharing of genetic variants.*** Eur J Hum Genet, 29(12):1796-1803.

Foroozan R, 2018. ***Vigabatrin: Lessons Learned From the United States Experience.*** J Neuroophthalmol, 38(4):442-450.

Franz DN, Belousova E, Sparagana S, Bebin EM, Frost MD, Kuperman R, Witt O, Kohrman MH, Flamini JR, Wu JY, Curatolo P, de Vries PJ, Berkowitz N, Niolat J, Jóźwiak S, 2016. ***Long-Term Use of Everolimus in Patients with Tuberous Sclerosis Complex: Final Results from the EXIST-1 Study.*** PLoS One, 11(6):e0158476.

Goorden SM, van Woerden GM, van der Weerd L, Cheadle JP, Elgersma Y, 2007. ***Cognitive deficits in Tsc1+/- mice in the absence of cerebral lesions and seizures.*** Ann Neurol, 62(6):648-55.

Haji N, Riebe I, Aguilar-Valles A, Artinian J, Laplante I, Lacaille JC, 2020. ***Tsc1 haploinsufficiency in Nkx2.1 cells upregulates hippocampal interneuron mTORC1 activity, impairs pyramidal cell synaptic inhibition, and alters contextual fear discrimination and spatial working memory in mice.*** Mol Autism, 11(1):29.

Hancock E & Osborne JP, 1999. ***Vigabatrin in the treatment of infantile spasms in tuberous sclerosis: literature review.*** J Child Neurol, 14(2):71-4.

Henske E, Jóźwiak S, Kingswood J, Sampson JR, Thiele EA, 2016. ***Tuberous sclerosis complex.*** Nat Rev Dis Primers 2, 16035.

Hortopan GA, Dinday MT, Baraban SC, 2010. ***Zebrafish as a model for studying genetic aspects of epilepsy.*** Dis Model Mech, 3(3-4):144-8.

House PM, Holst B, Lindenau M, Voges B, Kohl B, Martens T, Lanz M, Stodieck S, Huppertz HJ, 2015. ***Morphometric MRI analysis enhances visualization of cortical tubers in tuberous sclerosis.*** Epilepsy Res, 117:29-34.

Huang J, Dibble CC, Matsuzaki M, Manning BD, 2008. ***The TSC1-TSC2 complex is required for proper activation of mTOR complex 2.*** Mol Cell Biol, 28(12):4104-15.

Im K, Ahtam B, Haehn D, Peters JM, Warfield SK, Sahin M, Ellen Grant P, 2016. ***Altered Structural Brain Networks in Tuberous Sclerosis Complex.*** Cereb Cortex, 26(5):2046-58.

Jansen FE, Vincken KL, Algra A, Anbeek P, Braams O, Nellist M, Zonnenberg BA, Jennekens-Schinkel A, van den Ouweland A, Halley D, van Huffelen AC, van Nieuwenhuizen O, 2008. ***Cognitive impairment in tuberous sclerosis complex is a multifactorial condition.*** Neurology, 70(12):916-923.

Józwiak S, Mandera M, Młynarski W, 2020 (accessed 2025). ***Zalecenia dotyczące pozarejestracyjnego stosowania rapamycyny (Rapamune) w stwardnieniu guzowatym*** [Internet]. Polskie Towarzystwo Neurologów Dziecięcych, Gdańsk, Poland. Available from: https://stwardnienie-guzowate.eu/wp-content/uploads/2020/09/Zalecenia-dotyczace-stosowania-pozarejestracyjnego-rapamycyny.pdf

Kadish NE, Riedel C, Stephani U, Wiegand G, 2020. ***Developmental outcomes in children/adolescents and one adult with tuberous sclerosis complex (TSC) and refractory epilepsy treated with everolimus.*** Epilepsy Behav, 111:107182.

Kedra M, Banasiak K, Kisielewska K, Wolinska-Niziol L, Jaworski J, Zmorzynska J, 2020. ***TrkB hyperactivity contributes to brain dysconnectivity, epileptogenesis, and anxiety in zebrafish model of Tuberous Sclerosis Complex.*** Proc Natl Acad Sci U S A, 117(4):2170-2179.

Kim SH, Speirs CK, Solnica-Krezel L, Ess KC, 2011. ***Zebrafish model of tuberous sclerosis complex reveals cell-autonomous and non-cell-autonomous functions of mutant tuberin.*** Dis Model Mech, 4(2):255-67.

Kingswood JC, d'Augères GB, Belousova E, Ferreira JC, Carter T, Castellana R, Cottin V, Curatolo P, Dahlin M, de Vries PJ, Feucht M, Fladrowski C, Gislimberti G, Hertzberg C, Jozwiak S, Lawson JA, Macaya A, Nabbout R, O'Callaghan F, Benedik MP, Qin J, Marques R, Sander V, Sauter M, Takahashi Y, Touraine R, Youroukos S, Zonnenberg B, Jansen AC; TOSCA consortium and TOSCA investigators, 2017. ***TuberOus SClerosis registry to increase disease Awareness (TOSCA) - baseline data on 2093 patients.*** Orphanet J Rare Dis, 12(1):2.

Kobayashi T, Minowa O, Sugitani Y, Takai S, Mitani H, Kobayashi E, Noda T, Hino O, 2001. ***A germ-line Tsc1 mutation causes tumor development and embryonic lethality that are similar, but not identical to, those caused by Tsc2 mutation in mice.*** Proc Natl Acad Sci U S A, 98(15):8762-7.

Kotulska K, Kwiatkowski DJ, Curatolo P, Weschke B, Riney K, Jansen F, Feucht M, Krsek P, Nabbout R, Jansen AC, Wojdan K, Sijko K, Głowacka-Walas J, Borkowska J, Sadowski K, Domańska-Pakieła D, Moavero R, Hertzberg C, Hulshof H, Scholl T, Benova B, Aronica E, de

Ridder J, Lagae L, Jóźwiak S; EPISTOP Investigators, 2021. ***Prevention of Epilepsy in Infants with Tuberous Sclerosis Complex in the EPISTOP Trial.*** Ann Neurol, 89(2):304-314.

Lebrun-Julien F, Bachmann L, Norrmén C, Trötzmüller M, Köfeler H, Rüegg MA, Hall MN, Suter U, 2014. ***Balanced mTORC1 activity in oligodendrocytes is required for accurate CNS myelination.*** J Neurosci, 34(25):8432-48.

Lee WS, Macdonald-Laurs E, Stephenson S, D'Arcy C, Maixner W, Harvey AS, Lockhart PJ, Leventer RJ, 2023. ***Pathogenic RHEB Somatic Variant in a Child With Tuberous Sclerosis Complex Without Pathogenic Variants in TSC1 or TSC2.*** Neurology, 101(2):78-82.

Magri L, Cominelli M, Cambiaghi M, Cursi M, Leocani L, Minicucci F, Poliani PL, Galli R, 2013. ***Timing of mTOR activation affects tuberous sclerosis complex neuropathology in mouse models.*** Dis Model Mech, 1185-1197.

Man A, Di Scipio M, Grewal S, Suk Y, Trinari E, Ejaz R, Whitney R, 2024. ***The Genetics of Tuberous Sclerosis Complex and Related mTORopathies: Current Understanding and Future Directions.*** Genes (Basel), 15(3):332.

Moavero R, Napolitano A, Cusmai R, Vigevano F, Figà-Talamanca L, Calbi G, Curatolo P, Bernardi B, 2016. ***White matter disruption is associated with persistent seizures in tuberous sclerosis complex.*** Epilepsy Behav, 60:63-67.

Mori S & Aggarwal M, 2014. ***In vivo magnetic resonance imaging of the human limbic white matter.*** Front Aging Neurosci, 6:321.Neuman NA & Henske EP, 2011. ***Non-canonical functions of the tuberous sclerosis complex-Rheb signaling axis.*** EMBO Mol Med, 3(4):189-200.

Normand EA, Crandall SR, Thorn CA, Murphy EM, Voelcker B, Browning C, Machan JT, Moore CI, Connors BW, Zervas M, 2013. ***Temporal and mosaic Tsc1 deletion in the developing thalamus disrupts thalamocortical circuitry, neural function, and behavior.*** Neuron, 78(5):895-909.

Northrup H, Koenig MK, Pearson DA, Au KS, 1999 (Updated 2024). ***Tuberous Sclerosis Complex.*** In: Adam MP, Feldman J, Mirzaa GM, et al., editors. GeneReviews® [Internet]. University of Washington; Seattle, WA, USA. Available from: https:// ncbi.nlm.nih.gov/books/NBK1220/

Numis AL, Major P, Montenegro MA, Muzykewicz DA, Pulsifer MB, Thiele EA, 2011. ***Identification of risk factors for autism spectrum disorders in tuberous sclerosis complex.*** Neurology, 76(11):981-7.

Onda H, Lueck A, Marks PW, Warren HB, Kwiatkowski DJ, 1999. ***Tsc2(+/-) mice develop tumors in multiple sites that express gelsolin and are influenced by genetic background.*** J Clin Invest, 104(6):687-95.

Orlova KA & Crino PB, 2010. ***The tuberous sclerosis complex.*** Ann N Y Acad Sci, 1184:87-105.

Overwater IE, Rietman AB, Mous SE, Bindels-de Heus K, Rizopoulos D, Ten Hoopen LW, van der Vaart T, Jansen FE, Elgersma Y, Moll HA, de Wit MY; ENCORE Expertise Centre for

Neurodevelopmental Disorders, 2019. ***A randomized controlled trial with everolimus for IQ and autism in tuberous sclerosis complex.*** Neurology, 93(2):e200-e209.

Peters JM, Prohl A, Kapur K, Nath A, Scherrer B, Clancy S, Prabhu SP, Sahin M, Franz DN, Warfield SK, Krueger DA, 2019. ***Longitudinal Effects of Everolimus on White Matter Diffusion in Tuberous Sclerosis Complex.*** Pediatr Neurol, 90:24-30.

Prentzell MT, Rehbein U, Cadena Sandoval M, De Meulemeester AS, Baumeister R, Brohée L, Berdel B, Bockwoldt M, Carroll B, Chowdhury SR, von Deimling A, Demetriades C, Figlia G; Genomics England Research Consortium; de Araujo MEG, Heberle AM, Heiland I, Holzwarth B, Huber LA, Jaworski J, Kedra M, Kern K, Kopach A, Korolchuk VI, van 't Land-Kuper I, Macias M, Nellist M, Palm W, Pusch S, Ramos Pittol JM, Reil M, Reintjes A, Reuter F, Sampson JR, Scheldeman C, Siekierska A, Stefan E, Teleman AA, Thomas LE, Torres-Quesada O, Trump S, West HD, de Witte P, Woltering S, Yordanov TE, Zmorzynska J, Opitz CA, Thedieck K, 2021. ***G3BPs tether the TSC complex to lysosomes and suppress mTORC1 signaling.*** Cell, 184(3):655-674.e27.

Prohl AK, Scherrer B, Tomas-Fernandez X, Davis PE, Filip-Dhima R, Prabhu SP, Peters JM, Bebin EM, Krueger DA, Northrup H, Wu JY, Sahin M, Warfield SK; TACERN Study Group, 2019. ***Early white matter development is abnormal in tuberous sclerosis complex patients who develop autism spectrum disorder.*** J Neurodev Disord, 11(1):36.

Ragupathi A, Kim C, Jacinto E, 2024. ***The mTORC2 signaling network: targets and cross-talks.*** Biochem J, 481(2):45-91.

Ravi V & Venkatesh B, 2008. ***Rapidly evolving fish genomes and teleost diversity.*** Curr Opin Genet Dev, 18(6):544-50.

Reith RM, McKenna J, Wu H, Hashmi SS, Cho SH, Dash PK, Gambello MJ, 2013. ***Loss of Tsc2 in Purkinje cells is associated with autistic-like behavior in a mouse model of tuberous sclerosis complex.*** Neurobiol Dis, 51:93-103.

Rosengren T, Nanhoe S, de Almeida LGD, Schönewolf-Greulich B, Larsen LJ, Hey CAB, Dunø M, Ek J, Risom L, Nellist M, Møller LB, 2020. ***Mutational analysis of TSC1 and TSC2 in Danish patients with tuberous sclerosis complex.*** Sci Rep, 10(1):9909.

Ruppe V, Dilsiz P, Reiss CS, Carlson C, Devinsky O, Zagzag D, Weiner HL, Talos DM, 2014. ***Developmental brain abnormalities in tuberous sclerosis complex: A comparative tissue analysis of cortical tubers and perituberal cortex.*** Epilepsia, 55(4):539–550.

Salussolia CL, Klonowska K, Kwiatkowski DJ, Sahin M, 2019. ***Genetic Etiologies, Diagnosis, and Treatment of Tuberous Sclerosis Complex.*** Annu Rev Genomics Hum Genet, 20:217-240.

Santos VR, Jerow LG, LaSarge CL, 2025. ***Behavioral analyses in rodent models of tuberous sclerosis complex.*** Epilepsy Behav, 165:110313.

Sato A, Kasai S, Kobayashi T, Takamatsu Y, Hino O, Ikeda K, Mizuguchi M, 2012. ***Rapamycin reverses impaired social interaction in mouse models of tuberous sclerosis complex.*** Nat Commun, 3:1292.

Sato A, Tominaga K, Iwatani Y, Kato Y, Wataya-Kaneda M, Makita K, Nemoto K, Taniike M, Kagitani-Shimono K, 2022. ***Abnormal White Matter Microstructure in the Limbic System Is Associated With Tuberous Sclerosis Complex-Associated Neuropsychiatric Disorders.*** Front Neurol, 13:782479.

Scheldeman C, Mills JD, Siekierska A, Serra I, Copmans D, Iyer AM, Whalley BJ, Maes J, Jansen AC, Lagae L, Aronica E, de Witte PAM, 2017. ***mTOR-related neuropathology in mutant tsc2 zebrafish: Phenotypic, transcriptomic and pharmacological analysis.*** Neurobiol Dis, 108:225-237.

Schubert-Bast S & Strzelczyk A, 2021. ***Review of the treatment options for epilepsy in tuberous sclerosis complex: towards precision medicine.*** Ther Adv Neurol Disord, 14:17562864211031100.

Specchio N, Nabbout R, Aronica E, Auvin S, Benvenuto A, de Palma L, Feucht M, Jansen F, Kotulska K, Sarnat H, Lagae L, Jozwiak S, Curatolo P, 2023. ***Updated clinical recommendations for the management of tuberous sclerosis complex associated epilepsy.*** Eur J Paediatr Neurol, 47:25-34.

Switon K, Kotulska K, Janusz-Kaminska A, Zmorzynska J, Jaworski J, 2017. ***Molecular neurobiology of mTOR.*** Neuroscience, 341, 112–153.

Thiele EA, Bebin EM, Bhathal H, Jansen FE, Kotulska K, Lawson JA, O'Callaghan FJ, Wong M, Sahebkar F, Checketts D, Knappertz V; GWPCARE6 Study Group, 2021. ***Add-on Cannabidiol Treatment for Drug-Resistant Seizures in Tuberous Sclerosis Complex: A Placebo-Controlled Randomized Clinical Trial.*** JAMA Neurol, 78(3):285-292.

Tsai PT, Hull C, Chu Y, Greene-Colozzi E, Sadowski AR, Leech JM, Steinberg J, Crawley JN, Regehr WG, Sahin M, 2012. ***Autistic-like behaviour and cerebellar dysfunction in Purkinje cell Tsc1 mutant mice.*** Nature, 488(7413):647-51.

Tsai PT, Rudolph S, Guo C, Ellegood J, Gibson JM, Schaeffer SM, Mogavero J, Lerch JP, Regehr W, Sahin M, 2018. ***Sensitive Periods for Cerebellar-Mediated Autistic-like Behaviors.*** Cell Rep, 25(2):357-367.e4.

Tyburczy ME, Dies KA, Glass J, Camposano S, Chekaluk Y, Thorner AR, Lin L, Krueger D, Franz DN, Thiele EA, Sahin M, Kwiatkowski DJ, 2015. ***Mosaic and Intronic Mutations in TSC1/TSC2 Explain the Majority of TSC Patients with No Mutation Identified by Conventional Testing.*** PLoS Genet, 11(11):e1005637.

Uematsu M, Numata-Uematsu Y, Aihara Y, Kobayashi T, Fujikawa M, Togashi N, Shiihara T, Ohashi K, Hattori A, Saitoh S, Kure S, 2020. ***Behavioral problems and family distress in tuberous sclerosis complex.*** Epilepsy Behav, 111:107321.

de Vries PJ, Whittemore VH, Leclezio L, Byars AW, Dunn D, Ess KC, Hook D, King BH, Sahin M, Jansen A, 2015. ***Tuberous sclerosis associated neuropsychiatric disorders (TAND) and the TAND Checklist.*** Pediatr Neurol, 52(1):25-35.

de Vries PJ, Belousova E, Benedik MP, Carter T, Cottin V, Curatolo P, Dahlin M, D'Amato L, d'Augères GB, Ferreira JC, Feucht M, Fladrowski C, Hertzberg C, Jozwiak S, Kingswood JC, Lawson JA, Macaya A, Marques R, Nabbout R, O'Callaghan F, Qin J, Sander V, Sauter M, Shah S, Takahashi Y, Touraine R, Youroukos S, Zonnenberg B, Jansen AC; TOSCA Consortium and TOSCA Investigators, 2018. ***TSC-associated neuropsychiatric disorders (TAND): findings from the TOSCA natural history study.*** Orphanet J Rare Dis, 13(1):157.

Waltereit R, Welzl H, Dichgans J, Lipp HP, Schmidt WJ, Weller M, 2006. ***Enhanced episodic-like memory and kindling epilepsy in a rat model of tuberous sclerosis.*** J Neurochem, 96(2):407-13.

Waltereit R, Japs B, Schneider M, de Vries PJ, Bartsch D, 2011. ***Epilepsy and Tsc2 haploinsufficiency lead to autistic-like social deficit behaviors in rats.*** Behav Genet, 41(3):364-72.

West HD, Nellist M, Brouwer RWW, van den Hout-van Vroonhoven MCGN, de Almeida LGD, Hendriks F, Elfferich P, Raja M, Giles P, Alfano RM, Peron A, Sznajer Y, De Waele L, Jansen A, Koopmans M, Kievit A, Farach LS, Northrup H, Sampson JR, Thomas LE, van IJcken WFJ, 2023. ***Targeted Genomic Sequencing of TSC1 and TSC2 Reveals Causal Variants in Individuals for Whom Previous Genetic Testing for Tuberous Sclerosis Complex Was Normal.*** Hum Mutat, 2023:4899372.

Wong M, 2019. ***The role of glia in epilepsy, intellectual disability, and other neurodevelopmental disorders in tuberous sclerosis complex.*** J Neurodev Disord, 11(1):30.

Yuan E, Tsai PT, Greene-Colozzi E, Sahin M, Kwiatkowski DJ, Malinowska IA, 2012. ***Graded loss of tuberin in an allelic series of brain models of TSC correlates with survival, and biochemical, histological and behavioral features.*** Hum Mol Genet, 21(19):4286-300.

Chapter 3. The zebrafish model of Tuberous sclerosis complex to study epilepsy

O. Doszyn[¥], T. Dulski[¥], J. Zmorzynska*

[¥] equal contribution

*corresponding author

Chapter 19 of the Handbook of Animal Models in Neurological Disorders, edited by Colin R. Martin, Vinood B. Patel, Victor R. Preedy, Elsevier 2023; 227-240.

DOI: 10.1016/B978-0-323-89833-1.00031-8.

Abstract

Zebrafish are being widely used to study central nervous system diseases such as epilepsy. Over the last two decades research on zebrafish models contributed to our understanding of brain development as well as pathological processes involved in disease. Tuberous Sclerosis Complex (TSC) is a genetic disease resulting from mutations in *TSC1* or *TSC2* genes. TSC patients suffer from seizures associated with dysregulated mTOR signaling. Here, we focused on specific methodologies used to study epilepsy-like phenotype in the TSC fish highlighting the value of zebrafish as a model to study epilepsy. The availability of powerful and effective techniques like brain activity imaging, behavioral tracking, and high-resolution microscopy in developing animals make zebrafish useful to study epilepsy pathogenesis on different levels. Moreover, ex utero development, quick maturation, and ease of genetic manipulation are also advantageous. Furthermore, we also summarize other genetic or chemically induced epilepsy models made in zebrafish. Comprehensive knowledge in this chapter may help researchers to design their own studies using zebrafish as an animal model.

Key Words

Tuberous Sclerosis Complex (TSC), TSC zebrafish model, TSC-associated epilepsy, zebrafish epilepsy model, epilepsy, seizures, behavioral tracking, brain activity imaging

1. Introduction

Tuberous sclerosis complex (TSC) is an autosomal dominant genetic disease resulting from mutations inactivating the *TSC1* or *TSC2* genes (encoding Hamartin or Tuberin, respectively) but the latter is more common and accounts for 76% of cases (Salussolia et al., 2019). Hamartin and Tuberin proteins form an inhibitory complex which regulates the signaling pathway of mammalian target of rapamycin (mTOR). The outcome of either the *TSC1* or *TSC2* mutation is loss of the Hamartin-Tuberin functional complex and hyperactivity of the mTOR pathway (Switon et al., 2017).

The major clinical manifestations of TSC are epilepsy and benign tumors in multiple organs, however, 90% of patients suffer also from TSC-associated neuropsychiatric disorders (Crino et al., 2006; Ess, 2006; Salussolia et al., 2019). The first symptoms of TSC are usually seizures or characteristic skin changes, e.g., facial angiofibromas, which often occur during first two years of life (Salussolia et al., 2019). Structural lesions in the brain have long been associated with epilepsy. However in TSC, benign tumors in the cortex (tubers) are not solely responsible for epileptic seizures but cellular dysplasia and dysregulated mTOR signaling in the perituberal tissue also play a role. In fact, some studies suggest that the abnormal mTOR activity alone might result in epileptogenesis (Ruppe et al., 2014). The epilepsy image is very complex in patients with TSC. Focal seizures are the most common (50% of epilepsy cases), followed by generalized seizures which occur in 27% and mixed seizures in 18% of the TSC patients with epilepsy. Seizures can be of every type, e.g., clonic, tonic, atonic, or absence (Specchio & Pietrafusa, 2020). Childhood epilepsy in TSC often manifests also as infantile spasms (37% of children with TSC) and will often turn into a refractory form (Salussolia et al., 2019).

Moreover, the TSC patients with mutations in the *TSC2* gene tend to have an earlier onset and higher frequency of seizures. Earlier epilepsy onset is also associated in TSC with more pronounced cognitive decline (Salussolia et al, 2019). Therefore, studies of the early developmental mechanisms underlying epilepsy in TSC are still needed.

2. Details of the Animal Model

The *tsc2*^{vu242} mutant line was generated by Kim *et al*. (2011) by introducing a nonsense mutation into the zebrafish *tsc2* gene leading to premature STOP codon. The homozygotes *tsc2*$^{vu242/vu242}$ (the TSC fish) are considered the zebrafish model of TSC. The authors reported that the TSC fish have disrupted gray and white matter compartments in the brain and overgrown cells in multiple body regions. The large neurons in the brain exhibited hyperactive mTOR signaling similarly to TSC patients (Kim et al., 2011). Later, the TSC fish have been also shown to display behavioral alterations, neuronal hyperactivity in the brain, and disruptions in brain development, such as pallium malformations, thinner commissures, and disturbances in axon fasciculation – all changes corresponding to TSC symptoms (Kedra et al., 2020; Scheldeman et al., 2017). Scheldeman *et al*. (2017) also demonstrated seizures in the TSC fish using local field potential (LFP) recordings and we discovered that these were non-motor seizures caused by increased neuronal activity in the brain (Kedra et al., 2020). We also mapped specific characteristics of the TSC fish behavior to phenotypes similar to epilepsy and anxiety to facilitate high-throughput drug screens (Kedra et al., 2020). In this review, we focus on specific methodologies used to study epilepsy-like phenotype in the TSC fish.

2.1. Breeding and genotyping of the TSC fish

The TSC fish are sensitive to hypoxic conditions and thus water should be exchanged daily. The mutation is lethal when homozygous and homozygotic larvae die earlier when water is not exchanged frequently. Early mortality makes it necessary to breed and cross adult heterozygotic fish to gain homozygotic embryos and sibling controls for experiments. Efficient genotyping is thus crucial. There are two methods frequently used for genotyping the TSC fish – amplification of the allele by polymerase chain reaction (PCR) and digestion with the restriction enzyme HpyCHIV4 (Figure 1A) or amplification of the allele by quantitative PCR (qPCR) and analysis by high-resolution melting (HRM) technique (Figure 1B). Genotyping is done from the tail region and heads are used for experiments. The timing of genomic DNA isolation for genotyping depends on the experimental design. For example the genotyping is done before the extraction of tissue for immunofluorescence or for isolation of proteins or RNA. On the other hand, behavioral assays, electrophysiological recordings, and live imaging experiments are done blindly concerning the genotype and the extraction of genomic DNA is done after the recordings are taken.

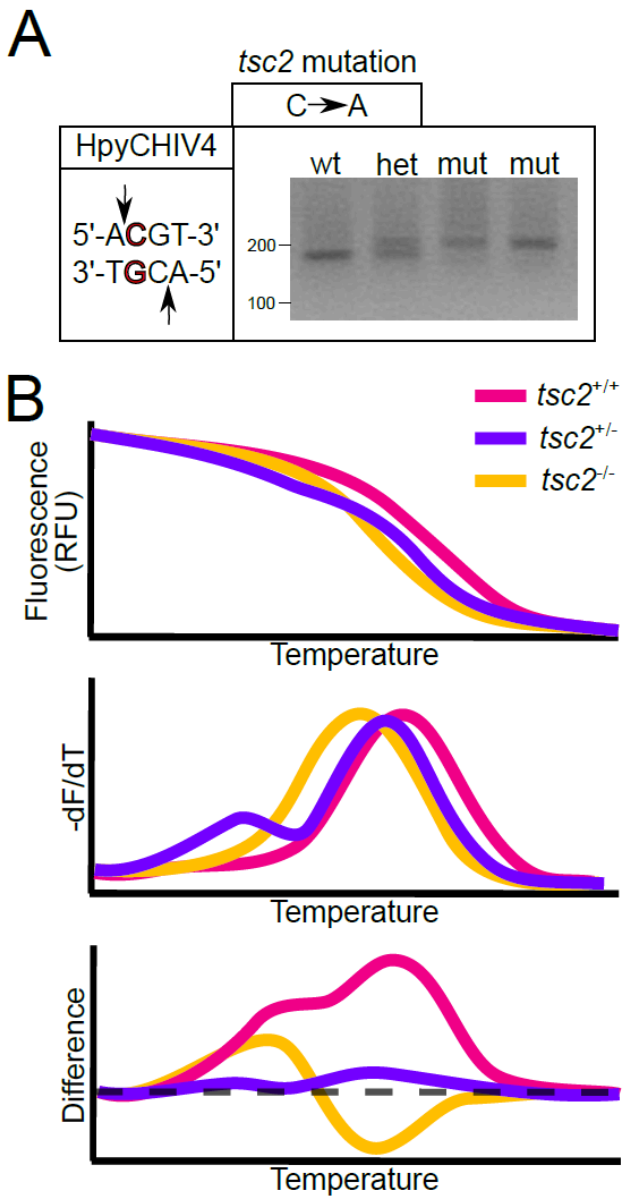

Figure 1. Strategies for genotyping the TSC fish.

A. Genotyping of the TSC fish and its sibling controls by PCR and restriction enzyme analysis. The mutation in the *tsc2* causes loss of restriction site for HpyCHIV4 enzyme. B. Genotyping of the TSC fish and its sibling controls by HRM analysis. The mutation in the *tsc2* causes a temperature shift.

2.2. Brain activity measurements in the TSC fish

One of the most imperative methods for the epilepsy research concerns brain activity measurements. For this purpose, transgenic lines expressing genetically encoded calcium indicator GCaMP are used. GCaMPs are fusion proteins of green fluorescent protein (GFP) and calcium-binding protein calmodulin. They increase their fluorescence when bound to calcium ions which facilitates live imaging of the brain activity on a single-cell level (Lin and Schnitzer,

2016). Using this approach, the zebrafish brain activity can be imaged and measured in a specific region of interest (Figure 2). Additional fusion of GCaMP with synaptophysin facilitates imaging of neuronal activity in the synapses as fusion with synaptophysin drives the synaptic localization of the fluorescent probe (Akerboom et al., 2012).

Anesthetics are used for mounting and stabilizing the fish for imaging. The commonly used Tricaine (or MS-222) is not suitable for the brain activity experiments, as it inhibits it. Thus, other approaches need to be taken like using 2% agarose of a low-melting point and freeing the tail in order for fish to move it freely or adding non-depolarizing muscle relaxants to the imaging medium, e.g., pancuronium bromide.

Our team studied the brain activity in the TSC fish in *Tg(HuC:GCaMP5G)* transgenic background (Ahrens et al., 2013). We also injected *Tg(HuC:GCaMP5G)* fish with morpholino (MO) against *g3bp1* for gene knockdown. *g3bp1* encodes protein that tethers the Hamartin-Tuberin complex to the lysosome enabling its function (Prentzell et al., 2021). Imaging of the neuronal activity in the pallium of the *Tg(HuC:GCaMP5G)* fish was performed using lightsheet microscope. Change in fluorescence intensity across time was calculated in the whole pallium and was also measured in single cells mislocalized to pallial white matter compartments (Kedra et al., 2020; Prentzell et al., 2021). We showed increased activity of the whole pallium in the TSC fish compared to wildtype siblings (Figure 2) (Kedra et al., 2020). Moreover, with this method we also discovered that cells mislocalized in the white matter compartments of the pallium may be the foci for the increased brain activity (Prentzell et al., 2021).

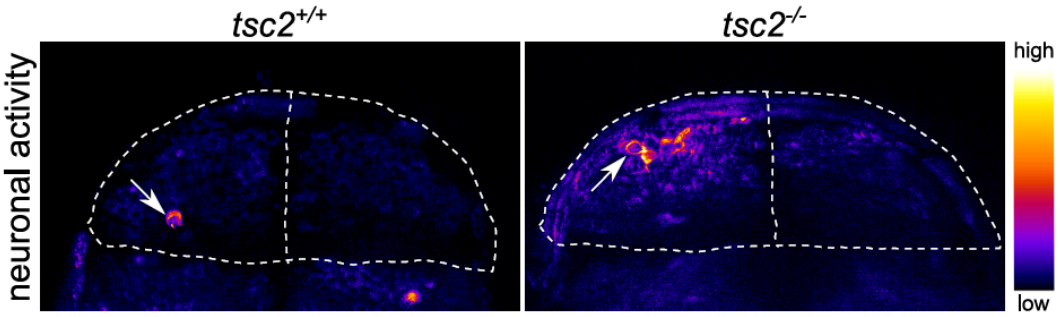

Figure 2. Calcium imaging of neuronal activity in the TSC fish.

The TSC fish shows higher overall neuronal activity in the brain compared to sibling controls.

The other approach to measure brain activity in the TSC fish is to perform electroencephalographic (EEG) recordings or LFP (LFP method has been recently reviewed by Gawel et al., 2020). A pioneer study by Baraban et al. (2005) established protocols to observe EEG activity and seizures in larval zebrafish exposed to pentylenetetrazole (PTZ). EEG recordings have shown similarities to those of humans regarding ictal discharge frequency (2–7 Hz). However, high gamma oscillations (80–150 Hz) present in humans and rodents were not observed (Weiss et al., 2013). It is also important to note that ongoing activity in the larval zebrafish brain looks different than in mammals,

with discontinuous bursts of activity, therefore electrographic signatures will differ between species (Zdebik et al., 2013).

These electrophysiological methods are complementary to calcium imaging using GCaMP transgenic lines as they have better temporal resolution, but lower spatial resolution. Although, GCaMP probes that have been lately generated facilitate imaging of neuronal activity with a very good temporal resolution. The LFP recordings are usually done in a region-specific manner in comparison to measurements using GCaMP probes which resolve neuronal activity to the single-cell level. The challenge using genetically encoded GCaMP probes is to image the same brain cells in the same brain region of multiple fish. This can be done by imaging of large portions of the brain, which can be later mapped into reference brain, but this approach causes loss of temporal resolution. Alternatively, GCaMP fish can be crossed into transgenic background in which the specific neurons of interest express reporter protein with different optical properties than GFP, e.g., red fluorescent protein (RFP). Then the imaging of these RFP-positive cells can be done in a temporally continuous mode across one z-plane which gives a very high temporal resolution.

2.3. Behavioral characteristics of the TSC fish

Behavior is ultimately connected to the brain function and therefore it is also crucial for the epilepsy research. The freely moving zebrafish larvae exhibit velocity in a range of 0.5–2 cm/s. Fish velocity above 2 cm/s is considered as hyperactivity and therefore can be used as a proxy for motor seizures. Motor seizures are acute and can be seen by burst swimming, left and right movements, and erratic, circular movements (Afrikanova et al., 2013). Tracking of basic locomotion should show differences between fish having motor seizures and seizure-free animals usually by large increase in activity and velocity in seizing animals (Figure 3A). Still, there are also non-motor seizures that result in loss of consciousness and decreased activity like in the TSC fish (Figure 3B). One may use 0.02% tricaine (g/vol) and 2.5–5 mM PTZ as negative and positive controls for motor seizures (Figure 3C).

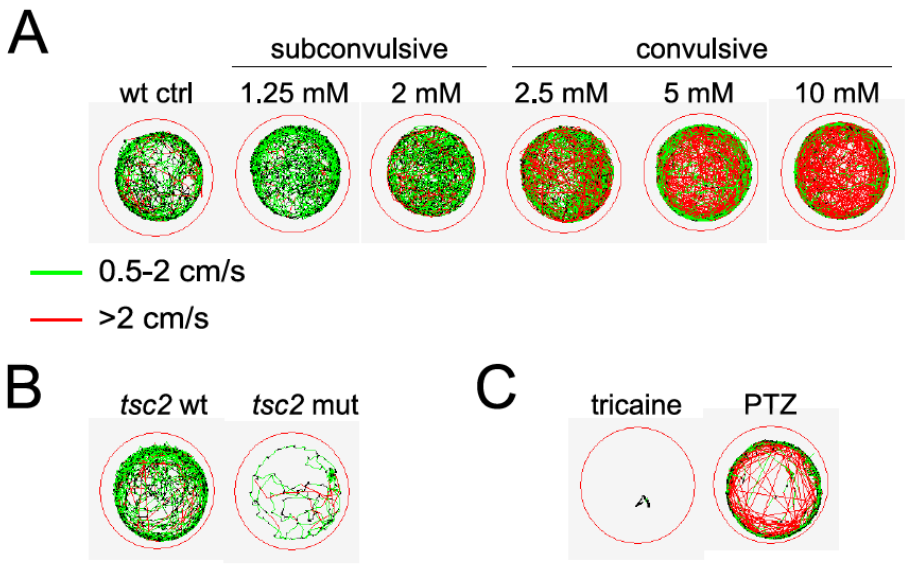

Figure 3. Behavioral analysis of seizures in the TSC fish.

A. Tracks from behavioral analysis of locomotor activity of wildtype zebrafish after treatment with various doses of PTZ. Motor seizures can be seen by increased activity in a hypervelocity range (red tracks). Green tracks represent normal activity. B. Tracks from behavioral analysis of locomotor activity of the TSC fish and its sibling controls. Non-motor seizures can be seen as decreased overall activity. C.

Tracks from behavioral analysis of locomotor activity of wildtype zebrafish treated with tricaine or PTZ that can be used as experimental controls.

Analysis of behavior connected to seizures in zebrafish is relatively easy using video recordings and commercially available automated tracking systems. Recordings of fish in 96-well plates with one fish per well offer very high throughput, however, it is not advisable for larvae older than 4 days post-fertilization (dpf). 12-well or 24-well plates would give much more information about characteristics of behavior such as repetitive movements, circling behavior, erratic movements, distance from center or from the wall, etc., as the recording area is bigger, and tracks are more informative.

Basic behavioral assays are suitable for screens of anti-epileptic properties of chemical compounds. They also can be used to assess compound toxicity. However, proper controls should be included in the experiment like non-treated siblings and solvent-treated fish of all genotypes. Commonly used dimethyl sulfoxide changes behavioral properties of zebrafish larvae by increasing their activity and velocity and is especially toxic for development in concentrations above 0.5%. Also, alcohols are toxic for zebrafish embryos and larvae, thus, they should be avoided.

The TSC fish exhibits decreased activity compared to wildtype siblings (Figure 3B), which can be seen by lower duration of activity, lower distance traveled, and lower mean velocity. We mapped this decreased activity to non-motor seizures which could be rescued by overnight treatment with 25 μM ethosuximide or 60 μM vigabatrin. 200 nM rapamycin also can be used to rescue the behavioral phenotype of the TSC fish. Moreover, the velocity in the hyperactivity range (> 2 cm/s) was increased in the TSC fish. Although it was not connected to seizures but to the anxiety-like behavior and could be rescued by rapamycin or anti-anxiety drugs such as ANA-12 or diazepam (Kedra et al., 2020).

2.4. Epileptogenesis studies in the TSC fish

Epileptogenesis can also be studied in zebrafish on a behavioral level. Taking advantage of the zebrafish external development, one can measure the spontaneous activity during very early developmental stage. The spontaneous movements of zebrafish embryos start at 17 hours post-fertilization (hpf), increase in time till 28 hpf, and then slowly decrease being the lowest at 36 hpf (de Oliveira et al., 2021). The stage of 24 hpf is advisable for this experiment as at 20 hpf high movement variability is observed, but it can also be done at 32 hpf. Staging should be performed before this experiment (usually at blastula stage) to assure that all embryos were born at the same time and are developing in equal pace. Assessment of spontaneous movements in zebrafish embryos can be done with low magnification bright-field microscope which is connected to a camera. Recordings should be done with a frame rate of at least 10 fps. Number of movements can be calculated manually or in an automatic manner using recently developed macro for ImageJ software (Kurnia et al., 2021). Increased number of spontaneous movements at 24 hpf has been linked to seizure development in the TSC fish and other zebrafish models of epilepsy (Kedra et al., 2020; Wager et al., 2016).

Another approach to study epileptogenesis is to subject zebrafish larvae to subconvulsive doses of

epileptogenic compounds such as PTZ, which induces motor seizures in larval zebrafish from 2.5 mM (Winter et al., 2008). We treated the TSC fish and their siblings with 1.25 mM PTZ for 6 min. before behavioral analysis and tracked their locomotion for 10 min. in darkness (Figure 4). The TSC fish treated with subconvulsive concentration of PTZ exhibited lower overall duration of activity, similarly to the untreated TSC fish. However, after PTZ, the TSC fish showed increased number of peaks of high activity in the hypervelocity range (> 2cm/s) and also increased number of peaks of higher velocity compared to sibling controls. The increase in locomotor activity in a hypervelocity range after treatment with PTZ is associated with motor seizures (Figure 4).

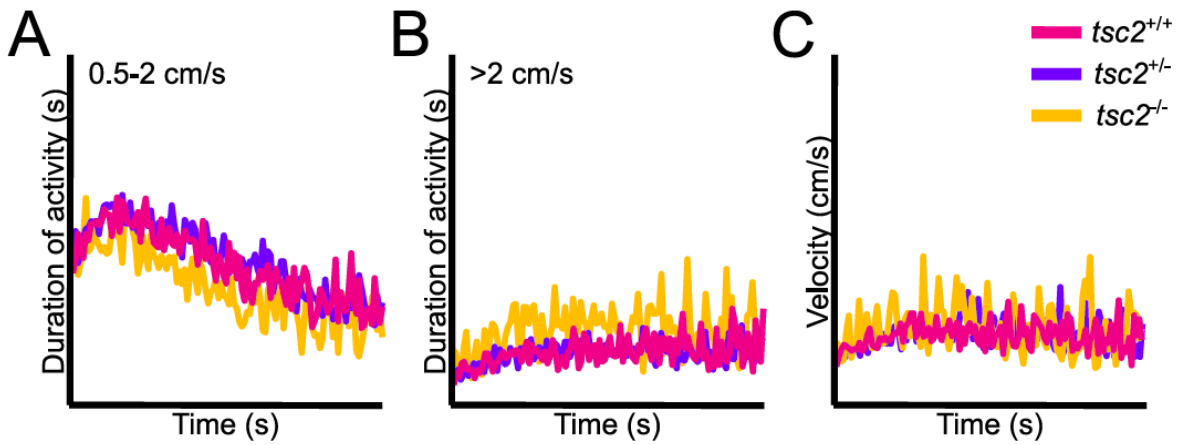

Figure 4. Behavioral analysis of the TSC fish treated with a subconvulsive dose of PTZ.

A. Activity over time in a 0.5-2 cm/s range shows decreased locomotion in the TSC fish compared to sibling controls. B. Activity over time in a hypervelocity range show increased locomotion in the TSC fish. C. Velocity over time shows high velocity peaks in the TSC fish.

2.5. Studies of pathomechanisms in the TSC fish

Epilepsy research imperatively also includes brain morphology and molecular studies to unravel the underlying mechanisms of pathogenesis. Multiple techniques of molecular and cell biology are available in zebrafish. The most informative techniques are not only qualitative, but also quantitative, and include the spatial context of the whole brain. These are whole-mount immunofluorescence techniques or whole-mount fluorescent *in situ* hybridization if antibodies are not available (Figure 5A). Inevitably, genetic techniques also can be used to study molecular mechanisms of pathogenesis.

The mechanism underlying seizures is presumably imbalance between inhibition and excitation in the neuronal activity, when excitation overcomes inhibition (reviewed by Staley, 2015). However, what drives the imbalance between the two neuronal systems to produce seizures, thus which mechanisms prompt epileptogenesis and ictogenesis in TSC, is still debated. The TSC fish can bring answers to these questions. Studies of the brain pathology of the TSC fish and *g3bp1* morphants in early development may resolve molecular or cellular mechanisms between mTOR pathway hyperactivation and increased neuronal excitability. Knockdown of *g3bp1* with MO caused

loss of function of Hamartin-Tuberin complex by disruption of its localization, phenocopying the TSC fish (Prentzell et al., 2021). Mislocalized cells in white matter compartments of pallia were present both in the TSC fish and the *g3bp1* morphants. In both models, these cells exhibited hyperactivated mTOR pathway (Kedra et al., 2020; Prentzell et al., 2021). In *g3bp1* morphants, ectopic cells in white matter compartments were acting as ictal foci propagating the neuronal activity into the whole pallium. Moreover, live imaging of migrating neuronal progenitors in the developing zebrafish frontbrains revealed increased migration dynamics in the *g3bp1* morphants compared to controls (Prentzell et al., 2021). This suggests that dysregulated migration may underlie the mislocalization of neurons in the white matter compartments that drive seizures in TSC (Figure 5).

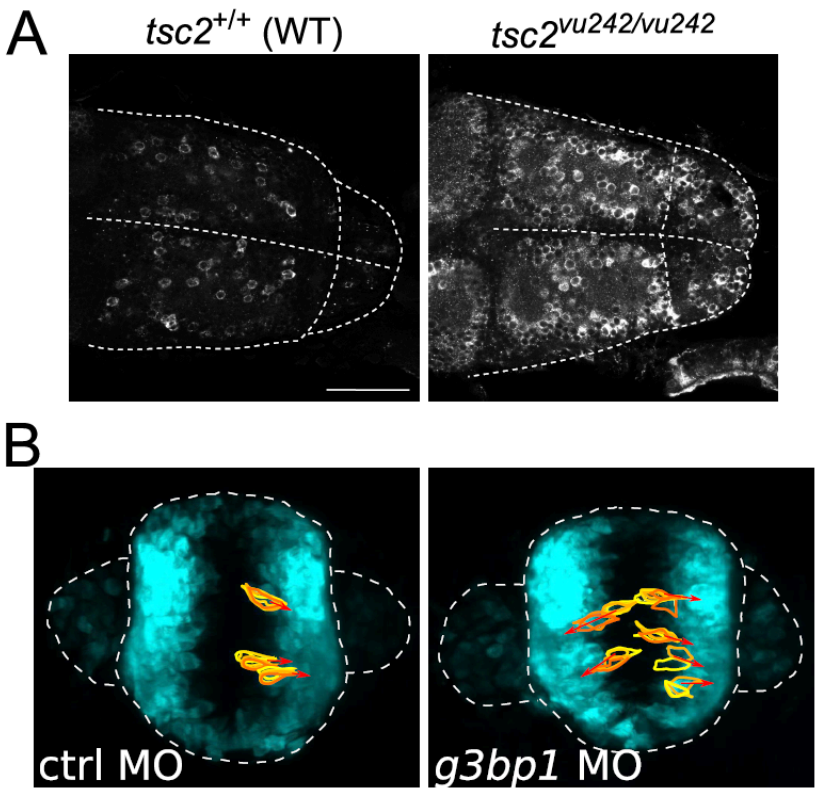

Figure 5. Single-cell resolution in the context of the whole brain.

A. Whole-mount immunofluorescence using anty-phosphorylated Rps6 antibody shows overactivated mTOR signaling and ectopic cells in white matter compartments in the pallium of the TSC fish compared to wildtype siblings (scale bar = 40 µm). B. Live imaging of HuC-positive neurons at 24 hpf brains shows increased number of migrating cells in the frontbrain of *g3bp1* morphants compared to control.

3. Advantages and Disadvantages

*Z*ebrafish emerged as a model organism for studying development and disease in the 1980s, with pioneer work by George Streisinger, who began to establish tools for its genetic analysis (Streisinger et al., 1981). However, rats and mice are still used in the bulk of neuroscience research, and zebrafish-based studies, although growing in popularity, are rarer in comparison. Because of prevalence of rodent models, neuroscientists less frequently train and specialize in working with zebrafish, and multiple techniques that are well-developed for rodents still require adjustments and validation in zebrafish. Nevertheless, there are numerous advantages of using zebrafish as a model animal for epilepsy research.

Zebrafish are small, with the adults growing only to 3-4 cm in length and the larvae of approx. 3 mm in length. They mature quickly, reaching larval stage by 72 hpf, and sexual maturity in approx. 3 months. Until 120 hpf, the larvae do not require feeding. A pair of adult zebrafish can generate 50-200 embryos every week, and the aquatic system allows for relatively straightforward and cheap maintenance of colonies (Bradford et al., 2017; Hortopan et al., 2010). Zebrafish develop externally, which is a major advantage over mammalian models, particularly when studying the earliest stages of development, and allows easy observation of living embryos. This is especially advantageous in studying conditions such as TSC, in which the pathogenesis starts during fetal development. Homozygous *TSC1* or *TSC2* rodent knockouts are lethal during embryonic development (Kobayashi et al., 2001; Onda et al., 1999). Similarly, the TSC fish die around 11 dpf, but their *ex-utero* development allows for observation of alive larvae up to that point. The developing zebrafish are transparent, which makes them highly convenient for microscopic analysis, including imaging of neuronal activity (Khan et al., 2017). The small size of zebrafish can also be a limitation for certain techniques. For example, deep brain stimulation therapies are practically impossible to carry out in larval zebrafish (Cho et al., 2017).

While small and easily accessible, the zebrafish brain is sufficiently complex, containing approximately 100,000 neurons at 7 dpf. It displays the anatomical divisions typical for vertebrates, with high functional homology to mammalian counterparts (Panula et al., 2010). All the major adult brain subdivisions are present in larvae. The zebrafish telencephalon is everted (with the ventricular region located externally), while in mammals it forms by invagination. Due to such major differences in mechanism of neurodevelopment, the homologous brain regions are located differently than in mammalian brain. However, many brain regions are still present in zebrafish (Hortopan et al., 2010). Apart from the overall architecture, the zebrafish and mammalian brains share similar cellular morphology, as well as key neurotransmitters, receptors, and transporters with comparable spatial and temporal distribution (Panula et al., 2010). Cell types responsible for the generation of excitatory discharges within a network, such as excitatory or inhibitory neurons, are present in both adult and immature zebrafish (Hortopan et al., 2010). Because the zebrafish brain is smaller, containing less neurons, some structures of the human brain do not have a direct zebrafish homologous region, however, their functions are shared by selected groups of specialized neurons (Khan et al., 2017). Nonetheless, zebrafish do lack major portion of the human cortex, which is considered a limiting factor in some studies, especially those concerning higher cognitive functions (Parker et al., 2013).

The high fecundity, ease of maintenance, and external development of zebrafish makes them more suitable for high-throughput drug screening than rodents (Bradford et al., 2017). 70% of epileptic patients develop the symptoms during childhood, therefore, screenings of anti-epileptic compounds should be performed using immature animals. Neonatal rodents are increasingly being used (Auvin et al., 2012; Galanopoulou & Moshé, 2015), but the ease of treating and observing zebrafish during early development is their obvious advantage. Drugs can be administered to fish in the bathing medium, which is much more efficient than injections, ensures equalized exposure and simultaneous treatment of multiple cohorts of fish.

Zebrafish are highly amenable to genetic manipulation using genome engineering methods based on MOs, RNA interference, synthetic mRNA injection, expression plasmid injection, or genome editing technologies such as zinc finger nucleases (ZFNs), transcription activator-like effector

nucleases (TALENs), and clustered regularly interspaced short palindromic repeats (CRISPR). Such techniques are often easier, cheaper, and faster to perform on zebrafish than on other laboratory animals (Koster and Sassen, 2015). Around 70% of human genes have corresponding zebrafish orthologs. Zebrafish are teleosts, which underwent a whole genome duplication in the Devonian period. Some of these duplicated genes are redundant, while others have acquired new functions, making molecular studies of disease pathomechanisms more complicated. Nevertheless, zebrafish mutants displayed similar neurological phenotype to patients with epilepsy, serving as useful models of pediatric epilepsy.

4. Other Model Systems

Seizures in zebrafish can be induced chemically, by genetic mutation, or by other methods. In this section, we briefly describe various zebrafish models of epilepsy.

4.1. Chemically induced epilepsy models in zebrafish

Chemically induced seizures in zebrafish at all ages cause similar behavioral response characterized by erratic whirlpool-like swimming, convulsive swimming, and eventually loss of posture or death during long exposition to a proconvulsive drug (Afrikanova et al., 2013). To model epilepsy in zebrafish, fish are exposed to different concentrations of a drug usually added to water or administered via injection into the yolk sac at the embryonic or larval stages or intraperitoneally in adults.

One of the first drugs used to induce epileptic seizures was PTZ (Baraban et al., 2005). Zebrafish larvae treated with PTZ display behavioral, electrophysiological, and molecular alterations which are observed from few seconds to minutes after PTZ administration (Afrikanova et al., 2013). PTZ was shown to induce convulsive effects in concentration range 2.5-20 mM (Winter et al., 2008).

Other drugs used to induce epilepsy in zebrafish are (concentration ranges for larvae in brackets): kainic acid (KA; 50-500 μM), (D, L)-allylglycine (AG; 50-300 mM), linopirdine (25-200 μM), XE991 (25-200 μM), ginkgotoxin (0.2-1 mM), picrotoxin (0.3-60 mM), caffeine (0.04 mg/L), 1,3,5-trinitroperhydro-1,3,5-triazine (RDX; 0.1-1 mM), etc. (Table1). All these drugs induce electrophysiological and behavioral response. However, lower doses cause less severe and higher doses cause more severe manifestations, e.g., high doses of KA decreased locomotion of zebrafish larvae being attributed to a loss of posture (Menezes et al., 2014). The timing of behavioral response also varies between different drugs. In larval zebrafish, PTZ induced seizures after minutes or seconds, while AG or ginkgotoxin after approx. 2 hours (Baraban et al., 2005; Chege et al., 2012; Lee et al., 2012).

4.2. Genetic Epilepsy Models in zebrafish

Genetic mutations account for approx. 1-2% of diseases which manifest with epilepsy. These mutations are often localized to genes encoding for neuronal ion channels and receptors, or γ-aminobutyric acid pathway components, leading to abnormal neuronal activity and seizures (Devinsky et al., 2018). Genetic models of epilepsy are therefore useful to study pathomechanisms of epilepsy. The first genetic models of epilepsy in zebrafish were obtained using MOs (Nasevicius

and Ekker, 2000), however, nowadays CRISPR/Cas9 method is the most used to introduce stable gene knockouts in zebrafish.

One of the most common disease with childhood epilepsy is Dravet syndrome (DS) caused by mutations in *SCN1A* which encodes for a subunit of voltage-gated sodium channel NaV1.1. In zebrafish, multiple techniques were used to inactivate *scn1lab* encoding this protein: mutagenesis (Schoonheim et al., 2010), MO (Zhang et al., 2015), or CRISPR (Tiraboschi et al., 2020). All these models exhibited hyperactivity, seizures, loss of posture, and repetitive jerking. Moreover, *scn1lab* zebrafish mutants showed epileptiform brain activity by LFP recordings (Sourbron et al., 2017). Recently, single-cell transcriptome analysis of *scn1lab* mutant developed with CRISPR/Cas9 mutagenesis revealed loss of inhibitory neurons during early stages of development starting to unravel molecular mechanisms of epilepsy-like phenotypes (Tiraboschi et al., 2020).

Similarly, a zebrafish model of febrile seizures caused by *stx1b* mutations, model of generalized epilepsy generated by mutation in *gabra1a* gene, the model of pyridoxine-dependent epilepsy carrying mutation in *aldh7a1*, or another model of DS generated by *chd2* knockdown with MO exhibited motor seizures often with circular swimming, body convulsions, and loss of posture (Table1). Also, increased brain activity or epileptiform events seen by LFP recordings were observed in these models. However, these phenotypes developed in different stages ranging from 4 dpf to 10 dpf.

On the other hand, there are zebrafish models with non-motor seizures, e.g., *cacna1aa* knockdown, a model of absence seizures and episodic ataxia type 1 (Gawel et al., 2020). Knockdown of *cacna1aa* by MO decreased locomotor activity in zebrafish larvae. Together with epileptiform events present in the brains of *cacna1aa* morphants, this phenotype can be interpreted as non-motor seizures. Another example is *depdc5* mutant generated using CRISPR/Cas9 method to model DEPDC5-related epilepsy (Swaminathan et al., 2018). This gene encodes for one of proteins of the GATOR1 complex inhibiting the mTOR pathway. Homozygous *depdc5* mutants exhibited decreased locomotor activity and increased number of epileptiform events in the brain. Furthermore, they showed higher susceptibility to seizures after PTZ and hyperactivation of mTOR (Swaminathan et al., 2018), resembling the TSC fish phenotype molecularly, morphologically, and behaviorally.

As seen from examples above, the behavioral responses can differ among various zebrafish epilepsy models. It is therefore indispensable to measure brain activity by EEG, LFP, or calcium imaging for further validation of seizure presence.

4.3. Other epilepsy models in zebrafish

Post-traumatic epilepsy model in adult zebrafish has been developed by induction of traumatic brain injury with high-intensity ultrasound (Cho et al., 2020). Moreover, protocols for hyperthermia-induced seizures were generated to model febrile seizures (Hunt et al., 2012). Zebrafish is also commonly used to model fetal alcohol spectrum disorder, which is caused by alcohol uptake by a pregnant mother and often results in seizures in the infant (Fernandes et al., 2018).

5. Mini-Dictionary of Terms

Epileptogenesis: cellular and molecular mechanisms leading to development of spontaneous seizures and epilepsy.

GCaMP: genetically encoded calcium indicators which consists of three key domains: the calcium-binding protein calmodulin (CaM), a peptide sequence from myosin light-chain kinase that interacts with CaM (M13), and GFP. Neuronal activity causes fluctuations in intracellular free calcium, which in turn induces conformational changes in the CaM–M13, resulting in an increased fluorescent signal from GFP. This allows to monitor neuronal activity *in vivo* by microscopy.

Lightsheet microscopy: a microscopy technique based on optical sectioning using a sheet of light illuminating a region in the focal plane. Compared to confocal microscopy, lightsheet offers higher scanning speed, lower phototoxicity, and higher penetration. It also allows to obtain images from multiple angles by rotating the specimen around its axis, which makes it particularly suitable for imaging complex three-dimensional structures, such as zebrafish embryos and larvae.

Morpholino oligonucleotides (MOs): oligomers of morpholine bases which decrease expression through complementary binding to the RNA of interest. They effectively hinder transcript processing (via inhibition of the spliceosome assembly) and translation (by preventing ribosome assembly at translational start site).

PTZ (pentylenetetrazol): a $GABA_A$ antagonist used to trigger acute seizures in animal models of epilepsy, usually for the purpose of testing anticonvulsive drugs.

Stages of development: The stages of zebrafish development are defined by morphological changes of the embryo across hours (hpf) and days (dpf) post-fertilization. The standard timeline of zebrafish development is based on optimal conditions of incubation in 28.5°C without overcrowding. While embryos develop normally at the temperatures between 25°C and 33°C, this will respectively slow down or accelerate the development. It should also be noted that water heats or cools slower than air, and thus should be prepared at the right temperature for particularly sensitive experiments.

6. Key Facts on zebrafish:

- It is a small, freshwater fish from Bangladesh.
- It is transparent till 24 hpf and then mostly transparent till larval stage with few melanophores in the skin and eyes.
- Scientists can stop generation of melanophores in the skin and eyes by using phenylthiourea in the culturing water.
- One pair of adult zebrafish can give hundreds of eggs.
- When setting the breeders, scientists usually use two males and one female zebrafish to get as many fertilized embryos as possible.

- The culturing water for zebrafish embryos is called E3 (5 mM NaCl, 0.17 mM KCl, 0.33 mM CaCl2, 0.33 mM MgSO4).
- Zebrafish underwent genome duplication in the Devonian period.
- The zebrafish brain is sufficiently complex for neurodevelopmental studies.
- Zebrafish are also genetically similar to humans.

7. Summary Points

- Tuberous sclerosis complex (TSC) results from mutations in the *TSC1* or *TSC2* gene, causing their loss of function and hyperactivity of the mTOR pathway.
- The major clinical manifestations of TSC are epilepsy and benign tumors in multiple organs, as well as TSC-associated neuropsychiatric disorders. Seizures in TSC patients can be of various types.
- The homozygous $tsc2^{vu242/vu242}$ zebrafish are considered the TSC disease model. Those fish display disruptions and alterations in mTOR signaling, brain development, neuronal activity, and behavior – consistent with data from TSC patients.
- Brain activity in the TSC fish can be measured using genetically encoded calcium indicators, or by LFP or EEG recordings.
- Epileptogenesis can be studied in zebrafish on a behavioral level.
- Compared to rodent models, zebrafish are more suitable for high-throughput studies. Their external development also allows for easy observation of living embryos.
- Seizures in zebrafish can be induced chemically by a proconvulsive drug, genetic mutation, or other methods, e.g., severe head injury.

Compound /gene	seizure induction method	type of seizures	LFP/EEG	Behavioral characteristics	Possible mechanisms	Drugs that rescue epilepsy-like phenotype	Reference
PTZ	chemical	motor	ictal discharge frequency (2–7 Hz)	hyperactivity-like behaviors, circular movements, tonic-clonic-like seizures characterized by spasms and loss of posture	associate with GABAergic synaptic transmission	diazepam, valproic acid,	Afrikanova et al. 2013; Baraban et al. 2005
KA			short-lived (100-200 msec) and longer (4-5 sec) bursting EEG discharges on average 8 events/min.	clonic-like convulsions in higher doses	agonist of AMPA/KA glutamatergic receptors	6,7-dinitroquinoxaline-2,3-dione	Alfaro et al. 2011; Menezes et al. 2014
AG			16 events per 10-min. recording, lasting 700 msec on average	increase in locomotor activity, rapid whirlpool-like circling, clonic-like convulsions leading to a loss of posture	irreversible inhibition of glutamic acid decarboxylase (GAD)	diazepam, sodium valproate, topiramate	Leclercq et al. 2015
linopirdine and XE991			multi-spike burst discharge activity, 200 to 300 ms of duration	increased locomotor activity with fast whole-body twitch-like convulsions	inhibits neuronal K(v)7 channels (also termed KCNQ channels)	-	Chege et al. 2012
ginkgotoxin			-	hyperactive swimming pattern with short bursts of rapid jerking lasting up to a few seconds	interference with the B6 vitamin-dependent GABA synthesis in neurons	phenytoin, gabapentin and primidone	Lee et al. 2012
picrotoxin			-	reduced normal swimming, episodes of hyperactivity, occurrence of spasms, tonic-clonic seizures	GABAA receptor antagonist; induces expression of c-fos in the forebrain	sodium valproate	Wong et al. 2010
caffeine			-	hyperactivity, spasms and increased corkscrew and circular swimming	inhibits adenosine A1 and A2A receprotors	-	Wong et al. 2010
RDX			-	reduced exploration, increased freezing, bouts of hyperactivity, spasms, and corkscrew swimming	associate with GABAergic synaptic transmission	-	Williams et al. 2012
scn1laa	genetic	motor	interictal spikes and ictal epileptiform discharges	hyperactivity, convulsive seizure behavior, loss of posture, repetitive jerking	loss of function mutations of gene encoding for an α subunit sodium channel NaV1.1	valproate, diazepam, potassium bromide, stiripentol	Sourbron et al., 2017; Tiraboschi et al. 2020;
scn1lab			interictal spikes and polyspiking discharges 1−1.5 event/min. lasting 400 msec	sudden hyperactivity, myoclonic jerk sand tremor	loss of function mutations of gene encoding for an α subunit sodium channel NaV1.1	clobazam, stiripentol, topiramate, sodium	Zhang et al. 2015

						valproate	
kcnj10b			clusters of spikes/poly-spikes, frequency: 2−4 Hz	ataxia, renal tubulopathy, burst activity, spontaneous body contractions, loss of posture	loss of function mutations of gene encodes potassium channel Kir4.1	pentobarbitone	Mahmood et al. 2013; Zdebik et al. 2013
stx1b			polyspiking discharges below 80 Hz; high frequency oscillations (100−200 Hz frequency), 1.3 events/min., lasting 100 msec	increased orofacial (jaw) and pectoral fin movements, myoclonus-like jerks	encode plasma membrane synaptic protein Syntaxin-1B involded in exocytosis	-	Schubert et al. 2014
gabra1a			-	tonic-clonic-like seizures in light exposure	encode α1 subunit of GABAA	valproic acid, clonazepam, levetiracetam	Samarut et al. 2018
aldh7a1			high amplitude ictal and low amplitude interictal EEG discharges	hyperactivity, rapid circling swimming, body convulsions,	pyridoxine-dependent epilepsy, accumulation of lysine metabolites in central nervous system	-	Pena et al. 2017
chd2			multiple upward spikes with occasional ictal patterns	whirlpool-like events, pectoral fin and jaw twitching, whole-body trembling	loss of function of chromodomain helicase DNA-binding protein involved in chromatin remodelin, gene expression, DNA repair, cell cycle	-	Suls et al. 2013
cacna1aa		non-motor	abrupt spike-wave complexes, polyspike-wave discharges and high-voltage spikes	hypoactive in both the light and dark phases	loss of function in neurotransmitters relase by knock-down gene encode α1 subunit of P/Q calcium channel	ethosuximide, topiramate	Gawel et al. 2020
depdc5			increased number of epileptiform events in the brain comparing to sibling controls	decreased locomotor activity	hyperactivation of mTORC1	rapamycin	Swaminathan et al. 2018
stxbp1a and stxbp1b			spontaneous epileptic seizure events only in stxbp1b	decreased locomotion, decreased mobility, reduced heart rate and metabolism in stxbp1a	loss of function of SNARE complex	-	Grone et al. 2016
tsc2			approx. 4 seizures per 10 min. recording	decreased locomotion, increased anxiety, no light preference	aberrant migration of neuronal progenitors	rapamycin, ethosuximide, ANA-12	Kedra et al., 2020 Scheldeman et al., 2017

Table 1. Chemically induced and genetic zebrafish models used in epilepsy studies.

References

Afrikanova, T, Serruys, ASK, Buenafe, OEM, Clinckers, R, Smolders, I, de Witte, PAM, Crawford, AD, and Esguerra, CV (2013). Validation of the Zebrafish Pentylenetetrazol Seizure Model: Locomotor versus Electrographic Responses to Antiepileptic Drugs, *PLoS ONE*, *8*(1).

Ahrens, MB, Orger, MB, Robson, DN, Li, JM, and Keller, PJ (2013). Whole-brain functional imaging at cellular resolution using light-sheet microscopy. *Nature Methods*, *10*(5).

Akerboom, J, Chen, TW, Wardill, TJ, Tian, L, Marvin, JS, Mutlu, S, Calderon, NC, Esposti, F, Borghuis, BG, Sun, XR, Gordus, A, Orger, MB, Portugues, R, Engert, F, Macklin, JJ, Filosa, A, Aggarwal, A, Kerr, RA, Takagi, R, … Looger, LL (2012). Optimization of a GCaMP Calcium Indicator for Neural Activity Imaging. *Journal of Neuroscience*, *32*(40).

Alfaro, JM, Ripoll-Gómez, J, Burgos, JS (2011). Kainate administered to adult zebrafish causes seizures similar to those in rodent models. *European Journal of Neuroscience*, *33*(7).

Auvin, S, Pineda, E, Shin, D, Gressens, P, and Mazarati, A (2012). Novel Animal Models of Pediatric Epilepsy. *Neurotherapeutics*, *9*(2).

Baraban, SC, Taylor, MR, Castro, PA, and Baier, H (2005). Pentylenetetrazole induced changes in zebrafish behavior, neural activity and c-fos expression. *Neuroscience*, *131*(3).

Bradford, YM, Toro, S, Ramachandran, S, Ruzicka, L, Howe, DG, Eagle, A, Kalita, P, Martin, R, Taylor Moxon, SA, Schaper, K, and Westerfield, M (2017). Zebrafish Models of Human Disease: Gaining Insight into Human Disease at ZFIN. *ILAR Journal*, *58*(1).

Chege, SW, Hortopan, GA, Dinday, M, and Baraban, SC (2012). Expression and function of KCNQ channels in larval zebrafish. *Developmental Neurobiology*, *72*(2).

Cho, S, Park, E, Telliyan, T, Baker, A, & Reid, AY (2020). Zebrafish model of posttraumatic epilepsy. *Epilepsia*, *61*(8).

Cho, SJ, Byun, D, Nam, TS, Choi, SY, Lee, BG, Kim, MK, & Kim, S (2017). Zebrafish as an animal model in epilepsy studies with multichannel EEG recordings. *Scientific Reports*, *7*(1).

Crino, PB, Nathanson, KL, & Henske, EP (2006). The Tuberous Sclerosis Complex. *New England Journal of Medicine*, *355*(13).

de Oliveira, A, Brigante, T, & Oliveira, D (2021). Tail Coiling Assay in Zebrafish (Danio rerio) Embryos: Stage of Development, Promising Positive Control Candidates, and Selection of an Appropriate Organic Solvent for Screening of Developmental Neurotoxicity (DNT). *Water*, *13*(2).

Devinsky, O, Vezzani, A, O'Brien, TJ, Jette, N, Scheffer, IE, de Curtis, M, & Perucca, P (2018). Epilepsy. *Nature Reviews Disease Primers*, *4*(1).

Ess, KC (2006). The Neurobiology of Tuberous Sclerosis Complex. *Seminars in Pediatric Neurology*, *13*(1).

Fernandes, Y, Rampersad, M, Jones, EM, Eberhart, JK (2018). Social deficits following embryonic ethanol exposure arise in post-larval zebrafish. *Addiction Biology*, 24(5).

Galanopoulou, AS, & Moshé, SL (2015). Pathogenesis and new candidate treatments for infantile spasms and early life epileptic encephalopathies: A view from preclinical studies. *Neurobiology of Disease*, *79*.

Gawel, K, Turski, WA, van der Ent, W, Mathai, BJ, Kirstein-Smardzewska, KJ, Simonsen, A, and Esguerra, CV (2020). Phenotypic Characterization of Larval Zebrafish (Danio rerio) with Partial Knockdown of the cacna1a Gene. *Molecular Neurobiology*, *57*(4).

Grone, BP, Marchese, M, Hamling, KR, Kumar, MG, Krasniak, CS, Sicca, F, Santorelli, FM, Patel, M, Baraban, SC (2016). Epilepsy, Behavioral Abnormalities, and Physiological Comorbidities in Syntaxin-Binding Protein 1 (STXBP1) Mutant Zebrafish. *PLOS ONE*, *11*(3).

Hortopan, GA, Dinday, MT, Baraban, SC (2010). Zebrafish as a model for studying genetic aspects of epilepsy. *Disease Models & Mechanisms*, *3*(3–4).

Hunt, RF, Hortopan, GA, Gillespie, A, Baraban, SC (2012). A novel zebrafish model of hyperthermia-induced seizures reveals a role for TRPV4 channels and NMDA-type glutamate receptors. *Experimental Neurology*, *237*(1).

Kedra, M, Banasiak, K, Kisielewska, K, Wolinska-Niziol, L, Jaworski, J, Zmorzynska, J (2020). TrkB hyperactivity contributes to brain dysconnectivity, epileptogenesis, and anxiety in zebrafish model of Tuberous Sclerosis Complex. *Proceedings of the National Academy of Sciences*, *117*(4).

Khan, KM, Collier, AD, Meshalkina, DA, Kysil, E, Khatsko, SL, Kolesnikova, T, Morzherin, YY, Warnick, JE, Kalueff, A, Echevarria, DJ (2017). Zebrafish models in neuropsychopharmacology and CNS drug discovery. *British Journal of Pharmacology*, *174*(13).

Kim, SH, Speirs, CK, Solnica-Krezel, L, Ess, KC (2011). Zebrafish model of tuberous sclerosis complex reveals cell-autonomous and non-cell-autonomous functions of mutant tuberin. *Disease Models & Mechanisms*, *4*(2).

Kobayashi, T, Minowa, O, Sugitani, Y, Takai, S, Mitani, H, Kobayashi, E, Noda, T, Hino, O (2001). A germ-line Tsc1 mutation causes tumor development and embryonic lethality that are similar, but not identical to, those caused by Tsc2 mutation in mice. *Proceedings of the National Academy of Sciences*, *98*(15).

Koster, R, and Sassen, WA (2015). A molecular toolbox for genetic manipulation of zebrafish. *Advances in Genomics and Genetics*.

Kurnia, KA, Santoso, F, Sampurna, BP, Audira, G, Huang, JC, Chen, KHC, Hsiao, CD (2021). TCMacro: A Simple and Robust ImageJ-Based Method for Automated Measurement of Tail Coiling Activity in Zebrafish. *Biomolecules*, *11*(8).

Leclercq, K, Afrikanova, T, Langlois, M, de Prins, A, Buenafe, OE, Rospo, CC, van Eeckhaut, A, de Witte, PAM, Crawford, AD, Smolders, I, Esguerra, CV, Kaminski, RM (2015). Cross-species pharmacological characterization of the allylglycine seizure model in mice and larval zebrafish. *Epilepsy & Behavior*, *45*.

Lee, GH, Sung, SY, Chang, WN, Kao, TT, Du, HC, Hsiao, TH, Safo, MK, Fu, TF (2012). Ginkgotoxin exposed zebrafish larvae exhibit seizure-like behavior that is relieved by pyridoxal-5'-phosphate, GABA and anti-epileptic drugs. *Disease Models & Mechanisms*.

Lin, MZ, and Schnitzer, MJ (2016). Genetically encoded indicators of neuronal activity. *Nature Neuroscience*, *19*(9).

Mahmood, F, Mozere, M, Zdebik, AA, Stanescu, HC, Tobin, J, Beales, PL, Kleta, R, Bockenhauer, D, Russell, C (2013). Generation and validation of a zebrafish model of EAST (Epilepsy, ataxia, sensorineural deafness and tubulopathy) syndrome. *Disease Models & Mechanisms*, *6*(3).

Menezes, FP, Rico, EP, da Silva, RS (2014). Tolerance to seizure induced by kainic acid is produced in a specific period of zebrafish development. *Progress in Neuro-Psychopharmacology and Biological Psychiatry*, *55*.

Nasevicius, A, and Ekker, SC (2000). Effective targeted gene 'knockdown' in zebrafish. *Nature Genetics*, *26*(2).

Onda, H, Lueck, A, Marks, PW, Warren, HB, Kwiatkowski, DJ (1999). Tsc2+/– mice develop tumors in multiple sites that express gelsolin and are influenced by genetic background. *Journal of Clinical Investigation*, *104*(6).

Panula, P, Chen, YC, Priyadarshini, M, Kudo, H, Semenova, S, Sundvik, M, Sallinen, V (2010). The comparative neuroanatomy and neurochemistry of zebrafish CNS systems of relevance to human neuropsychiatric diseases. *Neurobiology of Disease*, *40*(1).

Parker, MO, Brock, AJ, Walton, RT, Brennan, CH (2013). The role of zebrafish (Danio rerio) in dissecting the genetics and neural circuits of executive function. *Frontiers in Neural Circuits*, *7*.

Pena, IA, Roussel, Y, Daniel, K, Mongeon, K, Johnstone, D, Weinschutz Mendes, H, Bosma, M, Saxena, V, Lepage, N, Chakraborty, P, Dyment, DA, van Karnebeek, CDM, Verhoeven-Duif, N, Bui, TV, Boycott, KM, Ekker, M, MacKenzie, A (2017). Pyridoxine-Dependent Epilepsy in Zebrafish Caused by Aldh7a1 Deficiency. *Genetics*, *207*(4).

Prentzell, MT, Rehbein, U, Cadena Sandoval, M, de Meulemeester, A, Baumeister, R, Brohée, L, Berdel, B, Bockwoldt, M, Carroll, B, Chowdhury, SR, von Deimling, A, Demetriades, C, Figlia, G, de Araujo, MEG, Heberle, AM, Heiland, I, Holzwarth, B, Huber, LA, Jaworski, J, … Thedieck, K (2021). G3BPs tether the TSC complex to lysosomes and suppress mTORC1 signaling. *Cell*, *184*(3).

Ruppe, V, Dilsiz, P, Reiss, CS, Carlson, C, Devinsky, O, Zagzag, D, Weiner, HL, Talos, DM (2014). Developmental brain abnormalities in tuberous sclerosis complex: A comparative tissue analysis of cortical tubers and perituberal cortex. *Epilepsia*, *55*(4).

Salussolia, CL, Klonowska, K, Kwiatkowski, DJ, Sahin, M (2019). Genetic Etiologies, Diagnosis, and Treatment of Tuberous Sclerosis Complex. *Annual Review of Genomics and Human Genetics*, *20*(1).

Samarut, É, Swaminathan, A, Riché, R, Liao, M, Hassan-Abdi, R, Renault, S, Allard, M, Dufour, L, Cossette, P, Soussi-Yanicostas, N, & Drapeau, P (2018). γ-Aminobutyric acid receptor alpha 1 subunit loss of function causes genetic generalized epilepsy by impairing inhibitory network neurodevelopment. *Epilepsia*, *59*(11).

Scheldeman, C, Mills, JD, Siekierska, A, Serra, I, Copmans, D, Iyer, AM, Whalley, BJ, Maes, J, Jansen, AC, Lagae, L, Aronica, E, de Witte, PAM (2017). mTOR-related neuropathology in mutant tsc2 zebrafish: Phenotypic, transcriptomic and pharmacological analysis. *Neurobiology of Disease*, *108*.

Schoonheim, PJ, Arrenberg, AB, del Bene, F, Baier, H (2010). Optogenetic Localization and Genetic Perturbation of Saccade-Generating Neurons in Zebrafish. *Journal of Neuroscience*, *30*(20).

Schubert, J, Siekierska, A, Langlois, M, May, P, Huneau, C, Becker, F, Muhle, H, Suls, A, Lemke, JR, de Kovel, CGF, Thiele, H, Konrad, K, Kawalia, A, Toliat, MR, Sander, T, Rüschendorf, F, Caliebe, A, Nagel, I, Kohl, B, … Lerche, H (2014). Mutations in STX1B, encoding a presynaptic protein, cause fever-associated epilepsy syndromes. *Nature Genetics*, *46*(12).

Sourbron, J, Smolders, I, de Witte, P, Lagae, L (2017). Pharmacological Analysis of the Anti-epileptic Mechanisms of Fenfluramine in scn1a Mutant Zebrafish. *Frontiers in Pharmacology*, *8*.

Specchio, N, and Pietrafusa, N (2020). New‐onset refractory status epilepticus and febrile infection‐related epilepsy syndrome. *Developmental Medicine & Child Neurology*, *62*(8).

Staley, K (2015). Molecular mechanisms of epilepsy. *Nature Neuroscience*, *18*(3).

Streisinger, G, Walker, C, Dower, N, Knauber, D, Singer, F (1981). Production of clones of homozygous diploid zebra fish (Brachydanio rerio). *Nature*, *291*(5813).

Suls, A, Jaehn, J A., Kecskés, A, Weber, Y, Weckhuysen, S, Craiu, DC, Siekierska, A, Djémié, T, Afrikanova, T, Gormley, P, von Spiczak, S, Kluger, G, Iliescu, CM, Talvik, T, Talvik, I, Meral, C, Caglayan, HS, Giraldez, BG, Serratosa, J, … Ivanović, V (2013). De Novo Loss-of-Function Mutations in CHD2 Cause a Fever-Sensitive Myoclonic Epileptic Encephalopathy Sharing Features with Dravet Syndrome. *The American Journal of Human Genetics*, *93*(5).

Swaminathan, A, Hassan-Abdi, R, Renault, S, Siekierska, A, Riché, R, Liao, M, de Witte, PAM, Yanicostas, C, Soussi-Yanicostas, N, Drapeau, P, Samarut, É (2018). Non-canonical

mTOR-Independent Role of DEPDC5 in Regulating GABAergic Network Development. *Current Biology*, *28*(12).

Switon, K, Kotulska, K, Janusz-Kaminska, A, Zmorzynska, J, Jaworski, J (2017). Molecular neurobiology of mTOR. *Neuroscience*, *341*.

Tiraboschi, E, Martina, S, Ent, W, Grzyb, K, Gawel, K, Cordero‐Maldonado, ML, Poovathingal, SK, Heintz, S, Satheesh, SV, Brattespe, J, Xu, J, Suster, M, Skupin, A, Esguerra, CV (2020). New insights into the early mechanisms of epileptogenesis in a zebrafish model of Dravet syndrome. *Epilepsia*, *61*(3).

Wager, K, Zdebik, AA, Fu, S, Cooper, JD, Harvey, RJ, Russell, C (2016). Neurodegeneration and Epilepsy in a Zebrafish Model of CLN3 Disease (Batten Disease). *Plos ONE*, *11*(6).

Weiss, SA, Banks, GP, McKhann, GM, Goodman, RR, Emerson, RG, Trevelyan, AJ, Schevon, CA (2013). Ictal high frequency oscillations distinguish two types of seizure territories in humans. *Brain*, *136*(12).

Winter, MJ, Redfern, WS, Hayfield, AJ, Owen, SF, Valentin, J, Hutchinson, TH (2008). Validation of a larval zebrafish locomotor assay for assessing the seizure liability of early-stage development drugs. *Journal of Pharmacological & Toxicological Methods*, 57(3).

Williams, LR, Wong, K, Stewart, A, Suciu, C, Gaikwad, S, Wu, N, DiLeo, J, Grossman, L, Cachat, J, Hart, P, Kalueff, A (2012). Behavioral and physiological effects of RDX on adult zebrafish. *Comparative Biochemistry and Physiology Part C: Toxicology & Pharmacology*, *155*(1).

Wong, K, Stewart, A, Gilder, T, Wu, N, Frank, K, Gaikwad, S, Suciu, C, DiLeo, J, Utterback, E, Chang, K, Grossman, L, Cachat, J, Kalueff, A (2010). Modeling seizure-related behavioral and endocrine phenotypes in adult zebrafish. *Brain Research*, *1348*.

Yaksi, E, Jamali, A, Diaz Verdugo, C, Jurisch‐Yaksi, N (2021). Past, present and future of zebrafish in epilepsy research. *The FEBS Journal*.

Zdebik, AA, Mahmood, F, Stanescu, HC, Kleta, R, Bockenhauer, D, Russell, C (2013). Epilepsy in kcnj10 Morphant Zebrafish Assessed with a Novel Method for Long-Term EEG Recordings. *PLoS ONE*, *8*(11).

Zhang, Y, Kecskés, A, Copmans, D, Langlois, M, Crawford, AD, Ceulemans, B, Lagae, L, de Witte, PAM, Esguerra, CV (2015). Pharmacological Characterization of an Antisense Knockdown Zebrafish Model of Dravet Syndrome: Inhibition of Epileptic Seizures by the Serotonin Agonist Fenfluramine. *PLOS ONE*, *10*(5).

Chapter 4. Diving into the zebrafish brain: exploring neuroscience frontiers with genetic tools, imaging techniques, and behavioral insights

O. Doszyn[¥], T. Dulski[¥], J. Zmorzynska*

[¥] equal contribution and first authorship

*corresponding author

Frontiers in Molecular Neuroscience, 2024 Mar 12; 17:1358844.

DOI: 10.3389/fnmol.2024.1358844.

Abstract

The zebrafish (*Danio rerio*) is increasingly used in neuroscience research. Zebrafish are relatively easy to maintain, and their high fecundity makes them suitable for high-throughput experiments. Their small, transparent embryos and larvae allow for easy microscopic imaging of the developing brain. Zebrafish also share a high degree of genetic similarity with humans, and are amenable to genetic manipulation techniques, such as gene knockdown, knockout, or knock-in, which allows researchers to study the role of specific genes relevant to human brain development, function, and disease. Zebrafish can also serve as a model for behavioral studies, including locomotion, learning, and social interactions. In this review, we present state-of-the-art methods to study the brain function in zebrafish, including genetic tools for labeling single neurons and neuronal circuits, live imaging of neural activity, synaptic dynamics and protein interactions in the zebrafish brain, optogenetic manipulation, and the use of virtual reality technology for behavioral testing. We highlight the potential of zebrafish for neuroscience research, especially regarding brain development, neuronal circuits, and genetic-based disorders and discuss its certain limitations as a model.

Keywords

modern methods for neuroscience, brain development, genetic tools, behavioral studies, optogenetics, brain imaging, virtual reality, zebrafish.

1. Introduction

Since early work in the 1980s (Streisinger *et al*., 1981), the zebrafish (*Danio rerio*) has been increasingly used as a model organism. Although the zebrafish is a relatively new model organism for complex brain diseases, it is of great interest to scientists for a comprehensive analysis of the processes involved in the development and regeneration of the nervous system, as evidenced by the increasing number of publications using this model each year (Fig1).

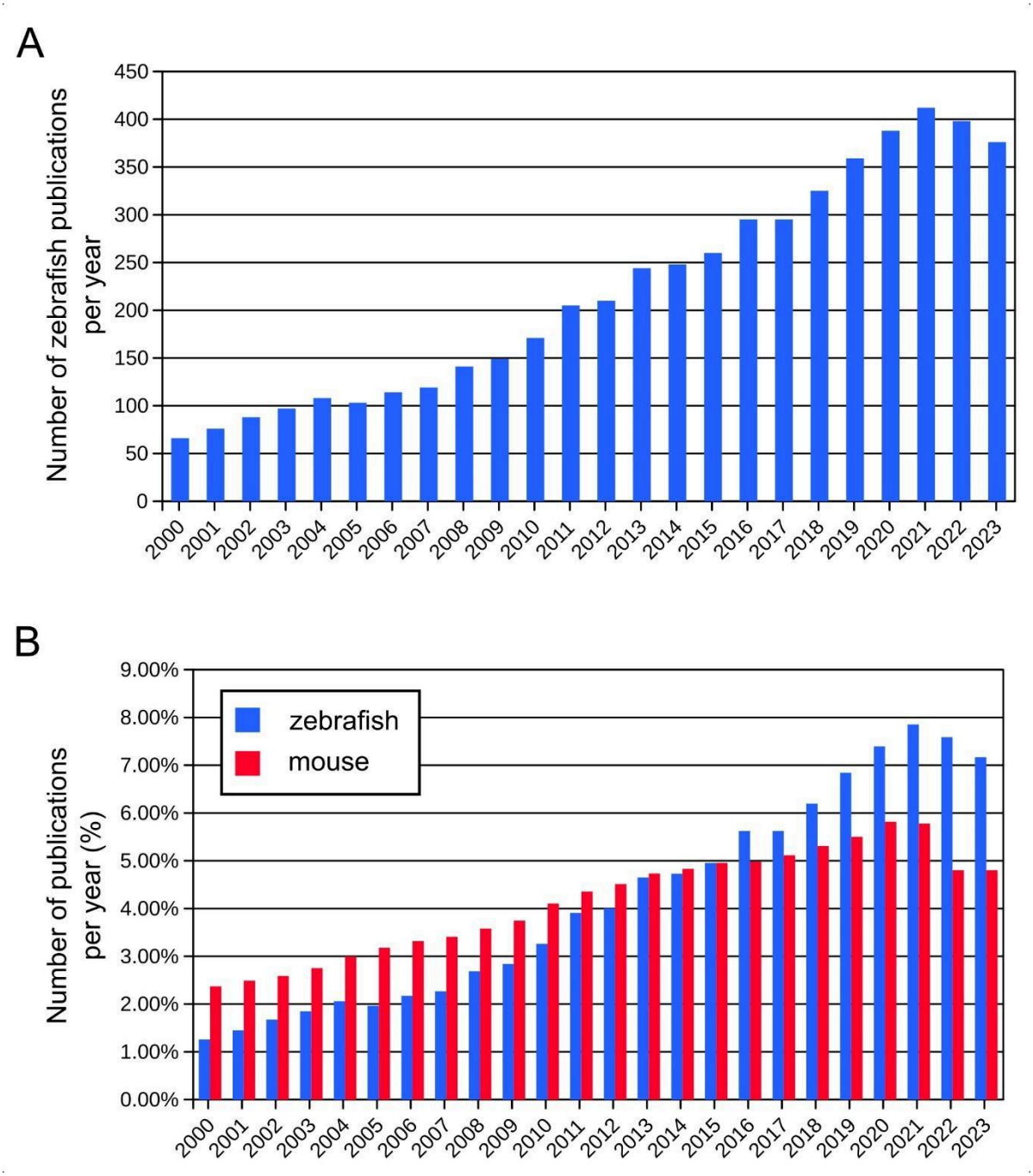

Figure 1. A. Number of publications per year using zebrafish since year 2000 (from Pubmed database). B. Comparison of relative numbers of publications per year using zebrafish and

mouse models showing dynamic growth of the zebrafish research.

The use of zebrafish in neuroscience research has several advantages. Zebrafish embryos and larvae are transparent, allowing researchers to easily visualize and study the development and function of the brain. This transparency, together with external development, makes it possible to observe the formation of neural circuits and the development of individual neurons in a living organism. Zebrafish share many genetic similarities with humans. The zebrafish genome and transcriptome have been sequenced revealing 70% sequence similarity between zebrafish and human (Howe *et al*., 2013; Shehwana & Konu, 2019). These features allow researchers to study fundamental processes in brain development and function that are relevant to humans (Hortopan *et al*., 2010; Panula *et al*., 2010). Also, zebrafish embryos develop quickly making them an ideal model for studying the early stages of brain development. Researchers can easily manipulate genetically and analyze the effects of genetic mutations or experimental treatments during this rapid developmental period. Zebrafish are amenable to gene knockdown, knockout, or knock-in, which allow researchers to investigate the roles of specific genes in brain development and function. These techniques – summarized in section 2 – have provided valuable insights into the genetic basis of brain-related disorders. Zebrafish exhibit a range of behaviors that can be investigated providing understanding into the neural basis of various behaviors, including locomotion, learning, and social interactions (Kalueff *et al*., 2014). Their behaviors can be assessed using automated tracking systems, making it easier to conduct high-throughput experiments. Advanced behavioral analyses, together with neuronal activity imaging techniques are described in section 3 of this review. Zebrafish are relatively easy and cost-effective to maintain in a laboratory setting, which makes them an attractive model organism. Overall, zebrafish have become a valuable tool in the field of brain research because of their unique combination of characteristics that allow researchers to analyze various aspects of brain development, function, and pathology. In this review, we describe highly advanced tools for studying the brain connectivity development, brain activity, and function using zebrafish as an animal model.

2. Methods to study development of the brain connectivity

2.1 Genetic tools for selective gene expression

Various genetic strategies are used to visualize neurons (Fig2). One of the common approaches in molecular and cell biology is the use of strategies that require the presence of two transgenes in the same cell to activate the expression of the fluorescent reporter gene. An example of this is the galactose transcription factor (Gal4) – upstream activating sequence (UAS) system that is widely used in zebrafish research (Halpern *et al*., 2008). In this system, two transgenic lines are used – one with Gal4 expression in a specific region or tissue and the other with expression of the gene of interest under the UAS, e.g., green fluorescent protein (GFP). Expression of Gal4 is restricted to a specific region or to a specific tissue because it is under the control of a specific promoter. This method allows researchers to achieve highly specific and controlled gene expression patterns that enable precise manipulation and analysis

of target cell populations (Fig2A). The Gal4-UAS system is a versatile and effective tool for exploring gene functionality, observing subcellular structures, labeling specific cells or tissues, or their selective removal.

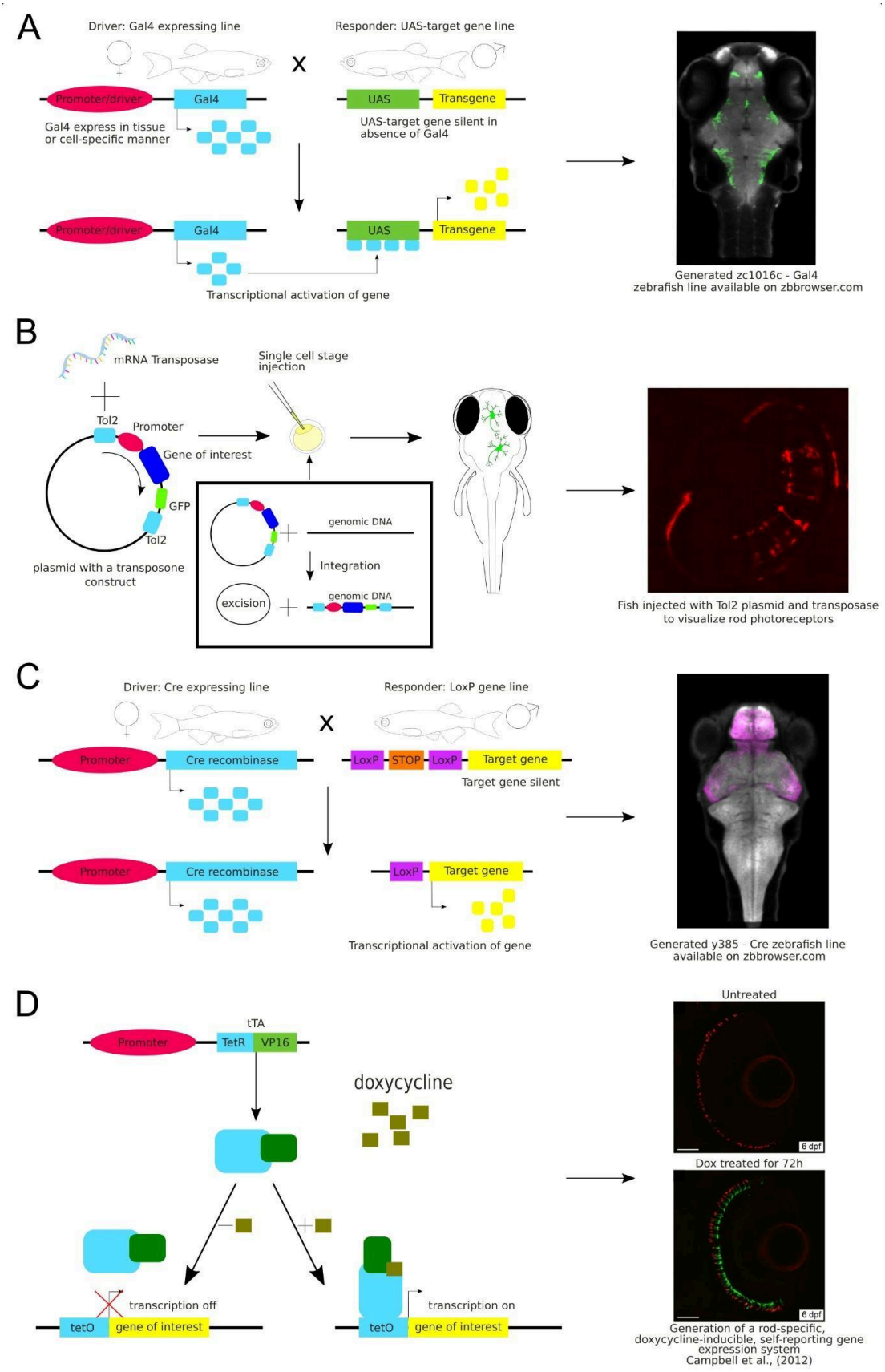

Figure 2. A. Schematic visualization and exemplary image of the use of the Gal4-UAS system. B. Schematic visualization and exemplary image of the use of the Tol2 system. C. Schematic visualization and exemplary image of the use of the Cre-loxP system. D. Schematic visualization and exemplary image of the use of the Tet-ON system.

Gal4 is a yeast transcription factor consisting of a DNA-binding domain and a transcription activation domain. It binds to UAS and activates transcription from the basal promoter placed downstream of UAS. The Gal4-UAS system was first used in zebrafish by Scheer and Campos-Ortega (Scheer & Campos-Ortega, 1999). They constructed a plasmid with the full-length yeast GAL4 gene. However, the expression of Gal4 was weak. Since then, the method has been continuously improved. To overcome the weak expression, Köster and Fraser have used Gal4-VP16, a fusion of the DNA-binding domain of Gal4 with the transcriptional activation domain of the VP16 protein from the herpes simplex virus, which has stronger transcriptional activity (Köster & Fraser, 2001). Another commonly used version of Gal4 is Gal4FF, a modified version of the Gal4 that has two activator segments of VP16 in addition to the DNA-binding domain of Gal4. Gal4FF has been shown to be better tolerated in vertebrate cells than Gal4-VP16 (Asakawa et al., 2008).

Another approach to achieve higher expression of the reporter gene was an insertion of a repeated UAS sequence in the transgene. However, Goll et al. found that the UAS sequence repeated 14 times was highly methylated, so expression of the reporter protein was silenced (Goll *et al.*, 2009). Silencing and methylation were lower for UAS repeats of 5 or 4. Fish lines containing such repeats have been shown to be reliable and reproducible over more than 15 generations (Kawakami *et al.*, 2016).

So far, many transgenic zebrafish lines expressing modified Gal4 in specific cells, organs, and tissues have been created. Several research labs have produced these Gal4 zebrafish lines in a high-throughput manner and organized them into collections available for the scientific community. These collections can be used in genetic and developmental biology research to study gene expression or manipulate gene function in a controlled and tissue-specific or temporal manner. Each Gal4 driver line in the collection is typically designed to express Gal4 in a specific tissue or cell type, e.g., Tg(chat:Gal4) expresses Gal4 in brain areas positive for choline acetyltransferase (ChAT) or Tg(gad1b:Gal4) with Gal4 expression in brain areas positive γ-aminobutyric acid (GABA) (Förster et al., 2017). This specificity of expression allows researchers to study development of these regions or to target them by genetic manipulations. It is important to highlight that recently the Zebrafish Brain Browser (ZBB) and its updated version, ZBB2 (Tabor et al., 2019), have become accessible online. These resources house images displaying the cellular expression patterns of various Gal4 collections, as well as transgenic lines that express fluorescent proteins in specific defined patterns (Marquart *et al.*, 2015). This platform is particularly valuable for investigating the functional mapping of neuronal circuits. These atlases have transformed research capabilities, enabling users to easily conduct 3D spatial searches and efficiently identify lines with reporter expression in regions of interest.

In making these zebrafish transgenic lines, scientists employed the Tol2 transposon transgenesis (Fig2B). The Tol2 system includes two key parts: a donor plasmid containing the gene of interest flanked by Tol2-transposon repeats (a Tol2 construct) and the Tol2 transposase (Kawakami, 2007). These two components are microinjected into fertilized eggs at the one-cell stage. The Tol2 construct is removed from the donor plasmid and incorporated into the genome during embryonic development. Consequently, these insertions are inherited by the subsequent fish generations. The latest generated vectors for Tol2-based transgenesis in zebrafish expand a selection of fluorescent protein choice, are coupled to Cre system or Gal4 system, and thus are adaptable for various applications. Integration of these vectors enhance the range of available tools for consistent, quality-controlled Tol2 transgenesis and gene-regulatory element testing in zebrafish and other model organisms (Kemmler *et al.*, 2023). By using the Tol2 system combined with the Gal4-UAS, Lal et al. identified a pallial amygdala in the zebrafish brain essential for fear conditioning suggesting that it is the mammalian functional equivalent. They also provided additional bricks in our understanding of the brain evolution and diversification of neuronal networks (Lal *et al.*, 2018).

The caveat of Tol2 transgenesis is that it uses transposon sites in the genome randomly and some of the insertions are not inherited through-out the generations. Lalonde et al. optimized targeted vector integration system in zebrafish, by converting well-established, validated, and inherited Tol2 sites into landing sites recognized by the phiC31 integrase (Lalonde *et al.*, 2023). They called it pIGLET, phiC31 Integrase Genomic Loci Engineered for Transgenesis. This system enables targeted insertion into a place in the zebrafish genome that is stable across generations, reducing the number of animals needed for generation of transgenic lines.

Another approach to target specific neurons is the Cre-lox system, a genetic recombination system that can be used to manipulate gene expression in a cell-specific manner (Fig2C). This system is widely used in mouse models. It also uses two transgenic lines: one that expresses the Cre recombinase enzyme in a specific subset of neurons, and another that contains a gene of interest flanked by loxP sites. When these two lines are crossed, the Cre enzyme binds to the loxP sites and e.g. excises the gene of interest resulting in a cell-specific knockout (Lin et al., 2013). Both systems, Gal4-UAS and Cre-lox, have successfully been used in zebrafish (Förster *et al.*, 2017; Tabor *et al.*, 2018), making this a promising strategy to achieve targeted reporter expression in neurons.

Another approach worth mentioning is the Tet-On system, an inducible gene expression system that uses tetracycline (Tet) or doxycycline (Dox) to timely control the activation of transgene expression (Fig2D). This system has been successfully used in mammals and zebrafish (Bockamp *et al.*, 2008; Knopf *et al.*, 2010; Ma *et al.*, 2017). Campbell *et al.* employed the Tet-On system to induce gene expression in rod photoreceptors. This proof-of-concept research shed light on the timed development and migration of these cells within the growing retina (Campbell *et al.*, 2012).

2.2 Tools to study single neurons within the brain and neuronal morphology development

Photoconvertible and photoactivatable fluorescent proteins are widely used to study neuronal morphology, especially projecting axons and neuronal connectivity, as they allow timed visualization of single neurons within a neuronal population (Fig3A). Photoconvertible proteins are a class of fluorescent proteins that change their emission wavelengths and thus can be activated in response to specific wavelengths of light (Chow & Vermot, 2017). They are widely used in biological research, particularly to visualize and track specific structures by fluorescence microscopy. Once activated, most photoactivatable proteins cannot be easily deactivated. On the other hand, the photoconvertible proteins emit fluorescence in one spectrum and undergo irreversible conversion to other fluorescence spectrum when exposed to violet or ultraviolet (UV) light. The first photoconvertible fluorescent protein was Kaede, and it was produced by accident. Kaede initially emits green fluorescence. When exposed to violet or UV light (350-400 nm), it undergoes irreversible conversion into a red light-emitting fluorophore (Ando *et al*., 2002). The use of the Kaede protein provides possibility to distinguish individual neurons from each other in the living zebrafish. In the study by Sato *et al*., a transgenic line *Tg(HuC:Kaede)* expressed Kaede in neurons under the neuron-specific HuC promoter and the photoconversion of Kaede enabled the labeling of a single neuron within the tectum to study development of dendritic arborization in time (Sato *et al*., 2006).

Examples of well-known photoactivatable and photoconvertible proteins include Photoactivatable Green Fluorescent Protein (PA-GFP), Dendra2, or mEos. PA-GFP is a non-fluorescent variant of GFP that can be activated by UV light and then it emits green fluorescence (Patterson & Lippincott-Schwartz, 2002). Similarly to Kaede, Dendra2 is a photoconvertible fluorescent protein converting from green to red. Dendra2 can also be photoconverted by initially exposing the protein to blue light and subsequently to near-infrared light, so called “primed conversion” (Mohr *et al*., 2016). mEos is another photoconvertible protein that transitions from green to red fluorescence when illuminated with UV light. Another fluorescent protein discovered both with photoconvertible and photoactivatable properties is Dronpa. The interesting feature of this protein allows its fluorescence to be deactivated with blue light and reactivated with violet light (Habuchi *et al*., 2005). Aramaki and Hatta used Dronpa in zebrafish to visualize the development of axonal arborizations of single spinal neurons during time-lapse imaging. They photoconverted Dronpa in soma to anterogradely label the axonal terminus of a single neurons or in the axon to retrogradely label somas which the axons belong to (Aramaki & Hatta, 2006). This approach enabled to map intertwined neuronal circuitries. Along with the years, new fluorescent proteins were discovered, such as PSmOrange, with red-shifted excitation and emission wavelengths (Subach *et al*., 2011). Using the PSmOrange photoconversion within GFP transgenic background, Beretta *et al*. explored the neural circuit development of the ventral habenula by employing 2-photon microscopy time-lapse imaging. Their investigation yielded compelling evidence of the thalamic-epithalamic origin of the ventral habenula neurons (Beretta *et al*., 2013).

2.3 Remodeling of neuronal connectivity using laser ablation

One of the innovative methods used to study plasticity of neuronal connectivity in the brain is laser ablation of neuronal cells (Fig3B). It may be also employed to study the role of a subpopulation of neurons in behavior (Muto & Kawakami, 2018) or to study single neurons connectivity development within a circuit (Hiyoshi *et al*., 2021). Laser ablation can be performed using a two-photon laser microscope and is especially well-suited for disrupting the activity of a limited number of specific neurons. Expression of fluorescent proteins in the specific population of neurons allows for the ablation of these neurons at desirable locations and timing at a high spatial resolution (single-cell level). Hiyoshi *et al*. used two-photon laser ablation of the inferior olive combined with long-term live imaging of the whole brain and showed structural remodeling of the olivo-cerebellar circuit at a single-cell resolution. Irreversible ablation of neurons caused severe damage in the inferior olive and enabled live observation of remodeling of the circuit (Hiyoshi *et al*., 2021).

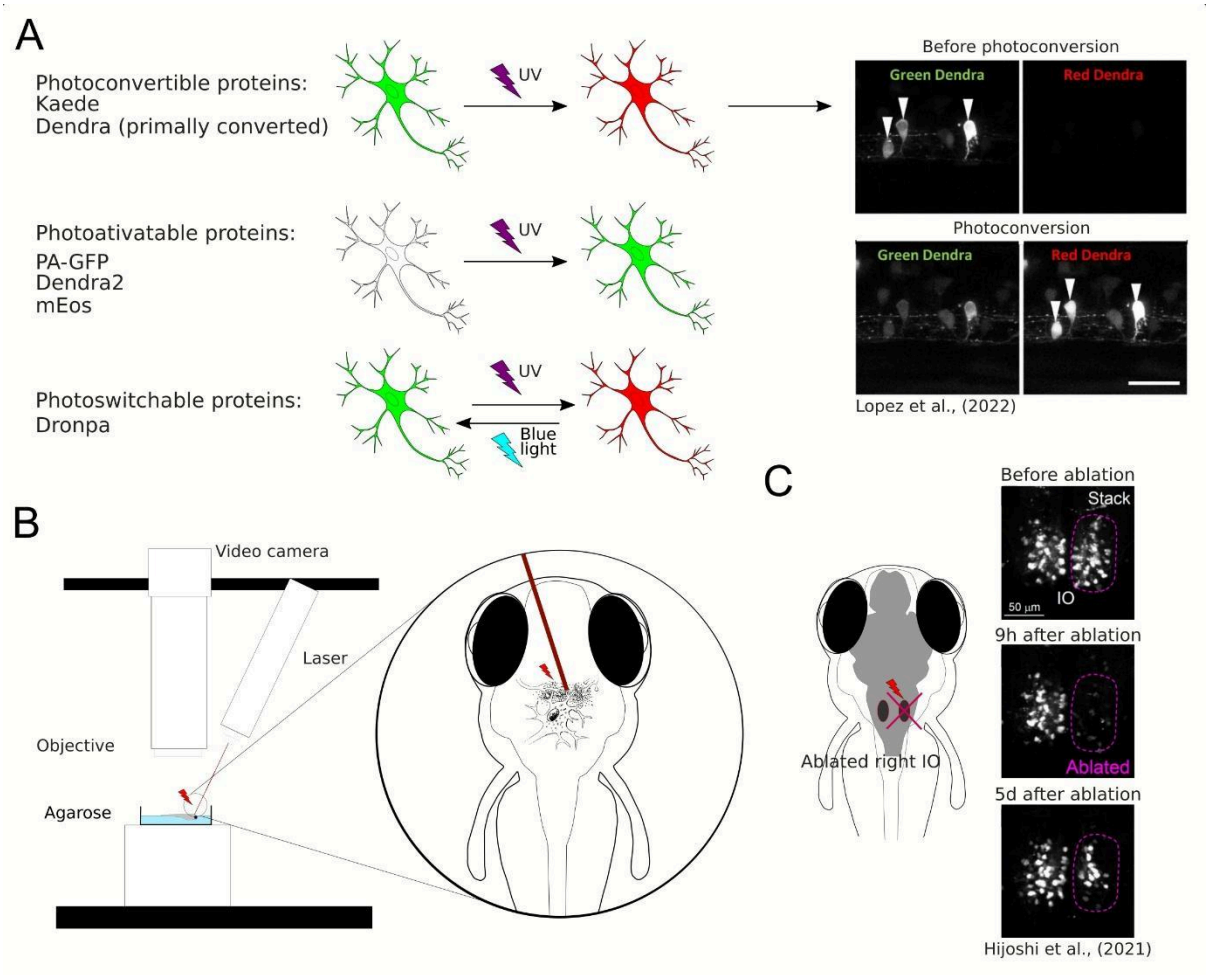

Figure 3. A. Schematic visualization and exemplary image of the use of photoconvertible and photoactivatable proteins. B. Schematic visualization and exemplary image of the use of the laser ablation method.

2.4 Tools to investigate synapse maturation live and neuronal connectivity mapping

Zebrafish have become a valuable model organism for studying synaptic structure and function. They offer several advantages for investigating synapses and neuronal connectivity mapping, including their optical transparency, rapid development, and genetic flexibility. One of the modern ways for visualizing synapses in living zebrafish larvae is the use of specialized approach such as FingRs to fluorescently label specific synaptic components. The transTANGO approach in turn, by labeling synaptically connected cells, is used to track synaptic connections. These labels can be introduced through genetic modification in a stable manner (transgenic zebrafish lines as in section 2.1) or by microinjection of plasmids encoding these components. Then, the observation of synaptic dynamics in real time can be done using time-lapse imaging including synaptic plasticity and the formation and elimination of synapses during development or pathology.

FingRs, the fibronectin intrabodies generated by mRNA, are antibody-like proteins fused to fluorescent proteins that target endogenous synaptic proteins (Fig4) (Son *et al*., 2016). FingRs can be used to visualize proteins in living cells without compromising structure and function of synaptic components (Gross *et al*., 2013). They offer a significant advance over the conventional immunofluorescence technique, which requires cell fixation and permeabilization. Additionally, expression of FingRs is regulated by a transcriptional feedback system that utilizes a zinc-finger DNA binding domain that matches the expression level of its endogenous target (Gross *et al*., 2013). Thus, FingRs can be used to comprehensively map the locations, numbers, and size of synaptic connections onto specific neurons in the developing intact brain.

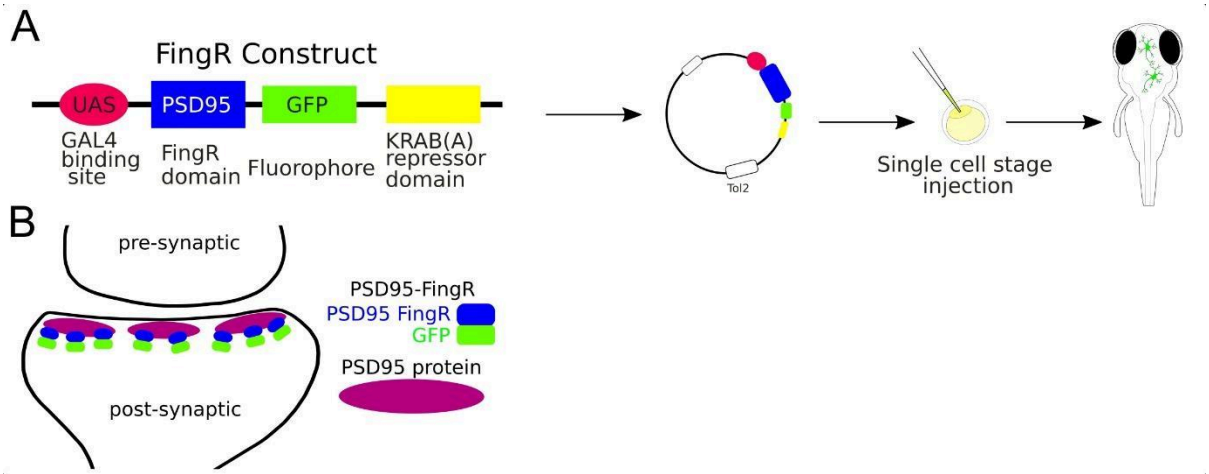

Figure 4. A. Schematic visualization of the use of the FingRs. B. FingR-PSD95 binds endogenous PSD-95 protein at the postsynaptic density.

FingRs have been used in zebrafish to target such proteins as postsynaptic density protein 95

(PSD-95), which is localized to the excitatory synapses, or Gephyrin (GPHN), which is a component of the postsynaptic protein network of inhibitory synapses. The PSD-95 is known to interact with synaptic receptors and have been well established as a marker for the size and location of postsynaptic densities of glutamatergic synapses (Dakoji *et al*., 2003). Thus FingRs targeting PSD-95 allow to precisely map the excitatory synapses in terms of their sizes and locations in the living animal. Son *et al*. have shown that FingRs for GPHN identified sites where GABA can be uncaged in close proximity to inhibitory synapses, providing an approach for investigating inhibitory circuitry. Furthermore, the amount of GPHN at postsynaptic inhibitory sites correlated with GABA or Glycine receptors (Son *et al*., 2016).

The trans-Tango method is a powerful and innovative technique used in neuroscience to delineate the synaptic connections between neurons in the brain (Fig5).

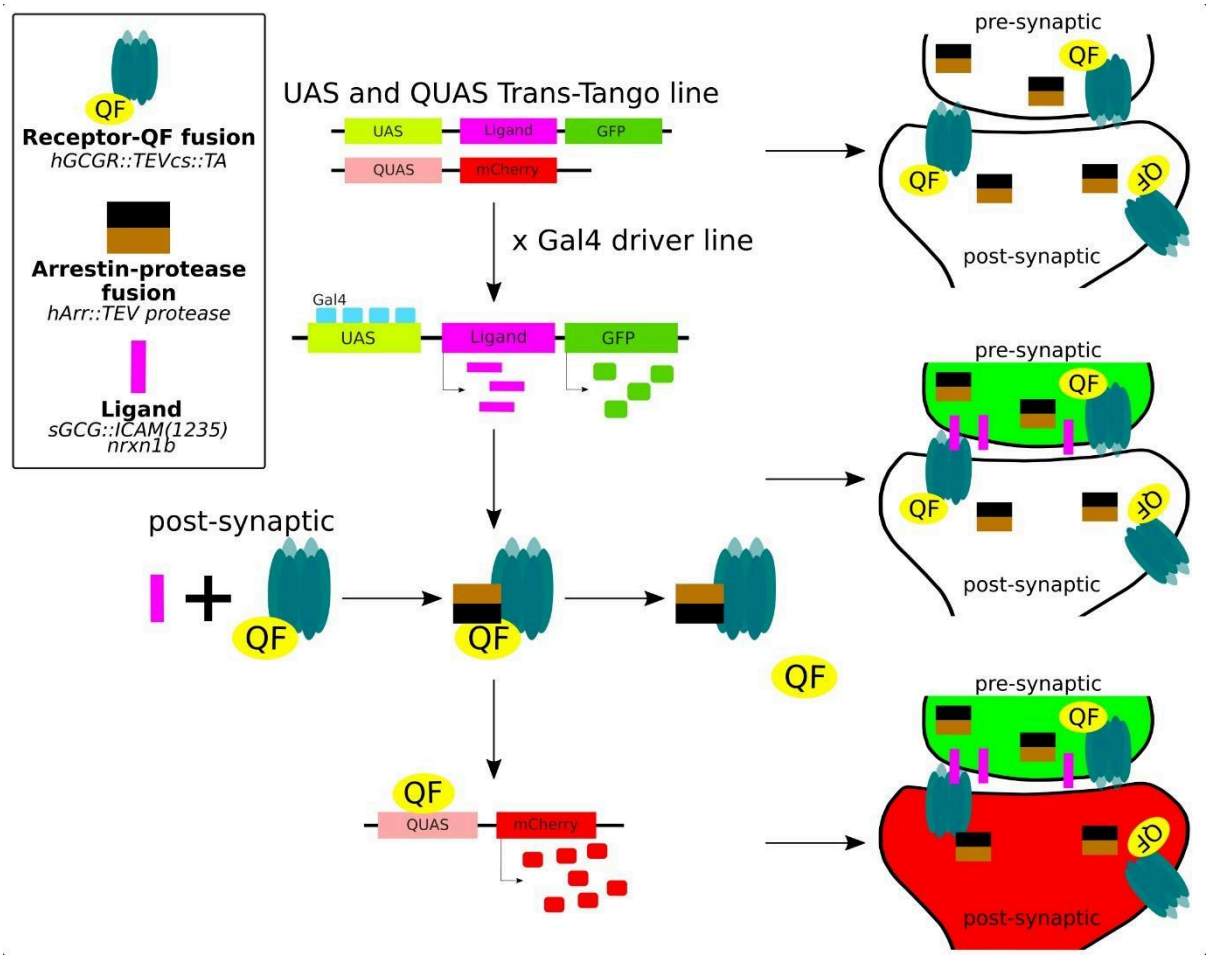

Figure 5. Trans-Tango method for live trans-synaptic tracing in zebrafish.

It is a variant of a method of identification of cells that are connected by a synapse with a specific "bait" neurons, called Tango (Barnea et al., 2008). The trans-Tango method was originally developed for anterograde trans-synaptic tracing in the *Drosophilla melanogaster*

olfactory system and it has been particularly useful for studying the complex neural circuits in the brain (Talay *et al*., 2017). In trans-Tango adopted for zebrafish, specific neurons of interest are chosen and are defined by expression of ligand that serves as a "bait" to identify their synaptic partners. Ligand expression is controlled by UAS, and thus by a Gal4 driver line of interest. The ligand is derived from human glucagon (sGCG), is tethered to the presynaptic membrane through the transmembrane domain of zebrafish Nrxn1b, and extended into the synaptic cleft through the linker sequence (Talay *et al*., 2017). All neurons in the central nervous system are genetically modified to express 1) a G protein coupled receptor (GPCR) fused to QF transcription factor on their cell surface, and 2) a fusion of TEV protease and Arrestin. GPCR-QF fusion is regulated by TEV protease because the TEV cleavage site lies in between the two proteins. In presynaptic neurons, Gal4 binds to UAS resulting in the expression of the sGCG ligand and its presentation on the presynaptic membrane. The presynaptically-presented sGCG ligand binds to the GPCR-QF fusion protein on the postsynaptic membrane, causing recruitment of Arrestin-TEV and cleavage of QF. QF then translocates to the nucleus and promotes transcription of a fluorescent marker under QUAS. This marker helps identify the cells that are synaptically connected to the bait neuron. The advantage of this method is that it works with any neural circuit regardless of the neurotransmitter that it uses (Coomer *et al*., 2023; Talay *et al*., 2017).

2.5 Fluorescence Resonance Energy Transfer (FRET) to study protein interactions or conformation in the living brain

FRET is a powerful and widely used technique in molecular and cellular biology that allows researchers to study interactions and conformational changes between molecules, typically within the nanometer scale. FRET relies on the transfer of energy between two fluorescent molecules when they are in close proximity (Fig6). This transfer happens from a donor fluorophore to an acceptor fluorophore. In the context of zebrafish research, FRET can be used to investigate various biological processes and molecular interactions, including interactions between proteins or within a protein in the living zebrafish (Kardash *et al*., 2011). By genetically fusing a donor fluorophore to one protein and an acceptor fluorophore to another, researchers can measure the proximity of these proteins and infer whether they are interacting in specific cellular contexts. To detect conformational changes in proteins, the donor and acceptor fluorophores are attached to different parts of a protein of interest and the changes in protein shape or structure in response to various stimuli or biological processes can be monitored by FRET in the living zebrafish neurons (Fig6B).

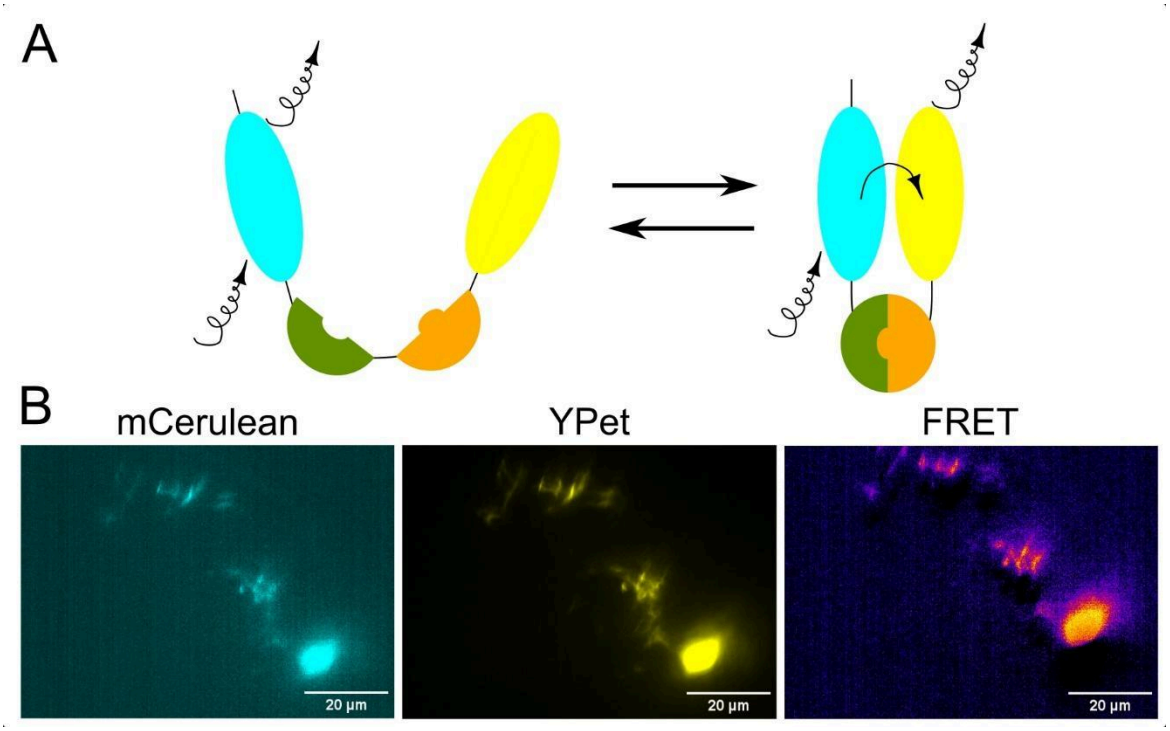

Figure 6. A. Schematic visualization of the FRET principle. B. Exemplary image of neurons in the zebrafish brain showing FRET.

3. Methods to study brain activity and behavior

3.1. Tools for single-cell neuronal activity analysis in the zebrafish brain

Neuronal activity causes rapid changes in intracellular free calcium. Using this mechanism, genetically encoded calcium indicators (GECIs) allow for real-time, *in vivo*, non-invasive measurement of neuronal activity, on a spatial scale ranging from synapses (Chen *et al*., 2013) to large populations of neurons (Ahrens *et al*., 2013). Currently, GFP-based GECIs are most widely used (Chen *et al*., 2013). The original GCaMP probe consisted of circularly permuted green fluorescent protein (cpGFP), the calcium-binding protein calmodulin (CaM), and CaM-interacting M13 peptide (Nakai *et al*., 2001). The major principle of GCaMP action is based on conformational changes in CaM/M13 upon calcium ion binding, resulting in increased brightness of the green fluorescence (Chen *et al*., 2013; Dana *et al*., 2016). Since the discovery of GCaMP, many variants of this fusion protein have been generated and widely used in many *in vitro* and *in vivo* models. For example, the GCaMP5G reporter (Ahrens *et al*., 2013) was used by us to examine epilepsy in the zebrafish model of Tuberous Sclerosis Complex. Whole-brain imaging of *tsc2*^{vu242}*;Tg(GCaMP5G) larvae* with light-sheet microscopy has revealed hyperexcitability in the pallial neurons of the *tsc2*$^{vu242/vu242}$ mutant fish (Kedra *et al*., 2020).

Subsequent iterations of GCaMP calcium indicators have evolved from the original structure

to enhance sensitivity and response kinetics. While the precise biophysical mechanisms governing these improvements are not yet fully elucidated, a trade-off appears to exist between the sensitivity and kinetics of GCaMP sensors. Consequently, distinct variants have been developed, optimized either for heightened sensitivity (e.g., GCaMP6s, GCaMP7s) or accelerated response kinetics (e.g., GCaMP6f, GCaMP7f) (Chen *et al.*, 2013; Dana *et al.*, 2019). Furthermore, large-scale neuronal activity imaging often encounters challenges related to signal cross-talk stemming from white matter regions and the nuclear expression of GECIs limit the imaging speed (C. K. Kim *et al*., 2014). Addressing this, Shemesh *et al*. have engineered cell body-targeted GCaMP6f and GCaMP7f which exhibited superior signal-to-noise ratios and reduced false-positive correlations when employed in the imaging of dense neural circuits (Shemesh *et al*., 2020). More recently, Zhang *et al*. have introduced the 8th generation of GCaMP indicators, denoted as jGCaMP8 sensors. These sensors offer rapid response kinetics, along with heightened sensitivity compared to preceding GECIs. jGCaMP8 variants are available, each optimized for either sensitivity or speed (Zhang *et al*., 2023). jGCaMP8s has recently been used as the calcium reporter in a newly developed platform that combines Ca2+ imaging and optogenetics in freely moving zebrafish (Chai *et al.*, 2024). SyjGCaMP8m, a variant of GCaMP8 expressed in synaptic terminals, has been used to image bipolar cells in the inner retina of larval zebrafish, in order to investigate the role of amacrine and bipolar cells in processing of color information (Wang *et al.*, 2023).

Notwithstanding the sensitivity and signal-to-noise ratio offered by GFP-based GECIs, their utility is restrained by the characteristics of their excitation and emission spectra (Table). Notably, these indicators are incompatible with transgenic organisms that already express GFP-based proteins. Also, the excitation spectrum of GCaMP partially overlaps with that of rhodopsin-based ion channels frequently employed in optogenetic investigations. To circumvent these constraints, the adoption of red GECIs has emerged as a solution. Red GECIs not only alleviate these issues but also exhibit diminished susceptibility to light scattering and absorption within tissues, along with reduced phototoxicity. Dana *et al*. have devised two enhanced red GECIs based on mRuby (jRCaMP1a and jRCaMP1b) and mApple (jRGECO1a). Beyond their application in cultured rat hippocampal neurons, mice, *Drosophilla*, *C. elegans*, and zebrafish, where they were pan-neuronally expressed under the HuC promoter, these red GECIs have displayed striking advantages over previously available RFP-based sensors. They have exhibited sensitivities similar to GCaMP6 and have maintained stable performance over time. Particularly jRGECO1a has shown superior sensitivity compared to jRCaMP1, representing an advance in the detection of neural activity relative to prior generations of red GECIs. Notably, jRCaMP1a and jRCaMP1b have demonstrated resistance to photoswitching following blue light exposure, a contrast to jRGECO1a, which undergoes such a conversion (Dana *et al*., 2016). The concurrent utilization of both green and red GECIs was demonstrated by Mu *et al*. in a study featuring zebrafish expressing GCaMP6f in neurons and jRGECO1b in radial astrocytes. This dual application facilitated the separate but simultaneous imaging of the two distinct cell types, thereby elucidating the dynamic interplay between neuronal and glial activity in the modulation of motor and passive states (Mu *et al*., 2019).

A slightly different approach is offered by the genetically encoded indicator CaMPARI, the second generation of which has been released recently (Fosque *et al*., 2015; Moeyaert *et al*., 2018). CaMPARI is a photoconvertible green fluorescent protein that, under UV light exposure, undergoes irreversible photoconversion to a red fluorescent form, but only in the presence of free calcium ions. Importantly, the degree of red-to-green fluorescence is contingent upon the levels of calcium allowing for the precise capture of neuronal activity in response to specific stimuli, both *in vivo* and *in vitro*. While CaMPARI probes have not been as extensively used as GCaMPs, they have proven to be valuable tool for the screens aimed at assessing the neurotoxicity of environmental contaminants or pharmaceuticals (Biechele-Speziale *et al*., 2023; Kanyo *et al*., 2021). Recently, live imaging of zebrafish larvae expressing CaMPARI was instrumental in elucidating the mechanism of Kv7 voltage-gated potassium channel inhibition (Kanyo *et al*., 2023).

Another approach to visualize and measure calcium dynamics upon neuronal activity is to use FRET-based calcium indicators called cameleons. Similarly to GECIs, cameleons are genetically encoded Ca^{2+} indicators based on fluorescent proteins and CaM (Fan *et al*., 2007). Cameleons are especially valuable for assessing basal-level activity and have found application in functional mapping and connectivity mapping studies in zebrafish (Tao *et al*., 2011). There are currently several different cameleons classified by composition of their Ca^{2+} binding domains. One of the most widely used cameleon is Yellow cameleon that consists of two fluorescent proteins, cyan CFP and yellow YFP. The neural activity can be visualized by FRET between these fluorescent proteins (Hasani *et al*., 2023). This technique has been used to observe Ca^{2+} dynamics in sensory and spinal cord neurons in zebrafish (Higashijima *et al*., 2003).

Cameleons typically use two fluorophores, a donor and an acceptor, which can be engineered to emit different wavelengths of light upon calcium binding and they can be used in combination with other FRET-based sensors targeting different molecules (e.g., cAMP, pH) to simultaneously monitor multiple cellular processes within the same cell. Moreover, cameleons provide ratiometric measurements comparing the emission of the donor and acceptor fluorophores, which reduces the impact of factors like indicator concentration and illumination intensity, resulting in more quantitative and accurate calcium measurements. FRET-based indicators often exhibit a higher signal-to-noise ratio compared to some single-fluorophore indicators like GCaMP probes. This means that cameleons can provide more robust and reliable measurements, especially in challenging experimental conditions. They can be designed to have a wider dynamic range, allowing them to detect both small and large changes in calcium concentrations. However, it's essential to note that cameleons can be more technically challenging to implement than the single-fluorophore indicators, as they often require more complex microscopy setups. The choice between FRET-based indicators and other approaches will depend on the specific experimental goals, the availability of equipment, and the expertise of the researchers. Both types of indicators have their strengths and are valuable tools in the field of calcium imaging and zebrafish research.

In parallel with the ongoing efforts to improve the kinetics and sensitivity of calcium

indicators, researchers have explored genetically encoded voltage indicators (GEVIs; Table). These indicators are based on naturally occurring ion channel voltage sensor domains fused to fluorescent proteins or, in later iterations, microbial rhodopsin proteins (reviewed in (Xu *et al*., 2017)). Voltage imaging is technically challenging, necessitating fast imaging speeds without compromising brightness or sensitivity. One innovative approach, proposed by Abdelfattah *et al*., involves the creation of a hybrid "chemigenetic" voltage indicator named Voltron. This indicator combines a voltage-sensitive microbial rhodopsin domain with a dye-capture protein domain, allowing for the binding of synthetic fluorophores such as Janelia Fluor. In this approach, transmembrane voltage-dependent changes in the rhodopsin domain modulate the fluorescence quenching of the dye molecule through FRET. Voltron excels in terms of brightness and photostability when compared to previous GEVIs. In zebrafish experiments, Voltron has been utilized to detect action potentials and subthreshold voltage signals during swim bouts in response to visual cues, providing insights into sensorimotor integration at an unprecedented temporal resolution (Abdelfattah *et al*., 2019). Recently, Abdelfattah *et al.* have also developed an improved version of this indicator, Voltron2, optimized for higher sensitivity to action potentials, subthreshold potential fluctuations, and it was tested in vivo in zebrafish olfactory neurons (Abdelfattah *et al.*, 2023).

An alternative approach to monitor neuronal activity *in vivo* is tracking of neurotransmitter release. For example, a genetically encoded G-protein-coupled receptor-based dopamine sensor ($GRAB_{DA}$) was engineered by coupling a conformationally sensitive cpGFP to a selected human dopamine receptor. It allows for rapid, sensitive, and specific detection of extracellular dopamine enabling quantitation of dopamine release in the living animals. $GRAB_{DA}$ was successfully used in zebrafish larvae to observe dopamine dynamics in response to a threatening looming stimulus (Sun *et al*., 2018). A year later, an analogous norepinephrine sensor was developed by Feng *et al*., and similarly validated in zebrafish larvae, also by observing the response to a looming stimulus (Feng *et al*., 2019). Both sensors showed high specificity, sensitivity, brightness, photostability, and lack of phototoxicity (Feng *et al*., 2019; Sun *et al*., 2018). Using a similar strategy, Wan *et al*. have developed the $GRAB_{5\text{-}HT1.0}$ sensor for detection of serotonin (Wan *et al*., 2021), and while it has not yet been used in zebrafish studies, it likely could be adapted for zebrafish similarly to its predecessors.

Moreover, iGluSnFR is a glutamate reporter constructed from *E. coli* GltI and cpGFP, originally shown to reliably report glutamate release from excitatory synapses in zebrafish (Marvin *et al*., 2013, James *et al*., 2019). It has been recently improved by postsynaptic targeting, achieved by the fusion of iGluSnFR with glutamate receptor auxiliary proteins γ-2 and γ-8, creating the SnFR-γ2 and SnFR-γ8 reporters (Hao *et al*., 2023). However, they have not yet been tested in zebrafish. For differential properties of various approaches to study brain activity see Table.

3.2. The virtual reality for the analysis of behavior

Virtual Reality (VR) is an emerging tool to study zebrafish behavior. VR arenas, displaying 2D or 3D environments, can be programmed to provide realistic visual cues and feedback, serving to analyze how the fish interact with their surroundings. This technology enables the execution of assays wherein the ongoing simulation is dynamically adjusted to the fish's behavior. This capability facilitates the observation of intricate, purpose-driven behaviors, including goal-directed navigation, hunting, or social interactions, all within the limits of a comparatively confined physical setting. The VR configuration effectively mitigates the spatial constraints associated with traditional behavioral tests. The mobile projection can persist for variable duration and at diverse speeds, and it can follow any trajectory. Additionally, it allows for simulating any desired visual stimuli, ranging from simple shapes and patterns to complex environments.

The simplest VR assays involve the projection of an animated virtual object on the walls of the tank. Zebrafish react to a moving dot stimulus as if it were a potential predator or prey depending on the dot size (Barker & Baier, 2015). Since this discovery, multiple studies have used such stimuli to examine the mechanisms of prey tracking (Antinucci *et al*., 2019; Barker & Baier, 2015; Jouary *et al*., 2016; Trivedi & Bollmann, 2013). More recently, researchers have also used the VR projection of conspecifics for the analysis of shoaling, and how the presence and behavior of conspecifics affects decision making in both freely swimming (Harpaz *et al*., 2021; Oscar *et al*., 2023) as well as head-restrained zebrafish (Huang *et al*., 2020). In the case of larvae, it has been demonstrated that a simple shape corresponding in size and movement patterns to a real zebrafish larva, is sufficient to provoke the same social responses as live conspecifics (Harpaz *et al*., 2021). However, in the case of adults, Huang *et al*. have shown that the fish are able to differentiate between a simple shape and a more detailed projection, and require a more realistic image of an adult zebrafish to trigger social behavior (Huang *et al*., 2020). And while the currently available technology, based on rendering the VR environment from the perspective of a single animal, does not allow for simultaneous testing of multiple fish in a single arena, virtual projections of conspecifics can be sufficiently sophisticated and accurate to the real-world behavior that they have been used to create models of sensorimotor control during schooling in juvenile zebrafish. In addition to studying social behavior in zebrafish, these models were used to refine the movement of autonomous vehicles, showing that insights gained from zebrafish behavioral studies can find application outside the field of neuroscience, or even biology (Li *et al.*, 2023).

Another simple type of a VR assay, developed by Portugues and Engert, is based on displaying a 2D drifting striped pattern to create the impression of movement. Presented with the moving stimulus, the fish responds by tail movements corresponding to behavior observed during free swimming, and the visual feedback can be controlled by the researcher to create a closed-loop environment (Portugues & Engert, 2011). In a more complex application of this method, Torigoe *et al*. have created a 3D arena with moving patterns of various colors. By pairing different projections with the absence or presence of an electric shock, they were able to induce a positive or negative associations with the displayed stimuli,

and demonstrated how the fish use this information to choose a safe environment and learn new information when the visual cues were changed (Torigoe *et al*., 2021).

Researchers have harnessed the advanced capabilities of VR tools to conduct innovative experiments. For instance, the FreemoVR system developed by Stowers *et al*. enables "virtual teleportation", wherein fish experience a seamless transition to a new projected environment as they move within a designated region (Stowers *et al*., 2017). 3D VR environments such as FreemoVR are usually created using open-source software for game developers (Huang *et al*., 2020; Stowers *et al*., 2017). However, such tools might require optimization to make them suitable for behavioral research. BonVision, created by Lopes *et al*, is an open-source software package for creating and displaying 2D and 3D VR environments, compatible with various display devices, equipped with a library of predefined 3D structures, and capable of real-time control and automatic calibration of the virtual environment using deep neural networks (Lopes *et al*., 2021). BonZeb, similarly based on the open-source visual programming language Bonsai, is a specialized set of modular software packages designed for high-resolution zebrafish behavioral tracking, both in head-fixed and free-swimming virtual assays (Guilbeault *et al*., 2021). VR environments offer immense potential for behavioral research, with tools like BonVision and BonZeb facilitating the generation of 2D and 3D VR environments, real-time control, and precise calibration, all tailored for zebrafish studies.

3.3. Calcium imaging coupled to behavior to study brain function

A distinct advantage of VR over traditional experimental setups is the possibility of simulating a changing, moving environment while the fish remains fixed in place, allowing for simultaneous microscopic imaging of brain activity together with behavioral assay. A fictive swimming assay, developed by Masino and Fetcho for the analysis of spinal motor patterns using electrophysiological recordings (Masino & Fetcho, 2005) was adapted for a behavioral test in VR, where immobilized zebrafish larvae are placed inside a water-filled chamber fitted with screens for projecting stimuli (Mu *et al.*, 2019). Alternatively, specific parts of the larval body, such as the tail and eyes, may be freed from agarose while still maintaining immobilization (Jouary *et al*., 2016; Trivedi & Bollmann, 2013). When studying behaviors that necessitate the use of adult fish, which cannot be easily immobilized in agarose, methods include head fixation (Huang *et al*., 2020) or the use of custom-made harnesses (Torigoe *et al*., 2021). In fictive swimming experiments, the firing of motor neurons in the tail is monitored to quantify movement speed and direction, enabling precise visual feedback (Masino & Fetcho, 2005; Ahrens *et al*., 2012; Mu *et al*., 2019). In instances where the fish's tail remains mobile, swimming patterns can be predicted based on tail curvature (Huang *et al*., 2020) or extrapolated from tail movements recorded during previous free-swimming periods (Jouary *et al*., 2016). Unlike traditional setups, VR permits the withholding or modification of visual stimuli, enabling the investigation of the fish's responses to these alterations. For instance, Mu *et al*. explored how fish respond to repeated futile movements and adapt their behavioral strategy in response to failure. The presented visual pattern was abruptly halted while the fish continued to "move" (Mu *et al*., 2019). In a

study by Yang *et al.*, which investigated the mechanisms of self-location and positional homeostasis, artificial movement was played in reverse, creating the illusion of struggling against a water current. This allowed an examination of how zebrafish react to perceived displacement and maintain their position (Yang *et al*., 2022). These studies, elucidating neuronal circuits underpinning specific motor behaviors, exemplify the capacity of VR to facilitate *in vivo* brain imaging during simulated movements.

VR experiments involving fictive swimming allow for *in-vivo*, real time monitoring of neuronal activity during a behavioral test. For this, two-photon microscopy is the most suitable providing robust 3D resolution with minimal photo-damage. Additionally, the infrared light used for excitation should not elicit visual responses in zebrafish (Renninger & Orger, 2013), and therefore should not interfere with the behavioral assay. Vladimirov *et al*. have developed an alternative approach for neuronal activity imaging during fictive swimming. This setup was based on lightsheet microscopy in which one laser beam scanned the brain from the front, imaging the forebrain between the eyes. At the same time, the second beam scanned the fish from the side, switching off when it passed over the eye, thus avoiding direct stimulation of the retina that would confound the results of the behavioral test (Vladimirov *et al*., 2014). Other groups have also constructed behavioral testing chambers coupled with imaging systems built to suit their particular needs. Vanwalleghem *et al*. placed immobilized zebrafish larvae in a microfluidic device designed to deliver water flow stimuli, and imaged them on a custom-built light-sheet microscope (Vanwalleghem *et al*., 2020). Constantin *et al*. also utilized a custom-built light-sheet microscope to measure neuronal activity in response to visual and auditory stimuli (Constantin *et al*., 2020). While the smaller larval brain is more accessible for imaging, two-photon microscopy was also used to perform calcium imaging during behavioral tests in adult fish (Huang *et al*., 2020; Torigoe *et al*., 2021). Huang *et al*. were able to visualize individual somata and neurites up to a depth of >200 μm below the brain surface (Huang *et al*., 2020).

However, the methods described above require restraining the fish, which limits the range of behaviors that can be studied or might result in unnatural movements. Immobilizing the head causes reactive forces in the body that do not naturally occur during free swimming, and restricts the movement to a horizontal plane, causing aberrant vestibular feedback. The CaMPARI calcium indicator (described in section 3.1) allows for irreversible marking of active cells during free swimming (Fosque *et al*., 2015). Furthermore, Kim *et al.* have devised a sophisticated tracking microscope system that incorporates a motorized stage with a motion-cancellation mechanism that cancels brain motion in three dimensions enabling brain imaging in freely-swimming fish (Kim *et al.*, 2017). The motion cancellation is coupled with a differential illumination focal filtering (DIFF) microscopy approach, based on an earlier technique called HiLo microscopy, described by Lim *et al.* HiLo microscopy used uniform and spatially modulated illumination in a speckled or grid pattern and combined these raw images resulting in an image of higher resolution (Lim *et al.*, 2011). In DIFF microscopy, the images are acquired with a pair of complementary grid illumination patterns (Kim *et al.*, 2017). This integrated system facilitates the continuous real-time imaging of neural activity in the brain of freely swimming larval zebrafish for extended periods.

3.4. Optogenetic approaches coupled to behavioral analysis

Optogenetic tools allow for specific and reversible manipulation of activity of selected neurons in a living organism, enabling researchers to experimentally test the link between neuronal activity and behavioral responses (Fig7). Moreover, the transparent zebrafish larvae allow for non-invasive optogenetic modulation of neural activity throughout the brain (Portugues *et al*., 2013). The cation channelrhodopsins (ChR1 and ChR2), originally found in the green alga *Chlamydomonas reinhardtii*, are among the most popular optogenetic tools. They are light-activated cation channels that allow the passage of positively charged ions upon light activation. They consist of rhodopsin, a seven-transmembrane helix protein with covalently linked retinal, acting as the chromophore. Upon illumination with light of specific wavelength, they generate action potentials in normally light-insensitive neurons which result in activation of the neuronal circuit (Berthold *et al*., 2008; Nagel *et al*., 2003). Anion channelrhodopsins are a type of optogenetic tool derived from microbial rhodopsins that are able to inactivate neuronal circuit. When exposed to specific light spectrum, anion channelrhodopsins open and enable the influx of negatively charged ions, primarily chloride ions, into the target neurons, leading to hyperpolarization of the cell membrane and suppression of neuronal activity (Mohamed *et al*., 2017). By expressing anion channelrhodopsins in specific neurons and then illuminating them with the appropriate light, researchers can inhibit neuronal firing and investigate the functional role of these neurons in various physiological and behavioral processes in a precise and temporally controlled manner. Both cation and anion channelrhodopsins have become valuable tools for studying neural circuits and their functions in neuroscience research.

A toolkit of nine transgenic zebrafish lines expressing optogenetic actuators under UAS – CoChR, CheRiff, $ChR2_{(H134R)}$, eArch3.0, GtACR1, GtACR2, Chronos, ChrimsonR and eNpHR3.0 – was generated by Antinucci *et al*., and tested using high-throughput behavioral assays and *in vivo* whole-cell electrophysiological recordings, providing a resource for design and calibration of opsin-expressing zebrafish lines in specific regions (Antinucci *et al*., 2020). These lines utilize the Gal4-UAS system for targeted opsin expression, and provide stable, reproducible opsin expression levels across cells and generations. Optogenetic interrogation of simple behaviors are done with modified microscopes or automated tracking systems that include LED lights (Antinucci *et al*., 2020; Oikonomou *et al*., 2019). Concurrently, the Raspberry Pi Virtual Reality (PiVR) system was purpose-built for the optogenetic stimulation of unrestrained animals to study more complex behaviors. The PiVR platform offers the capability to present virtual environments while automating behavioral tracking and facilitating feedback based on the animal's behavioral responses. Optogenetic manipulations are achieved through the use of a LED light source that remains focused on the animal during its locomotion. Although this setup has been utilized in phototaxis experiments with zebrafish larvae, it's important to note that to date the optogenetic component has been exclusively tested in *Drosophilla* (Tadres & Louis, 2020).

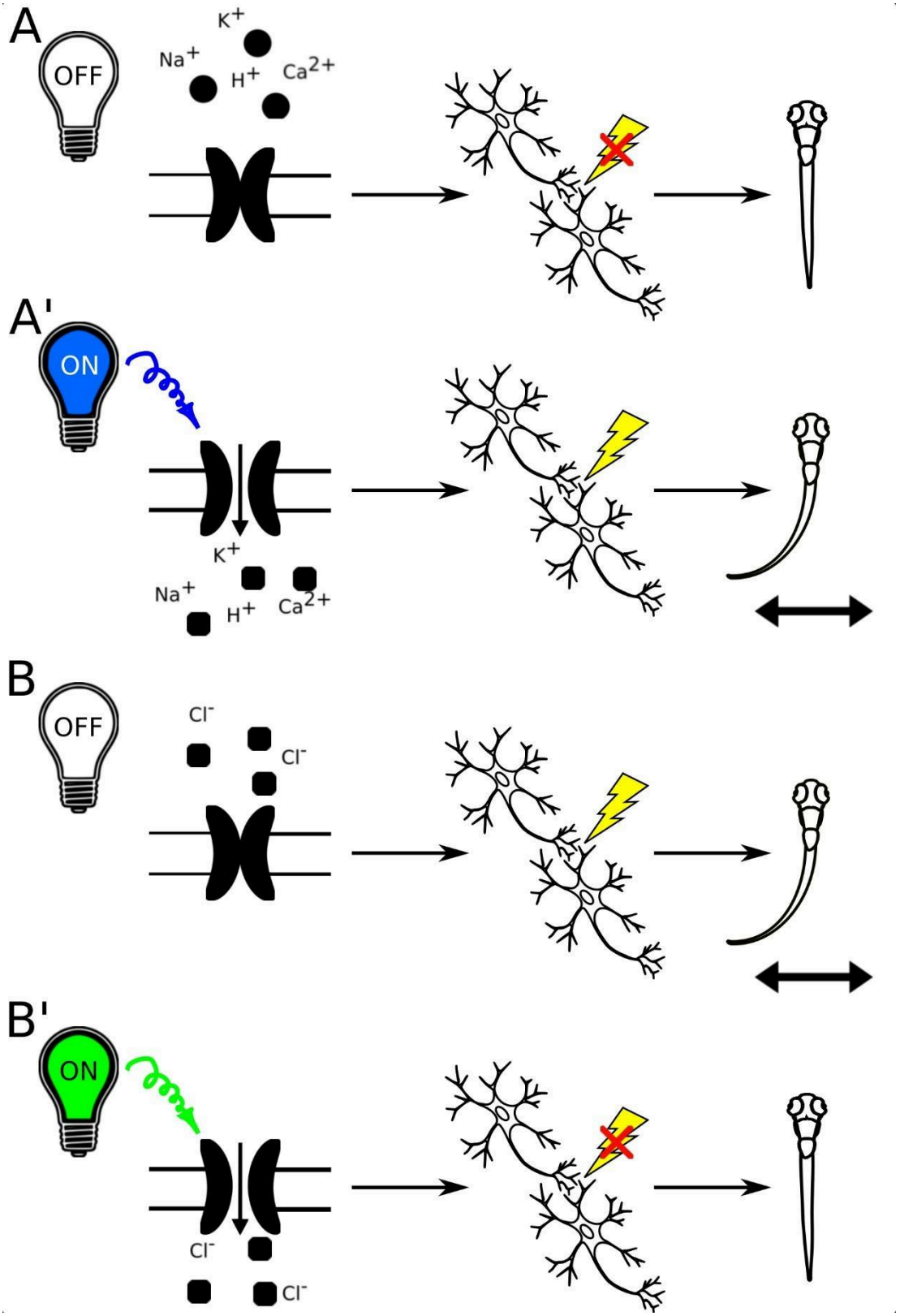

Figure 7. A. Schematic representation of the use of channelrhodopsins to activate neuronal circuits with light-off (A) and light-on conditions (A'). B. Schematic representation of the use of anion channelrhodopsins to inactivate neuronal circuits with light-off (B) and light-on

conditions (B’).

In zebrafish, the photoactivation of ChR2 in somatosensory neurons or ear hair cells has been demonstrated to elicit escape responses, as documented in multiple studies (Douglass *et al*., 2008; Monesson-Olson *et al*., 2014; Ozdemir *et al*., 2021). Notably, optogenetic manipulation using ChR2 was also employed in Barker and Baier's research concerning responses to moving dot stimuli, revealing that the activation of a specific subset of glutamatergic tectal interneurons prompted an increased approach toward small-sized objects mimicking prey (Barker & Baier, 2015). Recent investigations have further harnessed ChR2 to unveil two distinct modules of hypothalamic dopaminergic neurons in zebrafish. These modules were found to play pivotal roles in the initiation of locomotor activity, responsiveness to acoustic stimuli, and the impact of olfactory cues on decision-making processes (Barrios *et al*., 2020).

GtACR1 and GtACR2 represent anion channelrhodopsins derived from the alga *Guillardia theta*. These optogenetic tools have demonstrated their efficacy in inhibiting spontaneous coiling movements in larval zebrafish, underscoring their utility for the optical modulation of behavior in zebrafish larvae (Mohamed *et al*., 2017). However, it is important to acknowledge the limitations of GtACRs. Activation of these pumps in cells with elevated intracellular chloride levels may result in depolarization. Also, they can induce neuronal depolarization upon light cessation, potentially causing a burst of neural activity. Additionally, there is uncertainty regarding their sustained functionality beyond a one-minute time frame. Consequently, GtACRs are primarily suited for the observation of acute processes confined to the duration of light application (Mohamed *et al*., 2017). Nonetheless, as optogenetic inhibitors, GtACRs can serve as valuable controls alongside cation channelrhodopsins. For instance, in a study by Cheng *et al*., the identification of a nucleus in the anterior thalamus that responds to light stimuli, subsequently evoking a response in the habenula, was initially achieved by stimulating this nucleus with ChR2. This elicited depolarization in the habenula and an increase in neuronal activity, as measured by GCaMP6f fluorescence. Conversely, the application of GtACR1 inhibited the light response and disrupted phototaxic behavior, thereby confirming the nucleus's role in regulating habenula function (Cheng *et al*., 2017).

Another approach to inhibit neuronal activity is the PAC-K silencer, based on photoactivated adenylyl cyclases (PACs) and the small cyclic nucleotide-gated potassium channel SthK. PAC-K acts as a light-controlled K^+ channel, allowing for controlled hyperpolarization of neurons (Bernal Sierra *et al*., 2018). One advantage of the PAC-K silencer is that it is sensitive to longer wavelengths of light compared to GtACRs. This can be beneficial because longer wavelengths of light penetrate tissues more effectively, allowing for deeper and more precise light activation *in vivo*. Also, the PAC-K silencer typically requires lower light intensities for activation compared to GtACRs. This can be less phototoxic and reduce the risk of heating in the tissue, which is important for long-term experiments or when studying sensitive neural circuits. GtACRs and other anion channelrhodopsins are sensitive to intracellular chloride levels. If a cell has high intracellular chloride concentrations, activating GtACR may lead to depolarization rather than hyperpolarization. PAC-K is less affected by

intracellular chloride levels, making it a more reliable tool in diverse cellular contexts (Bernal Sierra *et al*., 2018). Anion channelrhodopsins like GtACR can sometimes cause depolarization of neurons when the light is turned off. PAC-K may exhibit a reduced off-response, making it more suitable for experiments, where the precise timing of inhibition is crucial. PAC-K can also be activated for a longer duration compared to GtACRs, which may be advantageous for experiments that require sustained inhibition of neural activity. The choice between these optogenetic tools depends on the specific experimental requirements and the characteristics of the neural circuit being studied.

Additionally, the combination of optogenetic circuit interrogation and calcium imaging has been realized through the innovative work of Dal Maschio *et al*. They developed a comprehensive protocol employing both ChR2 and GCaMP6s to facilitate concurrent 3D two-photon optogenetic stimulation and calcium imaging. This study harnessed two-photon computer-generated holography for photostimulation, leveraging a spatial light modulator to project intricate illumination patterns. Additionally, the co-expression of photoactivatable PA-GFP, ChR2, and GCaMP6s enabled the labeling and visualization of cells of interest, providing insights into their morphology subsequent to functional characterization. This methodology was instrumental in the identification of neuronal ensembles in the tegmentum of larval zebrafish associated with the control of tail bending (Dal Maschio *et al*., 2017). Until now, such experiments have usually been conducted on head-restrained zebrafish, and optogenetic manipulation in freely swimming fish required full-field illumination, and in consequence the generation of fish lines expressing the photosensitive proteins in the selected brain region. However, Chai *et al.* have recently developed a system for targeted brain imaging and optogenetics in freely-moving fish. The use of light-field microscopy allows for rapid recording of neuronal activity. In addition to the GFP-based Ca2+ indicator, the fish also expressed an activity-independent RFP, serving as a reference signal. By using this reference channel alongside a machine learning-based image detection and registration algorithm, researchers were able to correct Ca2+ signal artifacts caused by zebrafish movements. The tracking system was also used to deliver photostimulation to the region of interest previously chosen in the software, based on the ZBB atlas data (Chai *et al.*, 2024). This approach allows to study zebrafish brain activity during more naturalistic behavior than possible in experimental setups requiring the restraining of fish.

3.5. In vivo electrophysiological studies of the zebrafish brain

The easily accessible zebrafish brain also allows for electrophysiological recordings. In particular, multiple zebrafish models of epilepsy are used, in which the presence of seizures is confirmed by recording of electrical discharges in the brain. Epileptic seizures in zebrafish were first shown by Baraban using extracellular field recording. A microelectrode was inserted several microns into the forebrain of larval zebrafish, and the electrical activity of the brain was recorded, showing seizure-like discharges following the administration of convulsant drugs, or in genetically modified fish carrying a mutation in the *tsc1a* gene, associated with the disease Tuberous Sclerosis Complex, the symptoms of which include

epilepsy (Baraban, 2013). Later, Eimon *et al*. have developed a platform for simultaneous recording of local field potentials (LFP) in multiple fish, and have used it to analyze brain activity in the zebrafish model of a different genetic disease resulting in epilepsy, Dravet syndrome (Eimon *et al*., 2018). More recently, LFP recording has been combined with Ca^{2+} imaging in order to map epileptiform activity in the brains of *kcnj10a* morphant zebrafish as well as fish treated with the proconvulsant drug pentylentetrazole (PTZ), and evaluate the efficacy of the anti-epileptic drug valproate in these models (Cozzolino *et al.*, 2020). In the meantime, Pinion *et al*. have analysed and catalogued electrographic signatures of LFPs in zebrafish treated with different pro-convulsant agents, and compared these recordings with the results of electrophysiological studies in mammals, further illustrating the translational potential of zebrafish models for studies of epilepsy (Pinion *et al*., 2022).

The utility of electrophysiological studies in zebrafish is not however limited to studying epilepsy. In the previously mentioned study by Masino and Fetcho, foundational to establishing the paradigm of fictive behavior, whole cell patch clamp recordings were taken to measure the activity of motor neurons during the behavioral test (Masino & Fetcho, 2005). Intracellular recordings of the Mauthner neurons, responsible for integration of sensory information and evoking a motor response, were used to test the precise effect of commonly used anaesthetics on different aspects of sensory processing, providing with a method to evaluate potential novel anaesthetic compounds (Machnik *et al*., 2018). Vestibulospinal neurons were targeted in voltage- and current-clamp recordings aimed to elucidate how the larval zebrafish utilize vestibulospinal input to maintain posture. The use of these methods revealed the role of both inhibitory and excitatory inputs in posture stabilization, demonstrating the utility of zebrafish in studying the function of neuronal circuits, particularly when, in contrast to mammals, they are more accessible for *in vivo* patch clamp recording (Hamling *et al*., 2023).

Hong *et al*. have developed a system for non-invasive, long-term electrophysiological recording of zebrafish, through the use of a microfluidic system. The so-called Zebrafish Analysis Platform (iZAP) involves a central chamber where multiple zebrafish larvae can swim freely, and from there enter single channels where they become restrained. There, multiple electrodes are positioned in contact with the head, and field potentials from the dorsal side of the zebrafish forebrain, optic tectum, midbrain and hindbrain are measured. This system was successfully validated through recording of PTZ-induced seizures in zebrafish larvae, and allowed for nearly continuous 130 hour recording of brain activity – a length of recording not possible with previously established, more invasive techniques, requiring immobilization in agarose and penetrating electrodes. The iZAP system also allows for changing of the medium without disturbing the larvae, making it useful for high-throughput drug testing (Hong *et al*., 2016). More recently, Tomasello and Sive have also developed a simple method of measuring brain and spinal cord activity in larval zebrafish, based on a previously available microelectrode array from Axion Biosystems. This system was validated by collecting LFP recordings from zebrafish larvae at 7 dpf, with the anticonvulsant drug valproic acid used as a positive control for lowered brain activity. While this method does involve immobilizing the fish in agarose, and therefore cannot be used for

such extended periods of time as the iZAP method, it is a useful tool for non-invasive electrophysiological recordings in live zebrafish, making use of an easy to use, commercially available technology (Tomasello & Sive, 2020).

4. Discussion

While zebrafish are a valuable and versatile model organism for brain research, they do have certain limitations that researchers should consider when designing experiments and interpreting results. Zebrafish have a less complex brain compared to mammals. Some areas of the brain found in mammals are absent or simplified in zebrafish. This means that findings in zebrafish may not always directly translate to humans. Zebrafish behaviors are less complex than those of humans, which can make it challenging to model complex behaviors and cognitive functions in zebrafish. Zebrafish do not possess language or consciousness, which makes it challenging to study brain functions related to these aspects of cognition and behavior. While there is genetic homology between zebrafish and humans, there are also significant differences in the genetic makeup. This can limit the extent to which zebrafish findings can be extrapolated to mammals. Also, the small size of zebrafish can be a limitation when conducting invasive experiments or when detailed anatomical or electrophysiological measurements are required. Zebrafish have a relatively short lifespan compared to some other model organisms, which can be a limitation when studying long-term processes.

While genetic tools for manipulating the zebrafish genome have advanced significantly, they may not be as extensive as those available for other model organisms like mice. Zebrafish research is still relatively young compared to research in mice and rats. This means that there may be gaps in our knowledge, and some areas of zebrafish neuroscience are still emerging. Despite these limitations, zebrafish remain a valuable tool in brain research, particularly in areas related to early brain development, neural circuitry, and certain neurological and neuropsychiatric conditions. One example of a success story in zebrafish research is a discovery of an anti-seizure medication called clemizole. In a drug-repurposing study that tested the approved medications in zebrafish model of pediatric epilepsy, Dravet syndrome, clemizole was identified as a potent drug with anti-seizure actions with the use of high-throughput behavioral tests and validation by electrophysiological recordings (Baraban *et al.*, 2013). This discovery was a foundation of clinical trials testing safety and efficacy of clemizole as a treatment for Dravet syndrome, of which the phase II are to be completed by the end of 2024 (NCT04069689, NCT04462770, ClinicalTrials.gov). They are often used in combination with other model organisms to provide a more comprehensive understanding of brain function and dysfunction. Researchers should carefully consider these limitations when using zebrafish and design experiments to address specific questions that can be effectively tackled using this model organism.

Author contributions

JZ: study concept and design. OD, TD: search for information, draft of the manuscript. OD, TD, JZ: manuscript writing and editing. All authors contributed to and approved the article.

Funding

Authors were supported by OPUS grant no. 2020/37/B/NZ3/02345 from National Science Center (Poland).

Acknowledgments

We thank J. Jaworski for critical reading and H.L. Jezierska for copy editing the manuscript.

Conflict of interest

The authors declare no conflict of interest.

Table. Tools for visualization of the neuronal activity live.

Name	Targeted mechanism	Fluorophore	Excitation/emission wavelengths	Utility	References
GCaMP5G/6/7/8	Ca^{2+} influx	cpGFP**	488/507	Visualising neuronal activity dynamics	Ahrens et al., 2013 Kedra et al., 2019 Shemesh et al., 2020 Zhang et al., 2023
jRCaMP1a/1b	Ca^{2+} influx	mRuby	558/605	Visualising neuronal activity dynamics; can be used together with GFP-based sensor for labelling distinct cell populations	Dana et al., 2016
jRGECO1a	Ca^{2+} influx	mApple	568/592		
CaMPARI2	Ca^{2+} influx	EosFP*	Green: 502/516 Red: 562/577	Marking of active neuronal populations by irreversible	Moeyaert et al., 2018

				photoconversion	
Ratiometric cameleons	Ca^{2+} influx	Two fluorophores that allow FRET to occur between them		Visualising neuronal activity dynamics compare to the basal levels of Ca^{2+}	Fan et al., 2007 Tao et al., 2011
Voltron/Voltron2	Membrane potential	Janelia Fluor525/549/552/585	JF525: 525/549 JF549: 549/571 JF552: 552/575 JF585: 585/609	Detection of action potentials and subthreshold voltage signals	Abdelfattah et al., 2019 Abdelfattah et al., 2023
ASAP1	Membrane potential	cpGFP	488/507		St-Pierre et al., 2014 Silic et al, 2022
zArchon1	Membrane potential	GFP	488/507		Piatkevich et al., 2018 Böhm et al, 2022
$GRAB_{DA}$	Dopamine release and uptake	cpGFP	488/507	Visualising dopaminergic signaling	Sun et al., 2018
$GRAB_{NE}$	Norepinephrine release and uptake	cpGFP	488/507	Visualising norepinephrinergic signaling	Feng et al., 2019
$GRAB_{5\text{-}HT1.0}$	Serotonin release and uptake	cpGFP	488/507	Visualising serotonergic signaling	Wan et al., 2021
iGluSnFR	Glutamate release and uptake	cpGFP	488/507	Visualising glutamatergic signaling	Marvin et al., 2013

*FP = fluorescent protein; **cpGFP = circularly permuted GFP

References

Abdelfattah, A. S., Kawashima, T., Singh, A., Novak, O., Liu, H., Shuai, Y., Huang, Y.-C., Campagnola, L., Seeman, S. C., Yu, J., Zheng, J., Grimm, J. B., Patel, R., Friedrich, J., Mensh, B. D., Paninski, L., Macklin, J. J., Murphy, G. J., Podgorski, K., … Schreiter, E. R.

(2019). Bright and photostable chemigenetic indicators for extended in vivo voltage imaging. Science, 365(6454). https://doi.org/10.1126/science.aav6416

Abdelfattah, A.S., Zheng, J., Singh, A., Schreiter, E.R., Hasseman, J.P., Kolb, I. (2023). Sensitivity optimization of a rhodopsin-based fluorescent voltage indicator. Neuron 111(10). https://doi.org/10.1016/j.neuron.2023.03.009

Ahrens, M. B., Li, J. M., Orger, M. B., Robson, D. N., Schier, A. F., Engert, F., & Portugues, R. (2012). Brain-wide neuronal dynamics during motor adaptation in zebrafish. *Nature*, *485*(7399). https://doi.org/10.1038/nature11057

Ahrens, M. B., Orger, M. B., Robson, D. N., Li, J. M., & Keller, P. J. (2013). Whole-brain functional imaging at cellular resolution using light-sheet microscopy. *Nature Methods*, *10*(5). https://doi.org/10.1038/nmeth.2434

Ando, R., Hama, H., Yamamoto-Hino, M., Mizuno, H., & Miyawaki, A. (2002). An optical marker based on the UV-induced green-to-red photoconversion of a fluorescent protein. *Proceedings of the National Academy of Sciences*, *99*(20). https://doi.org/10.1073/pnas.202320599

Antinucci, P., Dumitrescu, A., Deleuze, C., Morley, H. J., Leung, K., Hagley, T., Kubo, F., Baier, H., Bianco, I. H., & Wyart, C. (2020). A calibrated optogenetic toolbox of stable zebrafish opsin lines. *ELife*, *9*. https://doi.org/10.7554/eLife.54937

Antinucci, P., Folgueira, M., & Bianco, I. H. (2019). Pretectal neurons control hunting behaviour. *ELife*, *8*. https://doi.org/10.7554/eLife.48114

Aramaki, S., & Hatta, K. (2006). Visualizing neurons one‐by‐one in vivo: Optical dissection and reconstruction of neural networks with reversible fluorescent proteins. *Developmental Dynamics*, *235*(8). https://doi.org/10.1002/dvdy.20826

Asakawa, K., Suster, M. L., Mizusawa, K., Nagayoshi, S., Kotani, T., Urasaki, A., Kishimoto, Y., Hibi, M., & Kawakami, K. (2008). Genetic dissection of neural circuits by *Tol2* transposon-mediated Gal4 gene and enhancer trapping in zebrafish. *Proceedings of the National Academy of Sciences*, *105*(4). https://doi.org/10.1073/pnas.0704963105

Baraban, S.C. (2013). Forebrain electrophysiological recording in larval zebrafish. *J Vis Exp 71*. doi: 10.3791/50104.

Baraban, S., Dinday, M. & Hortopan, G. (2013). Drug screening in Scn1a zebrafish mutant identifies clemizole as a potential Dravet syndrome treatment. *Nat Commun 4*. https://doi.org/10.1038/ncomms3410

Barker, A. J., & Baier, H. (2015). Sensorimotor Decision Making in the Zebrafish Tectum. *Current Biology*, *25*(21). https://doi.org/10.1016/j.cub.2015.09.055

Barnea, G., Strapps, W., Herrada, G., Berman, Y., Ong, J., Kloss, B., Axel, R., & Lee, K. J. (2008). The genetic design of signaling cascades to record receptor activation. *Proceedings of the National Academy of Sciences*, *105*(1). https://doi.org/10.1073/pnas.0710487105

Barrios, J. P., Wang, W.-C., England, R., Reifenberg, E., & Douglass, A. D. (2020). Hypothalamic Dopamine Neurons Control Sensorimotor Behavior by Modulating Brainstem Premotor Nuclei in Zebrafish. *Current Biology*, *30*(23). https://doi.org/10.1016/j.cub.2020.09.002

Beretta, C. A., Dross, N., Bankhead, P., & Carl, M. (2013). The ventral habenulae of zebrafish develop in prosomere 2 dependent on Tcf7l2 function. *Neural Development*, *8*.

Bernal Sierra, Y. A., Rost, B. R., Pofahl, M., Fernandes, A. M., Kopton, R. A., Moser, S., Holtkamp, D., Masala, N., Beed, P., Tukker, J. J., Oldani, S., Bönigk, W., Kohl, P., Baier, H., Schneider-Warme, F., Hegemann, P., Beck, H., Seifert, R., & Schmitz, D. (2018). Potassium channel-based optogenetic silencing. *Nature Communications*, *9*(1). https://doi.org/10.1038/s41467-018-07038-8

Berthold, P., Tsunoda, S. P., Ernst, O. P., Mages, W., Gradmann, D., & Hegemann, P. (2008). Channelrhodopsin-1 Initiates Phototaxis and Photophobic Responses in *Chlamydomonas* by Immediate Light-Induced Depolarization. *The Plant Cell*, *20*(6). https://doi.org/10.1105/tpc.108.057919

Biechele-Speziale, D., Camarillo, M., Martin, N. R., Biechele-Speziale, J., Lein, P. J., & Plavicki, J. S. (2023). Assessing CaMPARI as new approach methodology for evaluating neurotoxicity. *NeuroToxicology*, *97*. https://doi.org/10.1016/j.neuro.2023.05.013

Bockamp, E., Sprengel, R., Eshkind, L., Lehmann, T., Braun, J. M., Emmrich, F., & Hengstler, J. G. (2008). Conditional transgenic mouse models: from the basics to genome-wide sets of knockouts and current studies of tissue regeneration. *Regenerative Medicine*, *3*(2). https://doi.org/10.2217/17460751.3.2.217

Böhm, U. L., Kimura, Y., Kawashima, T., Ahrens, M. B., Higashijima, S., Engert, F., & Cohen, A. E. (2022). Voltage imaging identifies spinal circuits that modulate locomotor adaptation in zebrafish. *Neuron*, *110*(7). https://doi.org/10.1016/j.neuron.2022.01.001

Campbell, L. J., Willoughby, J. J., & Jensen, A. M. (2012). Two Types of Tet-On Transgenic Lines for Doxycycline-Inducible Gene Expression in Zebrafish Rod Photoreceptors and a Gateway-Based Tet-On Toolkit. *PLoS ONE*, *7*(12). https://doi.org/10.1371/journal.pone.0051270

Chai Y., Qi K., Wu, Y., Mu, Y., Shen, C., Wen, Q. (2024). All-optical interrogation of brain-wide activity in freely swimming larval zebrafish. *iScience 27*(1). https://doi.org/10.1016/j.isci.2023.108385

Chen, T.-W., Wardill, T. J., Sun, Y., Pulver, S. R., Renninger, S. L., Baohan, A., Schreiter, E. R., Kerr, R. A., Orger, M. B., Jayaraman, V., Looger, L. L., Svoboda, K., & Kim, D. S. (2013). Ultrasensitive fluorescent proteins for imaging neuronal activity. *Nature*, *499*(7458). https://doi.org/10.1038/nature12354

Cheng, R.-K., Krishnan, S., Lin, Q., Kibat, C., & Jesuthasan, S. (2017). Characterization of a thalamic nucleus mediating habenula responses to changes in ambient illumination. *BMC Biology*, *15*(1). https://doi.org/10.1186/s12915-017-0431-1

Chow, R. W.-Y., & Vermot, J. (2017). The rise of photoresponsive protein technologies applications in vivo: a spotlight on zebrafish developmental and cell biology. *F1000Research*, *6*. https://doi.org/10.12688/f1000research.10617.1

Constantin, L., Poulsen, R. E., Scholz, L. A., Favre-Bulle, I. A., Taylor, M. A., Sun, B., Goodhill, G. J., Vanwalleghem, G. C., & Scott, E. K. (2020). Altered brain-wide auditory networks in a zebrafish model of fragile X syndrome. *BMC Biology*, *18*(1). https://doi.org/10.1186/s12915-020-00857-6

Coomer, C., Naumova, D., Talay, M., Zolyomi, B., Snell, N. J., Sorkaç, A., Chanchu, J.-M., Cheng, J., Roman, I., Li, J., Robson, D., Barnea, G., & Halpern, M. E. (2023). Transsynaptic labeling and transcriptional control of zebrafish neural circuits. *BioRxiv* preprint. https://doi.org/10.1101/2023.04.03.535421

Cozzolino, O., Sicca, F., Paoli, E., Trovato, F., Santorelli, F.M., Ratto, G.M., Marchese, M. (2020). Evolution of Epileptiform Activity in Zebrafish by Statistical-Based Integration of Electrophysiology and 2-Photon Ca2+ Imaging. *Cells* 9(3). https://doi.org/10.3390/cells9030769

Dakoji, S., Tomita, S., Karimzadegan, S., Nicoll, R. A., & Bredt, D. S. (2003). Interaction of transmembrane AMPA receptor regulatory proteins with multiple membrane associated guanylate kinases. *Neuropharmacology*, *45*(6). https://doi.org/10.1016/S0028-3908(03)00267-3

dal Maschio, M., Donovan, J. C., Helmbrecht, T. O., & Baier, H. (2017). Linking Neurons to Network Function and Behavior by Two-Photon Holographic Optogenetics and Volumetric Imaging. *Neuron*, *94*(4). https://doi.org/10.1016/j.neuron.2017.04.034

Dana, H., Mohar, B., Sun, Y., Narayan, S., Gordus, A., Hasseman, J. P., Tsegaye, G., Holt, G. T., Hu, A., Walpita, D., Patel, R., Macklin, J. J., Bargmann, C. I., Ahrens, M. B., Schreiter, E. R., Jayaraman, V., Looger, L. L., Svoboda, K., & Kim, D. S. (2016). Sensitive red protein calcium indicators for imaging neural activity. *ELife*, *5*. https://doi.org/10.7554/eLife.12727

Dana, H., Sun, Y., Mohar, B., Hulse, B.K., Kerlin, A.M., Hasseman, J.P., Tsegaye, G., Tsang, A., Wong, A., Patel, R., Macklin, J.J., Chen, Y., Konnerth, A., Jayaraman, V., Looger, L.L., Schreiter, E.R., Svoboda, K., Kim D.S. (2019). High-performance calcium sensors for

imaging activity in neuronal populations and microcompartments. *Nat Methods 16*, 649–657. https://doi.org/10.1038/s41592-019-0435-6

Deán-Ben, X. L., Sela, G., Lauri, A., Kneipp, M., Ntziachristos, V., Westmeyer, G. G., Shoham, S., & Razansky, D. (2016). Functional optoacoustic neuro-tomography for scalable whole-brain monitoring of calcium indicators. *Light: Science & Applications*, *5*(12). https://doi.org/10.1038/lsa.2016.201

Douglass, A. D., Kraves, S., Deisseroth, K., Schier, A. F., & Engert, F. (2008). Escape Behavior Elicited by Single, Channelrhodopsin-2-Evoked Spikes in Zebrafish Somatosensory Neurons. *Current Biology*, *18*(15). https://doi.org/10.1016/j.cub.2008.06.077

Eimon, P.M., Ghannad-Rezaie, M., De Rienzo, G., Allalou, A., Wu, Y., Gao, M., Roy, A., Skolnick, J., Yanik, M.F. (2018). Brain activity patterns in high-throughput electrophysiology screen predict both drug efficacies and side effects. *Nat Commun 9*(219). https://doi.org/10.1038/s41467-017-02404-4

Fan, X., Majumder, A., Reagin, S. S., Porter, E. L., Sornborger, A. T., Keith, C. H., & Lauderdale, J. D. (2007). New statistical methods enhance imaging of cameleon fluorescence resonance energy transfer in cultured zebrafish spinal neurons. *Journal of Biomedical Optics*, *12*(3). https://doi.org/10.1117/1.2745263

Feng, J., Zhang, C., Lischinsky, J. E., Jing, M., Zhou, J., Wang, H., Zhang, Y., Dong, A., Wu, Z., Wu, H., Chen, W., Zhang, P., Zou, J., Hires, S. A., Zhu, J. J., Cui, G., Lin, D., Du, J., & Li, Y. (2019). A Genetically Encoded Fluorescent Sensor for Rapid and Specific In Vivo Detection of Norepinephrine. *Neuron*, *102*(4). https://doi.org/10.1016/j.neuron.2019.02.037

Förster, D., Arnold-Ammer, I., Laurell, E., Barker, A. J., Fernandes, A. M., Finger-Baier, K., Filosa, A., Helmbrecht, T. O., Kölsch, Y., Kühn, E., Robles, E., Slanchev, K., Thiele, T. R., Baier, H., & Kubo, F. (2017). Genetic targeting and anatomical registration of neuronal populations in the zebrafish brain with a new set of BAC transgenic tools. *Scientific Reports*, *7*(1). https://doi.org/10.1038/s41598-017-04657-x

Fosque, B. F., Sun, Y., Dana, H., Yang, C.-T., Ohyama, T., Tadross, M. R., Patel, R., Zlatic, M., Kim, D. S., Ahrens, M. B., Jayaraman, V., Looger, L. L., & Schreiter, E. R. (2015). Labeling of active neural circuits in vivo with designed calcium integrators. *Science*, *347*(6223). https://doi.org/10.1126/science.1260922

Goll, M. G., Anderson, R., Stainier, D. Y. R., Spradling, A. C., & Halpern, M. E. (2009). Transcriptional Silencing and Reactivation in Transgenic Zebrafish. *Genetics*, *182*(3). https://doi.org/10.1534/genetics.109.102079

Gross, G. G., Junge, J. A., Mora, R. J., Kwon, H.-B., Olson, C. A., Takahashi, T. T., Liman, E. R., Ellis-Davies, G. C. R., McGee, A. W., Sabatini, B. L., Roberts, R. W., & Arnold, D. B. (2013). Recombinant Probes for Visualizing Endogenous Synaptic Proteins in Living Neurons. *Neuron*, *78*(6). https://doi.org/10.1016/j.neuron.2013.04.017

Guilbeault, N. C., Guerguiev, J., Martin, M., Tate, I., & Thiele, T. R. (2021). BonZeb: open-source, modular software tools for high-resolution zebrafish tracking and analysis. *Scientific Reports*, *11*(1). https://doi.org/10.1038/s41598-021-85896-x

Habuchi, S., Ando, R., Dedecker, P., Verheijen, W., Mizuno, H., Miyawaki, A., & Hofkens, J. (2005). Reversible single-molecule photoswitching in the GFP-like fluorescent protein Dronpa. *Proceedings of the National Academy of Sciences*, *102*(27). https://doi.org/10.1073/pnas.0500489102

Halpern, M. E., Rhee, J., Goll, M. G., Akitake, C. M., Parsons, M., & Leach, S. D. (2008). Gal4/UAS Transgenic Tools and Their Application to Zebrafish. *Zebrafish*, *5*(2). https://doi.org/10.1089/zeb.2008.0530

Hamling, K.R., Harmon, K., Schoppik, D. (2023). The Nature and Origin of Synaptic Inputs to Vestibulospinal Neurons in the Larval Zebrafish. *eNeuro 10*(6). https://doi.org/10.1523/ENEURO.0090-23.2023

Hao, Y., Toulmé, E., König, B., Rosenmund, C., & Plested, A. J. (2023). Targeted sensors for glutamatergic neurotransmission. *ELife*, *12*. https://doi.org/10.7554/eLife.84029

Harpaz, R., Nguyen, M. N., Bahl, A., & Engert, F. (2021). Precise visuomotor transformations underlying collective behavior in larval zebrafish. *Nature Communications*, *12*(1). https://doi.org/10.1038/s41467-021-26748-0

Hasani, H., Sun, J., Zhu, S. I., Rong, Q., Willomitzer, F., Amor, R., McConnell, G., Cossairt, O., & Goodhill, G. J. (2023). Whole-brain imaging of freely-moving zebrafish. *Frontiers in Neuroscience*, *17*. https://doi.org/10.3389/fnins.2023.1127574

Higashijima, S. I., Masino, M. A., Mandel, G., & Fetcho, J. R. (2003). Imaging Neuronal Activity during Zebrafish Behavior with a Genetically Encoded Calcium Indicator. *Journal of Neurophysiology*, *90*(6), 3986–3997. https://doi.org/10.1152/jn.00576.2003

Hiyoshi, K., Saito, K., Fukuda, N., Matsuzaki, T., Yoshikawa, H. Y., & Tsuda, S. (2021). Two-Photon Laser Ablation and In Vivo Wide-Field Imaging of Inferior Olive Neurons Revealed the Recovery of Olivocerebellar Circuits in Zebrafish. *International Journal of Environmental Research and Public Health*, *18*(16). https://doi.org/10.3390/ijerph18168357

Hong, S., Lee, P., Baraban, S., Lee, L.P. (2016). A Novel Long-term, Multi-Channel and Non-invasive Electrophysiology Platform for Zebrafish. *Sci Rep* 6. https://doi.org/10.1038/srep28248

Hortopan, G. A., Dinday, M. T., & Baraban, S. C. (2010). Zebrafish as a model for studying genetic aspects of epilepsy. *Disease Models & Mechanisms*, *3*(3–4). https://doi.org/10.1242/dmm.002139

Howe, K., Clark, M. D., Torroja, C. F., Torrance, J., Berthelot, C., Muffato, M., Collins, J. E., Humphray, S., McLaren, K., Matthews, L., McLaren, S., Sealy, I., Caccamo, M., Churcher, C., Scott, C., Barrett, J. C., Koch, R., Rauch, G.-J., White, S., … Stemple, D. L. (2013). The zebrafish reference genome sequence and its relationship to the human genome. *Nature*, *496*(7446). https://doi.org/10.1038/nature12111

Huang, K.-H., Rupprecht, P., Frank, T., Kawakami, K., Bouwmeester, T., & Friedrich, R. W. (2020). A virtual reality system to analyze neural activity and behavior in adult zebrafish. *Nature Methods*, *17*(3). https://doi.org/10.1038/s41592-020-0759-2

James, B., Darnet, L., Moya-Díaz, J., Seibel, S.-H., & Lagnado, L. (2019). An amplitude code transmits information at a visual synapse. *Nature Neuroscience*, *22*(7). https://doi.org/10.1038/s41593-019-0403-6

Jouary, A., Haudrechy, M., Candelier, R., & Sumbre, G. (2016). A 2D virtual reality system for visual goal-driven navigation in zebrafish larvae. *Scientific Reports*, *6*(1). https://doi.org/10.1038/srep34015

Kalueff, A. V., Stewart, A. M., & Gerlai, R. (2014). Zebrafish as an emerging model for studying complex brain disorders. *Trends in Pharmacological Sciences*, *35*(2). https://doi.org/10.1016/j.tips.2013.12.002

Kanyo, R., Amin, M. R., Locskai, L. F., Bouvier, D. D., Olthuis, A. M., Allison, W. T., & Ali, D. W. (2021). Medium-throughput zebrafish optogenetic platform identifies deficits in subsequent neural activity following brief early exposure to cannabidiol and Δ9-tetrahydrocannabinol. *Scientific Reports*, *11*(1). https://doi.org/10.1038/s41598-021-90902-3

Kanyo, R., Lamothe, S. M., Urrutia, A., Goodchild, S. J., Allison, W. T., Dean, R., & Kurata, H. T. (2023). Site and Mechanism of ML252 Inhibition of Kv7 Voltage-Gated Potassium Channels. *Function*, *4*(4). https://doi.org/10.1093/function/zqad021

Kardash, E., Bandemer, J., & Raz, E. (2011). Imaging protein activity in live embryos using fluorescence resonance energy transfer biosensors. *Nature Protocols*, *6*(12). https://doi.org/10.1038/nprot.2011.395

Kawakami, K. (2007). Tol2: a versatile gene transfer vector in vertebrates. *Genome Biology*, *8*(Suppl 1). https://doi.org/10.1186/gb-2007-8-s1-s7

Kawakami, K., Asakawa, K., Hibi, M., Itoh, M., Muto, A., & Wada, H. (2016). *Gal4 Driver Transgenic Zebrafish*. https://doi.org/10.1016/bs.adgen.2016.04.002

Kedra, M., Banasiak, K., Kisielewska, K., Wolinska-Niziol, L., Jaworski, J., & Zmorzynska, J. (2020). TrkB hyperactivity contributes to brain dysconnectivity, epileptogenesis, and anxiety in zebrafish model of Tuberous Sclerosis Complex. *Proceedings of the National Academy of Sciences*, *117*(4). https://doi.org/10.1073/pnas.1910834117

Kemmler, C. L., Moran, H. R., Murray, B. F., Scoresby, A., Klem, J. R., Eckert, R. L., Lepovsky, E., Bertho, S., Nieuwenhuize, S., Burger, S., D'Agati, G., Betz, C., Puller, A. C., Felker, A., Ditrychova, K., Bötschi, S., Affolter, M., Rohner, N., Lovely, C. B., Kwan, K. M., Burger, A., & Mosimann, C. (2023). Next-generation plasmids for transgenesis in zebrafish and beyond. *Development*, 150(8). https://doi.org/10.1242/dev.201531

Kim, C. K., Miri, A., Leung, L. C., Berndt, A., Mourrain, P., Tank, D. W., & Burdine, R. D. (2014). Prolonged, brain-wide expression of nuclear-localized GCaMP3 for functional circuit mapping. *Frontiers in Neural Circuits*, *8*. https://doi.org/10.3389/fncir.2014.00138

Kim, D. H., Kim, J., Marques, J. C., Grama, A., Hildebrand, D. G. C., Gu, W., Li, J. M., & Robson, D. N. (2017). Pan-neuronal calcium imaging with cellular resolution in freely swimming zebrafish. *Nature Methods*, *14*(11). https://doi.org/10.1038/nmeth.4429

Knopf, F., Schnabel, K., Haase, C., Pfeifer, K., Anastassiadis, K., & Weidinger, G. (2010). Dually inducible TetON systems for tissue-specific conditional gene expression in zebrafish. *Proceedings of the National Academy of Sciences*, *107*(46). https://doi.org/10.1073/pnas.1007799107

Köster, R. W., & Fraser, S. E. (2001). Tracing Transgene Expression in Living Zebrafish Embryos. *Developmental Biology*, *233*(2). https://doi.org/10.1006/dbio.2001.0242

Lal P., Tanabe H., Suster M.L., Ailani D., Kotani Y., Muto A., Itoh M., Iwasaki M., Wada H., Yaksi E. & Kawakami K. (2018). Identification of a neuronal population in the telencephalon essential for fear conditioning in zebrafish. *BMC Biology 16*(45). https://doi.org/10.3389/fnana.2022.837527

Lalonde, L.R., Wells, H.H., Kemmler, C.L., Nieuwenhuize, S., Lerma, R., Burger, A., Mosimann, C. (2023). pIGLET: Safe harbor landing sites for reproducible and efficient transgenesis in zebrafish. *bioRxiv* preprint. https://doi.org/10.1101/2023.12.08.570868

Li, L., Nagy, M., Amichay, G., Wang, W., Deussen, O., Rus, D., Couzin, I. (2023). Reverse engineering the control law for schooling in zebrafish using virtual reality. *ResearchSquare* preprint. https://doi.org/10.21203/rs.3.rs-2801869/v1

Lim, D., Ford, T. N., Chu, K. K., & Metz, J. (2011). Optically sectioned in vivo imaging with speckle illumination HiLo microscopy. *Journal of Biomedical Optics*, *16*(1). https://doi.org/10.1117/1.3528656

Lin, H.-J., Lee, S.-H., Wu, J.-L., Duann, Y.-F., & Chen, J.-Y. (2013). Development of Cre–loxP technology in zebrafish to study the regulation of fish reproduction. *Fish Physiology and Biochemistry*, *39*(6). https://doi.org/10.1007/s10695-013-9806-6

Lopes, G., Farrell, K., Horrocks, E. A., Lee, C.-Y., Morimoto, M. M., Muzzu, T., Papanikolaou, A., Rodrigues, F. R., Wheatcroft, T., Zucca, S., Solomon, S. G., & Saleem, A.

B. (2021). Creating and controlling visual environments using BonVision. *ELife*, *10*. https://doi.org/10.7554/eLife.65541

Lopez A., Gorb A., Palha N., Fleming A., Rubinsztein D.C. (2022). A New Zebrafish Model to Measure Neuronal α-Synuclein Clearance In Vivo. Genes 13(868). https://doi.org/10.3390/genes13050868

Ma, Z., Zhu, P., Pang, M., Guo, L., Chang, N., Zheng, J., Zhu, X., Gao, C., Huang, H., Cui, Z., Xiong, J.-W., Peng, J., & Chen, J. (2017). A novel inducible mutagenesis screen enables to isolate and clone both embryonic and adult zebrafish mutants. *Scientific Reports*, *7*(1). https://doi.org/10.1038/s41598-017-10968-w

Machnik, P., Schirmer, E., Glück, L., Schuster, S. (2018). Recordings in an integrating central neuron provide a quick way for identifying appropriate anaesthetic use in fish. *Sci Rep 8*. https://doi.org/10.1038/s41598-018-36130-8

Marquart, G. D., Tabor, K. M., Brown, M., Strykowski, J. L., Varshney, G. K., LaFave, M. C., Mueller, T., Burgess, S. M., Higashijima, S., & Burgess, H. A. (2015). A 3D Searchable Database of Transgenic Zebrafish Gal4 and Cre Lines for Functional Neuroanatomy Studies. *Frontiers in Neural Circuits*, *9*. https://doi.org/10.3389/fncir.2015.00078

Marvin, J. S., Borghuis, B. G., Tian, L., Cichon, J., Harnett, M. T., Akerboom, J., Gordus, A., Renninger, S. L., Chen, T.-W., Bargmann, C. I., Orger, M. B., Schreiter, E. R., Demb, J. B., Gan, W.-B., Hires, S. A., & Looger, L. L. (2013). An optimized fluorescent probe for visualizing glutamate neurotransmission. *Nature Methods*, *10*(2). https://doi.org/10.1038/nmeth.2333

Masino, M.A., & Fetcho, J.R. (2005). Fictive Swimming Motor Patterns in Wild Type and Mutant Larval Zebrafish. *J Neurophysiol 93*(6). https://doi.org/10.1152/jn.01248.2004

Moeyaert, B., Holt, G., Madangopal, R., Perez-Alvarez, A., Fearey, B. C., Trojanowski, N. F., Ledderose, J., Zolnik, T. A., Das, A., Patel, D., Brown, T. A., Sachdev, R. N. S., Eickholt, B. J., Larkum, M. E., Turrigiano, G. G., Dana, H., Gee, C. E., Oertner, T. G., Hope, B. T., & Schreiter, E. R. (2018). Improved methods for marking active neuron populations. *Nature Communications*, *9*(1). https://doi.org/10.1038/s41467-018-06935-2

Mohamed, G. A., Cheng, R.-K., Ho, J., Krishnan, S., Mohammad, F., Claridge-Chang, A., & Jesuthasan, S. (2017). Optical inhibition of larval zebrafish behaviour with anion channelrhodopsins. *BMC Biology*, *15*(1). https://doi.org/10.1186/s12915-017-0430-2

Mohr, M. A., Argast, P., & Pantazis, P. (2016). Labeling cellular structures in vivo using confined primed conversion of photoconvertible fluorescent proteins. *Nature Protocols*, *11*, 2419–2431.

Monesson-Olson, B. D., Browning-Kamins, J., Aziz-Bose, R., Kreines, F., & Trapani, J. G. (2014). Optical Stimulation of Zebrafish Hair Cells Expressing Channelrhodopsin-2. *PLoS ONE*, *9*(5). https://doi.org/10.1371/journal.pone.0096641

Mu, Y., Bennett, D. V., Rubinov, M., Narayan, S., Yang, C.-T., Tanimoto, M., Mensh, B. D., Looger, L. L., & Ahrens, M. B. (2019). Glia Accumulate Evidence that Actions Are Futile and Suppress Unsuccessful Behavior. *Cell*, *178*(1). https://doi.org/10.1016/j.cell.2019.05.050

Muto, A., & Kawakami, K. (2018). Ablation of a Neuronal Population Using a Two-photon Laser and Its Assessment Using Calcium Imaging and Behavioral Recording in Zebrafish Larvae. *Journal of Visualized Experiments*, *136*. https://doi.org/10.3791/57485

Nagel, G., Szellas, T., Huhn, W., Kateriya, S., Adeishvili, N., Berthold, P., Ollig, D., Hegemann, P., & Bamberg, E. (2003). Channelrhodopsin-2, a directly light-gated cation-selective membrane channel. *Proceedings of the National Academy of Sciences*, *100*(24). https://doi.org/10.1073/pnas.1936192100

Nakai, J., Ohkura, M., & Imoto, K. (2001). A high signal-to-noise Ca2+ probe composed of a single green fluorescent protein. *Nature Biotechnology*, *19*(2). https://doi.org/10.1038/84397

Oikonomou, G., Altermatt, M., Zhang, R., Coughlin, G. M., Montz, C., Gradinaru, V., & Prober, D. A. (2019). The Serotonergic Raphe Promote Sleep in Zebrafish and Mice. *Neuron*, *103*(4). https://doi.org/10.1016/j.neuron.2019.05.038

Oscar, L., Li, L., Gorbonos, D., Couzin, I. D., & Gov, N. S. (2023). A simple cognitive model explains movement decisions in zebrafish while following leaders. *Physical Biology*, *20*(4). https://doi.org/10.1088/1478-3975/acd298

Ozdemir, Y. I., Hansen, C. A., Ramy, M. A., Troconis, E. L., McNeil, L. D., & Trapani, J. G. (2021). Recording Channelrhodopsin-Evoked Field Potentials and Startle Responses from Larval Zebrafish. In: Dempski, R. (eds) *Channelrhodopsin. Methods in Molecular Biology, 2191*. Humana, New York, NY. https://doi.org/10.1007/978-1-0716-0830-2_13

Panula, P., Chen, Y.-C., Priyadarshini, M., Kudo, H., Semenova, S., Sundvik, M., & Sallinen, V. (2010). The comparative neuroanatomy and neurochemistry of zebrafish CNS systems of relevance to human neuropsychiatric diseases. *Neurobiology of Disease*, *40*(1). https://doi.org/10.1016/j.nbd.2010.05.010

Patterson, G. H., & Lippincott-Schwartz, J. (2002). A Photoactivatable GFP for Selective Photolabeling of Proteins and Cells. *Science*, *297*(5588). https://doi.org/10.1126/science.1074952

Pinion, J., Walsh, C., Goodfellow, M., Randall, A.D., Tyler, C.R., Winter, M.J. (2022). Differential Electrographic Signatures Generated by Mechanistically-Diverse Seizurogenic Compounds in the Larval Zebrafish Brain. *eNeuro* *9*(2). https://doi.org/10.1523/ENEURO.0337-21.2022

Portugues, R., & Engert, F. (2011). Adaptive locomotor behavior in larval zebrafish. *Front. Syst. Neurosci. 5*. https://doi.org/10.3389/fnsys.2011.00072

Portugues, R., Severi, K. E., Wyart, C., & Ahrens, M. B. (2013). Optogenetics in a transparent animal: circuit function in the larval zebrafish. *Current Opinion in Neurobiology*, *23*(1). https://doi.org/10.1016/j.conb.2012.11.001

Piatkevich, K.D., Jung, E.E., Straub, C., Linghu C., Park D., Suk H.-J., Hochbaum D.R., Goodwin D., Pnevmatikakis E., Pak N., Kawashima T., Yang C.-T., Rhoades J.L., Shemesh O., Asano S., Yoon Y.-G., Freifeld L., Saulnier J.L., Riegler C., Engert F., Hughes T., Drobizhev M., Szabo B., Ahrens M.B., … Boyden E.S. (2018). A robotic multidimensional directed evolution approach applied to fluorescent voltage reporters. *Nature Chem Biol* 14. https://doi.org/10.1038/s41589-018-0004-9

Renninger, S. L., & Orger, M. B. (2013). Two-photon imaging of neural population activity in zebrafish. *Methods*, *62*(3). https://doi.org/10.1016/j.ymeth.2013.05.016

Sato, T., Takahoko, M., & Okamoto, H. (2006). HuC:Kaede, a useful tool to label neural morphologies in networks in vivo. *Genesis*, *44*(3), 136–142.

Scheer, N., & Campos-Ortega, J. A. (1999). Use of the Gal4-UAS technique for targeted gene expression in the zebrafish. *Mechanisms of Development*, *80*(2). https://doi.org/10.1016/S0925-4773(98)00209-3

Shehwana, H., & Konu, O. (2019). Comparative Transcriptomics Between Zebrafish and Mammals: A Roadmap for Discovery of Conserved and Unique Signaling Pathways in Physiology and Disease. *Frontiers in Cell and Developmental Biology*, *7*. https://doi.org/10.3389/fcell.2019.00005

Shemesh, O. A., Linghu, C., Piatkevich, K. D., Goodwin, D., Celiker, O. T., Gritton, H. J., Romano, M. F., Gao, R., Yu, C.-C. (Jay), Tseng, H.-A., Bensussen, S., Narayan, S., Yang, C.-T., Freifeld, L., Siciliano, C. A., Gupta, I., Wang, J., Pak, N., Yoon, Y.-G., … Boyden, E. S. (2020). Precision Calcium Imaging of Dense Neural Populations via a Cell-Body-Targeted Calcium Indicator. *Neuron*, *107*(3). https://doi.org/10.1016/j.neuron.2020.05.029

Silic, M. R., Dong, Z., Chen, Y., Kimbrough, A., & Zhang, G. (2022). Zebrafish Embryos Display Characteristic Bioelectric Signals during Early Development. *Cells*, *11*(22). https://doi.org/10.3390/cells11223586

Son, J.-H., Keefe, M. D., Stevenson, T. J., Barrios, J. P., Anjewierden, S., Newton, J. B., Douglass, A. D., & Bonkowsky, J. L. (2016). Transgenic FingRs for Live Mapping of Synaptic Dynamics in Genetically-Defined Neurons. *Scientific Reports*, *6*(1). https://doi.org/10.1038/srep18734

St-Pierre, F., Marshall, J., Yang, Y., Gong Y., Schnitzer M.J. & Lin M.Z. (2014). High-fidelity optical reporting of neuronal electrical activity with an ultrafast fluorescent voltage sensor. *Nature Neurosci* 17. https://doi.org/10.1038/nn.3709

Stowers, J. R., Hofbauer, M., Bastien, R., Griessner, J., Higgins, P., Farooqui, S., Fischer, R. M., Nowikovsky, K., Haubensak, W., Couzin, I. D., Tessmar-Raible, K., & Straw, A. D. (2017). Virtual reality for freely moving animals. *Nature Methods*, *14*(10). https://doi.org/10.1038/nmeth.4399

Streisinger, G., Walker, C., Dower, N., Knauber, D., & Singer, F. (1981). Production of clones of homozygous diploid zebra fish (Brachydanio rerio). *Nature*, *291*(5813), 293–296.

Subach, O. M., Patterson, G. H., Ting, L.-M., Wang, Y., Condeelis, J. S., & Verkhusha, V. V. (2011). A photoswitchable orange-to-far-red fluorescent protein, PSmOrange. *Nature Methods*, *8*(9). https://doi.org/10.1038/nmeth.1664

Sun, F., Zeng, J., Jing, M., Zhou, J., Feng, J., Owen, S. F., Luo, Y., Li, F., Wang, H., Yamaguchi, T., Yong, Z., Gao, Y., Peng, W., Wang, L., Zhang, S., Du, J., Lin, D., Xu, M., Kreitzer, A. C., … Li, Y. (2018). A Genetically Encoded Fluorescent Sensor Enables Rapid and Specific Detection of Dopamine in Flies, Fish, and Mice. *Cell*, *174*(2). https://doi.org/10.1016/j.cell.2018.06.042

Tabor, K. M., Marquart, G. D., Hurt, C., Smith, T. S., Geoca, A. K., Bhandiwad, A. A., Subedi, A., Sinclair, J. L., Rose, H. M., Polys, N. F., & Burgess, H. A. (2019). Brain-wide cellular resolution imaging of Cre transgenic zebrafish lines for functional circuit-mapping. *ELife*, *8*. https://doi.org/10.7554/eLife.42687

Tabor, K. M., Smith, T. S., Brown, M., Bergeron, S. A., Briggman, K. L., & Burgess, H. A. (2018). Presynaptic Inhibition Selectively Gates Auditory Transmission to the Brainstem Startle Circuit. *Current Biology*, *28*(16). https://doi.org/10.1016/j.cub.2018.06.020

Tadres, D., & Louis, M. (2020). PiVR: An affordable and versatile closed-loop platform to study unrestrained sensorimotor behavior. *PLOS Biology*, *18*(7). https://doi.org/10.1371/journal.pbio.3000712

Talay, M., Richman, E. B., Snell, N. J., Hartmann, G. G., Fisher, J. D., Sorkaç, A., Santoyo, J. F., Chou-Freed, C., Nair, N., Johnson, M., Szymanski, J. R., & Barnea, G. (2017). Transsynaptic Mapping of Second-Order Taste Neurons in Flies by trans-Tango. *Neuron*, *96*(4). https://doi.org/10.1016/j.neuron.2017.10.011

Tao, L., Lauderdale, J. D., & Sornborger, A. T. (2011). Mapping functional connectivity between neuronal ensembles with larval zebrafsh transgenic for a ratiometric calcium indicator. *Frontiers in Neural Circuits*, *5*(FEB). https://doi.org/10.3389/fncir.2011.00002

Tomasello, D.L., Sive, H. (2020). Noninvasive Multielectrode Array for Brain and Spinal Cord Local Field Potential Recordings from Live Zebrafish Larvae. *Zebrafish 17*(4).http://doi.org/10.1089/zeb.2020.1874

Torigoe, M., Islam, T., Kakinuma, H., Fung, C. C. A., Isomura, T., Shimazaki, H., Aoki, T., Fukai, T., & Okamoto, H. (2021). Zebrafish capable of generating future state prediction

error show improved active avoidance behavior in virtual reality. *Nature Communications*, *12*(1). https://doi.org/10.1038/s41467-021-26010-7

Trivedi, C. A., & Bollmann, J. H. (2013). Visually driven chaining of elementary swim patterns into a goal-directed motor sequence: a virtual reality study of zebrafish prey capture. *Frontiers in Neural Circuits*, *7*. https://doi.org/10.3389/fncir.2013.00086

Tsuruwaka, Y., Konishi, T., Miyawaki, A., & Takagi, M. (2007). Real-Time Monitoring of Dynamic Intracellular Ca $^{2+}$ Movement During Early Embryogenesis Through Expression of Yellow Cameleon. *Zebrafish*, *4*(4). https://doi.org/10.1089/zeb.2007.0519

Vanwalleghem, G., Schuster, K., Taylor, M. A., Favre-Bulle, I. A., & Scott, E. K. (2020). Brain-Wide Mapping of Water Flow Perception in Zebrafish. *The Journal of Neuroscience*, *40*(21). https://doi.org/10.1523/JNEUROSCI.0049-20.2020

Vladimirov, N., Mu, Y., Kawashima, T., Bennett, D. V., Yang, C. T., Looger, L. L., Keller, P. J., Freeman, J., & Ahrens, M. B. (2014). Light-sheet functional imaging in fictively behaving zebrafish. In *Nature Methods* (Vol. 11, Issue 9, pp. 883–884). Nature Publishing Group. https://doi.org/10.1038/nmeth.3040

Wan, J., Peng, W., Li, X., Qian, T., Song, K., Zeng, J., Deng, F., Hao, S., Feng, J., Zhang, P., Zhang, Y., Zou, J., Pan, S., Shin, M., Venton, B. J., Zhu, J. J., Jing, M., Xu, M., & Li, Y. (2021). A genetically encoded sensor for measuring serotonin dynamics. *Nature Neuroscience*, *24*(5). https://doi.org/10.1038/s41593-021-00823-7

Wang, X., Roberts, P.A., Yoshimatsu, T., Lagnado, L., Baden, T. (2023). Amacrine cells differentially balance zebrafish color circuits in the central and peripheral retina. *Cell Reports 42*(1). https://doi.org/10.1016/j.celrep.2023.112055

Xu, Y., Zou, P., & Cohen, A. E. (2017). Voltage imaging with genetically encoded indicators. *Current Opinion in Chemical Biology*, *39*. https://doi.org/10.1016/j.cbpa.2017.04.005

Yang, E., Zwart, M. F., James, B., Rubinov, M., Wei, Z., Narayan, S., Vladimirov, N., Mensh, B. D., Fitzgerald, J. E., & Ahrens, M. B. (2022). A brainstem integrator for self-location memory and positional homeostasis in zebrafish. *Cell*, *185*(26). https://doi.org/10.1016/j.cell.2022.11.022

Zhang, Y., Rózsa, M., Liang, Y., Bushey, D., Wei, Z., Zheng, J., Reep, D., Broussard, G. J., Tsang, A., Tsegaye, G., Narayan, S., Obara, C. J., Lim, J.-X., Patel, R., Zhang, R., Ahrens, M. B., Turner, G. C., Wang, S. S.-H., Korff, W. L., … Looger, L. L. (2023). Fast and sensitive GCaMP calcium indicators for imaging neural populations. *Nature*, *615*(7954). https://doi.org/10.1038/s41586-023-05828-9

Chapter 5. Hyperactive mTORC1 disrupts habenula function and light preference in zebrafish model of Tuberous sclerosis complex

Olga Doszyn[1,2,3], Magdalena Kedra[1,3], Justyna Zmorzynska[1,2,4]

[1] Laboratory of Molecular and Cellular Neurobiology, International Institute of Molecular and Cell Biology in Warsaw, 02-109 Warsaw, Poland
[2] Laboratory of Developmental Neurobiology, International Institute of Molecular Mechanisms and Machines, 02-247 Warsaw, Poland
[3] equal contribution
[4] Lead contact

iScience, 2024 May 28; 27(6):110149.
DOI: 10.1016/j.isci.2024.110149.

Summary

Mechanistic target of rapamycin complex 1 (mTORC1) is an integration hub for extracellular and intracellular signals necessary for brain development. Hyperactive mTORC1 is found in autism spectrum disorder (ASD) characterized by atypical reactivity to sensory stimuli, among other symptoms. In Tuberous Sclerosis Complex (TSC) inactivating mutations in the *TSC1* or *TSC2* genes result in hyperactivation of the mTORC1 pathway and ASD. Here, we show that lack of light preference of the TSC zebrafish model, *tsc2*$^{vu242/vu242}$ is caused by aberrant processing of light stimuli in the left dorsal habenula and *tsc2*$^{vu242/vu242}$ fish have impaired function of the left dorsal habenula, in which neurons exhibited higher activity and lacked habituation to the light stimuli. These characteristics were rescued by rapamycin. We thus discovered that hyperactive mTorC1 caused aberrant habenula function resulting in lack of light preference. Our results suggest that mTORC1 hyperactivity contributes to atypical reactivity to sensory stimuli in ASD.

Key words: atypical reactivity to sensory stimuli, autism spectrum disorder, mTORC1 hyperactivation, habenula, Tuberous Sclerosis Complex (TSC)

Introduction

Mechanistic target of rapamycin complex 1 (mTORC1) is an integration hub for extracellular and intracellular signals that controls cell homeostasis by regulating translation, protein degradation, transcription, and cytoskeleton dynamics[1]. mTORC1 is necessary for proper brain development and coordinates proliferation, migration, differentiation, synaptogenesis, and neuronal activity[1]. Hyperactivation of mTORC1 is a hallmark of many developmental diseases linked to an increased risk of developing autism spectrum disorder (ASD), including fragile X syndrome, Angelman syndrome, PTEN-associated ASD or tuberous sclerosis complex[2,3,4,5]. Additionally, dysregulation of mTORC1-dependent signaling has been reported in cases of non-syndromic ASD, both in animal models as well as patients[6,7,8,9]. ASD has a prevalence of 1% in general population and its symptoms include social deficits, atypical reactivity to sensory stimuli, repetitive behaviors, and speech delay[10].

Tuberous Sclerosis Complex (TSC) is an exemplary genetic disease with mTORC1 hyperactivation. Inactivating mutations in the *TSC1* or *TSC2* genes cause lack of functional TSC1-TSC2 complex and result in hyperactivation of the mTORC1 pathway[1]. Patients with TSC suffer from epilepsy, benign tumors, and TSC-associated neuropsychiatric disorders (TANDs). TANDs include ASD and do not fully correlate with tumor or seizure burden[11]. Approximately 40% of the TSC patients develop ASD, which makes TSC the most frequent hereditary cause of ASD[12]. However, the underlying pathomechanisms of the TSC-associated ASD are still obscure.

Aberrant sensory processing leading to “sensory overload” is a hallmark of ASD[13], however, the mechanism underlying this deficit is not fully understood. Individuals with ASD often attempt to avoid visual stimulation[14] and show high levels of mTORC1 activity[2,3,4,5,6,7,8,9]. Here, we investigated light processing in the light preference paradigm in the zebrafish model of TSC[15] to identify mTorC1 as an underlying cause for aberrant activity of the left dorsal habenula (LdHb) and for atypical response to light in the light-preference test. Our results show that mTORC1 hyperactivity underlies atypical reactivity to light stimuli in TSC and link sensory deficits seen in TSC patients suffering from ASD with hyperactive mTORC1.

Results

The *tsc2*$^{vu242/vu242}$ mutants lack light preference behavior

It has been long reported that adult zebrafish, presented with a choice between a black and white chamber, exhibit a strong dark preference[16]. It has also been shown that in a light/gray choice, adult zebrafish prefer the less brightly lit chamber, while in a gray/dark choice, they show no preference, and spend equal amounts of time in both chambers. This avoidance of bright light by the adult zebrafish has been linked to anxiety, as it was attenuated by known anxiolytic compounds. However, in the case of larval zebrafish placed in a light/dark choice, one- and two-week-old fish have shown preference for the light compartment, suggesting that a reversal of the light/dark preference behavior occurs during development. Although the

precise mechanism underlying this choice reversal is not known, it has been established that wild-type adult zebrafish show light avoidance, while wild-type larval zebrafish show light preference[17]. The light-preference assay measures anxiety by comparing times spent in the light and dark compartments. Increased preference for light of zebrafish larvae is indicative of anxiety-like behavior. We have previously shown that the *tsc2*$^{vu242/vu242}$ mutant zebrafish exhibit anxiety-like behavior and have elevated cortisol levels[18]. However, in the light-preference assay, the *tsc2*$^{vu242/vu242}$ fish exhibited decreased light preference compared to wild-type (wt) siblings, which strongly preferred the light compartment (Figure 1A-B). The total time moving was similar among genotypes (Figure 1D). The lack of light preference of the *tsc2*$^{vu242/vu242}$ fish was not prevented by pretreatment with anxiolytic drug ANA-12 (Figure 1B-C, Figure S1A). We have shown before that ANA-12 rescued anxiety-like behaviors of the *tsc2*$^{vu242/vu242}$ fish[18]. Thus, the lack of light preference was not likely to be associated with anxiety. Moreover, the *tsc2*$^{vu242/vu242}$ mutants did not have major developmental defects (Figure S1B) or visual problems as they responded to light changes similarly as siblings in the sudden-light-changes assay (Figure S1C-E). The lack of preference for light of the *tsc2*$^{vu242/vu242}$ fish was also not changed by treatment with an anti-epileptic drug vigabatrin (VGB) (Figure 1B-C). Interestingly, the pretreatment with a direct mTorC1 inhibitor rapamycin reversed the aberrant light response of the *tsc2*$^{vu242/vu242}$ mutants in the light-preference test (Figure 1B-C). These results led us to the hypothesis that hyperactive mTorC1 underlies the lack of light-preference of the *tsc2*$^{vu242/vu242}$ fish.

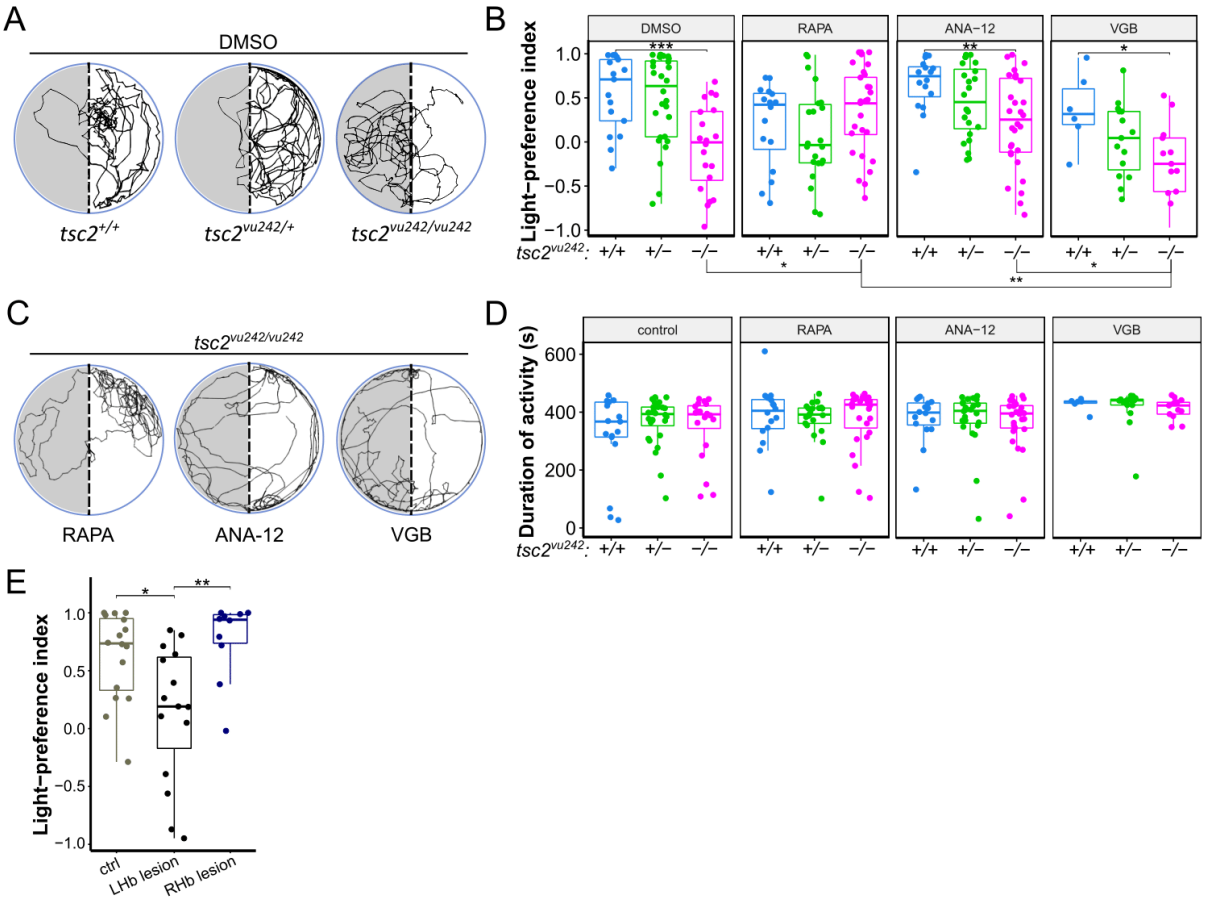

Figure 1. Light-preference test in *tsc2*^{vu242} fish.
(A) Exemplary tracks of *tsc2*^{vu242} fish from the light-preference test. (B) Light-preference index of *tsc2*^{vu242} fish after various treatments (*tsc2*$^{vu242/vu242}$ *vs.* *tsc2*$^{+/+}$: $p = 0.0009$ for DMSO, $p = 0.588$ for rapamycin (RAPA), $p = 0.005$ for ANA-12, $p = 0.044$ for vigabatrin (VGB); for *tsc2*$^{vu242/vu242}$ treated with DMSO *vs.* RAPA $p = 0.048$). The dots on the boxplots represent the number of fish in the experiment (N > 10 per experimental group, except VGB *tsc2*$^{+/+}$ where N = 6). (C) Exemplary tracks of *tsc2*$^{vu242/vu242}$ mutant treated with RAPA, ANA-12, or VGB from the light-preference test. (D) Cumulative activity of *tsc2*^{vu242} fish during the light-preference test. The dots on the boxplots represent the number of fish in the experiment (N > 10 per experimental group, except VGB *tsc2*$^{+/+}$ where N = 6). (E) Light-preference index of wt fish without lesions and with lesion of left (LHb) or right (Rhb) habenula (unlesioned *vs.* lesion of the left habenula: $p = 0.019$, lesion of the left habenula *vs.* lesion of the right habenula: $p = 0.009$). The dots on the boxplots represent the number of fish in the experiment (N > 10 per experimental group). See also Figure S1.

Neurons in the left dorsal habenula of *tsc2*$^{vu242/vu242}$ mutants show mTorC1 hyperactivation and aberrant response to light stimuli

The lack of light preference of the *tsc2*$^{vu242/vu242}$ fish, otherwise exhibiting increased anxiety-like behaviors, can be indicative of impaired sensory processing of the light stimulus. Habenula integrates various stimuli and regulates light-preference behavior[19,20,21]. We also confirmed that impairment of LdHb results in a lack of light preference in wt zebrafish (Figure 1E, Figure S1F). To test for mTorC1 hyperactivation in habenulae of the *tsc2*$^{vu242/vu242}$ mutants, we checked phosphorylation levels of mTORC1 downstream target: ribosomal protein s6 (Rps6). We found that the number of cells positive for phosphorylated Rps6 (pRps6) in the *tsc2*$^{vu242/vu242}$ mutants was increased specifically in the left dorsal habenula (LdHb) compared to wt siblings (Figure 2A-B). Also, the pRps6 intensity levels per cell were higher in the *tsc2*$^{vu242/vu242}$ LdHb neurons than in the wt fish (Figure 2C). The pRps6 levels were decreased after rapamycin pretreatment in both *tsc2*$^{vu242/vu242}$ and wt siblings (Figure 2A-C).

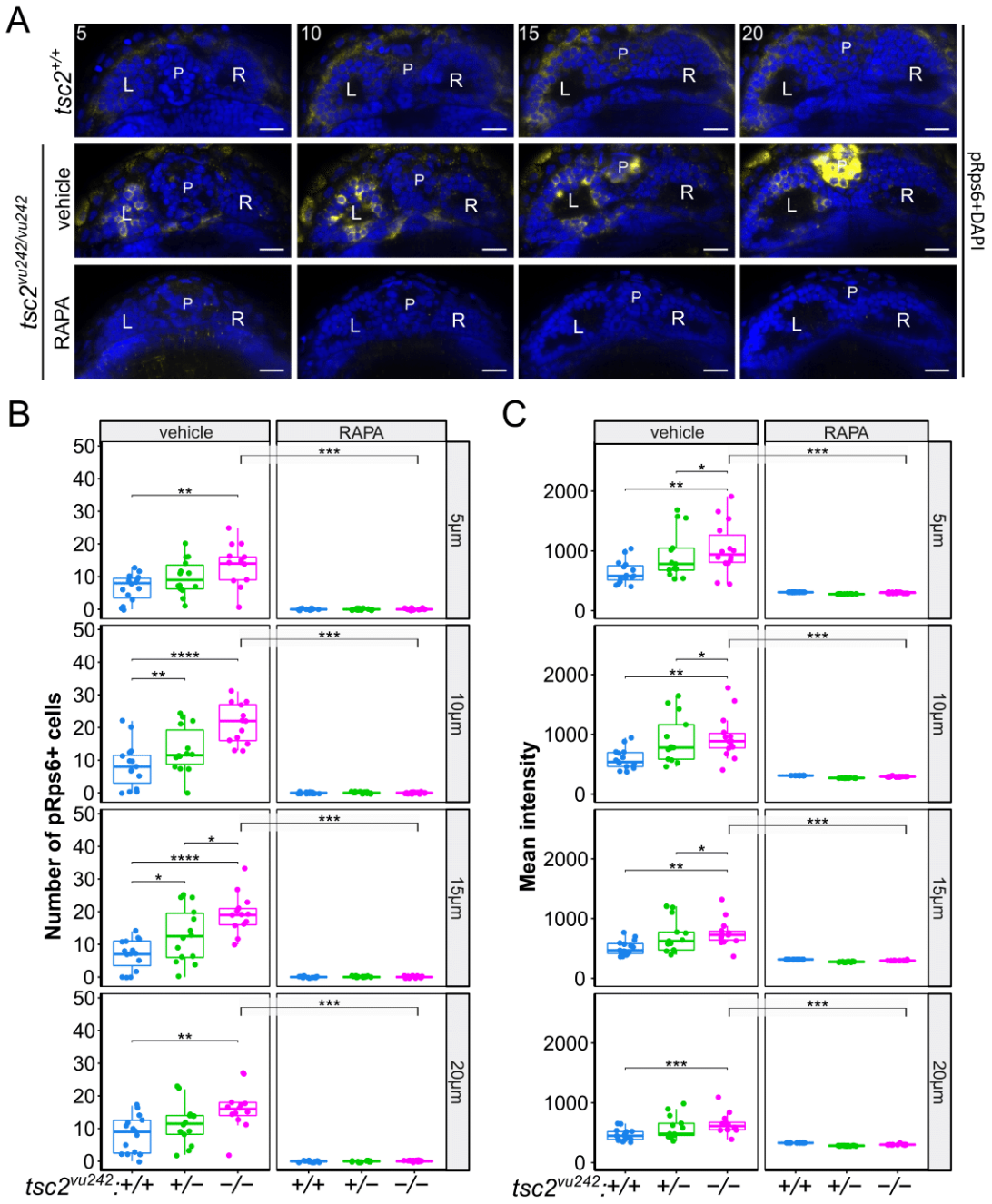

Figure 2. mTorC1 activation in *tsc2*^{vu242} fish habenulas.

(A) Representative optical sections through habenula of *tsc2*$^{vu242/vu242}$ fish and their wild-type *tsc2*$^{+/+}$ siblings at 5, 10, 15, and 20 μm from the top. pRps6 – yellow, nuclei – blue. L – left habenula, R – right habenula, P – pineal complex. Scale bars, 20 μm. (B) Number of pRps6-positive cells in LdHb of *tsc2*^{vu242} fish (5 μm: *tsc2*$^{vu242/vu242}$ control *vs.* *tsc2*$^{+/+}$ control p = 0.004 and *vs.* *tsc2*$^{vu242/vu242}$ treated with RAPA $p = 1.038 \times 10^{-5}$; 10 μm: *tsc2*$^{vu242/vu242}$ control *vs.* *tsc2*$^{+/+}$ control $p = 4.656 \times 10^{-5}$ and *vs.* *tsc2*$^{vu242/vu242}$ treated with RAPA $p = 1.038 \times 10^{-5}$; 15 μm: *tsc2*$^{vu242/vu242}$ control *vs.* *tsc2*$^{+/+}$ control $p = 1.584 \times 10^{-5}$ and *vs.* *tsc2*$^{vu242/vu242}$ treated with RAPA $p = 1.038 \times 10^{-5}$; 20 μm: *tsc2*$^{vu242/vu242}$ control *vs.* *tsc2*$^{+/+}$ control p = 0.004 and *vs.* *tsc2*$^{vu242/vu242}$ treated with RAPA $p = 1.038 \times 10^{-5}$). The dots on the boxplots represent the number of fish in

the experiment (N > 10 per experimental group). (C) Quantification of mean intensity of pRps6 fluorescence from LdHb of *tsc2*^{vu242} fish (5 μm: *tsc2*$^{vu242/vu242}$ control *vs.* *tsc2*$^{+/+}$ control $p = 0.0051$ and *vs.* *tsc2*$^{vu242/vu242}$ treated with RAPA $p = 1.0912 \times 10^{-5}$; 10 μm: *tsc2*$^{vu242/vu242}$ control *vs.* *tsc2*$^{+/+}$ control $p = 0.0017$ and *vs.* *tsc2*$^{vu242/vu242}$ treated with RAPA $p = 1.0912 \times 10^{-5}$; 15 μm: *tsc2*$^{vu242/vu242}$ control *vs.* *tsc2*$^{+/+}$ control $p = 0.001$ and *vs.* *tsc2*$^{vu242/vu242}$ treated with RAPA $p = 1.0912 \times 10^{-5}$; 20 μm: *tsc2*$^{vu242/vu242}$ control *vs.* *tsc2*$^{+/+}$ control $p = 0.0007$ and *vs.* *tsc2*$^{vu242/vu242}$ treated with RAPA $p = 1.0912 \times 10^{-5}$). The dots on the boxplots represent the number of fish in the experiment (N > 10 per experimental group).

LdHb contains light-responsive neurons and is responsible for mediating light-preference behavior in zebrafish larvae[19,21]. We performed 3D time-lapse imaging of the activity of LdHb neurons in *Tg(HuC:GCaMP5G);tsc2*^{vu242} expressing GCaMP5G calcium indicator under neuron-specific promoter. The single-cell analysis revealed that neuronal activity in LdHb was increased in *tsc2*$^{vu242/vu242}$ compared to wt siblings (Figure 3A-D). With analysis of neuronal activity dynamics across time, we discovered that the activity of light-responsive neurons in the most dorsal layers increased after light stimulation in the wt LdHb but decreased over time, indicative of habituation to constant light stimulus. In contrast, the activity of neurons in the *tsc2*$^{vu242/vu242}$ LdHb was lower at the initial stimulation but increased over time (Figure 3C-D, Figure S2). Rapamycin pretreatment normalized neuronal activity of the *tsc2*$^{vu242/vu242}$ LdHb (Figure 3E-F, Figure S2) implicating mTorC1 hyperactivation in the aberrant LdHb activity.

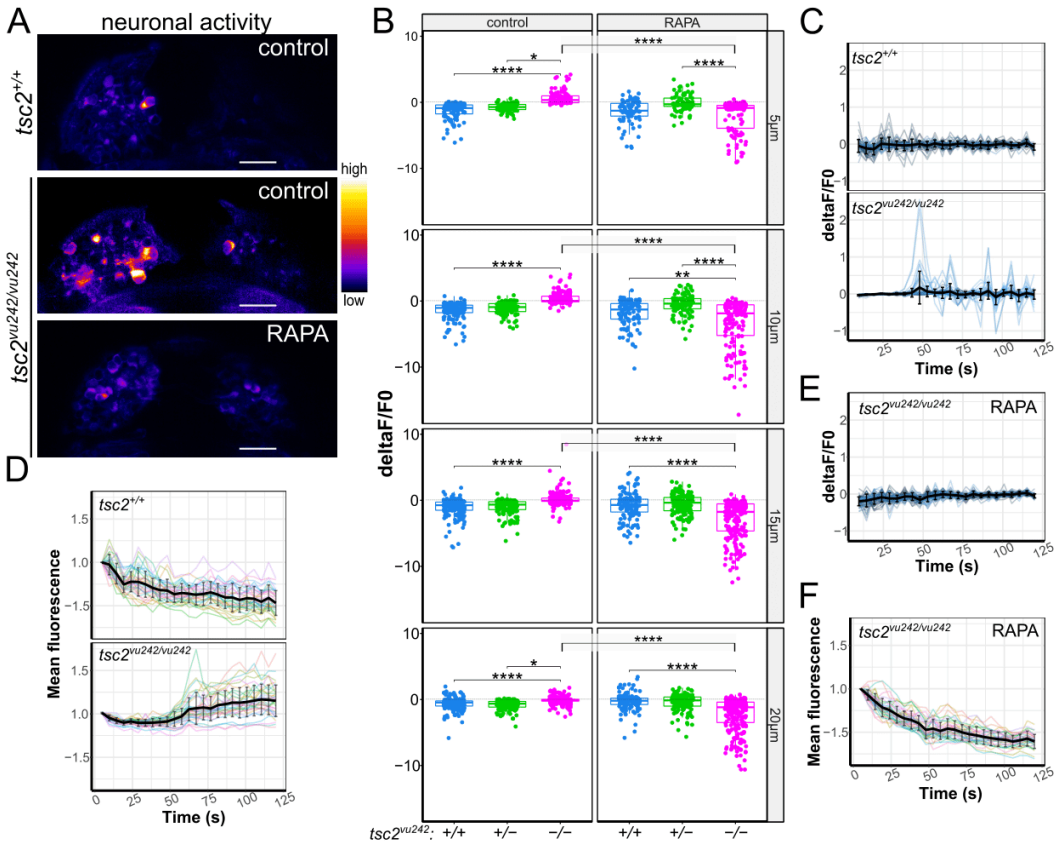

Figure 3. Neuronal activity in LdHb of *tsc2*^{vu242} fish.

(A) Representative images of neuronal activity in the habenulae of *tsc2*^{vu242} fish at 10 µm from the top. Scale bars, 20 µm. (B) Cumulative activity of the *tsc2*^{vu242} LdHb for all the layers of LdHb (5 µm: *tsc2*$^{vu242/vu242}$ control *vs.* *tsc2*$^{+/+}$ control $p = 6.528 \times 10^{-33}$ and *vs.* *tsc2*$^{vu242/vu242}$ treated with RAPA $p = 5.958 \times 10^{-34}$; 10 µm: *tsc2*$^{vu242/vu242}$ control *vs.* *tsc2*$^{+/+}$ control $p = 1.1232 \times 10^{-44}$ and *vs.* *tsc2*$^{vu242/vu242}$ treated with RAPA $p = 1.625 \times 10^{-47}$; 15 µm: *tsc2*$^{vu242/vu242}$ control *vs.* *tsc2*$^{+/+}$ control $p = 5.928 \times 10^{-31}$ and *vs.* *tsc2*$^{vu242/vu242}$ treated with RAPA $p = 4.68 \times 10^{-52}$; 20 µm: *tsc2*$^{vu242/vu242}$ control *vs.* *tsc2*$^{+/+}$ control $p = 1.104 \times 10^{-14}$ and *vs.* *tsc2*$^{vu242/vu242}$ treated with RAPA $p = 5.958 \times 10^{-34}$). Dots on boxplots represent single cells. (C) Neuronal activity change over time in the *tsc2*^{vu242} LdHb at 10 µm from the top. (D) Normalized mean GCaMP5F fluorescence over time in the *tsc2*^{vu242} LdHb at 10 µm from the top. (E) Neuronal activity change over time in the *tsc2*$^{vu242/vu242}$ mutant's LdHb at 10 µm from the top after RAPA pretreatment. (F) Normalized mean GCaMP5F fluorescence over time in the *tsc2*$^{vu242/vu242}$ mutant's LdHb at 10 µm from the top after RAPA. (C-F) The mean with SD is shown in black.

7 fish per genotype per treatment were analysed (N = 7 per experimental group). See also Figure S2.

mTorC1 hyperactivation in the left dorsal habenula causes lack of light-preference behavior of the *tsc2*$^{vu242/vu242}$ fish

To address further the involvement of hyperactive mTorC1 in LdHb in controlling light preference behavior of the *tsc2*$^{vu242/vu242}$ mutants, we microinjected rapamycin directly into the left habenula to locally inhibit mTorC1. The singular injection at 4 dpf did not change mTorC1 lactivation levels at 5 dpf (Figure S3A), thus we injected rapamycin on two consecutive days, at 3 dpf and 4 dpf (Figure S3B-C) and then we tested the injected fish for light preference at 5 dpf. The vehicle-injected *tsc2*$^{vu242/vu242}$ fish showed lack of light preference behavior similarly to uninjected mutants and rapamycin injection rescued this impairment (Figure 4A-D, Figure S3). The *tsc2*^{vu242} fish showed normal habenula morphology after injections and similar duration of activity during the light-preference test (Figure S3C-D). Analysis of fish activity over time showed that the light-preference index of the *tsc2*$^{vu242/vu242}$ mutants decreases over time during first two minutes of analysis (Figure 4D) indicating that they have high preference for dark compartment or aversion to light. After 200 s, the light-preference index of the *tsc2*$^{vu242/vu242}$ fish increased slightly but still stayed at the negative level (Figure 4D). This impairment was rescued by rapamycin injection into the LdHb.

The left habenula receives afferent inputs from the eminentia thalami (EmT), the pallium through stria medullaris (SM), and from the right habenula through the habenula commissure (HC)[19]. Therefore, we investigated the development of these afferents in the *tsc2*$^{vu242/vu242}$ mutants as their alterations could facilitate impaired LdHb function. The EmT fibers that innervate LdHb are calretinin-positive, thus, we checked anti-calretinin immunofluorescence in the LdHb in whole-mount brain preparations. We determined that the mean intensity of the anti-calretinin signal was similar across genotypes (Figure 4E), suggesting proper innervation of LdHb by EmT in the *tsc2*$^{vu242/vu242}$ fish. The immunofluorescence staining against acetylated Tubulin (AcTub) revealed that the lateral input to habenulae through SM was not significantly changed in *tsc2*$^{vu242/vu242}$ compared to wt (Figure 4F). However, the HC was thinner in the *tsc2*$^{vu242/vu242}$ fish compared to the wt siblings, and pretreatment with rapamycin reversed this to its proper width (Figure 4G-H) indicating that the right habenula input to LdHb may be involved in the LdHb aberrant function.

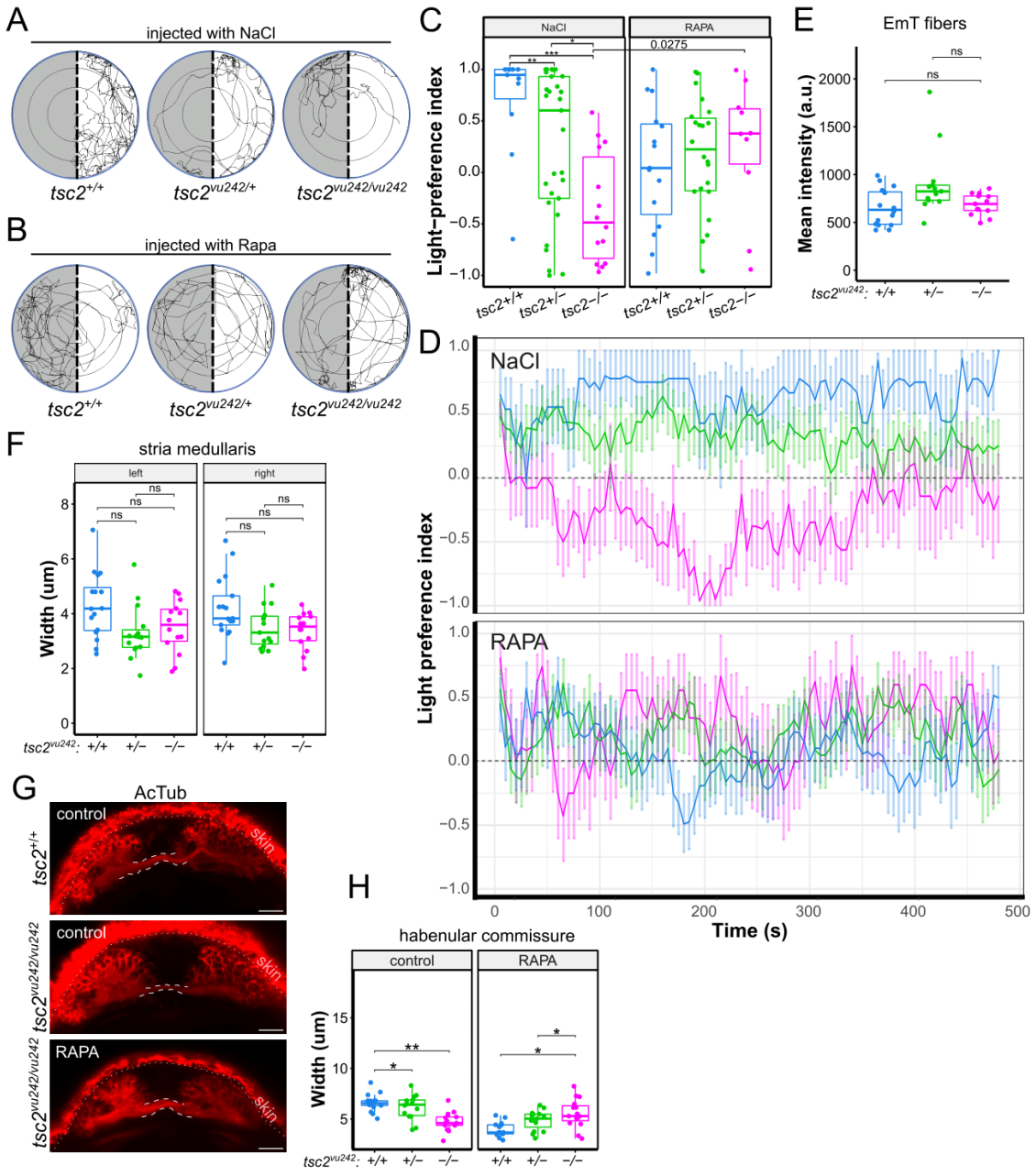

Figure 4. Rapamycin injections to the left habenula and afferent connectivity of LdHb in *tsc2*^{vu242} fish.

(A) Exemplary tracks of the *tsc2*^{vu242} fish injected to the left habenula with NaCl from the light-preference test. (B) Exemplary tracks of the *tsc2*^{vu242} fish injected to the left habenula with 1 µM rapamycin (Rapa) from the light-preference test. (C) Light-preference index of the *tsc2*^{vu242} fish after injections to the left habenula (*tsc2*$^{vu242/vu242}$ *vs.* *tsc2*$^{+/+}$: $p = 0.00015$ and *vs.* *tsc2*$^{+/-}$: $p = 0.006$ for NaCl, $p = ns$ for rapamycin (RAPA); *tsc2*$^{vu242/vu242}$ fish injected with RAPA *vs.* NaCl: $p = 0.0275$). The dots on the boxplots represent the number of fish in the experiment (N > 10 per experimental group). (D) Analysis of light-preference index over time of the *tsc2*^{vu242} fish after injections to the left habenula (data presented as mean ± SD). (E) Mean intensity of calretinin fluorescence in the left habenulae of the *tsc2*^{vu242} fish. The dots on the boxplots represent the number of fish in the experiment (N > 10 per experimental

group). (F) Width of SM in the *tsc2*^{vu242} fish brains. The dots on the boxplots represent the number of fish in the experiment (N > 10 per experimental group). (G) Representative horizontal optical sections through HC (outlined) of the *tsc2*^{vu242} fish (projection of 8 z-stacks). Scale bars, 20 μm. (H) HC width of the *tsc2*^{vu242} fish (*tsc2*$^{vu242/vu242}$ *vs.* *tsc2*$^{+/+}$: p = 0.002 for DMSO, p = 0.011 for RAPA). The dots on the boxplots represent the number of fish in the experiment (N > 10 per experimental group). See also Figure S3.

Discussion

We have shown that aberrant activity of the LdHb neurons was associated with hyperactivation of the mTorC1 pathway and decreased light preference in the *tsc2*$^{vu242/vu242}$ mutants. The involvement of mTORC1 in neuronal activity is well documented and hyperactive mTORC1 consistently produces neuronal hyperexcitability and seizures[22]. The increased neuronal activity of LdHb neurons in *tsc2*$^{vu242/vu242}$ can be indicative of decreased activation threshold which is seen in the pallium of *tsc2*$^{vu242/vu242}$ and is responsible for seizures[18]. However, anti-epileptic VGB did not rescue light-preference behavior and rapamycin did reverse both, increased neuronal activity of LdHb neurons and light-preference behavior in the *tsc2*$^{vu242/vu242}$ fish, suggesting that LdHb activity is not induced by seizures. Instead, hyperactive mTorC1 causes aberrant LdHb function and impairs sensory integration resulting in the lack of light preference of the *tsc2*$^{vu242/vu242}$ fish. LdHb integrates light stimuli from EmT and the right habenula with other inputs to produce light-preference behavior. In older zebrafish larvae, deactivation of LdHb by botulinum toxin decreased light preference, and activation of LdHb by optogenetic approach resulted in a preference for light in the wt zebrafish[21]. We also confirmed that deactivation of the left habenula decreases preference for light in the wt fish. In the *tsc2*$^{vu242/vu242}$ fish, however, the LdHb activity is impaired – low at initial stimulation, but increasing in time. It suggests that the threshold for activation may be higher but results in higher neuronal activity when crossed or that the habituation to the light stimulus is impaired. This in turn may cause aversion to the light stimulus and result in lack of light-preference behavior. It is possible that intracellular signaling pathways are abnormally functioning due to hyperactive mTorC1 and therefore the synaptic inputs to LdHb in the *tsc2*$^{vu242/vu242}$ fish are not integrated properly or timely.

However, caution should be taken when administering rapamycin or rapamycin derivatives (sirolimus and everolimus) to ASD patients without diagnosed genetic mutation linked to mTORC1 hyperactivity and we suggest that the levels of mTORC1 activation should be checked beforehand as rapamycin may exert some toxic effects. We have observed that after rapamycin treatment, wt fish loose the light preference while the *tsc2*$^{vu242/vu242}$ mutant fish show restored light-preference behavior. Rapamycin was previously reported to have deleterious effects on wt animals[23]. Rapamycin treatment resulted in highly exaggerated neuronal activity induced by kainic acid and induced brain morphology changes in wildtype rats[24]. Also in patients, rapamycin derivatives (sirolimus and everolimus), which are often used in cancer or after transplantation, exerted adverse effects when administered

systemically[25,26,27]. Consistently with this data, our results also show smaller habenulas after treatment with rapamycin. However, the loss of light preference of wt fish after rapamycin pretreatment may not have been associated with habenula function as the neuronal activity of habenular neurons was not distinguishable from wt fish treated with vehicle. Our results strongly link atypical sensory reactivity to light with hyperactive mTorC1 and suggest that rapamycin derivatives can be used to prevent atypical reactivity to sensory stimuli in ASD with hyperactivated mTorC1.

Limitations of the study

Modeling human diseases in zebrafish offers numerous advantages due to their genetic similarity and ease of manipulation, however, there are also limitations to consider. Zebrafish have a simpler nervous system and behavioral repertoire compared to humans. While they can display basic behaviors like response to light or movement, studying complex cognitive or emotional behaviors that are relevant to human psychiatric disorders such as ASD is challenging. Zebrafish may also metabolize drugs differently than humans, which can affect the efficacy and toxicity of potential treatments studied in zebrafish models. This can complicate translation of findings to human clinical trials. Zebrafish embryos develop externally, which allows for easier observation of development but the placental environment may serve a very important role in fetal brain development concerning ASD and TSC. Many human diseases are multifaceted and involve interactions between genetic, environmental, and lifestyle factors. Zebrafish models may oversimplify these interactions due to their controlled laboratory environment. Despite these limitations, zebrafish remain a valuable model organism for studying certain aspects of human disorders, especially in areas like developmental biology, genetics, and basic biological processes. Complementary studies using other model organisms and human cell-based assays are needed to validate findings and bridge the gap between zebrafish research and clinical applications.

Acknowledgments
We thank Kevin Ess (Vanderbilt University) for the *tsc2*$^{vu242/+}$ line and Michael Orger (Champalimaud Foundation) for the *Tg(HuC:GCaMP5G)* line, the IIMCB ZCF for assistance with the adult fish, and the IIMCB MCF for sharing the Lightsheet Z.1. This work was supported by an OPUS grant no. 2020/37/B/NZ3/02345 (JZ) and an ETIUDA grant no. 2020/36/T/NZ3/00132 (MK), both from National Science Centre, Poland.

Author Contributions (CRediT): OD: Investigation, Formal analysis (Fig.1-4), Writing – Review & Editing; MK: Investigation, Formal analysis (Fig.1); JZ: Conceptualization, Investigation, Formal analysis, Writing – Original Draft, Writing – Review & Editing, Visualization, Supervision, Project administration, Funding acquisition.

Declaration of Interests
The authors declare no competing interests.

STAR Methods

Key Resource Table

REAGENT or RESOURCE	SOURCE	IDENTIFIER
Antibodies		
Mouse monoclonal anti-acetyl-Lys40-Tubulin	GeneTex	Cat# GTX16292; RRID:AB_2887530
Rabbit polyclonal anti-Calretinin	SWant	Cat# 7697; RRID:AB_2721226
Rabbit polyclonal anti-pRps6 (Ser235/236)	Cell Signaling Technology	Cat# CS4858; RRID:AB_916156
Goat anti-Mouse IgG (H+L) Cross-Adsorbed Secondary Antibody, Alexa Fluor™ 568	Thermo Fisher Scientific	Cat# A-11004; RRID:AB_2534072
Goat anti-Rabbit IgG (H+L) Cross-Adsorbed Secondary Antibody, Alexa Fluor™ 488	Thermo Fisher Scientific	Cat# A-11008; RRID:AB_143165
Chemicals, peptides, and recombinant proteins		
ANA-12	Sigma-Aldrich/Merck	Cat# SML0209
Dimethyl sulfoxide	Sigma-Aldrich/Merck	Cat# D8418
E3 medium (for neuronal in vivo models): NaCl (sodium chloride) KCl (potassium chloride) CaCl2 (calcium chloride) MgCl2 (magnesium chloride)	Chempur	 Cat# 117941206 Cat# 117397402 Cat# 118748703 Cat# 116120500
Formaldehyde	Sigma-Aldrich/Merck	Cat# 47608
Glycerol	Sigma-Aldrich/Merck	Cat# G5516
Goat serum	Sigma-Aldrich/Merck	Cat# G9023
Heparin sodium salt from porcine intestinal mucosa	Sigma-Aldrich/Merck	Cat# H3149
Phenol Red	Sigma-Aldrich/Merck	Cat# P0290
Rapamycin	Sigma-Aldrich/Merck	Cat# 553210
RT PCR Mix EvaGreen®	A&A Biotechnology	Cat# 2008

TopVision low melting point agarose	Thermo Fisher Scientific	Cat# R0801
Tricaine	Sigma-Aldrich/Merck	Cat# E10521
Triton™ X-100	Sigma-Aldrich/Merck	Cat# T8787
Tween®20	Sigma-Aldrich/Merck	Cat# P1379
Vigabatrin	Sigma-Aldrich/Merck	Cat# V8261
Deposited data		
Raw and analyzed data	This paper	N/A
Experimental models: Organisms/strains		
Zebrafish: mixed wild-type strain AB/ TL	Zebrafish Core Facility, International Institute of Molecular and Cell Biology in Warsaw	ZFIN:ZDB-GENO-031202-1
Zebrafish: Tg(HuC:GCaMP5G);tsc2$^{vu242/+}$	Kedra et al.	N/A
Zebrafish: tsc2$^{vu242/+}$	Kim et al.	RRID:ZFIN_ZDB-GENO-180906-3
Zebrafish: tsc2$^{vu242/\ vu242}$	Kim et al.	RRID:ZFIN_ZDB-GENO-190115-9
Oligonucleotides		
Primer *tsc2* for HRM genotyping, Forward: GAGACCTGCCTGGACATGAT	Doszyn et al.	N/A
Primer *tsc2* for HRM genotyping, Reverse: CTTGGGCAGAGCAGAGAAGT	Doszyn et al.	N/A
Software and algorithms		
Fiji	Schindelin et al.	https://fiji.sc/
R 4.3.2	R Foundation for Statistical Computing	https://www.R-project.org
RStudio	Posit Software, PBC	https://posit.co/download/rstudio-desktop/
ZebraLab version 3.22	ViewPoint Behavior Technology	https://www.viewpoint.fr/product/zebrafish/fish-behavior-monitoring/zebralab
ZEN2014 SP1 (black edition)	Zeiss	https://www.micro-shop.zeiss.com/en/us/softwarefinder/software-categories/zen-black
Other		

Cokin CREATIVE light-absorbing photographic filters: Neutral grey ND4 – 0.6, Medium size Neutral grey ND8 – 0.9, Medium size	Cokin	 Cat# P153 Cat# P154
Borosilicate glass capillaries 0.75 mm inner diameter	Sutter Instruments	Cat# BF150-75-10
Lightsheet Z.1 microscope	Zeiss	https://www.zeiss.com/microscopy/en/products/light-microscopes/light-sheet-microscopes.html
ZebraBox	ViewPoint Behavior Technology	https://www.viewpoint.fr/product/zebrafish/fish-behavior-monitoring/zebrabox

Resource availability

Lead contact

Further information and requests for resources and reagents should be directed to and will be fulfilled by the Lead Contact, Justyna Zmorzynska (j.zmorzynska@imol.institute).

Materials Availability

This study did not generate new unique reagents. The fish mutant and transgenic lines are protected under material transfer agreement with the institutions that generated the lines. Upon appropriate agreement with these institutions, they can be requested from the Lead Contact.

Data and code availability

• Data: All data is included in the manuscript. Microscopy data reported in this paper will be shared by the lead contact upon request.
• Code: This paper does not report original code.
• Additional information: Any additional information required to reanalyze the data reported in this paper is available from the lead contact upon request.

Experimental Model and Study Participant details

Zebrafish breeding and genotyping

The following lines were used: *tsc2*$^{vu242/+}$ [15], wild-type (mixed strain AB x TL), and *Tg(HuC:GCaMP5G);tsc2*$^{vu242/+}$ [18,28]. Adult and larval zebrafish were bred according to international standards. Zebrafish larvae used in this study were up to 5 dpf and had no specified sex yet. All experiments performed were conducted in accordance with the Act of 15 January 2015 on the protection of animals used for scientific and educational purposes, Directive 2010/63/EU of the European Parliament and of the Council of 22 September 2010 on the protection of animals used for scientific purposes and were approved by the Animal

Welfare Commission of the IIMCB. The larvae were genotyped by PCR and high resolution melting technique using primers listed in the KeyResource Table[18,29]. Genotyping was performed after collection of behavioral or imaging data in live experiments or after collection of zebrafish heads for immunofluorescence (the tails were used for genotyping). Offspring of at least two parental pairs were used in each experiment.

Drug treatments

To prepare stock solutions, drugs were dissolved in E3 (5 mM NaCl, 0.17 mM KCl, 0.33 mM $CaCl_2$, 0.33 mM $MgSO_4$) or dimethylsulfoxide (DMSO) and were further diluted in E3 or in NaCl (for injections into the habenula). Drugs were administered directly into E3 with the same number of dechorionated fish. Treatments included: 200 nM rapamycin (Sigma-Aldrich/Merck, #553210) from 2 days post-fertilization (dpf), 50 nM ANA-12 or 60 μM VGB (both from Sigma-Aldrich/Merck, Darmstadt, Germany) 24 hours before the behavioral test. For injections into the habenula, 1 μM rapamycin was used.

Method details

Light-preference assay

Light-preference test was performed using live monitoring system Zebrabox (Viewpoint). One fish at a time was tracked in a Petri dish with half of a dish covered with light-absorbing photographic filters (ND4+ND8, Cokin.com) to produce darkness. Tracking was done for 8 min[18]. Lack of movement of the *tsc2*$^{vu242/vu242}$ mutants was mapped to non-motor seizures before[18], thus, not moving fish were excluded from the analysis. The light preference index was calculated as cumulative time spent in the dark compartment subtracted from cumulative time spent in the light compartment and divided by the total time of movement ((L-D)/(L+D)) as previously[21].

Habenula lesion

A borosillicate glass capillary (0.75 mm inner diameter, Sutter Instruments) was heat-pulled to obtain a micropipette with an open tip of ~15 μm. At 4 dpf, fish were sedated with 0.01% Tricaine (E10521, Sigma-Aldrich) and immobilized in 1% low-melting point agarose (Thermo Fisher Scientific) with head facing up. The habenulae were lesioned with the micropipette under a microscope to visualize the region with high accuracy. After 3-4 hours, the fish were freed from agarose and moved to E3 medium without Tricaine. At 5 dpf, the fish were tested for light preference and then fixed in 4% formaldehyde for habenula morphology analysis.

Whole-mount immunofluorescence

Heads of zebrafish larvae were fixed in 4% formaldehyde at 5 dpf (overnight at 4°C). Samples were bleached in freshly prepared 3% KOH, 1% H_2O_2 solution, permeabilized with PBS containing 0.2% Triton X-100, 20% DMSO, and 0.1% Tween-20, blocked with 3% bovine serum albumin and 10% goat serum, incubated with primary antibodies (anti-pRps6 antibody (Ser235/236), 1:200, CS4858, Cell Signaling Technology, RRID:AB_916156; anti-calretinin, 1:400, CR7697, Swant, RRID:AB_2721226; anti-acetyl-Lys40-tubulin, 1:100,

GTX16292, Genetex, RRID:AB_2887530) in PBS-Hep solution (PBS suplemented with 0.2% Tween-20 and 10 µg/ml heparin) at room temperature for 72 hours, washed overnight with PBS-Hep, incubated with secondary antibodies (goat anti-mouse Alexa Fluor 568, 1:1000, or goat anti-rabbit, Alexa Fluor 488, 1:1000, both from Thermo Fisher Scientific) in PBS-Hep for 48 hours, washed again, and mounted.

Microinjections into the habenula

A borosillicate glass capillary (0.75 mm inner diameter, Sutter Instruments) was heat-pulled to obtain a micropipette with an open tip of ~3 µm. The drop was set to 0.5 nL. At 3 and 4 dpf, fish were sedated with 0.01% Tricaine (E10521, Sigma Aldrich) and immobilized in 1% low-melting point agarose (Thermofisher Scientific) with head facing up. Then the solutions (0.9% NaCl or 1 µM rapamycin, containing 0.05% Phenol Red (Sigma-Aldrich) for visualization) were microinjected into the left habenula – the micropipette was inserted between the habenula and the blood vessel surrounding it. 4 drops were administered with 20 sec intervals. After 3-4 hours, the fish were freed from agarose and moved to E3 medium without Tricaine. At 5 dpf, the fish were tested for light preference and then fixed in 4% formaldehyde for whole-mount immunofluorescence.

Imaging

Images were acquired using a Zeiss Lightsheet Z.1 microscope (40✧ water immersion objective, NA = 1.3) at 1024 × 1024 pixel-resolution. Z-stacks of the images were taken with an interval of 0.5 µm for fixed samples and 1 µm for live imaging. The 3D time-lapse images were recorded every 5s for 2 min. at 28.5°C at 4 dpf. Time-lapse images included both habenulae and had an approximate range of 100 µm.

Quantification and Statistical analysis

Image analyses

Image analyses were performed using Fiji software. For pRps6, AcTub, and calretinin measurements, regions of interest (ROIs) were drawn manually and cell size, fluorescence intensity, or fiber width were measured using the measurement tool. For neuronal activity analysis, drift correction was performed using the Tischer script embedded in the Fiji software, ROIs were applied manually, measured using the measurement tool in Fiji, and then the fluorescence intensity and derivative (deltaF/F0, where F0 is the minimal intensity value of the cell) were calculated with Rstudio (cran.r-project.org; rstudio.com). All LdHb neurons from 7 fish per genotype per treatment were included in the analysis.

Statistical analysis

No predetermination of sample sizes was performed because the number of each genotype could not be predicted due to the random distribution and the early lethality of homozygotes (as previously reported[18]). Equality of variance and normality of residuals were assessed using Levene's test and Shapiro-Wilk test, respectively. Because these assumptions were not met, data were analyzed by Kruskal-Wallis test with *post-hoc* Wilcoxon test to correct for multiple comparisons. The adjusted $p < 0.05$ was considered statistically significant. Data are

presented as medians using boxplots with dots representing data points. Data points outside of boxplots and their whiskers are outliers. In majority of analyses, number of dots represent number of animals included (1 dot is 1 fish) – except for single-cell calcium imaging analysis where 7 fish per genotype per treatment were included. Adjusted p-values are reported on figures with * for $p < 0.05$, ** for $p < 0.01$, *** for $p < 0.001$, and **** for $p < 0.0001$. In most cases, randomization and blinding was assured by lack of knowledge about the genotypes while performing the experiments or collecting the fish for immunofluorescence. All data were analyzed with Rstudio.

Supplementary Figures 1-4

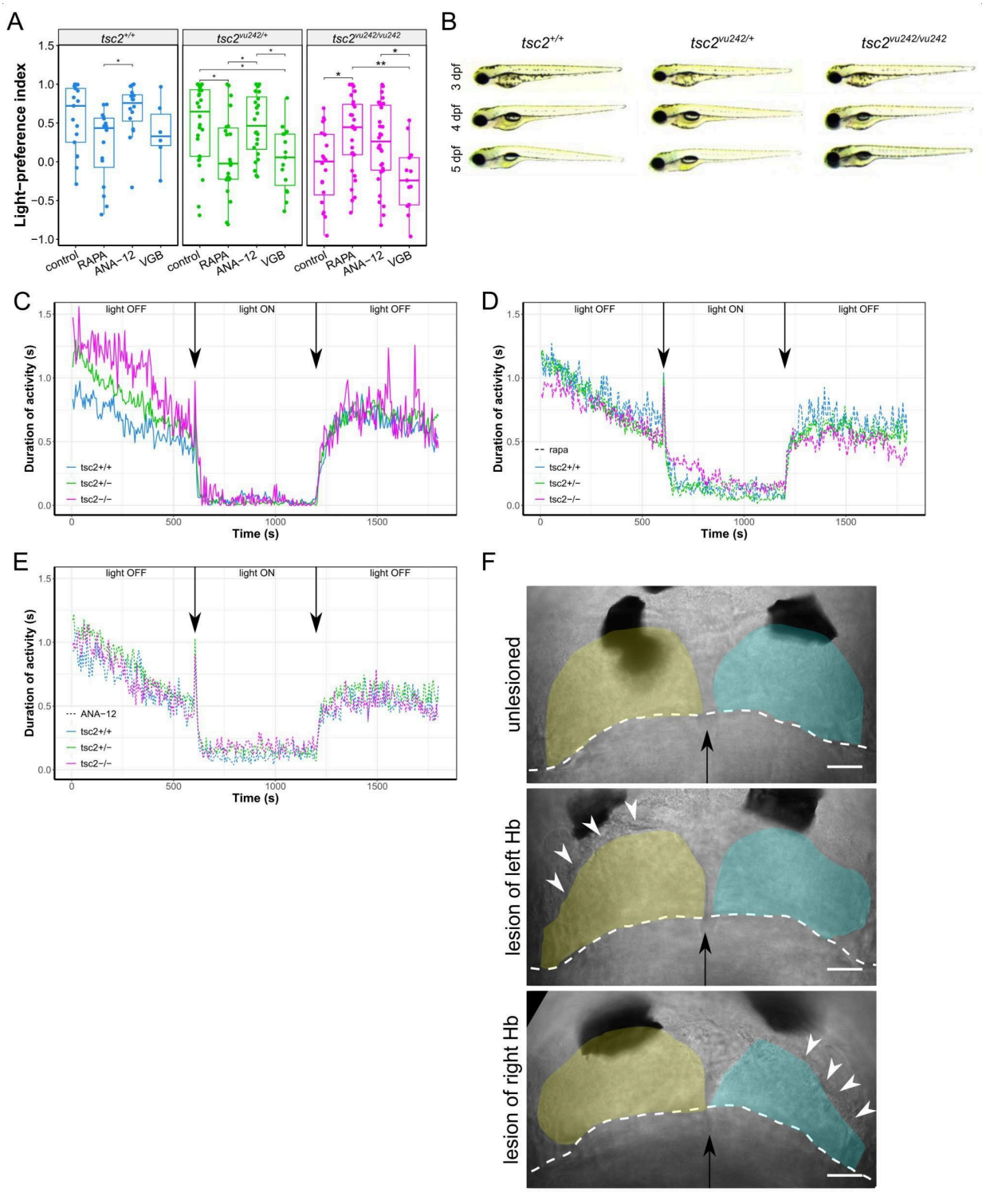

Supplementary Figure S1, related to Figure 1. Light-preference test in *tsc2*^{vu242} fish.

(A) Light-preference index of *tsc2*$^{+/+}$ sibling controls and *tsc2*$^{vu242/+}$ mutants with comparison statistics between treatments (*tsc2*$^{+/+}$: $p = 0.013$ for ANA-12 *vs.* RAPA, the rest – *ns*; *tsc2*$^{vu242/+}$: $p = 0.036$ for control *vs.* RAPA, $p = 0.027$ for control *vs.* VGB, $p = 0.036$ for ANA-12 *vs.* RAPA, $p = 0.036$ for ANA-12 *vs.* VGB). (B) Gross morphology of *tsc2*^{vu242} fish. dpf – days post-fertilization. (C) Mean activity over time for *tsc2*^{vu242} fish after sudden changes in light conditions, showing proper responses to light changes: hyperactivity in the dark phases and freezing behavior in the light phase. (D) Mean activity over time for *tsc2*^{vu242} fish treated with rapamycin after sudden changes in light conditions, showing proper responses to light changes: hyperactivity in the dark phases and freezing behavior in the light phase. (E) Mean activity over time for *tsc2*^{vu242} fish treated with ANA-12 after sudden changes in light conditions, showing proper responses to light changes: hyperactivity in the dark phases and freezing behavior in the light phase. (F) Exemplary bright-field images of habenulas morphology after lesions (taken at 4 dpf). The white dashed lines represent boundary between the optic tectum and the frontbrain, white arrows point the sites of the lesion, the black arrows point the midbrain boundary (between hemispheres). Left habenulas were colored in yellow and the right habenulas – in blue. Black patches are melanophores. Scale bars 20 μm.

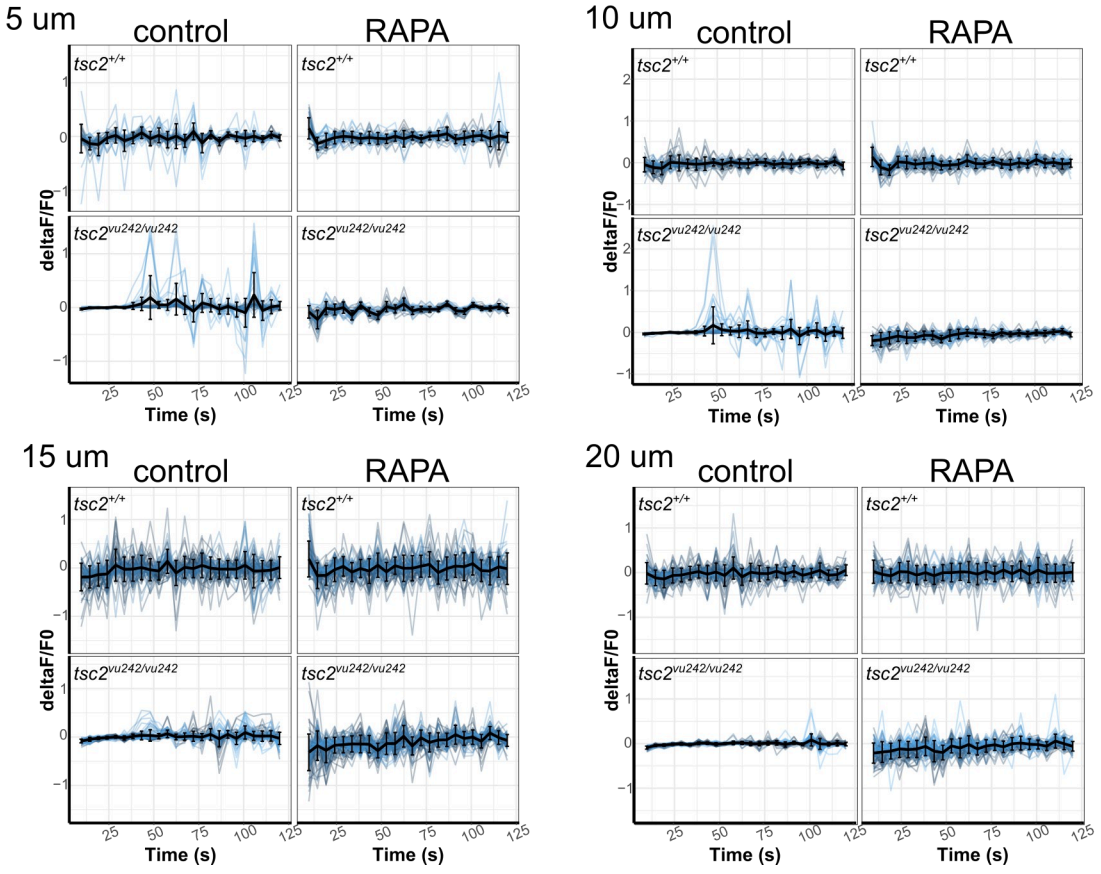

Supplementary Figure S2, related to Figure 3. Neuronal activity in LdHb of *tsc2*$^{vu242/vu242}$ fish and their wt siblings.

Neuronal activity change over time in the *tsc2*$^{+/+}$ and *tsc2*$^{vu242/vu242}$ LdHb at 5, 10, 15, and 20 µm from the top. In black – mean with SD.

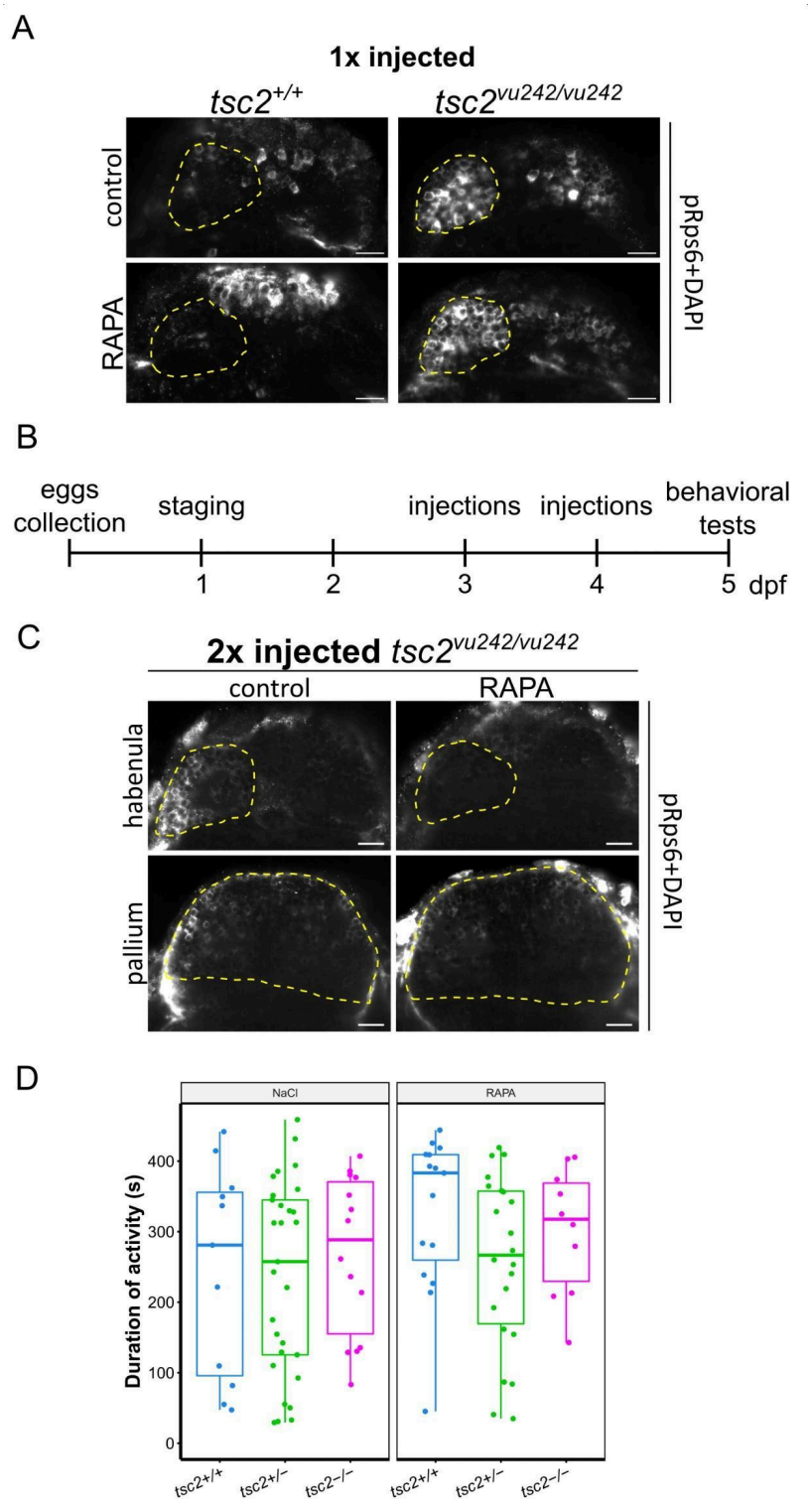

Supplementary Figure S3, related to Figure 4. Rapamacin injections to the left habenula and afferent connectivity of LdHb in *tsc2*^{vu242} fish.

(A) Exemplary images of P-Rps6-immunofluorescence intensity at the habenulae of the *tsc2*$^{vu242/vu242}$ fish and their wild-type *tsc2*$^{+/+}$ siblings after injections with rapamycin or NaCl at 4 dpf only. Injection at 4 dpf did not change P-Rps6 levels in the left habenula of the *tsc2*$^{vu242/vu242}$ mutant fish. Scale bars, 20 μm. (B) Timeline of the experiment of rapamycin injections into the habenula. (C) Exemplary images of P-Rps6-immunofluorescence intensity of the *tsc2*$^{vu242/vu242}$ fish after injections with rapamycin or NaCl at 3 dpf and 4 dpf depicting sections through habenulae and pallium. Injections at two consecutive days decreased the P-Rps6 levels in the left habenula of the *tsc2*$^{vu242/vu242}$ mutant fish, but did not change the P-Rps6 levels in the pallium. Scale bars, 20 μm. (D) Cumulative activity during the light-preference test calculated for *tsc2*^{vu242} fish injected with rapamycin or NaCl at 3 dpf and 4 dpf.

References

1. Switon, K., Kotulska, K., Janusz-Kaminska, A., Zmorzynska, J., Jaworski, J. (2017). Molecular neurobiology of mTOR. Neurosci 341, doi: 10.1016/j.neuroscience.2016.11.017.

2. Sharma, A., Hoeffer, C.A., Takayasu, Y., Miyawaki, T., McBride, S.M., Klann, E., Zukin, R.S. (2010). Dysregulation of mTOR Signaling in Fragile X Syndrome. J. Neurosci 30(2), 694-702, doi:10.1523/JNEUROSCI.3696-09.2010.

3. Sun, J., Liu, Y., Moreno, S., Baudry, M., Bi, X., (2015). Imbalanced mechanistic target of rapamycin C1 and C2 activity in the cerebellum of Angelman syndrome mice impairs motor function. J. Neurosci 35(11), 4706-4718, doi: 10.1523/JNEUROSCI.4276-14.2015.

4. Zhou, J., Blundell, J., Ogawa, S., Kwon, C.-H., Zhang, W., Sinton, C., Powell, C.M., Parada, L.F. (2009). Pharmacological Inhibition of mTORC1 Suppresses Anatomical, Cellular, and Behavioral Abnormalities in Neural-Specific Pten Knock-Out Mice. J. Neurosci 29(6), 1773-1783, doi: 10.1523/JNEUROSCI.5685-08.2009.

5. Sato, A., Kasai, S., Kobayashi, T., Takamatsu, Y., Hino, O., Ikeda, K., Mizuguchi, M. (2012). Rapamycin reverses impaired social interaction in mouse models of tuberous sclerosis complex. Nat. Commun. 3, 1292, doi:10.1038/ncomms2295.

6. Oguro-Ando, A., Rosensweig, C., Herman, E., Nishimura, Y., Werling, D., Bill, B.R., Berg, J.M., Gao, F., Coppola, G., Abrahams, B.S., Geschwind, D.H. (2014). Increased CYFIP1 dosage alters cellular and dendritic morphology and dysregulates Mtor. Mol. Psychiatry 20, 1069–1078, doi:10.1038/mp.2014.124.

7. Gkogkas, C.G., Khoutorsky, A., Ran, I., Rampakakis, E., Nevarko, T., Weatherill, D.B., Vasuta, C., Yee, S., Truitt, M., Dallaire, P., Major, F., Lasko, P., Ruggero, D., Nader, K., Lacaille, J.-C., Sonenberg, N. (2013). Autism-related deficits via dysregulated eIF4E-dependent translational control. Nature 493, 371–377, doi:10.1038/nature11628.

8. Nicolini, C., Ahn, Y., Michalski, B., Rho, J.M., Fahnestock, M. (2015). Decreased mTOR signaling pathway in human idiopathic autism and in rats exposed to valproic acid. Acta Neuropath. Comm. 3(3), doi:10.1186/s40478-015-0184-4.

9. Poopal, A.C., Schroeder, L.M., Horn, P.S., Bassell, G.J., Gross, C. (2016). Increased expression of the PI3K catalytic subunit p110δ underlies elevated S6 phosphorylation and protein synthesis in an individual with autism from a multiplex family. Mol. Autism 7(3), doi:10.1186/s13229-015-0066-4.

10. Zeidan, J., Fombonne, E., Scorah, J., Ibrahim, A., Durkin, M.S., Saxena, S., Yusuf, A., Shih, A., Elsabbagh, M. (2022). Global prevalence of autism: A systematic review update. Autism Research 15(5), 778-790, doi: 10.1002/aur.2696.

11. Feliciano, D.M. Lin, T.V., Hartman, N.W., Bartley, C.M., Kubera, C., Hsieh, L., Lafourcade, C., O'Keefe, R.A., Bordey, A. (2013). A circuitry and biochemical basis for tuberous sclerosis symptoms: from epilepsy to neurocognitive deficits. Int. J. Dev. Neurosci. 31(7), 667–678, doi: 10.1016/j.ijdevneu.2013.02.008.

12. Leclezio, L., and de Vries, P.J. (2015). Advances in the treatment of tuberous sclerosis complex. Curr. Opin. Psychiatry 28(2), 113–120, doi: 10.1097/YCO.0000000000000136.

13. Little, L.M., Dean, E., Tomchek, S., Dunn, W. (2018). Sensory Processing Patterns in Autism, Attention Deficit Hyperactivity Disorder, and Typical Development. Phys. Occup. Ther. Pediatr. 38(3), 243–254, doi: 10.1080/01942638.2017.1390809.

14. Marco, E.J., Hinkley, L.B.N., Hill, S.S., Nagarajan, S.S. (2011). Sensory Processing in Autism: A Review of Neurophysiologic Findings. Pediatr. Res. 69(5), 48R-54R, doi: 10.1203/PDR.0b013e3182130c54.

15. Kim, S.-H., Speirs, C.K., Solnica-Krezel, L., Ess, K.C. (2011). Zebrafish model of tuberous sclerosis complex reveals cell-autonomous and non-cell-autonomous functions of mutant tuberin. Dis. Models Mech. 4(2), doi: 10.1242/dmm.005587.

16. Serra, E.L., Medalha, C.C., Mattioli, R. (1999). Natural preference of zebrafish (Danio rerio) for a dark environment. Braz. J. Med. Biol. Res. 32(12), 1551–1553, doi: 10.1590/s0100-879x1999001200016

17. Lau, B.Y.B., Mathur, P., Gould, G.G., Guo, S. (2011). Identification of a brain center whose activity discriminates a choice behavior in zebrafish. Proc. Natl. Acad. Sci. USA. 108(6), 2581–2586, doi:10.1073/pnas.1018275108

18. Kedra, M., Banasiak, K., Kisielewska, K., Wolinska-Niziol, L., Jaworski, J. Zmorzynska, J. (2020). TrkB hyperactivity contributes to brain dysconnectivity, epileptogenesis, and anxiety in zebrafish model of Tuberous Sclerosis Complex. Proc. Natl. Acad. Sci. USA. 117(4), doi: 10.1073/pnas.1910834117.

19. Bianco, I.H., and Wilson, S.W. (2009). The habenular nuclei: a conserved asymmetric relay station in the vertebrate brain. Philos. Trans. R. Soc. Lond. B. Biol. Sci. 364(1519), 1005–1020, doi: 10.1098/rstb.2008.0213.

20. Dreosti, E., Vendrell Llopis, N., Carl, M., Yaksi, E., Wilson, S.W. (2014). Left-Right Asymmetry Is Required for the Habenulae to Respond to Both Visual and Olfactory Stimuli. Curr. Biol. 24(4), 440–445, doi: 10.1016/j.cub.2014.01.016.

21. Zhang, B., Yao, Y., Zhang, H., Kawakami, K., Du, J. (2017). Left Habenula Mediates Light-Preference Behavior in Zebrafish via an Asymmetrical Visual Pathway. Neuron 93(4), 914–928, doi: 10.1016/j.neuron.2017.01.011.

22. LaSarge, C.L., and Danzer, S.C. (2014). Mechanisms regulating neuronal excitability and seizure development following mTOR pathway hyperactivation. Front. Mol. Neurosci. 7, doi: 10.3389/fnmol.2014.00018.

23. Zhang, Z., Qiu, T., Zhou, J., Gong, X., Yang, K., Zhang, X., Lan, Y., Yang, C., Zhou, Z., Ji, Y. (2023). Toxic effects of sirolimus and everolimus on the development and behavior of zebrafish embryos. Biomed. Pharmacother. 166, doi:10.1016/j.biopha.2023.115397.

24. Macias, M., Blazejczyk, M., Kazmierska, P., Caban, B., Skalecka, A., Tarkowski, B., Rodo, A., Konopacki, J., Jaworski, J. (2013). Spatiotemporal characterization of mTOR kinase activity following kainic acid induced status epilepticus and analysis of rat brain response to chronic rapamycin treatment. PLoS One 8, doi:10.1371/journal.pone.0064455.

25. Vignot, S., Faivre, S., Aguirre, D., Raymond, E. (2005). mTOR-targeted therapy of cancer with rapamycin derivatives. Ann. Oncol. 16(4), 525–537, doi:10.1093/annonc/mdi113.

26. Kaplan, M.J., Ellis, C.N., Bata-Csorgo, Z., Kaplan, R.S., Endres, J.L., Fox, D.A. (1999). Systemic Toxicity Following Administration of Sirolimus (Formerly Rapamycin) for Psoriasis: Association of Capillary Leak Syndrome With Apoptosis of Lesional Lymphocytes. Arch. Dermatol. 135(5), 553–557, doi:10.1001/archderm.135.5.553.

27. Barlow, A.D., Nicholson, M.L., Herbert, T.P. (2013). Evidence for Rapamycin Toxicity in Pancreatic β-Cells and a Review of the Underlying Molecular Mechanisms. Diabetes 62(8), 2674–2682, doi:10.2337/db13-0106.

28. Ahrens, M.B., Orger, M.B., Robson, D.N., Li, J.M., Keller, P.J. (2013). Whole-brain functional imaging at cellular resolution using light-sheet microscopy. Nat. Meth. 10(5), doi: 10.1038/nmeth.2434.

29. Doszyn, O., Dulski, T., Zmorzynska, J. (2023). The zebrafish model of Tuberous sclerosis complex to study epilepsy. In Handbook of Animal Models in Neurological Disorders, Martin, C.R., Patel, V.B., Preedy, V.R. ed. (Elsevier), pp. 227–240, doi:10.1016/B978-0-323-89833-1.00031-8.

30. Schindelin, J., Arganda-Carreras, I., Frise, E., Kaynig, V., Longair, M., Pietzsch, T., Preibisch, S., Rueden, C., Saalfeld, S., Schmid, B., Tinevez, J.-Y., White, D.J., Hartenstein, V., Eliceiri, K., Tomancak, P., Cardona, A. (2012). Fiji: an open-source platform for biological-image analysis. Nat. Methods 9, 676–682, https://doi.org/10.1038/nmeth.2019.

Chapter 6. Protocol for visualization of pRps6-positive cells in larval zebrafish brains using whole-mount immunofluorescence and lightsheet microscopy

Olga Doszyn,[1,2] Tomasz Dulski[1], Justyna Zmorzynska[1,2,3,4,5]

[1]Laboratory of Developmental Neurobiology, International Institute of Molecular Mechanisms and Machines, 02-247 Warsaw, Poland
[2]Laboratory of Molecular and Cellular Neurobiology, International Institute of Molecular and Cell Biology in Warsaw, 02-109 Warsaw, Poland
[3]Technical contact
[4]Lead contact
[5]Technical contact

STAR Protocols, 2025 Mar 21; 6(1):103587.

DOI: 10.1016/j.xpro.2024.103587.

Summary

Due to their small size and transparency, larval zebrafish are a useful model for whole brain imaging. Here, we present a protocol for the visualization of phosphorylated Rps6, a marker of mTorC1 activity, in the zebrafish brains at 5 days post fertilization (dpf), using whole-mount immunofluorescence and lightsheet microscopy. We describe steps for sample preparation, storage, staining and imaging. This protocol can also be modified for staining with antibodies against other proteins.

For complete details on the use and execution of this protocol, please refer to Doszyn et al.[1]

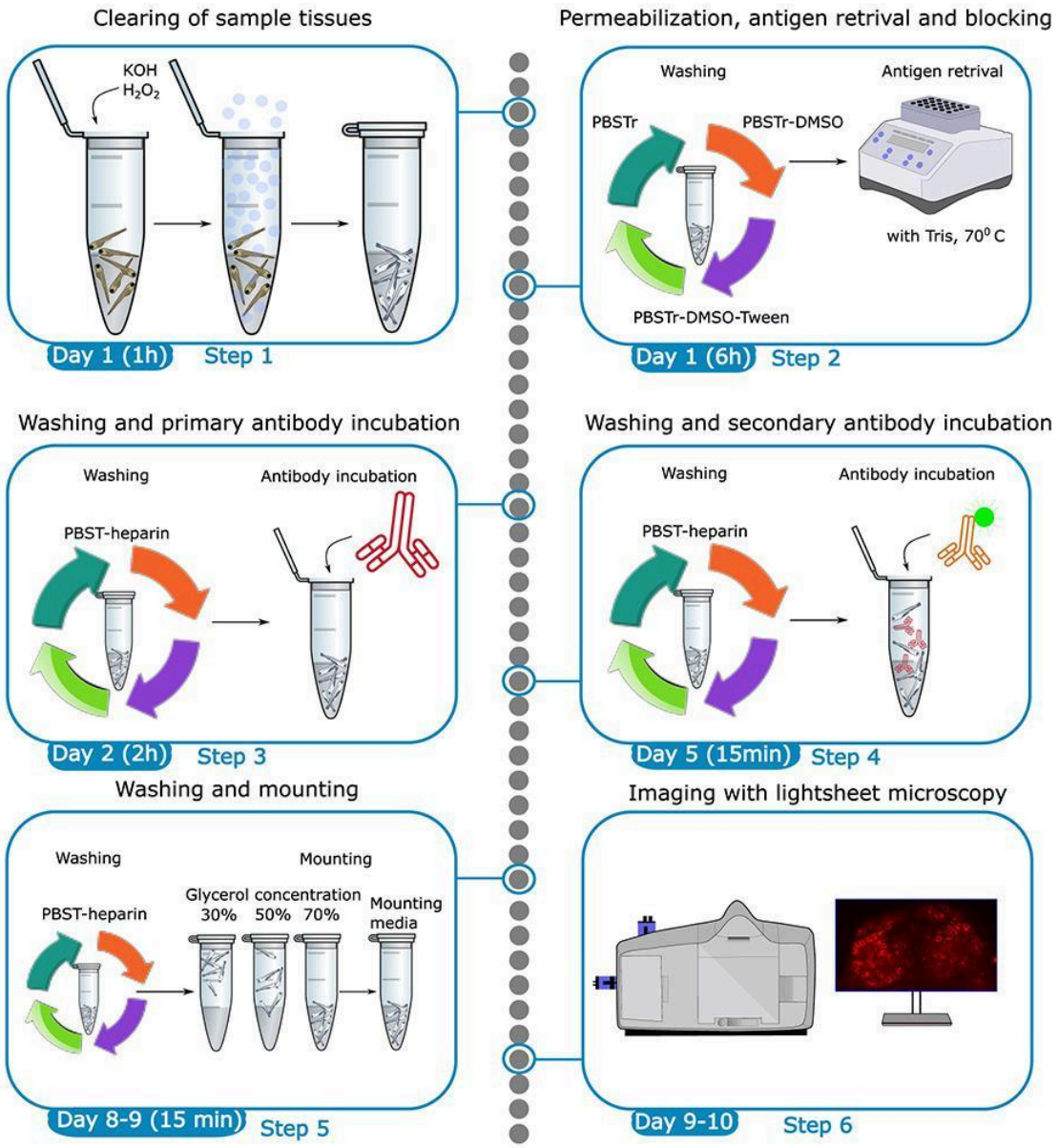

Before you begin

In this protocol, we provide detailed instructions for whole-mount immunofluorescence staining in larval zebrafish brains. The example provided here is visualization of phosphorylated Rps6 (Ribosomal S6 Protein) in the brain. As Rps6 is a downstream target of mTORC1 (Mechanistic Target of Rapamycin Complex 1), it can be used as an indicator of mTORC1 activity. However, we have used this protocol for all of our immunofluorescence staining experiments, and it can be adapted for staining against other proteins. Prior to the staining procedure, zebrafish larvae were bred and maintained according to international standards, and genotyped using methods described by Kedra et al.[2] and Doszyn et al.[3] We have used this protocol on zebrafish larvae up to 14 dpf; for older fish, additional optimalization (such as extending incubation times necessary for tissue penetration) might be required.

Institutional permissions

For the procedure described here, the *tsc2*$^{vu242/+}$ zebrafish line was used. All experiments performed were conducted in accordance with the Act of 15 January 2015 on the protection of animals used for scientific and educational purposes, Directive 2010/63/EU of the European Parliament and of the Council of 22 September 2010 on the protection of animals used for scientific purposes and were approved by the Animal Welfare Commission of the IMol and the IIMCB.

Any experiments using zebrafish older than 5 dpf require the permission of local ethical committee.

Preparation of buffers and stock solutions

Timing: 1-2 h

1. Prepare 20x Tricaine stock solution for larvae euthanasia.
    a. Dissolve 1 g of Tricaine in 244.75 mL of MilliQ H_2O.
    b. Dissolve 60.57 g of Tris base in 450 mL of MilliQ H_2O to obtain a 1 M solution. Adjust the pH to 9 with HCl, and top up the volume to 500 mL with MilliQ H_2O.
    c. Add 5.25 mL of 1 M Tris buffer to the Tricaine solution.
    d. Store at 4°C.

2. Prepare TE buffer for DNA extraction (if genotyping of larvae is required).
    a. Dissolve 60.57 g of Tris base in 450 mL of MilliQ H_2O to obtain a 1 M solution. Adjust the pH to 8 with HCl, and top up the volume to 500 mL with MilliQ H_2O.
    b. Dissolve 73.06 g of EDTA in 450 mL of MilliQ H_2O to obtain a 0.5 M solution. Adjust the pH to 8 with NaOH, and top up the volume to 500 mL with MilliQ H_2O.
    c. Add 5 mL of the Tris solution and 1 mL of the EDTA solution to 500 mL of MilliQ H_2O.
    d. Autoclave and store at 20°C–22°C.

3. Prepare 60x stock solution of the E3 medium for the maintenance of larvae (recipe included in materials and equipment). Autoclave and keep at 4°C.
    a. Prepare the E3 medium by diluting the stock to 1x in MilliQ H_2O.

4. Prepare 10% KOH solution for tissue clearing.
    a. Dissolve 5 g of solid KOH in 50 mL of ddH2O.
    b. Store at 4°C.

5. Prepare PBSTr solution for washing and permeabilization.
    a. Add 0.2% of Triton™ X-100 to PBS (e.g. add 100 µl Triton™ X-100 to prepare 50 ml of PBSTr solution).
    b. Store at 4°C.

    Critical: undiluted Triton™ X-100 should be handled under a chemical hood.

6. Prepare PBSTr-DMSO solution for washing and permeabilization.
    a. Add 0.2% of Triton™ X-100 and 20% DMSO to PBS (e.g. add 100 µl Triton™ X-100 and 10 ml DMSO to prepare 50 ml of PBSTr-DMSO solution).
    b. Store at 4°C.

7. Prepare PBSTr-DMSO-Tween solution for washing and permeabilization.
    a. Add 0.2% of Triton™ X-100, 20% DMSO and 0.1% TWEEN® 20 to PBS (e.g. add 100 µl Triton™ X-100, 10 ml DMSO, and 50 µl TWEEN® 20 to prepare 50 ml of PBSTr-DMSO-Tween solution).
    b. Store at 4°C.

8. Prepare 150 mM Tris buffer for antigen retrieval.
    a. Dissolve 9.0855 g of Tris base in 450 mL of ddH2O.
    b. Adjust the pH to 9 with HCl.
    c. Transfer the buffer to a volumetric flask and adjust to 500 mL with ddH2O.
    d. Transfer to a clean and sterile glass bottle.

9. Prepare 2x GDB-Tr blocking solution.
    a. Add 0.4% gelatin and 0.2% Triton™ X-100 to PBS (e.g. add 10 ml Gelatin solution and 100 µl Triton™ X-100 to prepare 50 ml of 2x GDB-Tr blocking solution).
    b. Aliquot and store at -20°C.

10. Prepare PBST-heparin solution for washing and antibody dilution.
    a. Add 0.2% TWEEN® 20 and 10 µg/mL heparin salt to PBS (e.g. add 100 µl TWEEN® 20 and 50 µl of prepared 10 mg/ml heparin salt stock).
    b. Store at 4°C.

11. Prepare mounting medium.

a. Dissolve 1 g of propyl gallate in 45 mL of glycerol.
b. Add 5 mL of PBS, mix using a magnetic stirrer.
c. Aliquot and store at -20°C protected from light.

12. Prepare a 2% low melting point agarose solution for imaging.
    a. Dissolve low melting point agarose in 1x E3 medium to the final concentration of 2%.
    b. If not prepared immediately before imaging, aliquot and store at 4°C.

13. Prepare 36% paraformaldehyde stock for fixation.
    a. Dissolve paraformaldehyde powder in PBS to the final concentration of 36%.
    b. Aliquot and store at -20°C.

Critical: paraformaldehyde must be handled under a chemical hood.

Zebrafish breeding
Timing: 1-2 h per day for 4 days

14. Prepare a spawning tank with male and female fish in a light-controlled room where the light is switched off overnight and switched on in the morning.
    a. If a light-controlled environment is not available, separate the fish by a divider, and remove it the following morning.

15. On the following morning, collect the eggs. Remove unfertilized eggs and debris. Place up to 60 eggs per a Ø100 mm Petri dish filled with 40 mL of 1x E3 medium. Keep at 28.5°C in an incubator set to a diurnal cycle of 14 h light/10 h darkness.

16. Every day until collection, remove dead larvae and debris, and replace the medium with fresh 1x E3 solution.

Sample fixation
Timing: 24 h

Critical: this step utilizes paraformaldehyde, which is harmful; therefore, all following steps must be performed under a chemical hood.

17. Freshly before use, prepare a 4% fixing solution of formaldehyde by diluting a 36% stock in PBS.
    a. Prepare 50 µl of fixing solution per larva. Leftover 4% solution can be stored at 4°C and used within 48 h, after which it should be discarded.

    Optional: if the samples will be stained against phosphorylated antibodies, add sodium fluoride (NaF) to the final concentration of 20 mM as a phosphatase inhibitor.

18. If genotyping is required, prepare two 96-well plates – one filled with 50 µl of fixing solution per well and the second – with 20 µl of TE buffer respectively.

19. Collect larvae into the fixing solution.
    b. Euthanize the larvae by adding the 20x Tricaine solution to the medium to the final concentration of 3x. If genotyping is not required, collect the larvae directly into 2 mL round or flat bottom tubes, remove remaining liquid, and add 1 mL of fixing solution.
    c. If genotyping is required, cut the larvae below the head. Collect the corresponding heads and tails into separate 96-well plates, placing the heads in the fixing solution, and the tails in TE buffer for DNA extraction and genotyping.
    d. Incubate the larvae in fixing solution overnight at 4°C for fixing.

20. Wash 3x with PBS. Store at 4°C in fresh PBS or proceed immediately to staining.

    Note: it is recommended to stain fixed samples within 2-3 weeks after fixing. During the storage, make sure to replenish evaporated PBS solution.

Key resource table

REAGENT or RESOURCE	SOURCE	IDENTIFIER
Antibodies		
Rabbit polyclonal anti-pRps6 (Ser235/236)	Cell Signaling Technology	Cat# CS4858; RRID:AB_916156
Goat anti-Rabbit IgG (H+L) Cross-Adsorbed Secondary Antibody, Alexa Fluor™ 488	Thermo Fisher Scientific	Cat# A-11008; RRID:AB_143165
Chemicals, peptides, and recombinant proteins		
Tricaine	Sigma-Aldrich/Merck	Cat# E10521
PBS tablets	Carl Roth	Cat# 0890.2
NaCl (sodium chloride)	Chempur	Cat# 117941206
KCl (potassium chloride)	Chempur	Cat# 117397402
$CaCl_2$ (calcium chloride)	Chempur	Cat# 118748703
$MgCl_2$ x $6H_2O$ (magnesium chloride hexahydrate)	Chempur	Cat# 116120500
Paraformaldehyde	Sigma-Aldrich/Merck	Cat# 158127
Sodium fluoride	Sigma-Aldrich/Merck	Cat# 221368

Potassium hydroxide, 90%	Sigma-Aldrich/Merck	Cat# 484016
Hydrogen peroxide, 30%	Carl Roth	Cat# 9681.1
Triton™ X-100	Sigma-Aldrich/Merck	Cat# X100
Dimethyl sulfoxide	Sigma-Aldrich/Merck	Cat# D8418
TWEEN® 20	Sigma-Aldrich/Merck	Cat# P1379
Tris base	Carl Roth	Cat# 4855.3
HCl	Chempur	Cat# 115752837
EDTA	Sigma-Aldrich/Merck	Cat# EDS
NaOH	Sigma-Aldrich/Merck	Cat# S5881
Gelatin solution, type B, 2% in H_2O	Sigma-Aldrich/Merck	Cat# G1393
Heparin sodium salt	Sigma-Aldrich/Merck	Cat# H3149
Propyl gallate	Sigma-Aldrich/Merck	Cat# P3130
Glycerol	Sigma-Aldrich/Merck	Cat# G5516
1-phenyl-2-thiourea (PTU)	Sigma-Aldrich/Merck	Cat# P7629
TopVision low melting point agarose	Thermo Fisher Scientific	Cat# R0801
Experimental models: Organisms/strains		
Zebrafish: $tsc2^{vu242/+}$ (mixed strain) larvae until 5 dpf;	Kim et al.[4]	RRID:ZFIN_ZDB-GENO-180906-3
Software and algorithms		
Fiji	Schindelin et al.[5]	https://fiji.sc/
R 4.3.2	R Foundation for Statistical Computing	https://www.Rproject.org
RStudio	Posit Software, PBC	https://posit.co/download/rstudiodesktop/

ZEN2014 SP1 (black edition)	Zeiss	https://www.microshop.zeiss.com/en/u s/softwarefinder/sof tware-categories/zen-black
Other		
ThermoMixer® C	Eppendorf	Cat# 2231001005
Lightsheet Z.1 microscope	Zeiss	https://www.zeiss.com/microscopy/en/products/lightmicroscopes/lightsheet-microscopes.html

Materials and equipment setup

60x E3 medium stock solution

Reagent	**Final concentration**	**Amount**
NaCl	297 mM	17,4 g
KCl	10,7 mM	0,8 g
$CaCl_2$	19,6 mM	2,18 g
$MgCl_2$ x $6H_2O$	24 mM	4,89 g
MilliQ H_2O	n/a	Fill up to 1 L
Total	**n/a**	**1 L**

[Can be stored long term at 4°C.]

Step-by-step method details

Note: For all steps, use 0.5 – 1 mL of solution per tube. When removing solutions, we recommend gently aspirating the liquid with glass Pasteur pipettes to avoid damage to the tissues, or sticking of tissue to the walls of a plastic pipette tip.

Clearing of sample tissues
Timing: 0.5 – 1 h

The first step (Fig. 1) removes pigmentation from the skin and eyes, in order to provide clear microscopic images. Additionally, H_2O_2 quenches autofluorescence, reducing background noise and false positive signals during imaging.

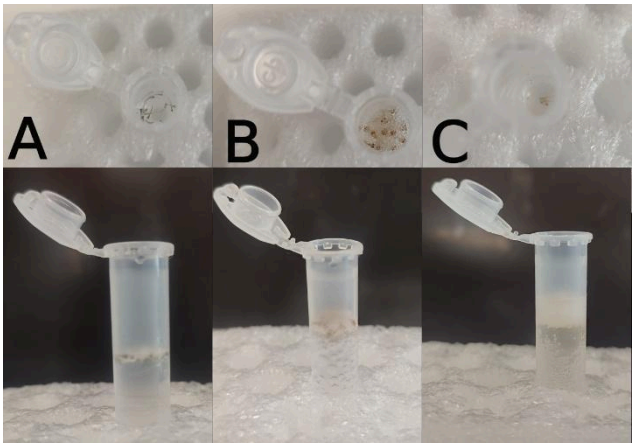

Figure 1. Clearing of sample tissues. A. Before adding KOH and H_2O_2. B. Samples after 15 min. C. Washed samples after 45 min. KOH removes pigmentation from the skin and eyes, in order to provide clear microscopic images. H_2O_2 quenches autofluorescence, reducing background noise and false positive signals during imaging.

Note: If the experiment uses transgenic zebrafish lines without pigmentation, such as *casper*, this step can be omitted. It is also possible to depigmentate fish form 1 dpf onward using 0.003% 1-phenyl-2-thiourea (PTU) in 1x E3 and then this step can be omitted. Depigmentation using PTU is not recommended for studies of brain as the chemical actions of PTU on the brain morphology and function are unknown.

1. Collect up to 20 larvae in a 2 mL tube with a flat or round bottom.

2. Just before starting, prepare a clearing solution of 1x KOH + 3% H_2O_2 in MilliQ H_2O.

3. Remove PBS from each tube with fixed larvae and add 1 mL of clearing solution per tube. Incubate at 20°C–22°C until the tissue is cleared (for larvae at 5 dpf, this takes approximately 45 min).
   Keep the tubes open during this time.

4. Rinse 2x with PBS and store in PBS at 4°C or proceed immediately to the next step.

Permeabilization, antigen retrieval and blocking
Timing: 6 h + 24 h

In this step, we describe the first, preparatory steps of the whole-mount immunofluorescence procedure, including tissue permeabilization, washing, antigen retrieval and blocking against nonspecific antibody binding. Triton™ X-100 and TWEEN® 20 are nonionic detergents, enhancing tissue penetration and reducing surface tension respectively, while DMSO removes lipids from cell membranes.

5. Wash the sample tissues (at 20°C–22°C).
   a. Wash cleared samples in PBSTr solution 2x for 1 h.
   b. Wash samples in PBSTr-DMSO solution for 1 h.
   c. Wash samples in PBSTr-DMSO-Tween solution for 1 h.
   d. Wash samples in PBSTr solution 2x for 1 h.

6. Perform antigen retrieval. **Troubleshooting 1**

a. Wash samples with 150 mM Tris.
b. Add fresh 150 mM Tris and incubate for 5 min at 20°C–22°C.
c. Incubate for 15 min at 70°C using a thermomixer.
d. Bring to 20°C–22°C before proceeding with the next step.

7. Block samples against non-specific antibody binding. **Troubleshooting 2**
    a. Prepare a blocking solution by diluting the GDB-Tr stock to 1x in PBS.
    b. Incubate samples in blocking solution overnight at 20°C–22°C.

Note: An alternative blocking solution of 0.2% Triton™ X-100, 20% DMSO, 0.3 M glycine and 6% goat or donkey serum in PBS can also be used, and may work better for some antibodies. Glycine binds aldehydes, and therefore reduces non-specific antibody binding, and can improve the quality of the staining. Serum blocks unspecific binding of the secondary antibody to the tissue, thus, the serum should be used from species that the secondary antibody comes from, e.g. goat serum should be used for blocking when the goat secondary antibodies are used for detection.

Washing and primary antibody incubation
Timing: 2 h + 3 days

This step clears the residue of blocking solution and incubation with the primary antibody. The addition of heparin to the buffer increases antibody diffusion in tissue.

8. Wash samples by incubating them for 2x 1 h at 20°C–22°C in PBST-heparin solution.

9. Incubate samples with the primary antibody. **Troubleshooting 1**
    a. Prepare a 1:200 solution of the rabbit polyclonal anti-pRps6 antibody in PBST-heparin.

Note: For staining with alternative antibodies, higher or lower dilutions might be more optimal. Follow the manufacturer's suggestions for each antibody.

    b. Incubate with antibody solution for 72 h at 20°C–22°C.

Washing and secondary antibody incubation
Timing: 15 min + 3 days

This step clears the residue of primary antibody and incubate with the secondary antibody.

10. Wash samples in PBST-heparin once.

11. Incubate samples in PBST-heparin overnight at 20°C–22°C.

12. Incubate samples with secondary antibody.

a. Prepare a 1:1000 solution of the Alexa Fluor™ 488 antibody in PBST-heparin.

Critical: when using the alternative blocking solution containing goat or donkey serum, remember to match the source species of the serum to the host species of the secondary antibody (e.g. when using a goat anti-rabbit secondary antibody, block the samples in goat serum).

b. Remove the PBST-heparin solution and add the antibody solution.
c. Incubate with antibody solution for 48 h at 20°C–22°C in darkness (e.g. cover with aluminum foil).

Critical: from this point onwards, keep samples protected from light.

Washing and mounting
Timing: 2 days + 15 min

This step clears the residue of secondary antibody and mounting samples in a glycerol-based medium for long-term storage.

13. Wash samples 2x in PBST-heparin.

14. Incubate samples in PBST-heparin overnight at 20°C–22°C.

15. Incubate samples in a glycerol gradient.
    a. Incubate in 30% glycerol in PBS for at least 2 h at 20°C–22°C (until the larvae fall to the bottom of the tube).
    b. Incubate in 50% glycerol in PBS for at least 2 h at 20°C–22°C (until the larvae fall to the bottom of the tube).
    c. Incubate in 70% glycerol in PBS overnight at 20°C–22°C (until the larvae fall to the bottom of the tube).

16. Transfer samples to mounting medium and store at 4°C in the dark until imaging.

Imaging with lightsheet microscopy
Timing: variable (approx. 1 min per sample)

This step explains the procedure of imaging zebrafish larvae with lightsheet microscopy.

17. Heat up the previously prepared 2% agarose solution to melt it. Keep it in a heat block at 55-60°C.

18. Wash samples with PBS to remove the mounting medium.

Note: When imaging the deeper structures of the brain, it might be necessary to remove the eyes and skin in order to increase the light penetration to the region of interest.

19. Place samples in a glass capillary tube filled with agarose.

20. Place the capillary in the imaging chamber filled with PBS.

Note: In this study, samples were imaged using a Zeiss Lightsheet Z.1 microscope (40× water immersion objective, NA = 1.3) at following settings: pivot scan, 1024 × 1024 pixel-resolution, Z-step size 0.5 µm, laser line 488 nm intensity 8%.

Note: Following imaging, samples can be placed back in the mounting medium and stored long-term at 4°C in the dark.

Expected outcomes

This protocol provides methodology for visualization of protein expression patterns in whole zebrafish larval brain. In case of P-Rps6, the fluorescent signal is visible in the cytoplasm (Fig. 2).

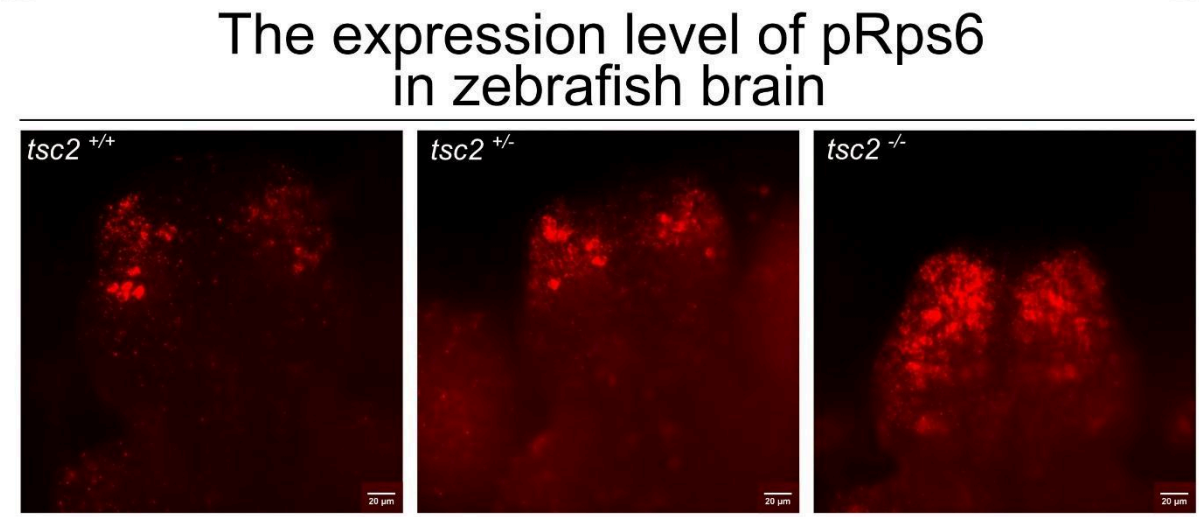

Figure 2. Expression of P-Rps6 in *tsc2*-zebrafish larval brain at 5 dpf. Representative images of P-Rps6positive cells in the pallium, showing differences in expression between genotypes.

Quantification and statistical analysis

Quantification can be performed in Fiji software (Fig. 3). Using the Measure tool (set measurements: area, mean fluorescence, min. and max. values), manually select cells in your region of interest, and record the cell size and signal intensity. The number of signal-positive cells can be counted manually. Afterwards, statistical analysis can be

performed in RStudio. Check for equality of variance and normality of residuals using Levene's test and Shapiro-Wilk test, respectively. If those assumptions are met, use an ANOVA test with post-hoc TukeyHSD for data analysis; if they are not, use the KruskalWallis test with *post-hoc* Wilcoxon test to correct for multiple comparisons.

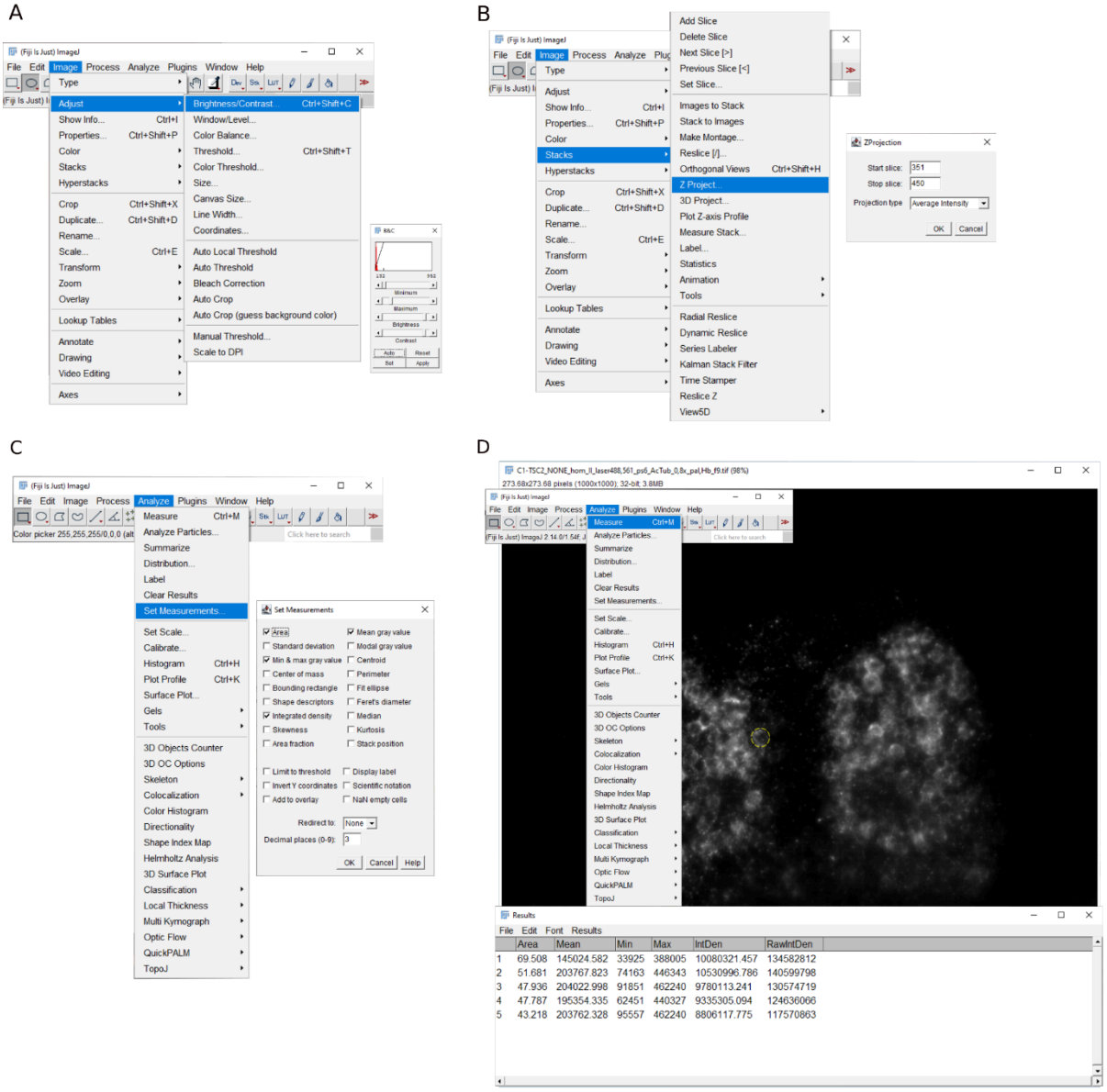

Figure 3. Quantification of P-Rps6 levels in the pallium performed in Fiji software. A. After loading the resized image stack into the Fiji software, in the brightness/contrast level adjustment, set the minimum and maximum value displayed on the image. These values depend on the fluorescence intensity of the images and must be selected individually for the experiment. All images must have the same values set. Therefore, after step B, the images must be verified and checked to make sure that the brightness is not too high and that single positive P-Rps6 cells are visible. B. This step requires selecting the brain area of interest. Select an equal number of slices from each sample in the stack. Then sum the slices using the projection type: Average Intensity. C. Set the measurements needed for analysis:

Average Intensity, Area, etc. D. Click the oval function to draw a circle around the positive P-Rps6 cell and measure the parameters. Do this for several representative cells per image. The average value of the measurements will be used to calculate the fluorescence intensity per cell.

Limitations

The main limitation of this protocol is the limited availability of antibodies designed for detection of zebrafish proteins. Therefore, the conservation of detected epitope between zebrafish and mammalian orthologs should be assessed and taken into account.

Troubleshooting

Problem 1:

Lack of or weak fluorescent signal (can be related to step 6 or 9).

Potential solution:

- Test whether the antigen retrieval step is required. For some proteins, the temperature or the buffer in which this step is performed might also need to be adjusted.

OR

- Increase the concentration of primary antibody.

Problem 2:

High background fluorescence (related to step 7).

Potential solution:

- Make sure you used the correct blocking solution; particularly when using a blocking solution containing goat or donkey serum, make sure to match it to the host species of the secondary antibody.

Resource availability

Lead contact

Further information and requests for resources and reagents should be directed to and will be fulfilled by the lead contact, Justyna Zmorzynska (j.zmorzynska@imol.institute).

Technical contact

Technical questions on executing this protocol should be directed to and will be answered by the technical contact, Justyna Zmorzynska (j.zmorzynska@imol.institute).

Materials availability

This study did not generate new unique reagents. The fish mutant and transgenic lines are protected under material transfer agreement with the institutions that generated the lines.

Upon appropriate agreement with these institutions, they can be requested from the lead contact.

Data and code availability

This study did not generate datasets or codes.

Acknowledgments

We thank Kevin Ess (Vanderbilt University) for the *tsc2*$^{vu242/+}$ zebrafish line, the IIMCB ZCF for assistance with the adult fish, and the IIMCB MCF for sharing the Lightsheet Z.1. This work was supported by an OPUS grant no. 2020/37/B/NZ3/02345 from National Science Centre, Poland. For the purpose of Open Access, the author has applied a CC-BY public copyright licence to any Author Accepted Manuscript (AAM) version arising from this submission.

Author contributions

This protocol was developed and optimized by J.Z. and O.D. The detailed procedure was written and edited by O.D., T.D., and J.Z. Resources and funding were secured by J.Z.

Declaration of interests

The authors declare no competing interests.

References

1. Doszyn, O., Kedra, M., Zmorzynska, J. (2024). Hyperactive mTORC1 disrupts habenula function and light preference in zebrafish model of Tuberous sclerosis complex. iScience 27(6), 110149. DOI: https://doi.org/10.1016/j.isci.2024.110149
2. Kedra, M., Banasiak, K., Kisielewska, K., Wolinska-Niziol, L., Jaworski, J., Zmorzynska, J. (2020). TrkB hyperactivity contributes to brain dysconnectivity, epileptogenesis, and anxiety in zebrafish model of Tuberous Sclerosis Complex. Proc. Natl. Acad. Sci. USA. 117, 2170-2179. DOI: https://doi.org/10.1073/pnas.1910834117
3. Doszyn, O., Dulski, T., Zmorzynska, J. (2023). The zebrafish model of Tuberous sclerosis complex to study epilepsy. in: Martin C.R. Patel V.B. Preedy V.R. Handbook of Animal Models in Neurological Disorders. Elsevier, 227-240. DOI: https://doi.org/10.1016/B978-0-323-89833-1.00031-8
4. Kim, S.-H., Speirs, C.K., Solnica-Krezel, L., Ess, K.C. (2011). Zebrafish model of tuberous sclerosis complex reveals cell-autonomous and non-cell-autonomous functions of mutant tuberin. Dis. Model. Mech. 4, 255-267. DOI: https://doi.org/10.1242/dmm.005587
5. Schindelin, J., Arganda-Carreras, I., Frise, E., Kaynig, V., Longair, M., Pietzsch, T., Preibisch, S., Rueden, C., Saalfeld, S., Schmid, B. et al., (2012). Fiji: an open-source platform for biologicalimage analysis. Nat. Methods. 9, 676-682. DOI: https://doi.org/10.1038/nmeth.2019

Chapter 7. Protocol for microinjection of rapamycin into the zebrafish habenula

Olga Doszyn,[1,2] Tomasz Dulski[1], Justyna Zmorzynska[1,2,3,4]

[1]Laboratory of Developmental Neurobiology, International Institute of Molecular Mechanisms and Machines, 02-247 Warsaw, Poland
[2]Laboratory of Molecular and Cellular Neurobiology, International Institute of Molecular and Cell Biology in Warsaw, 02-109 Warsaw, Poland
[3]Technical contact
[4]Lead contact

STAR Protocols, 2025 Mar 21; 6(1):103566.

DOI: 10.1016/j.xpro.2024.103566.

Summary

Mechanistic target of rapamycin complex 1 (mTorC1) activity plays a crucial role in brain development. Here, we present an approach for microinjection of rapamycin into the habenula of larval zebrafish, in order to achieve localized inhibition of the mTorC1 pathway and explore the role of mTorC1 in habenula function. The protocol includes details on the microinjections as well as maintaining zebrafish larvae before and after the procedure.

For complete details on the use and execution of this protocol, please refer to Doszyn et al.[1]

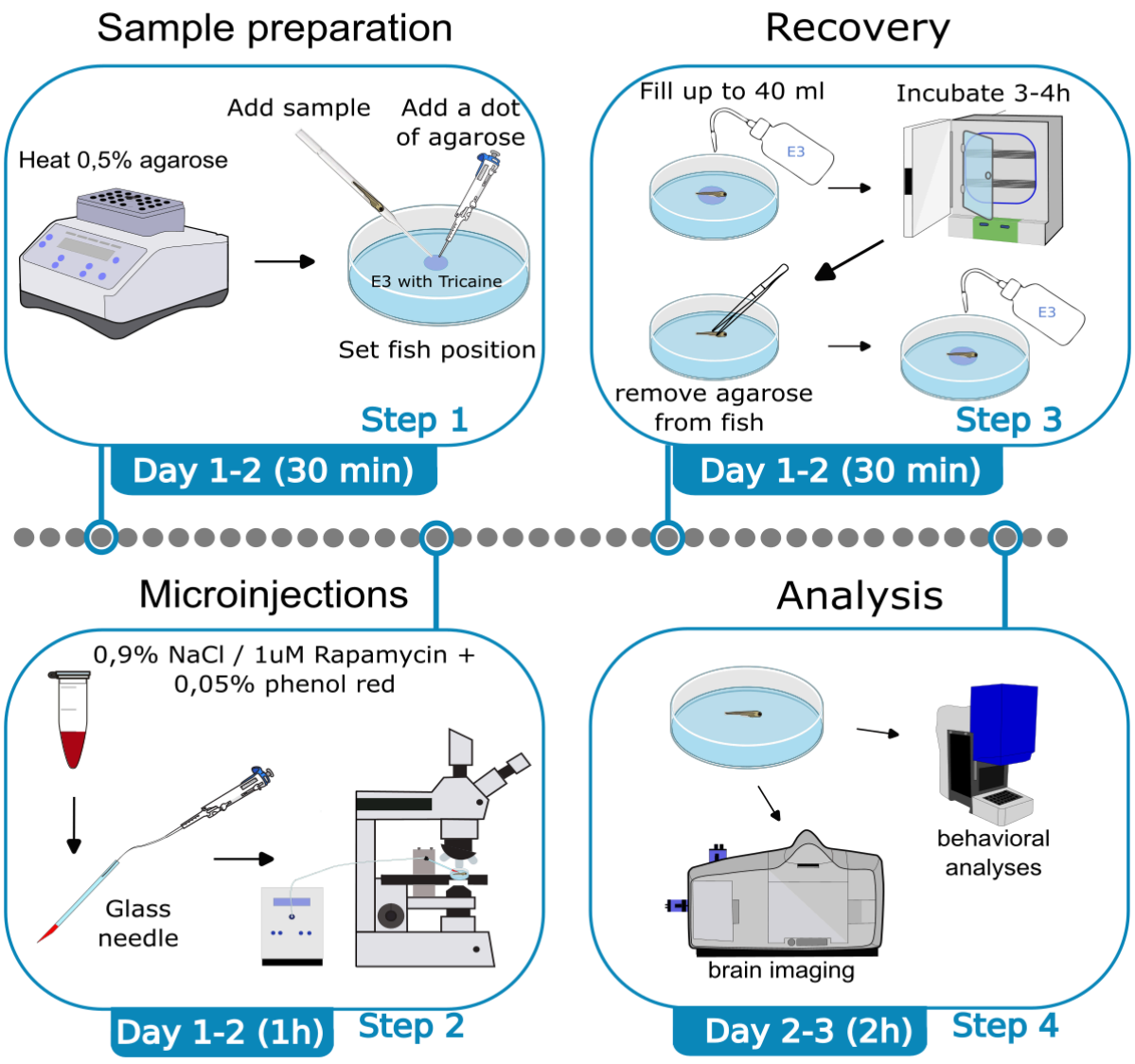

Before you begin

Mechanistic target of rapamycin complex 1 (mTorC1), integrates multiple extra- and intracellular signals in order to regulate transcription, translation, protein degradation and cytoskeleton dynamics. In the brain, it controls proliferation, migration, differentiation, synaptogenesis, and neuronal activity[2]. This protocol describes the procedure for injecting rapamycin, the direct mTorC1 inhibitor, into the zebrafish habenula, a bilateral structure located in the dorsal diencephalon. The morphology and function of the habenula is asymmetric, with the left and right habenula playing different roles in the integration of various sensory stimuli and regulation of behavioral response[3,4]. This protocol allows for localized mTorC1 inhibition. We have examined the role of mTorC1 in the light-preference behavior of tsc2vu242/+ zebrafish, which is regulated by the left habenula4. However, depending on the researcher's subject of interest, this protocol can also be adapted for microinjections of different drugs, as well as for other zebrafish lines. In such cases, it might be necessary to adjust parameters such as drug concentration or age of injected larvae; the technical aspects of the injection itself would remain the same.

Institutional permissions

For the procedure described here, the *tsc2*$^{vu242/+}$ zebrafish line was used. All experiments performed were conducted in accordance with the Act of 15 January 2015 on the protection of animals used for scientific and educational purposes, Directive 2010/63/EU of the European Parliament and of the Council of 22 September 2010 on the protection of animals used for scientific purposes and were approved by the Animal Welfare Commission of the IMol and the IIMCB.

As this protocol uses zebrafish younger than 5 days post-fertilization (dpf), it does not require the additional permission of local ethical committee.

Preparation of buffers and stock solutions
Timing: 1 h

1. Prepare the 60x E3 medium stock solution (recipe to be found in materials and equipment). Autoclave and keep at 4°C.
    a. Prepare the E3 medium by diluting the stock to 1x in MilliQ H_2O.
2. Prepare the Tricaine stock solution (recipe to be found in materials and equipment). Keep at 4°C in the dark.
3. Prepare a 1% solution of low melting point agarose in E3 medium.

Note: If the solution is being prepared prior to the day of the experiment, it can be stored at 4°C and melted as needed. If prepared immediately before injections, keep in liquid form at 55-60°C.

4. Prepare a 0,9% solution of NaCl. Store in room temperature for up to a week or in 4°C for a longer time. Bring to room temperature or keep in the incubator with the fish at 28.5°C before use.

5. Prepare a 1 µM rapamycin solution in 0,9% NaCl. Aliquot and keep at -20°C. Bring to room temperature or 28.5°C before use.

Zebrafish breeding

Timing: 1-2 h per day for 4 consecutive days

6. Set up a spawning tank with male and female fish (either separated by a divider to be removed on the next-day's morning, or in a light-controlled room where the light will be off during the night and will switch on in the morning).

7. On the following day, collect the fertilized eggs. Place up to 60 eggs per a Ø100 mm Petri dish filled with 40 mL of E3 medium. Incubate at 28.5°C, with a diurnal cycle of 14 h light/10 h darkness.

8. On the first and second day post fertilization (dpf), remove any debris, dead embryos or unfertilized eggs, and exchange the E3 medium.

Preparation of micropipettes

Timing: 30 min

9. Prepare the micropipettes.

    a. Insert a glass capillary into the heat puller and prepare the needles as described by Konadu et al.[5]. Briefly, to prepare microinjection needles, begin with a 10-cm-long borosilicate glass capillary (1.0 mm outer diameter, thin-walled) placed in the micropipette puller (e.g. from Sutter Instrument Company). Carefully load the capillary tube into the carriage, aligning it precisely within the groove and securing it with clamps. Glide the capillary through the heating filament to ensure consistent alignment across the entire length. Once positioned, initiate the pull program with settings tailored to heat, pull, velocity, delay, and pressure. After the pull process, the needle tip is formed at both ends that has to be broken open using fine forceps under a stereo microscope.

    b. Using fine forceps under a stereo microscope with good optics (at least 150x magnification), snap off the pointed end to obtain a micropipette with an open tip of ~3 µm. Use microscope calibration slide with ruler of 0.01 mm or microscope reticle to measure tip diameter.

    c. Load the micropipette with 3 µl of 0.9% NaCl or rapamycin solution.

10. Insert the micropipette into the injector pump holder. Put a drop of mineral oil on the calibration slide. Using the calibration slide with a ruler of 0.01 mm set the drop size to 0.5 nL by injecting a drop to the mineral oil, measuring it and adjusting the size with pressure. Workstation for microinjection with the necessary equipment is presented on Figure 1. **Troubleshooting 1**

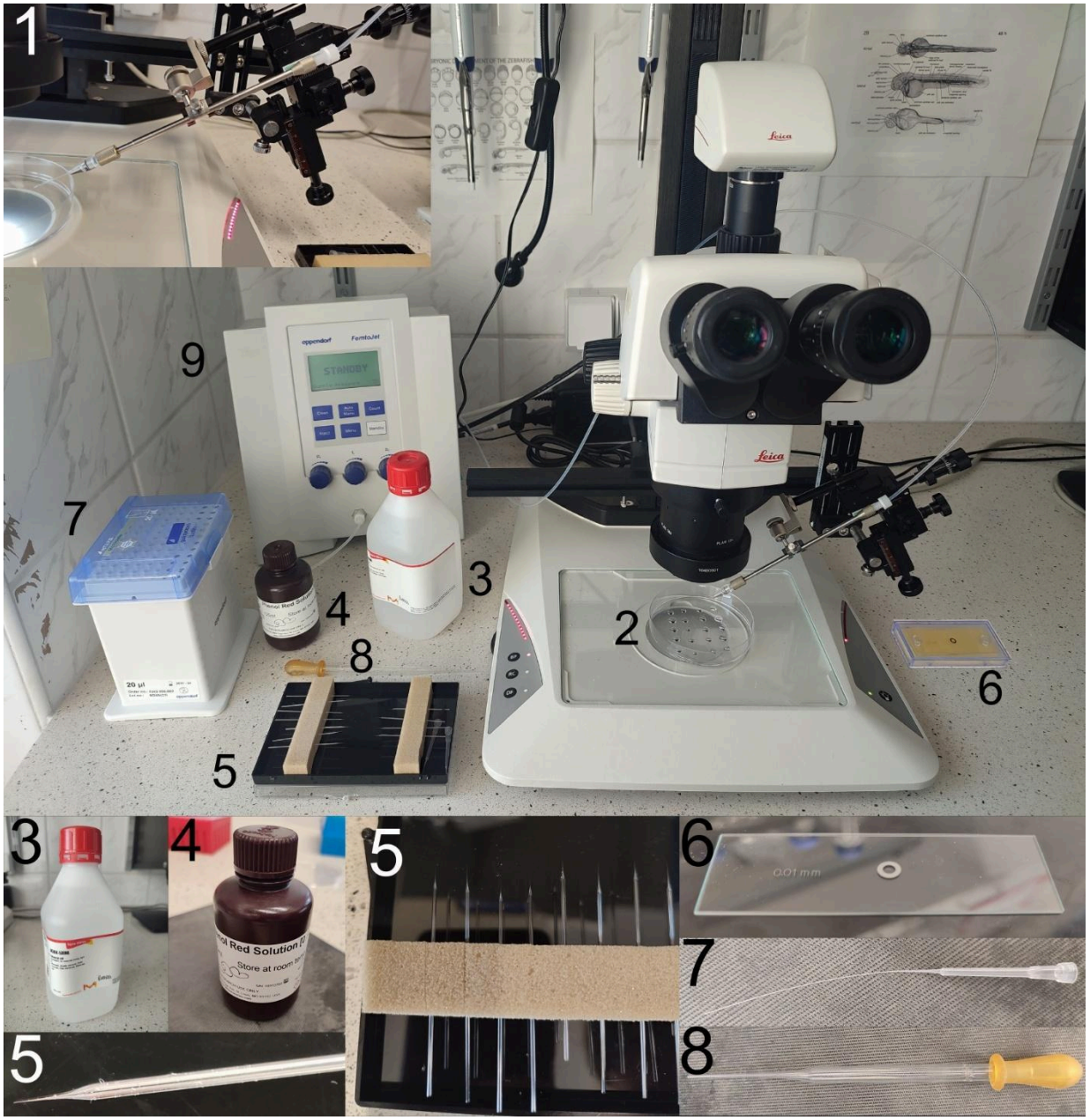

Figure 1. Workstation for injection. 1. Glass needle mounted on the injector pump holder. 2. Petri dish with fish mixed in each dot with E3 and agarose. 3. Mineral oil necessary for injection calibration. 4. Phenol Red solution. 5. Glass needles. 6. Microscope calibration slide. 7. Extended pipette tips for easy needle loading. 8. Pasteur pipette. 9. Injection pump.

Key resources table

REAGENT or RESOURCE	SOURCE	IDENTIFIER
Chemicals, peptides, and recombinant proteins		
NaCl (sodium chloride)	Chempur	Cat# 117941206
KCl (potassium chloride)	Chempur	Cat# 117397402
$CaCl_2$ (calcium chloride)	Chempur	Cat# 118748703
$MgCl_2$ x $6H_2O$ (magnesium chloride hexahydrate)	Chempur	Cat# 116120500
Tricaine	Sigma-Aldrich/Merck	Cat# E10521
Tris base	Carl Roth	Cat# 4855.3
HCl	Chempur	Cat# 115752837
Rapamycin	Sigma-Aldrich/Merck	Cat# 553210
Phenol Red	Sigma-Aldrich/Merck	Cat# P0290
TopVision low melting point agarose	Thermo Fisher Scientific	Cat# R0801
Experimental models: Organisms/strains		
Zebrafish: $tsc2^{vu242/+}$	Kim et al.[6]	RRID:ZFIN_ZDB-GENO-180906-3
Other		
Dry block thermostat Bio TDB-100	Biosan	Cat# BS-010412-AAA
Borosilicate glass capillaries (outer diameter 1,0 mm / inner diameter 0,75 mm)	Sutter Instrument	Cat# BF150-75-10
Flaming/Brown Micropipette Puller	Sutter Instrument	Cat# P-1000
Microscope Leica M165 FC 198x magnification	Leica	https://www.leica-microsystems.com/products/light-microscopes/stereo-microscopes/p/leica-m165-fc/
Injector pump FemtoJet™ 4i	Eppendorf	Cat# E5252000021

Materials and equipment setup

60x E3 medium stock solution

Reagent	**Final concentration**	**Amount**
NaCl	297 mM	17,4 g
KCl	10,7 mM	0,8 g
$CaCl_2$	19,6 mM	2,18 g
$MgCl_2$ x $6H_2O$	24 mM	4,89 g
MilliQ H_2O	n/a	Fill up to 1 L
Total	**n/a**	**1 L**

[Can be stored long term at 4°C.]

Tricaine stock solution

Reagent	**Final concentration**	**Amount**
Tricaine	15,3 mM	1 g
1M Tris-HCl pH 9	21 mM	5,25 mL
MilliQ H_2O	n/a	244,75 mL
Total	**n/a**	**250 mL**

[Can be stored long term at 4°C in the dark.]

Step-by-step method details

First microinjection

Timing: 2 h

This step describes the preparation of zebrafish larvae and the microinjection procedure. For rapamycin injections into the left habenula, it was performed at 3 dpf and then repeated again at 4 dpf, as this was previously established to be required for the sustained effect of the treatment. **Troubleshooting 2**

1. Heat the 1% agarose solution to melt. Keep it in the heat block at 55-60°C.

2. Prepare the 0.9% NaCl and 1 µM rapamycin solutions. Add 1 µl of 0.05% Phenol Red per every 10 µl of solution for visualization.

3. Add Tricaine solution into the E3 medium with the larvae to a final concentration of 0,01%.

Note: It is recommended to sedate a smaller number of larvae at a time, perform the microinjection procedure to the end, and repeat for the next batch.

4. Place single larva in one drop of approximately 20 µl of E3 with Tricaine on a Petri dish. You can put as many separate drops as you manage to inject (e.g. 20 per dish). Pipette an equal volume (approx. 20 µl) drop of 1% agarose solution (to the final concentration of 0,5%) onto the drop with the larva and position the larva with the dorsal side of the head facing up.
    a. Place the dish under the microscope. If necessary, using a thin pipette tip, carefully manipulate the larva to adjust its position, ensuring the habenulae are easily accessible.
    b. After the agarose solidifies, pipette a drop of E3 medium with Tricaine on top, ensuring that the fish is continuously sedated and submerged in water.

Critical: To increase efficiency of the procedure, several larvae can be mounted on a single dish, and injected in a batch. Extra attention must be then paid to ensure the E3 medium covering the larvae does not evaporate before the end of the injections. Add drops of fresh E3 medium with Tricaine when needed.

5. Insert the micropipette tip between the habenula and the surrounding blood vessel. Blood vessels should be easily visible under stereo microscope because the blood cells are floating in them (Fig 2.)

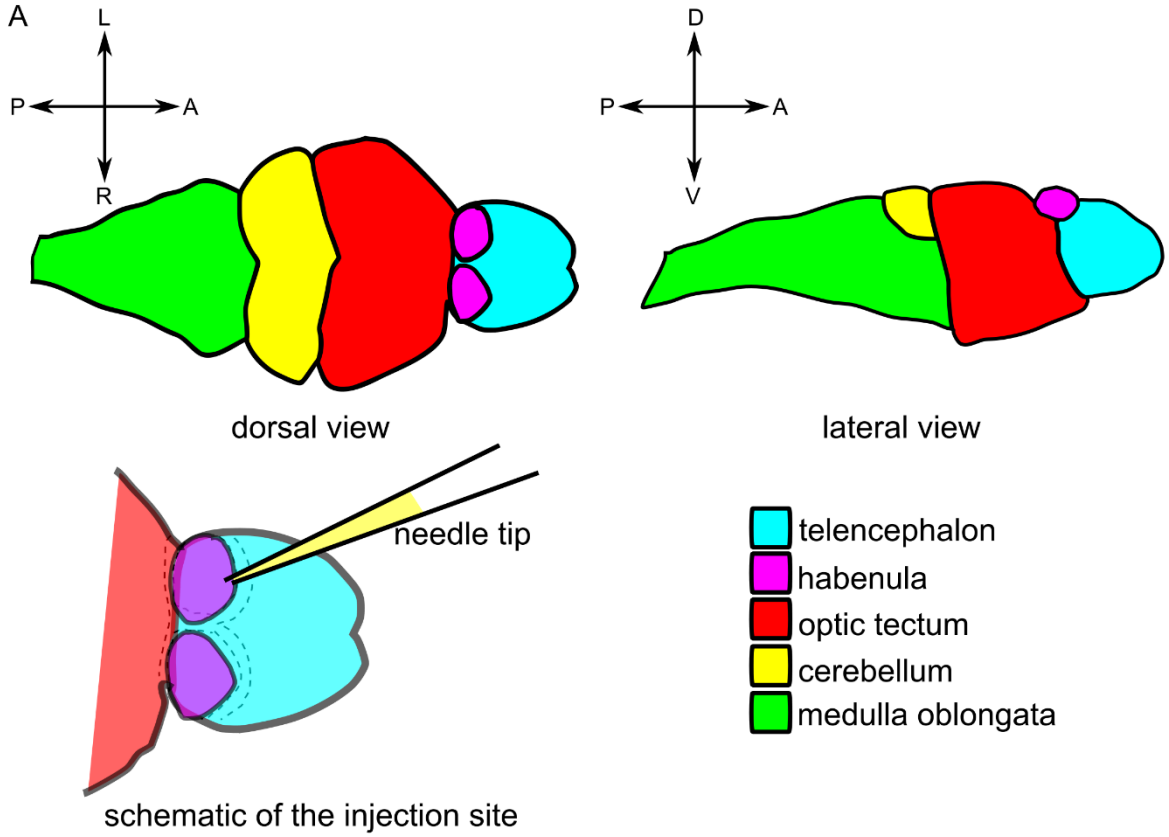

Figure 2.
(A) Schematic of the zebrafish habenulae location within the brain depicting also the injection site. Surrounding blood vessels are marked with dashed lines. A – anterior, P – posterior, L – left, R – right, D – dorsal, V – ventral. (B) An exemplary images of the zebrafish head with zoom-in onto the habenulas. Dark spots are melanophores in the skin. Scale bar – 200 µm.

6. Administer 4 drops of NaCl with Phenol Red or rapamycin with Phenol Red solutions by injecting 1 drop at a time at 20 s intervals. **Troubleshooting 3**

Note: For microinjection use the stereo microscope with at least 150x magnification.

Recovery

Timing: 3-4 h + 1 day

This step describes the recovery procedure after the injections.

7. After each batch of injections, fill the Petri dish containing immobilized larvae with 40 mL of E3 (without Tricaine), and place it back in the incubator.

8. After 3-4 hours, if the larvae did not freed themselves already, gently remove the agarose from around the larvae using a thin pipette tip. **Troubleshooting 4**
    a. Transfer the free larvae to a clean Petri dish with fresh E3 medium.

Note: Do not remove the agarose from the fish immediately after injection. Leaving the fish in agarose reduces the risk of damaging the fish. The fish can rest and recover after injection. Once they start moving, most of the fish can get out of the remaining agarose on their own. If not, be careful during removing the agarose with a tip, as the yolk sac can be easily damaged.

Second microinjection and recovery

Timing: 6 h + 1 day

This step is required in the case of rapamycin injections, in order to achieve sustained effect of the treatment.

9. On the following day (4 dpf), perform the microinjections again by repeating steps 1-6.

10. Allow the larvae to recover as described in steps 7-8.

11. On 5 dpf, the larvae can be used for further experiments, such as behavioral testing, brain imaging, or immunofluorescence staining.

Expected outcomes

The subsequent injections of 1 μM rapamycin at 3 and 4 dpf result in the inhibition of the mTorC1 activity localized to the injected region (left habenula). This can be verified by analyzing the phosphorylation levels of one of the target proteins of mTorC1, Rps6. Immunofluorescence staining shows lowered levels of phosphorylated Rps6 (pRps6) in the left habenula of *tsc2*$^{vu242/vu242}$ mutants at 5 dpf following rapamycin injections, in comparison to control group injected with NaCl, bringing them down to a level comparable with that found in the wild-type fish (Fig. 3). Additionally, we have previously shown that the *tsc2*$^{vu242/vu242}$ mutants, compared to wild-type siblings, display a lowered preference for light over dark environment in the light-dark choice assay. This aberrant behavioral response to light was rescued by rapamycin injections into the left habenula[1].

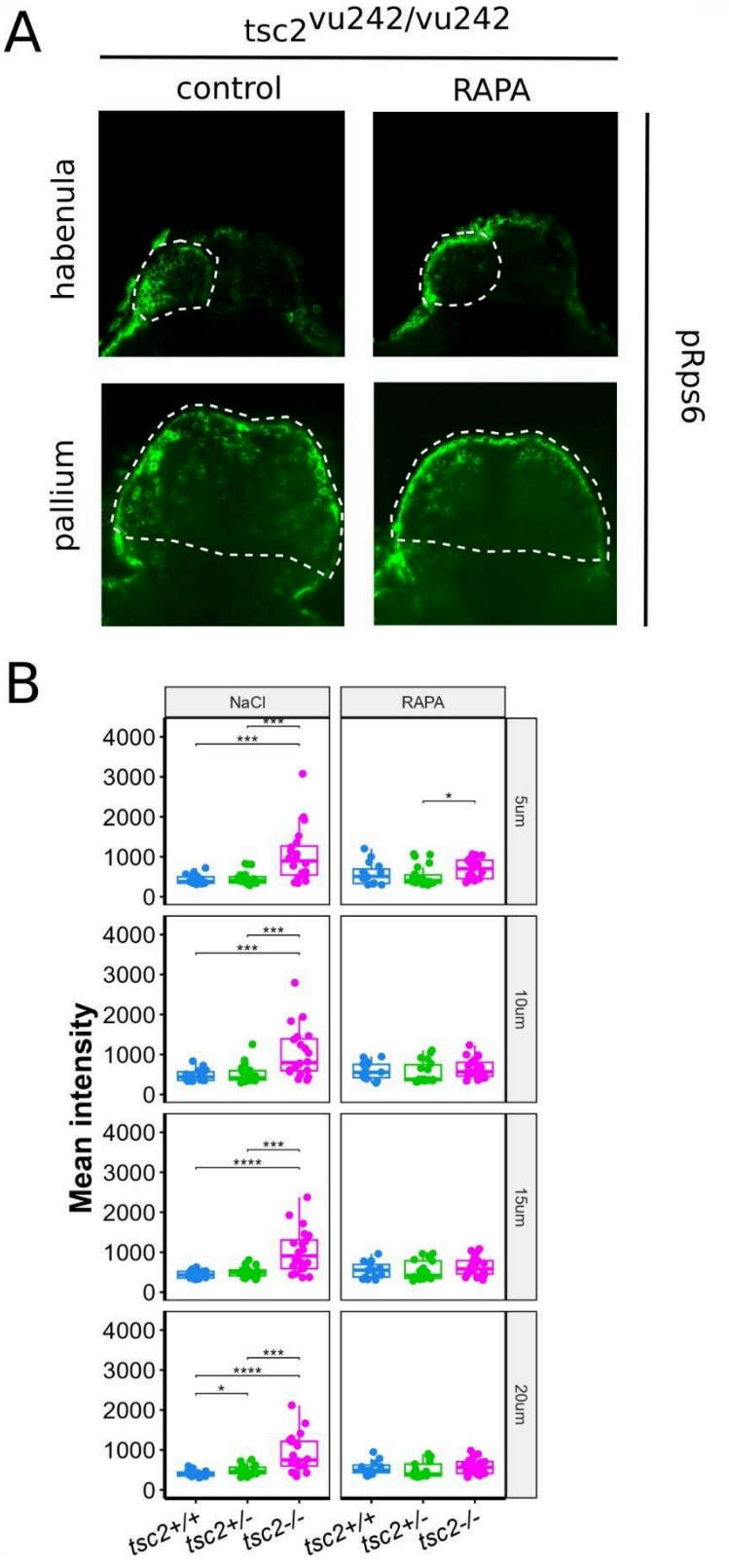

Figure 3. Expression levels of the pRps6 in the left habenula of tsc2$^{vu242/vu242}$ zebrafish.
(A) Representative optical sections through habenula and pallium of *tsc2*$^{vu242/vu242}$ fish injected at 3 and 4 dpf with NaCl or rapamycin, following immunofluorescence staining against pRps6. The images show a decrease in fluorescence intensity in the left habenula following rapamycin injections, but no significant change in fluorescence intensity in the pallium. (B) Quantification of mean intensity of pRps6 fluorescence from LdHb of *tsc2*^{vu242} fish injected at 3 and 4 dpf with NaCl or rapamycin (5 µm from the top of the habenula: *tsc2*$^{vu242/vu242}$ control vs. *tsc2*$^{+/+}$ control $p = 0.000107$ and vs. *tsc2*$^{vu242/+}$ control $p = 0.000244$; *tsc2*$^{vu242/vu242}$ treated with RAPA vs. *tsc2*$^{vu242/+}$ treated with RAPA $p = 0.022$. 10 µm: *tsc2*$^{vu242/vu242}$ control vs. *tsc2*$^{+/+}$ control $p = 0.000918$ and vs. *tsc2*$^{vu242/+}$ control $p = 0.000867$. 15 µm: *tsc2*$^{vu242/vu242}$ control vs. *tsc2*$^{+/+}$ control $p = 8.73e\text{-}05$ and vs. *tsc2*$^{vu242/+}$ control $p = 0.000456$. 20 µm: *tsc2*$^{vu242/vu242}$ control vs. *tsc2*$^{+/+}$ control $p = 7.5e\text{-}06$ and vs. *tsc2*$^{vu242/+}$ control $p = 0.000676$; *tsc2*$^{vu242/+}$ control vs. *tsc2*$^{+/+}$ control $p = 0.047$). The dots on the boxplots represent the number of fish in the experiment ($N > 10$ per experimental group).

Limitations

- The dose and timing of the administered drug should be tested prior to further experiments, especially as it might be different than when the drug is administered into the water. In our study, we have determined that two subsequent injections of 1 μM rapamycin at 3 and 4 dpf are required for effective inhibition of mTorC1 activity at 5 dpf, as a lower dose or a single injection did not result in significantly lowered levels of pRps6[1]. Similarly, efficacy of the treatment should be tested when considering injections of other drugs, or at other developmental stages.

- This protocol might also be used for injections into other parts of the brain, e.g. the cerebellum. However, due to the lack of stereotaxic instruments designed for zebrafish larvae, finding a very specific region of interest might require additional effort and care. Additionally, while the habenulae are positioned dorsally and easily accessible, injecting into the deeper parts of the brain might be more problematic.

Troubleshooting

Problem 1:

The ejected drops are too big or too small. The size of drops should be set to 0.5 nL. To set appropriate size use the microscope calibration slide with a ruler of 0.01 mm or microscope reticle.

Potential solutions:

- If the drop size is smaller than 0.5 nL, consider increasing the pressure in the injection pump. Do not increase the pressure too much (above 500 hPa), as you can damage the fish. If this solution will not resolve the problem, break the needle a little more under the stereoscope using the high magnification (at least 50x).
- If the drop size is bigger than 0.5 nL, consider decreasing the pressure in the injection pump. If this solution will not resolve the problem, then the diameter of the needle may be too big. Prepare another needle, breaking the tip off at a lower point. Always, break the needle under the stereoscope using the high magnification (at least 50x magnification).

Problem 2:

No effect of the drug is observed following the injection.

Potential solutions:

- Consider increasing the dose of the drug.

- Multiple injections on subsequent days might be required. With multiple injections especially, take extra care to make sure they don't cause sustained injury, and that the larvae have sufficient time to recover between injections.

Problem 3:

No drops are ejected from the needle.

Potential solutions:

- Check for air bubbles or any debris that might be blocking the needle.
- Check for any breaks or leaks in the needle or injector tubing.

Problem 4:

High mortality of larvae following injections. The mortality rate depends on many factors like injection time and drug dose. However, the critical factor is the user. For unskilled users the mortality rate can reach up to 50% whereas for skilled users mortality rate decreases to ~1%. Practice with wild-type larvae before your experiment to master the procedure.

Potential solutions:

- The most likely cause is damage to the body of the fish or rupturing the yolk during either mounting (step 4a) or freeing the fish from agarose (step 8). During those steps, take extra care not to damage the fish.
- The fish might also be damaged when the micropipette is inserted too deep into the tissue, or at the wrong place. Make sure you have located the habenula correctly, and that the fish is mounted in such a way that it is easily accessible, facing straight up.

Resource availability

Lead contact

Further information and requests for resources and reagents should be directed to and will be fulfilled by the lead contact, Justyna Zmorzynska (j.zmorzynska@imol.institute).

Materials availability

This study did not generate new unique reagents. The fish mutant and transgenic lines are protected under material transfer agreement with the institutions that generated the lines. Upon appropriate agreement with these institutions, they can be requested from the lead contact.

Data and code availability

This study did not generate datasets or codes.

Acknowledgments

We thank Kevin Ess (Vanderbilt University) for the *tsc2*$^{vu242/+}$ zebrafish line, and the IIMCB ZCF for assistance with the adult fish. This work was supported by an OPUS grant no. 2020/37/B/NZ3/02345 from National Science Centre, Poland. For the purpose of Open Access, the author has applied a CC-BY public copyright licence to any Author Accepted Manuscript (AAM) version arising from this submission.

Author contributions

This protocol was developed by J.Z. The detailed procedure was written and edited by O.D., T.D., and J.Z. Resources and funding were secured by J.Z.

Declaration of interests

The authors declare no competing interests.

References

1. Doszyn, O., Kedra, M., Zmorzynska, J. (2024). Hyperactive mTORC1 disrupts habenula function and light preference in zebrafish model of Tuberous sclerosis complex. iScience 27(6), 110149. DOI: https://doi.org/10.1016/j.isci.2024.110149
2. Switon, K., Kotulska, K., Janusz-Kaminska, A., Zmorzynska, J., Jaworski, J. (2017). Molecular neurobiology of mTOR. Neuroscience 341, 112-153. DOI: https://doi.org/10.1016/j.neuroscience.2016.11.017
3. Dreosti, E., Vendrell Llopis, N., Carl, M., Yaksi, E., Wilson, S.W. (2014). Left-Right Asymmetry Is Required for the Habenulae to Respond to Both Visual and Olfactory Stimuli. Curr. Biol. 24, 440-445. DOI: https://doi.org/10.1016/j.cub.2014.01.016
4. Zhang, B.B., Yao, Y.Y., Zhang, H.F., Kawakami, K., Du, J.L. (2017). Left Habenula Mediates Light-Preference Behavior in Zebrafish via an Asymmetrical Visual Pathway. Neuron 93, 914-928.e4. DOI: https://doi.org/10.1016/j.neuron.2017.01.011
5. Konadu, B., Cox, C.K., Gibert, Y. (2024). Protocol for the microinjection of free fatty acids and triacylglycerol in zebrafish embryos. STAR Protocols 5(2), 103086. DOI:https://doi.org/10.1016/j.xpro.2024.103086.
6. Kim, S.-H., Speirs, C.K., Solnica-Krezel, L., Ess, K.C. (2011). Zebrafish model of tuberous sclerosis complex reveals cell-autonomous and non-cell-autonomous functions of mutant tuberin. Dis. Model. Mech. 4, 255-267. DOI: https://doi.org/10.1242/dmm.005587

Chapter 8. Evolutionary Perspectives on Anxiety: Telencephalic Circuitry and the Anxiogenic Role of TrkB Signaling in Tuberous Sclerosis Complex

Olga Doszyn[1], Justyna Zmorzynska[1,2]

[1]Laboratory of Developmental Neurobiology, International Institute of Molecular Mechanisms and Machines, 02-247 Warsaw, Poland
[2]Lead contact

Biorxiv [preprint], 2025 Jun 25.

DOI: 10.1101/2025.06.23.661056.

Abstract

Tuberous Sclerosis Complex (TSC) is a genetic disease which manifests as a range of neurological symptoms, including benign brain tumors, epilepsy, and TSC-associated neuropsychiatric disorders (TANDs). Among the latter, according to recent reports, anxiety and mood disorders affect over 50% of patients. We have previously demonstrated anxiety-like behavioral symptoms in the zebrafish model of TSC, which were rescued by treatment with the TrkB antagonist ANA-12. Here, we aimed to investigate the mechanism of how ANA-12 regulates behavior by analyzing brain activity in the telencephalon of TSC zebrafish larvae, and we identified the affected regions as corresponding to the known mammalian circuitry involved in anxiety processing. Due to differences in development, the identification of telencephalic territories that are homologous between zebrafish and mammals remains challenging, particularly at early, dynamic stages of development. However, we were able to identify populations of neurons in the zebrafish habenula and ventral subpallium whose involvement in anxiety parallels that of mammals. Those regions were dysregulated in the TSC mutant. This dysregulation correlated with aberrant anxiety behavior and was rescued by treatment with ANA-12. Our results suggest that hyperactivation of TrkB in those regions is a major contributor to anxiety-like behavior as seen in TSC fish, and that those mechanisms could be evolutionarily conserved between zebrafish and mammals.

Introduction

Tuberous sclerosis complex (TSC) is a genetic disease caused by inactivating mutations in either the *TSC1* or *TSC2* gene. The products encoded by these genes, known as Hamartin and Tuberin respectively, together with the protein TBC1D7, form the TSC complex, acting as a negative regulator of mammalian/mechanistic target of rapamycin complex 1 (mTORC1) (Crino et al., 2006). mTORC1 is a hub for many signaling pathways, and in neuronal development, it regulates the processes of axon genesis and guidance, dendritogenesis, synaptic plasticity, learning and memory (Switon et al., 2017). In the brain, TSC presents with benign tumors, lesions and cortical dysplasia, epilepsy, and TSC-associated neuropsychiatric disorders (TANDs) (Crino et al., 2006; Salussolia et al., 2019). This term is used to describe a wide plethora of symptoms, ranging from intellectual disability and cognitive deficits, autism spectrum disorder, attention deficit–hyperactivity disorder (ADHD), to anxiety and mood disorders (de Vries et al., 2015). According to the recent statistics presented by the TANDem project, which aimed to establish an internationally standardized methodology for diagnosis and treatment of TANDs, anxiety and mood disorders affect up to 56% of TSC patients. At the same time, anxiety is believed to be underdiagnosed, especially when co-occurring with intellectual disabilities, which may make it difficult for the patient to effectively communicate their experiences. The TANDem project also concludes that more research is still needed to understand the underlying mechanisms by which anxiety arises in TSC patients, and find targeted treatments (de Vries et al., 2023).

In the previous study conducted by our group, we have found elevated cortisol levels and anxiety-like behavior exhibited by *tsc2*$^{vu242/vu242}$ (tsc2-deficient) zebrafish larvae. The increased high-range velocity in *tsc2*$^{vu242/vu242}$ fish, indicative of anxiety, was rescued by treatment with ANA-12, a selective TrkB inhibitor. ANA-12 also rescued the seizure-associated decreased activity of the *tsc2*$^{vu242/vu242}$ mutant, as well as the observed thinning of the anterior commissure, suggesting the role of TrkB signaling in brain connectivity and epileptogenesis, either of which could contribute to anxiety (Kedra et al., 2020). However, the question of how ANA-12 might affect the activity of pertinent brain regions in order to produce its effect on behavior remained unanswered.

In this study, we conducted an in-depth investigation into the anxiolytic effects of ANA-12 by performing additional behavioral assays in zebrafish. Furthermore, we examined neuronal activation patterns in the frontbrain of tsc2$^{vu242/+}$ zebrafish larvae using whole-brain imaging techniques to elucidate the neuroanatomical correlates of ANA-12-induced behavioral changes and we have found that ANA-12 regulates activity in regions linked to behavioral regulation and processing of stress and fear related information, such as the habenulae, striatum and septum. We have also putatively identified parts of the amygdaloid complex in the zebrafish brain at early stages of development.

Methods

Zebrafish breeding and genotyping

All experiments were performed using the *tsc2*$^{vu242/+}$ zebrafish line (Kim et al., 2011). Adult and larval zebrafish were maintained according to international standards. In each experiment, offspring of at least three parental pairs were used. The larvae were genotyped in order to distinguish wild-type fish from those hetero- or homozygous for the mutation in the *tsc2* gene. Behavioral experiments were performed blindly for the genotype, with larvae collected for genotyping afterwards; for the purpose of immunofluorescence staining, Western blot and ELISA assays, heads were collected for the experiment, and tails were used for genotyping. All genotyping was performed using the HRM method.

Drug treatments

All stock solutions of drugs used in this study were prepared in E3 medium (5 mM NaCl, 0.17 mM KCl, 0.33 mM $CaCl_2$, 0.33 mM $MgSO_4$) or dimethyl sulfoxide (DMSO; Sigma-Aldrich (Merck)). Working solutions were prepared in E3 medium. Drugs were administered into the bathing medium, containing up to 50 dechorionated larvae. Treatments included: 200 nM rapamycin from 2 days post-fertilization (dpf), and 50 nM ANA-12 or 60 μM vigabatrin (all from Sigma-Aldrich (Merck)) 24 hours before the behavioral test.

Behavioral tests

Behavioral tests were performed using zebrafish larvae at 5 dpf, following a 15-minute period of habituation to the behavioral testing room. Zebrafish activity was recorded using the ZebraBox system, with experimental parameters set using the dedicated ZebraLab software (both from ViewPoint Behavior Technology). Obtained raw data was processed and analyzed using RStudio software (cran.r-project.org; rstudio.com).

The open field test was performed as previously described (Kedra et al., 2020). Single larvae were placed in each well of a 6-well plate, filled with E3 medium. The plate was uniformly illuminated with bottom light set to 80% intensity. Activity was tracked for 8 min, with a 5 s time bin. Surround and central areas of each well were defined in ZebraLab software, and the cumulative activity in each area (normalized to the total time of movement) was calculated for each fish. Lack of movement of the *tsc2*$^{vu242/vu242}$ mutants was mapped to non-motor seizures before (Kedra et al., 2020), therefore not moving fish were excluded from the analysis.

For the sudden light changes test (Kedra et al., 2020), single larvae were placed in each well of a 24-well plate, filled with E3 medium. Activity was tracked for 30 min overall, with a 5 s time bin. The experiment consisted of three phases: dark-light-dark, of 10 min each. During the light phase, the plate was illuminated with bottom light set to 60% intensity.

Whole-mount immunofluorescence

At 5 dpf, heads of zebrafish larvae were collected into 4% PFA solution for overnight fixation at 4°C. For staining with antibodies against phosphorylated proteins, 2% (v/v) of 1 M NaF was added to the fixative solution as a phosphatase inhibitor. Fixed samples were then washed with 1x PBS, and incubated with 3% KOH, 1% H_2O_2 bleaching solution for approx. 30-45 min at room temp. to remove pigmentation. Samples were then stained with primary antibodies (anti-pRps6 (Ser235/236; Cell Signaling Technology), 1:200; anti-TrkB (Proteintech), 1:400; anti-ERK (Cell Signaling Technology), 1:400; anti-pERK (Cell Signaling Technology), 1:400; anti-VGlut1 (Synaptic Systems), 1:400; GAD65/67 (Abcam), 1:400; anti-calretinin (Swant), 1:200; anti-NPY (Abcam), 1:200; anti-parvalbumin (Genetex), 1:250) and secondary antibodies (donkey anti-mouse Alexa Fluor 568, 1:1000, or donkey anti-rabbit, Alexa Fluor 488, 1:1000, both from Thermo Fisher Scientific) according to a previously established protocol (Doszyn et al., 2025).

Protein extraction and Western blot

25-30 heads of each genotype were pooled into Ringer's solution supplemented with protease and phosphatase inhibitors (1 mM aprotinin, 1 mM leupeptin, 0.25 mM benzamidine hydrochloride, 0.25 mM Pefabloc® SC, 0.5 mM sodium orthovanadate, 1 mM sodium β-glycerophosphate, 0.25 mM tetrasodium pyrophosphate, 2.5 mM sodium fluoride), 1% Triton™ X-100 (Sigma-Aldrich (Merck)), 0.1% SDS, and 0.5 mM EDTA, sonicated, and placed on ice for 30 min. The samples were then centrifuged for 5 min at 4 ℃ at 9000 rpm, and concentrated Laemmli buffer was added to each sample to the final concentration of 1x. The samples were then denatured by incubation in 95 ℃ for 5 min using Thermomixer C (Eppendorf®), aliquoted and stored at -20 ℃.

SDS-PAGE electrophoresis was performed using the vertical Mini-PROTEAN system (Bio-Rad), in Tris-Glycine-SDS buffer. For the immunodetection of target proteins, the samples were transferred from the polyacrylamide gel onto a PVDF membrane (Sigma-Aldrich (Merck)) activated by submerging in 100% methanol. Transfer was performed using the vertical Mini Trans-Blot® Cell system (Bio-Rad), in Towbin buffer with SDS, at 4 ℃. The membrane was then washed with deionized water, and incubated in 5% milk in TBS buffer against non-specific binding for 1 h at room temp. After blocking, the membrane was washed with TBST, and incubated with primary antibodies: anti-Rps6 (Santa Cruz Biotechnology), 1:200; anti-pRps6 (Ser235/236 Cell Signaling Technology), 1:1000) in 5% BSA in TBST overnight at 4 ℃. On the following day, the membrane was washed thrice with TBST, and incubated with secondary antibodies (IRDye® 680RD Donkey anti-Rabbit IgG, 1:10 000, or IRDye® 800CW Donkey anti-Mouse IgG, 1:10 000, both from LI-COR Bioscience) in 5% BSA in TBST for 1 h at room temp. Afterwards, the membrane was again washed thrice with TBST, then imaged using the Odyssey DLx (LI-COR Bioscience), and analyzed using Image Studio Lite v.5.5 software (LI-COR Bioscience).

ELISA assay

The ELISA assays for P-TrkB and TrkB were performed on samples containing 20 heads each, according to manufacturers' instructions. The detection antibody in both assays was the biotin-conjugated anti-TrkB antibody (500 ng/ml working concentration; catalog no. BAF397, R&D) and streptavidin-horseradish peroxidase (1:200; R&D) to detect TrkB. The capture antibodies were anti-P-TrkB (catalog no. DYC688, R&D) and anti-TrkB (4 ng/l working concentration; catalog no. 13129-1-AP, ProteinTech).

Imaging and image analysis

All images were acquired using a Zeiss Lightsheet Z.1 microscope (40x water immersion objective, NA = 1.3) at 1024 × 1024 pixel-resolution, in a z-stack mode with an interval of 0,5 μm between z-slices, resulting in multi-layered images of brain tissue.

The images were then analyzed using Fiji software (Schindelin et al., 2012). For calretinin, the number of calretinin-positive cells in each region of interest (ROI) was counted manually. For phosphorylated ribosomal protein s6 (pRps6), 5 signal-positive cells per fish were randomly selected, mean signal intensity of each cell were measured using the Measure tool, and the mean intensity per fish was later calculated in Rstudio. For TrkB and parvalbumin, ROIs were selected manually, Z-slices were superimposed using the Sum slices tool, and the intensity or integrated density of the fluorescent signal were measured using the Measure tool. Integrated density was chosen as a proxy for the number of parvalbumin-positive cells due to the low optic resolution in the medial subpallium, making it difficult to distinguish single cells.

For, neuronal activity measurements using pERK-ERK method, the brains were firstly registered to the reference brain using Parallel Fiji CMTK Registration Plugin by Sandor Kovacs (github.com/sandorbx/Parallel-Fiji-CMTK-Registration). After accuracy analysis, the automated analysis of neuronal activity was performed similarly to previously described protocol (Randlett et al., 2015), except the commands were done in Fiji. These included preprocessing, division of pERK and ERK channels, gaussian blurring, and averaging. At least 20 images were averaged per genotype per treatment from two independent experiments. The statistics were calculated using FDR method versus randomized dataset. Only significant pixels are represented on the neuronal activity maps (images).

Statistical analysis

All data were analyzed with Rstudio software (cran.r-project.org; rstudio.com). Sample sizes could not be predetermined due to the random distribution of genotypes; however, this provided randomization and blinding for sample collection. Equality of variance and normality of residuals were determined with Levene's test and Shapiro-Wilk test, respectively. If data were normally distributed, they were analyzed by two-way ANOVA with post-hoc TukeyHSD test; otherwise, the Kruskal-Wallis test was used with post-hoc Wilcoxon test to correct for multiple comparisons. Data are presented as medians using boxplots, where each dot represents datapoint from one fish. Data points outside of the boxplot whiskers represent outliers. Adjusted p-values below 0.05 were considered

statistically significant, and are shown on figures with * for $p < 0.05$, ** for $p < 0.01$, *** for $p < 0.001$, and **** for $p < 0.0001$.

Results

ANA-12 rescues anxiety-like behavior in *tsc2*$^{vu242/vu242}$ fish

We have previously shown that the *tsc2*$^{vu242/vu242}$ fish exhibit hypervelocity, thigmotaxis in the open field test, and anxiety-like behavior in response to a sudden changes in light conditions. Additionally, hypervelocity was rescued by treatment with ANA-12 (Kedra et al., 2020). Here, we have performed the open field and sudden light changes tests using *tsc2*^{vu242} fish pretreated with ANA-12 versus untreated, and have confirmed a rescue of anxiety-like behaviors in those tests by ANA-12. Relative time spent next to the walls of the testing chamber was increased in *tsc2*$^{vu242/vu242}$ fish in comparison to wild-type *tsc2*$^{+/+}$ and heterozygous *tsc2*$^{vu242/+}$ siblings representing anxiety-like behavior. This was reduced in *tsc2*$^{vu242/vu242}$ homozygotes following treatment with ANA-12 (Fig.1 A-C). However, a reduction in thigmotaxis was also observed following pretreatment with the mTorC1 inhibitor rapamycin, and the antiepileptic drug vigabatrin (Fig.1 B-C). Mutant *tsc2*$^{vu242/vu242}$ fish also showed hyperactivity during the dark phases of the sudden light changes test, which is indicative of anxiety, although freezing during the light phase was not increased in relation to wild-type *tsc2*$^{+/+}$ siblings, whose activity levels also dropped drastically when the light was switched on (Fig.1 E). The hyperactivity of *tsc2*$^{vu242/vu242}$ during the dark phase was markedly reduced by treatment with ANA-12 or rapamycin (Fig.1 F-H).

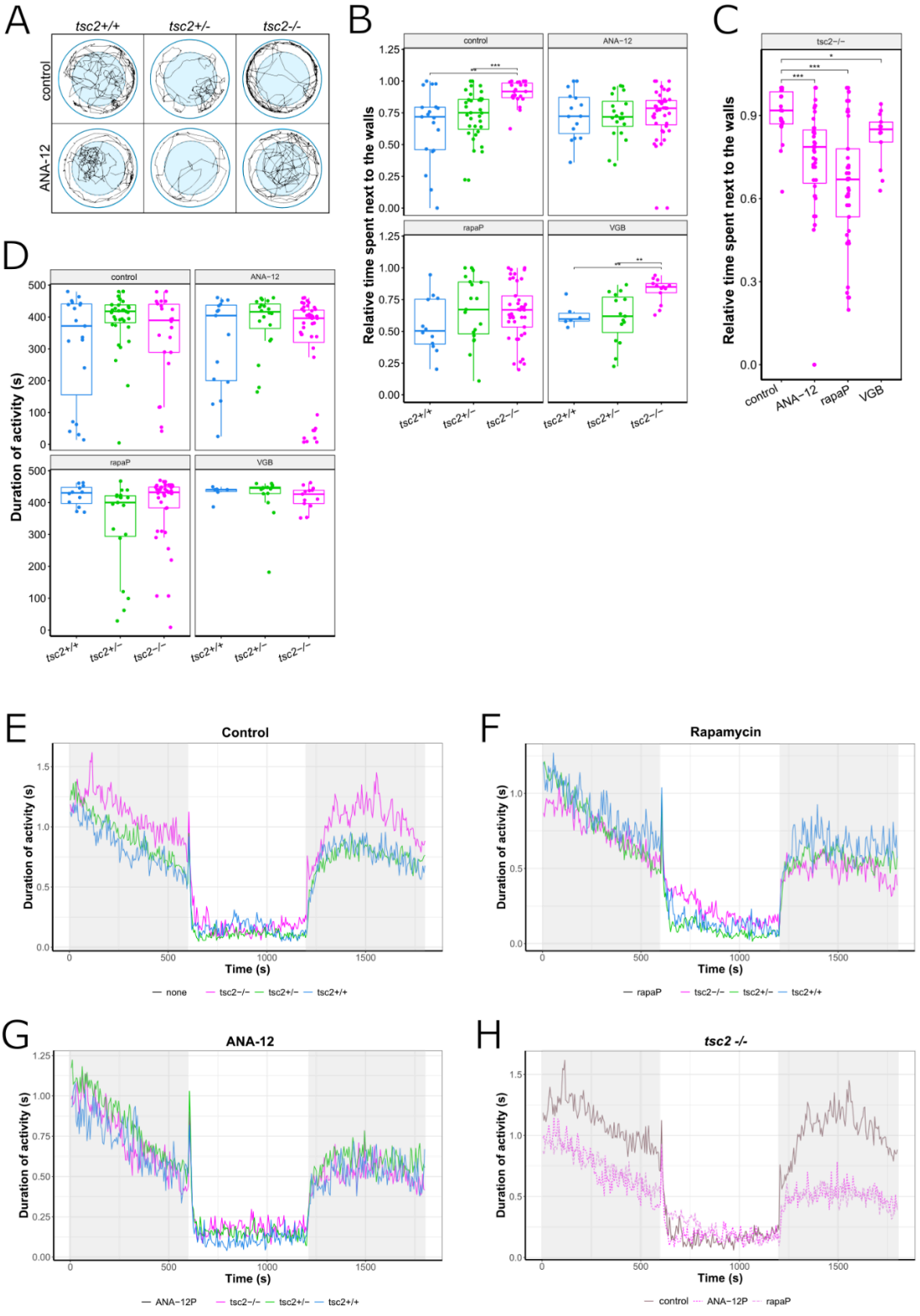

Figure 1. *Tsc2*$^{vu242/vu242}$ fish show anxiety-like behavior that is ameliorated by pretreatment with ANA-12. **(A)** Representative tracks from the open field test for each *tsc2*^{vu242} genotype in the control group vs. treated with ANA-12. Summary tracks from 8 min recordings show thigmotaxis behavior in *tsc2*$^{vu242/vu242}$ fish that is rescued by ANA-12 treatment. **(B)** Relative

time spent next to the walls of the dish [$p = 0.002$ for control *tsc2*$^{+/+}$ vs. control *tsc2*$^{vu242/vu242}$, $p = 0.000159$ for control *tsc2*$^{vu242/+}$ vs. control *tsc2*$^{vu242/vu242}$, $p = 0.002$ for VGB *tsc2*$^{+/+}$ vs. VGB *tsc2*$^{vu242/vu242}$, $p = 0.002$ for VGB *tsc2*$^{vu242/+}$ vs. VGB *tsc2*$^{vu242/vu242}$]. **(C)** Relative time next to the walls compared between *tsc2*$^{vu242/vu242}$ fish only [$p = 0.000227$ for control vs. ANA-12, $p = 0.000122$ for control vs. rapamycin]. **(D)** Duration of overall activity across all genotype and treatment groups. No significant difference between median activity of each group indicates that the relative activity differences are not caused by changes in overall motor activity. **(E-G)** Mean activity over time during suddenly changing light conditions (dark-light-dark) for control, rapamycin and ANA-12 treated groups respectively. **(H)** Mean activity over time during suddenly changing light conditions compared between *tsc2*$^{vu242/vu242}$ fish only.

RapaP – rapamycin pretreatment starting at 2 dpf in order to prevent the development of symptoms; VGB – vigabatrin.

ANA-12 treatment affects TrkB activation

First, we checked how treatment with ANA-12 affected the levels and activity of TrkB in the whole fish heads by ELISA assay to confirm ANA-12 actions. TrkB undergoes self-dimerization and autophosphorylation following the binding of BDNF (Huang & Reichardt, 2003). As we have demonstrated before (Kedra et al., 2020), *tsc2*$^{vu242/vu242}$ fish show increased levels of phosphorylated TrkB (pTrkB) in comparison to wild-type siblings. This effect was rescued by treatment with the direct TrkB antagonist ANA-12 (Fig.2 A). The immunofluorescence stainings of the intact zebrafish brains demonstrated that there was no significant difference between genotypes in either the amount or distribution of the TrkB protein in the pallium of *tsc2*^{vu242} fish, and that those parameters were also not affected by ANA-12 treatment (Fig.2 B-C).

ANA-12 treatment does not affect mTORC1 activity

The stimulation of TrkB by BDNF triggers the activation of multiple downstream pathways, including the phospholipaseCγ (PLCγ), mitogen-activated protein kinase/extracellular signal-regulated protein kinase (MAPK/ERK), and phosphatidylinositide 3-kinase (PI3K)-Akt-mTOR pathway (Huang & Reichardt, 2003; Takei et al., 2004). Although there is no functional TSC complex in the *tsc2*$^{vu242/vu242}$ fish, we checked whether ANA-12 could act through an unknown mechanism that impacts mTORC1 activity. We performed a Western blot assay to check the ratio of phosphorylated ribosomal protein s6 (P-Rps6) to non-phosphorylated form of this protein (Rps6) as it is one of the downstream targets of mTORC1. In the untreated *tsc2*$^{vu242/vu242}$ fish, the ratio of P-Rps6 to Rps6 was increased in comparison to wild-type *tsc2*$^{+/+}$ and heterozygous *tsc2*$^{vu242/+}$ siblings, owing to mTORC1 hyperactivity; and this ratio was preserved in the group treated with ANA-12 (Fig.2 D-E). Similarly, whole-mount immunofluorescence staining against P-Rps6 showed no effect of ANA-12 on neither the levels of P-Rps6 nor the distribution of P-Rps6 positive cells in the pallium of *tsc2*^{vu242} fish (Fig.2 F-G). Therefore, even though pretreatment with rapamycin

resulted in a similar rescue of behavioral symptoms as ANA-12, suggesting that both TrkB and mTORC1 signaling play a role in regulating anxiety, we have confirmed that the effect of ANA-12 on zebrafish behavior is not exerted directly through the mTORC1 pathway.

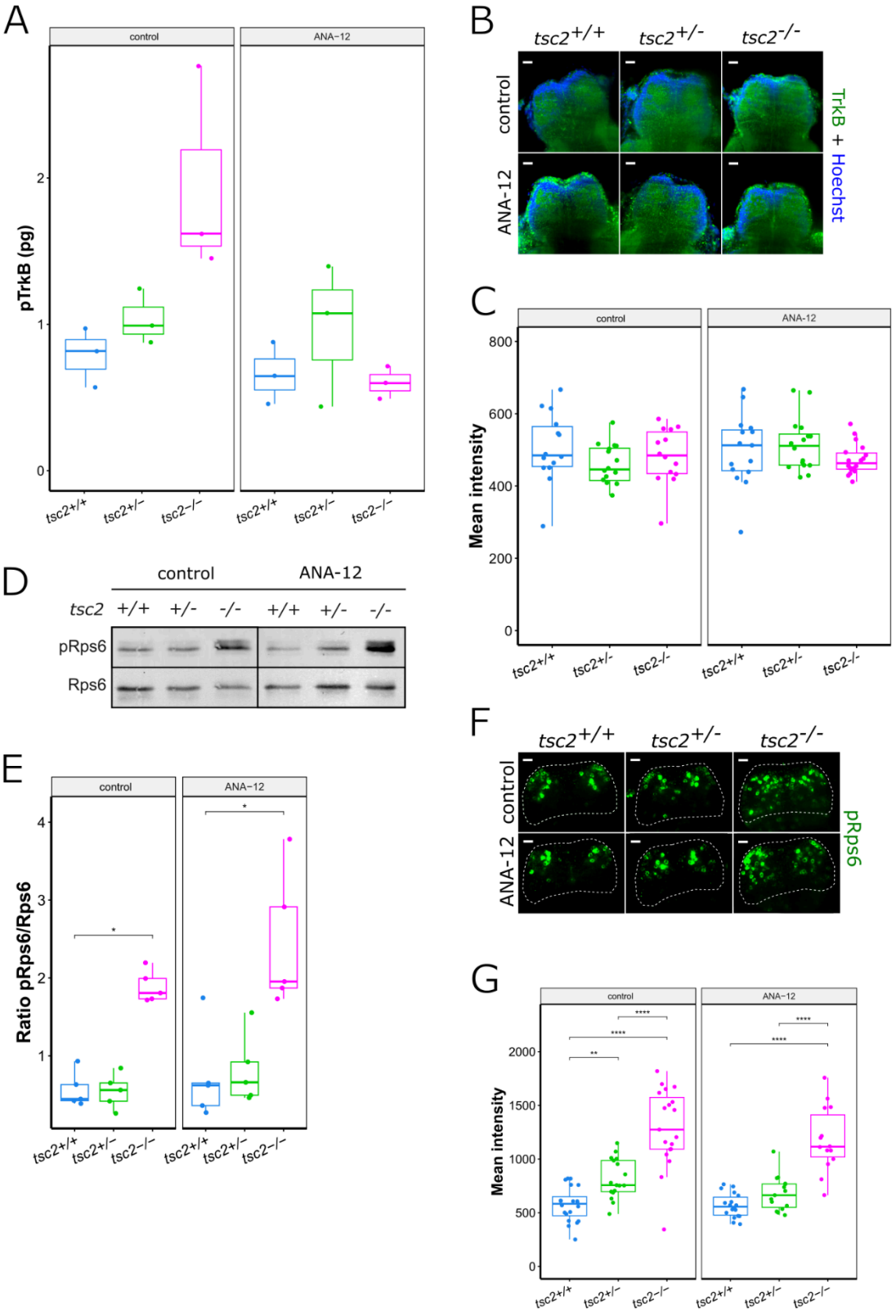

Figure 2. ANA-12 affects TrkB activation but not TrkB levels or mTorC1 activation. **(A)** pTrkB levels in *tsc2*^{vu242} fish ± ANA-12 as measured by ELISA assay. **(B)** Representative images of the *tsc2*^{vu242} zebrafish pallium stained with anti-TrkB antibody and Hoechst nuclear stain. Scale bar = 20 µm. **(C)** Mean intensity of TrkB signal in the pallium across all genotypes ± ANA-12. Each dot represents one fish. **(D)** Representative Western blot results showing the amount of pRps6 and Rps6 protein in whole brains of *tsc2*^{vu242} fish ± ANA-12. **(E)** Ratio of pRps6 to Rps6 protein in *tsc2*^{vu242} fish ± ANA-12 as measured by Western blot [p = 0.016 for control *tsc2*$^{+/+}$ vs. control *tsc2*$^{vu242/vu242}$, p = 0.032 for ANA-12 *tsc2*$^{+/+}$ vs. ANA-12 *tsc2*$^{vu242/vu242}$]. Each dot represents one sample pooled from at least 25 fish. **(F)** Representative images of the *tsc2*^{vu242} zebrafish pallium stained with anti-pRps6 antibody. Scale bar = 20 µm. **(G)** Mean intensity of pRps6 signal in the pallium across all genotypes ± ANA-12 [p = 0.00399 for control *tsc2*$^{+/+}$ vs. control *tsc2*$^{vu242/+}$, p = 3.636e-07 for control *tsc2*$^{+/+}$ vs. control *tsc2*$^{vu242/vu242}$, p = 8.52e-05 for control *tsc2*$^{vu242/+}$ vs. control *tsc2*$^{vu242/vu242}$, p = 3.054e-07 for ANA-12 *tsc2*$^{+/+}$ vs. control *tsc2*$^{vu242/vu242}$, p = 4.206e-05 for ANA-12 *tsc2*$^{vu242/+}$ vs. control *tsc2*$^{vu242/vu242}$]. Each dot represents an average intensity of five cells from one fish.

ANA-12 affects brain activity

The habenula (Hb), a bilateral structure located within the epithalamus, is split into two main subdivisions – medial and lateral in mammals, corresponding to dorsal and ventral in zebrafish respectively (Amo et al, 2010). In both zebrafish and mammals, the habenula is known to play a role in a multitude of processes and behaviors, including fear and anxiety, aversion and reward, sleep and circadian rhythm, reproductive and aggressive behaviors, and processing of sensory stimuli (Fore et al., 2018).

Previously, we have found hyperactive cells in the left dorsal habenula (LDHb) of larval zebrafish, which were also marked by hyperactivation of mTORC1. This hyperactivation was linked to aberrant processing of light stimuli. We have shown that pretreatment with the mTORC1 inhibitor rapamycin rescued both the behavioral symptoms and the dysregulation of neuronal activity (Doszyn et al., 2024). Here, we have imaged the whole left and right habenula following whole-mount staining with antibodies against extracellular signal-regulated kinase (ERK) and phosphorylated (activated) ERK. Since ERK is phosphorylated in response to the calcium influx following neuron depolarization, the ratio of pERK/ERK can be used as a readout of neuronal activity, and has been validated as such in zebrafish (Randlett et al., 2015). We have calculated the ratio of pERK/ERK in untreated *tsc2*^{vu242} fish and siblings treated with ANA-12, and created maps of neuronal activity in each group. Next, we have compared the composite difference maps of activity between *tsc2*$^{vu242/vu242}$ mutant *vs*. wild-type and between *tsc2*$^{vu242/vu242}$ treated with ANA-12 *vs*. untreated *tsc2*$^{vu242/vu242}$ in order to check what brain regions are hypo- or hyperactive in the mutant fish, and whether ANA-12 affect these differences. As seen before in calcium imaging experiments (Doszyn et al., 2024), we have observed significant hyperactivity in the dorsal part of the left habenula. Interestingly, ANA-12 lowered the activity in this region, even though it did not affect light preference behavior (Doszyn et al., 2024), indicating that the

effect of ANA-12 might be restricted to anxiety-like behaviors, even when the affected brain regions have other functions as well. Furthermore, ANA-12 treatment did not result in uniform dampening of neuronal activity, since some regions were unaffected by the treatment, and those that were hypoactive in the *tsc2*$^{vu242/vu242}$ mutant, such as in the right dorsal habenula, were hyperactivated by ANA-12 (Fig.3 A). A similar effect was observed around the habenula commissure, which appeared separated into two distinct hyper- and hypoactive tracts, whose levels of activity were reversed after ANA-12 treatment (Fig.3 B). In the ventral part of both left and right habenula, too, cells that were hypoactive in untreated *tsc2*$^{vu242/vu242}$ fish were more active after ANA-12, and vice versa (Fig.3 C). Therefore, we demonstrated that ANA-12 could rescue both hypo- and hyperactivity in dysregulated brain regions.

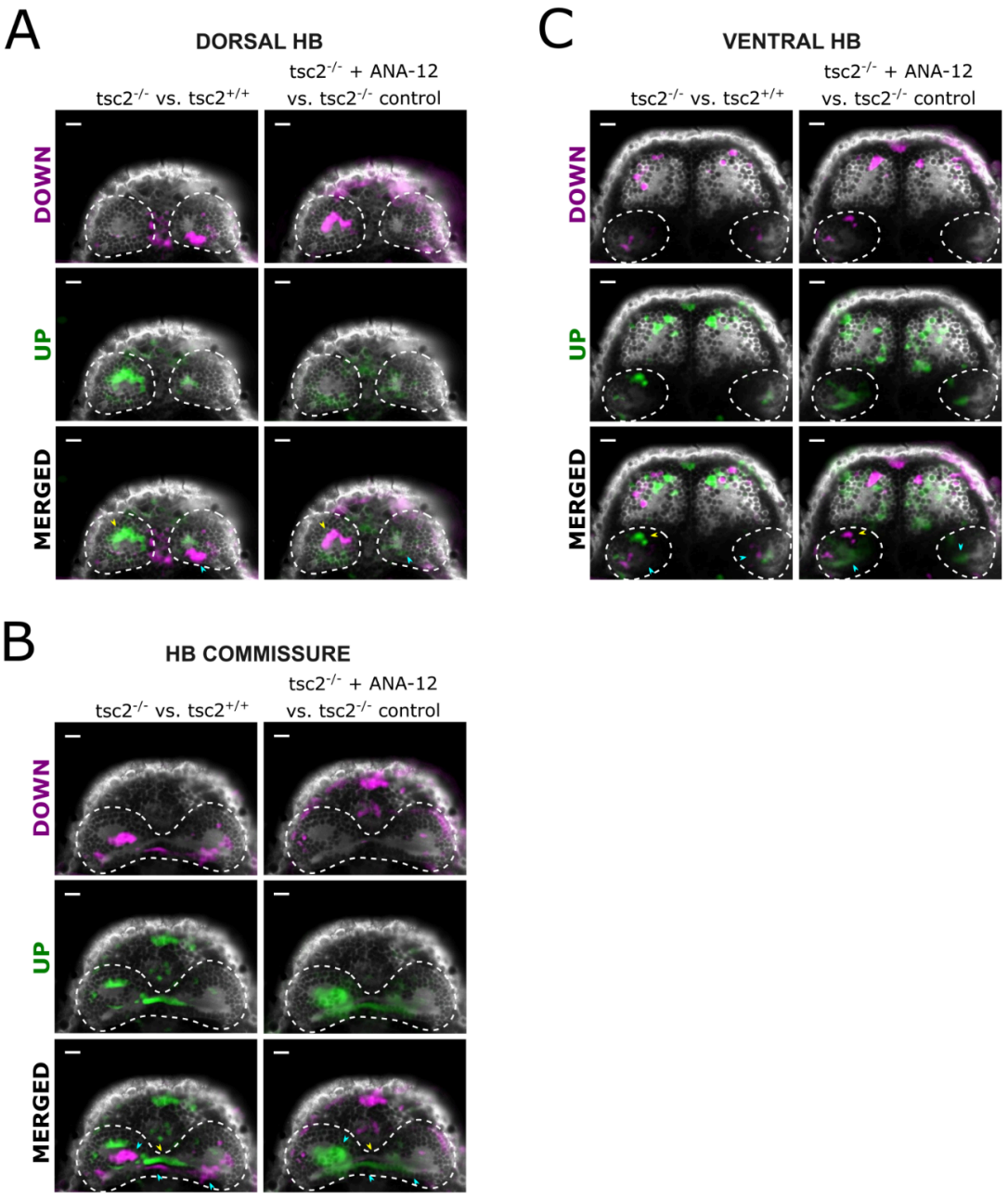

Figure 3. Single z-slices representative of the dorsal habenula **(A)**, area around the habenula commissure **(B)**, and ventral habenula **(C)**. Due to the asymmetry of the habenulae (left Hb being larger than right Hb) the pericommissural area shown here belongs to the dorsal left Hb and ventral right Hb. The images were selected from maps of neuronal activity as measured by the pERK/ERK ratio. Areas marked in magenta represent regions of lower activity in *tsc2*$^{vu242/vu242}$ fish vs. wild-type siblings (left), and *tsc2*$^{vu242/vu242}$ fish treated with ANA-12 vs. untreated *tsc2*$^{vu242/vu242}$ (right), while areas marked in green represent regions of increased activity respectively. The reference brain image is shown in black and white. The yellow and blue arrows point to areas that were upregulated in the mutant but downregulated after ANA-12, or vice versa. Scale bar = 20 μm.

The mammalian amygdaloid complex, located in the forebrain, plays a key role in sensory and behavioral regulation, emotion, and cognition (Pabba, 2013). Most importantly for this study, the amygdala is also crucial for proper responses to fear stimuli (LeDoux, 2000). While its functionality is evolutionarily conserved, a notable difference between zebrafish and mammals is that in the former, the telencephalon forms by eversion, rather than evagination. As a result, the regions of the pallium, while sharing functional homology, are oriented differently than in mammals, making the identification of corresponding structures challenging (Bally-Cuif & Vernier, 2010). While the amygdala has been identified in adult zebrafish (Lal et al., 2018; Porter & Mueller, 2020), there is still a knowledge gap with regards to amygdala development at early larval stages. We have used the pERK/ERK stainings to assess neuronal activity in the telencephalon of *tsc2*^{vu242} fish at 5 dpf, and have stained our samples against a number of markers known to be expressed in various pallial and subpallial territories, in an attempt to identify the amygdaloid nuclei in the developing zebrafish, and correlate the neuronal activity data with functional topology of the brain. Those were the GABAergic neuron marker GAD65/67, the glutamatergic marker VGlut1, neuropeptide Y (NPY), and the calcium-binding proteins calretinin and parvalbumin.

In the most dorsal layer of the *tsc2*$^{vu242/vu242}$ zebrafish pallium, we have found both hypo- and hyperactivated cells. Following treatment with ANA-12, most notably, there was an increase of activity along the midline in *tsc2*$^{vu242/vu242}$ fish (Fig.4 A). This region was also distinguished by clusters of calretinin-positive cells, located along the medial and posterior edges of the white matter compartments (Fig.4 B-C), although no statistically significant differences in the number of calretinin-positive cells were seen between neither genotypes nor treatment groups (Fig.4 D). Following treatment with ANA-12, sporadic parvalbumin-positive cells were seen in the lateral areas. GAD65/67 and VGlut1 were expressed throughout this layer, with a particularly strong enrichment in the white matter compartments (Fig.4 B).

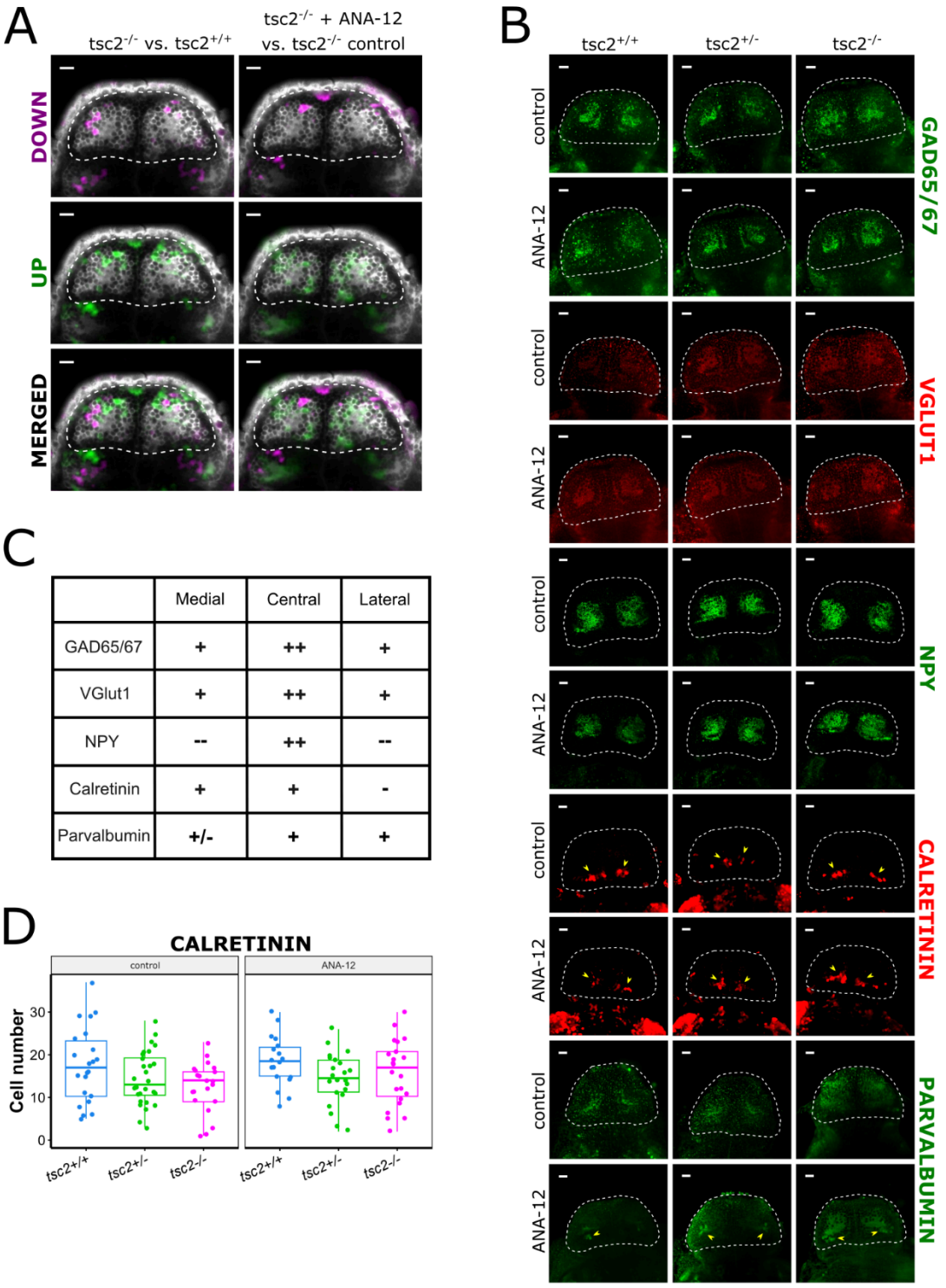

	Medial	Central	Lateral
GAD65/67	+	++	+
VGlut1	+	++	+
NPY	--	++	--
Calretinin	+	+	-
Parvalbumin	+/-	+	+

Figure 4. Representative data from the dorsal pallium. **(A)** Single z-slices from maps of neuronal activity as measured by the pERK/ERK ratio, as described previously. Scale bar = 20 µm. **(B)** Single z-slices from brains stained with antibodies against GAD65/67, VGlut1, NPY, calretinin and parvalbumin, selected from the corresponding region of the pallium. Yellow arrows point to distinct calretinin- and parvalbumin-positive cells. Scale bar = 20 µm. **(C)** Expression of markers in the medial, central and lateral areas of this layer, as found in

wild-type fish. **(D)** Number of calretinin-positive cells in the dorsal pallium across all genotypes in untreated vs. ANA-12-treated groups. Each dot represents one fish.

Below this region, moving in the dorsal-ventral axis, multiple hypo- and hyperactivated cells could be seen around the white matter compartments; some of them, though not all, responded to ANA-12 treatment (Fig.5 A). The strong expression of VGlut1/2 together with positive immunoreactivity for GAD65/67 and parvalbumin (Fig.5 A-C) would suggest that this region belongs to the intermediate zone of the subpallium, likely the posterior division of the medial amygdala (MeAp). However, in accordance with data published by Porter and Mueller (Porter & Mueller, 2020), MeA is distinguished by a high number of calretinin-positive cells, which, in our case, were present only sporadically in this layer (Fig.5 B-C).

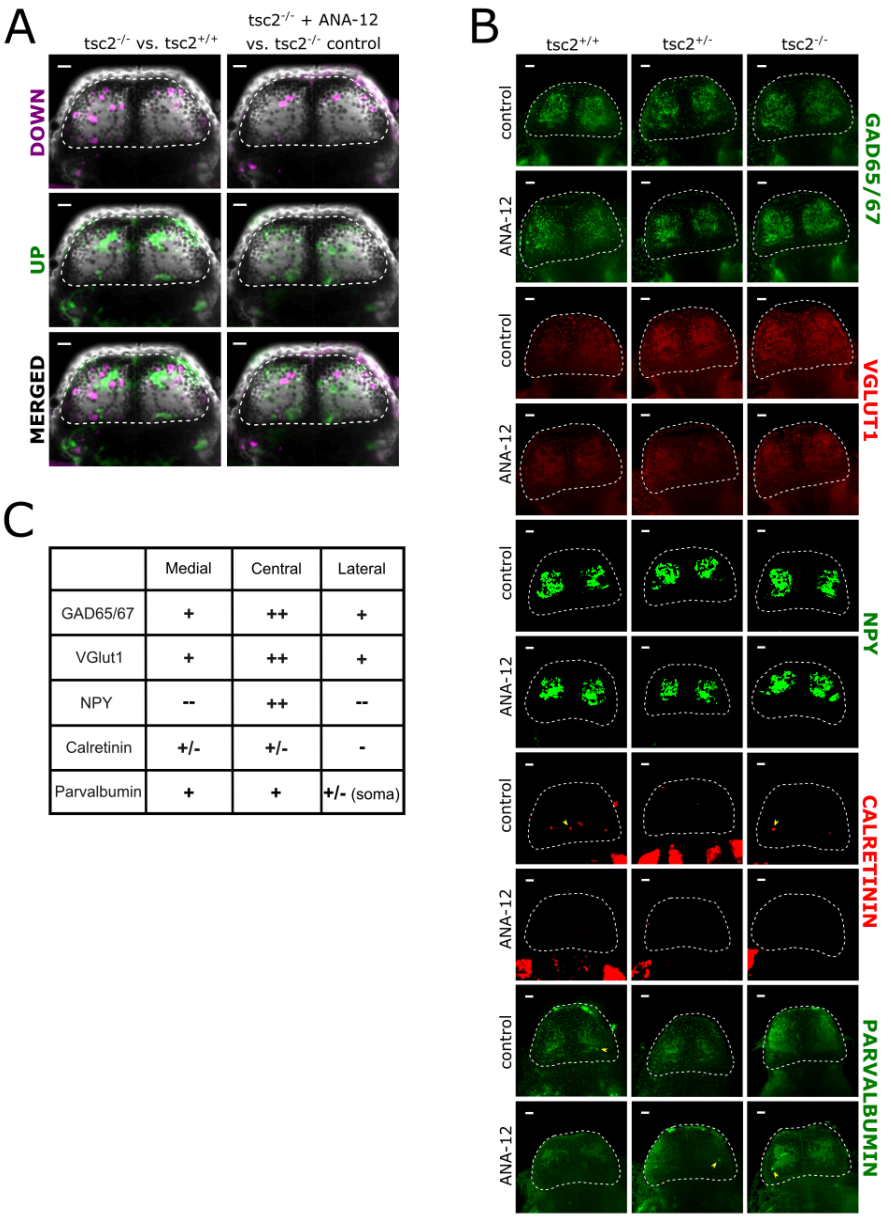

C

	Medial	Central	Lateral
GAD65/67	+	++	+
VGlut1	+	++	+
NPY	--	++	--
Calretinin	+/-	+/-	-
Parvalbumin	+	+	+/- (soma)

Figure 5. Representative data from the next pallial layer. **(A)** Single z-slices from maps of neuronal activity as measured by the pERK/ERK ratio, as described previously. Scale bar = 20 µm. **(B)** Single z-slices from brains stained with antibodies against GAD65/67, VGlut1, NPY, calretinin and parvalbumin, selected from the corresponding region of the pallium. Yellow arrows point to distinct calretinin- and parvalbumin-positive cells. Scale bar = 20 µm. **(C)** Expression of markers in the medial, central and lateral areas of this layer, as found in wild-type fish.

The next layer in the dorso-ventral axis showed a high increase in neuronal activity in *tsc2*$^{vu242/vu242}$ fish compared to wildtype *tsc2*$^{+/+}$ siblings (Fig.6 A). Along the brain midline, the neuronal activity was increased even further after ANA-12 treatment, although single hypoactive cells were also seen (Fig.6 A). This area coincided with high numbers of calretinin-positive cells, which was reduced in the *tsc2*$^{vu242/vu242}$ mutant, both in the control and treated groups (Fig.6 B-D). In ANA-12-treated fish, there were also downregulated clusters positioned laterally, which overlapped with the localization of parvalbumin-positive cells, and positive immunoreactivity for GAD65/67 (Fig.6 A-C). However, in both cases, it could not be determined for certain if those cells correspond to each other due to a lack of a triple pERK+ERK+parvalbumin or pERK+ERK+calretinin staining. The localization of this region in the dorsal-ventral axis, and the expression of tested markers (GAD65/67+, VGlut1-, calretinin+, parvalbumin+) suggest that this layer might correspond to the anterior division of bed nucleus stria terminalis (BNSTa; labelled as BSTa in Porter & Mueller, 2020), however, this could not be determined for certain. Ultimately, at this stage of development, and with the markers used, we were not able to delineate the precise boundaries between the nuclei of the medial and central amygdala, as well as the BNST.

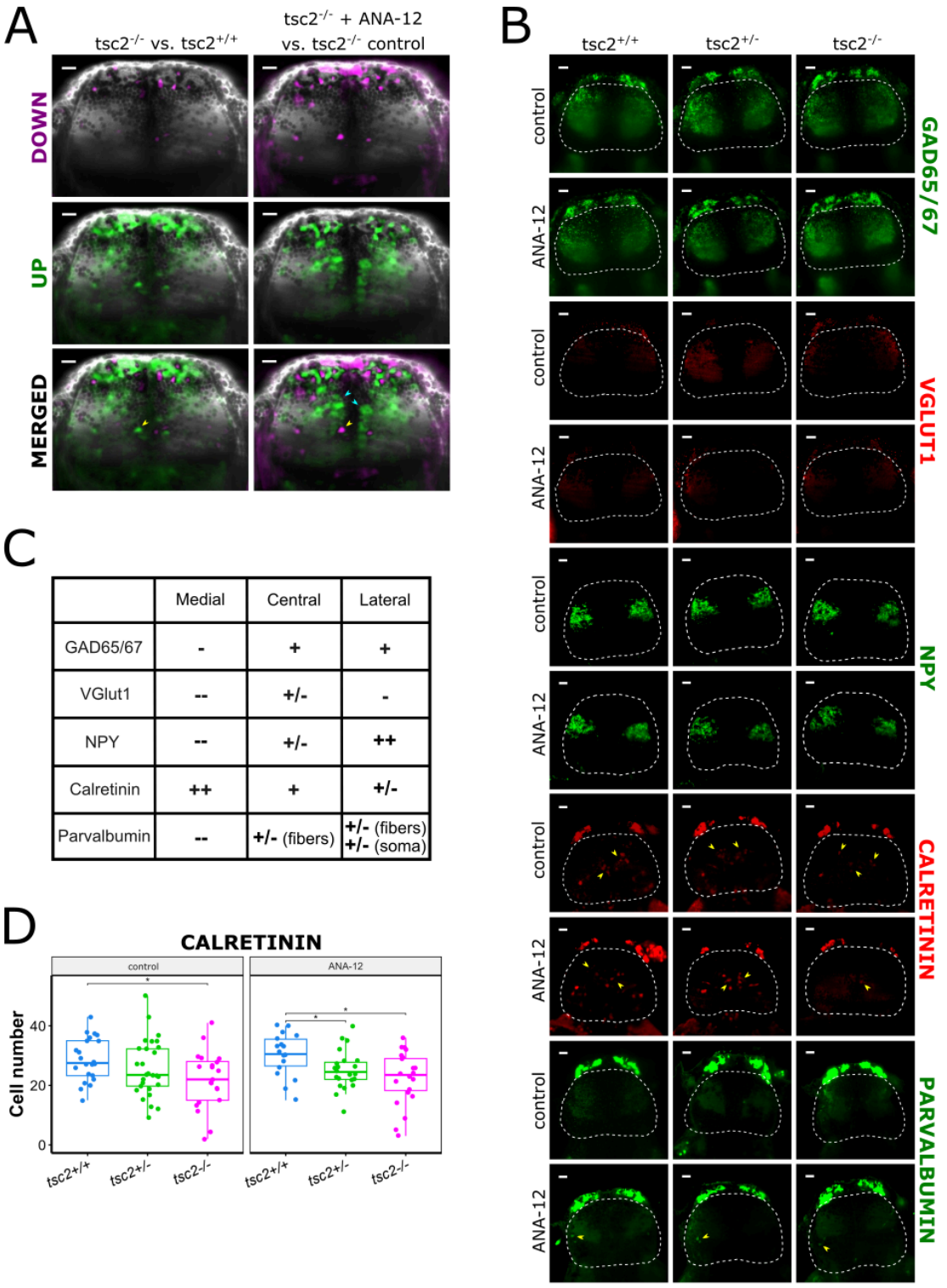

Figure 6. Representative data from the most dorsal layer of the subpallium. **(A)** Single z-slices from maps of neuronal activity as measured by the pERK/ERK ratio, as described previously. The yellow arrows point to one of the cells that were upregulated in the mutant but downregulated after ANA-12. The blue arrows point to the main area along the midline that was upregulated after ANA-12. Scale bar = 20 µm. **(B)** Single z-slices from brains stained with antibodies against GAD65/67, VGlut1, NPY, calretinin and parvalbumin, selected from the corresponding region of the pallium. Yellow arrows point to distinct

calretinin- and parvalbumin-positive cells. Scale bar = 20 μm. **(C)** Expression of markers in the medial, central and lateral areas of this layer, as found in wild-type fish. **(D)** Number of calretinin-positive cells in the subpallium across all genotypes in untreated vs. ANA-12-treated groups [$p = 0.036$ for control *tsc2*$^{+/+}$ vs. control *tsc2*$^{vu242/vu242}$, $p = 0.044$ for ANA-12 *tsc2*$^{+/+}$ vs. ANA-12 *tsc2*$^{vu242/+}$, $p = 0.011$ for ANA-12 *tsc2*$^{+/+}$ vs. ANA-12 *tsc2*$^{vu242/vu242}$]. Each dot represents one fish.

We have also found a population of hyperactive cells in the deeper subpallial layer of *tsc2*$^{vu242/vu242}$ telencephalon, which were downregulated by ANA-12 treatment (Fig.7 A). This layer showed negative immunoreactivity for Vglut1. The expression of GAD65/67 and parvalbumin was constrained to the olfactory pallium, where we have also observed a strong calretinin signal (Fig.7 B, D). Single calretinin-positive cells were also found in both the medial and lateral areas of this layer, however, there was no statistically significant difference in their number between neither genotypes nor treatment groups (Fig.7 B-C). Based on its topological position, we have labelled this region as the striatopallidum.

The most ventral layer of the *tsc2*$^{vu242/vu242}$ fish telencephalon showed strong neuronal hyperactivity in the anterior commissure and the precommissural area (Fig.8 A). By comparison, in *tsc2*$^{vu242/vu242}$ fish treated with ANA-12, the centrolaterally positioned regions showed decreased activity, while there was an increase of neuronal activity along the midline (Fig.8 A). We have also found a distinctive V-shaped cluster of parvalbumin-positive cells (Fig.8 B-C). Based on its topological location and immunoreactivity to brain markers, we identified this region as the septum. In the control group, the integrated density of the parvalbumin signal in this area tended towards higher in the *tsc2*$^{vu242/vu242}$ mutant, although the difference was not statistically significant. Conversely, in the group treated with ANA-12, the median signal density was higher in the wild-type fish, and significantly lowered in the *tsc2*$^{vu242/vu242}$ mutant, compared to both treated wild-type and untreated mutant (Fig.8 C).

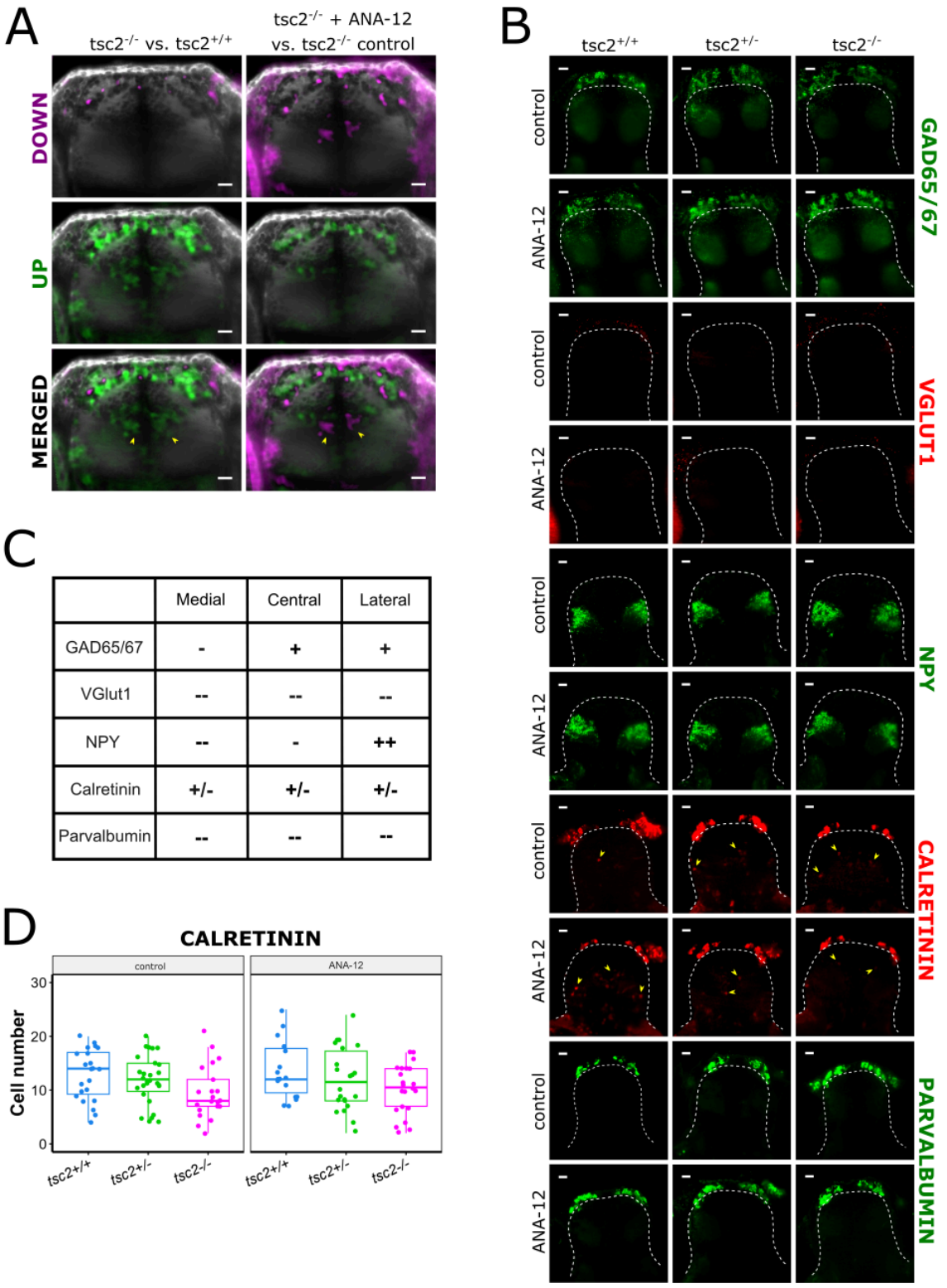

Figure 7. Representative data from the next subpallial layer. **(A)** Single z-slices from maps of neuronal activity as measured by the pERK/ERK ratio, as described previously. The yellow arrows point to clusters of cells along the midline that were upregulated in the mutant but downregulated after ANA-12. Scale bar = 20 µm. **(B)** Single z-slices from brains stained with antibodies against GAD65/67, VGlut1, NPY, calretinin and parvalbumin, selected from the corresponding region of the pallium. Yellow arrows point to distinct calretinin-positive cells.

Scale bar = 20 µm. **(C)** Expression of markers in the medial, central and lateral areas of this layer, as found in wild-type fish. **(D)** Number of calretinin-positive cells in the middle subpallial layer across all genotypes in untreated vs. ANA-12-treated groups. Each dot represents one fish.

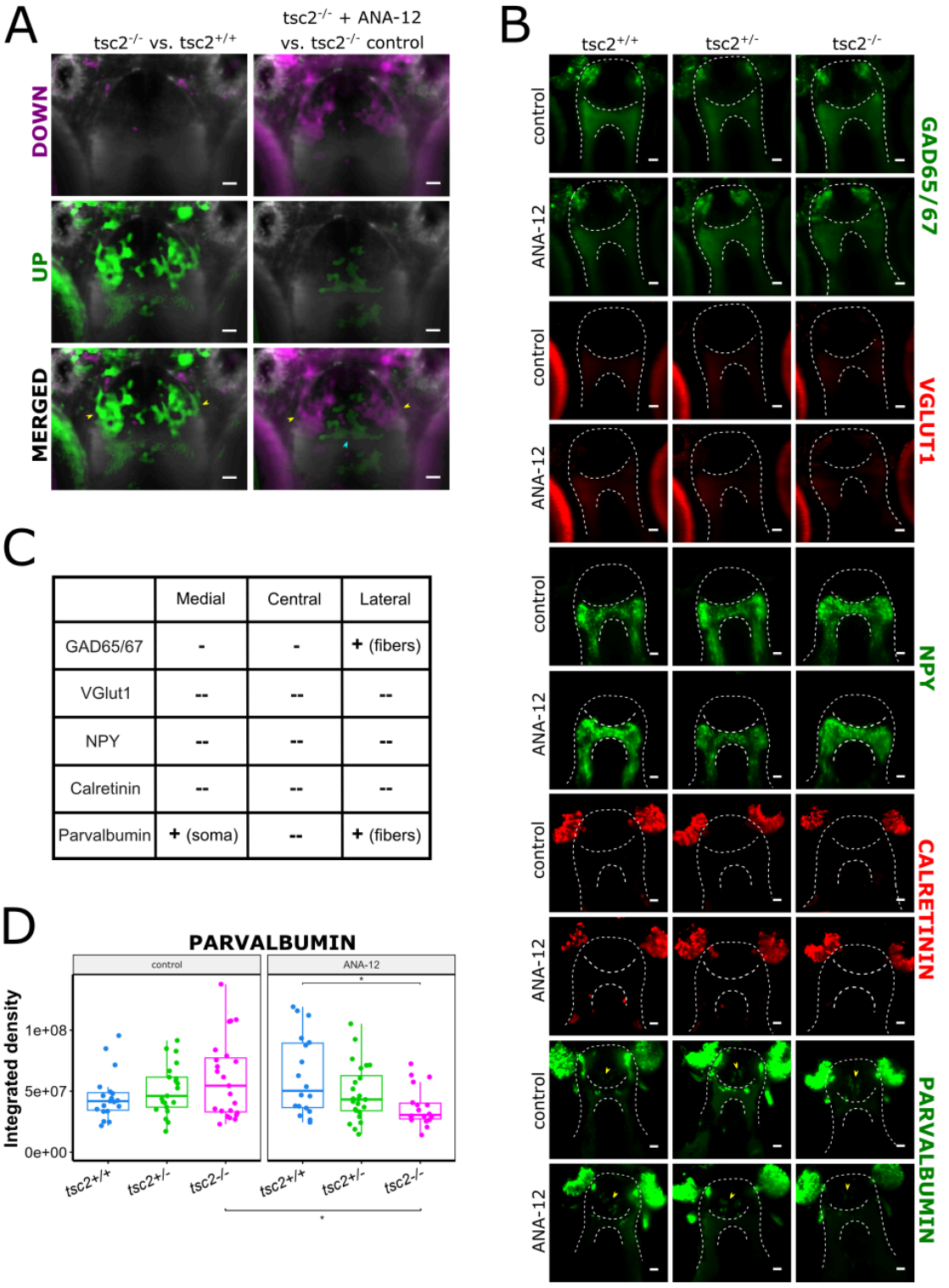

Figure 8. Representative data from the most ventral layer of the subpallium. **(A)** Single z-slices from maps of neuronal activity as measured by the pERK/ERK ratio, as described previously. The yellow arrows point to laterally positioned areas that that were upregulated in the mutant but downregulated after ANA-12. The blue arrow points to the cluster of cells along the midline that was upregulated after ANA-12. Scale bar = 20 µm. **(B)** Single z-slices from brains stained with antibodies against GAD65/67, VGlut1, NPY, calretinin and parvalbumin, selected from the corresponding region of the pallium. Yellow arrows point to a distinct cluster of parvalbumin-positive cells. Scale bar = 20 µm. **(C)** Expression of markers in the medial, central and lateral areas of this layer, as found in wild-type fish. **(D)** The integrated density count, representing the number and intensity of fluorescent signal, of parvalbumin-positive cells in the ventral subpallium across all genotypes in untreated vs. ANA-12-treated groups [p = 0.0129 for control *tsc2*$^{vu242/vu242}$ vs. ANA-12 *tsc2*$^{vu242/vu242}$, p = 0.032 for ANA-12 *tsc2*$^{+/+}$ vs. ANA-12 *tsc2*$^{vu242/+}$]. Each dot represents one fish.

Discussion

Following our previous findings concerning anxiety-like behavior in *tsc2*$^{vu242/vu242}$ fish, and the anxiolytic potential of the TrkB inhibitor ANA-12, our results support the finding that pretreatment with ANA-12 rescues anxiety-like symptoms in *tsc2*$^{vu242/vu242}$ larvae. We have confirmed that ANA-12 lowers the hyperactivation of TrkB seen in the *tsc2*$^{vu242/vu242}$ mutant, and acts independently of rapamycin-dependent activity of mTorC1. At the same time, we have observed that a 24 h treatment with ANA-12 had the same effect on anxiety-like behavior as treatment with rapamycin from 2 dpf. This suggests that dysregulation of mTorC1 signaling in early development contributes to the etiology of anxiety.

The dorsal habenula is known to regulate fear responses, as experiments with Hb-lesioned fish showed increased freezing behavior in response to conditioned aversive stimuli (Agetsuma et al., 2010; Lee et al., 2010) and increased anxiety in a novel environment (Mathuru & Jesuthasan, 2013) in the lesioned individuals. It was also found through rodent studies that the inhibition of both glutamatergic and GABAergic signalling within the lateral Hb, which corresponds to the ventral Hb in zebrafish, induced anxiety, as measured by exploration in the open field test (Lecourtier et al., 2023). Studies have also demonstrated the role of zebrafish ventral Hb in processing aversive stimuli and learning from negative outcomes (Amo et al., 2014; Chou et al., 2016). Crucially, interrupting the function of ventral Hb affects active avoidance learning, but not panic behavior, which might contribute to exaggerated fear responses as seen in anxiety disorders (Amo et al., 2014). We have found clusters of dysregulated neuronal activity in both dorsal (dHb) and ventral (vHb) habenulae of *tsc2*$^{vu242/vu242}$ mutant in comparison to wild-type siblings. The dysregulated neuronal activity that we have observed in the vHb of the *tsc2*$^{vu242/vu242}$ mutant might lead to impaired processing of anxiogenic stimuli, and produce a persistent anticipation of negative outcomes, leading to behavioral responses such as reduced exploration in the open field test. Treatment with ANA-12 would then ameliorate the exaggerated anxiety response. Moreover, in our previous work we have noted improper formation of commissural tracts in the *tsc2*$^{vu242/vu242}$

mutant, including the anterior (Kedra et al., 2020) and habenular (Doszyn et al., 2024) commissures. The habenula commissure (HC) is formed by tracts projected from the pallium, the eminentia thalami and the posterior tuberculum (Hendricks & Jesuthasan 2007). Here, we have found that neuronal activity in those tracts was dysregulated in the *tsc2*$^{vu242/vu242}$ mutant, potentially contributing to its stunted development, and improper processing of stress-related information by the habenulae. However, further experiments would be necessary to confirm the link between neuronal activity in the HC, habenula dysconnectivity and anxiety-like behavior.

Based on the topological models proposed by Porter and Mueller (Porter & Mueller, 2020), we attempted to identify components of the amygdaloid complex in the developing zebrafish telencephalon at 5 dpf. We were able to delineate five telencephalic zones, based on their location in the dorsal-ventral axis, as well as the expression patterns of GAD65/67, VGlut1/2, NPY, calretinin and parvalbumin (Fig. 9 A-C). We have putatively labelled them as dorsal telencephalon (D), posterior division of the medial amygdala (MeAp), anterior division of bed nucleus stria terminalis (BNSTa), striatopallidum (Str/PA), and septum (Se).

The basolateral amygdala (BLA) plays a crucial role in fear conditioning (LeDoux, 2000). Glutamatergic neurons found in the basolateral amygdala (BLA) are key to fear learning following aversive stimuli, and their inhibition impairs this process (Sengupta et al., 2018). The majority of GABAergic interneurons in the BLA express calcium-binding proteins parvalbumin or calretinin, though cells expressing those markers form separate populations (Sah et al., 2003). Studies on goldfish, and later also zebrafish, pointed to the dorsomedial telencephalon as its teleostan equivalent (Aoki et al., 2013; Portavella et al., 2002), and it is currently believed that the zebrafish central and pallial amygdala territories correspond to the mammalian BLA (Porter & Mueller, 2020). It is possible that in our horizontal sections of the brain, the calretinin-positive cells in the first dorsal layer belong to the pallial amygdala, however, we have not been able to confirm this; we have also not subjected our larvae to repeated aversive stimuli to determine whether they also experience a dysregulation in fear learning.

While we were not able to precisely define the boundaries of pallial, central and medial amygdala at this stage of development, we have identified the localization Str/PA and Se. We based our identification on their location in the dorsal-ventral axis, by comparing our results to previously published models of the zebrafish telencephalon (Gerlach & Wulliman, 2021; Porter & Mueller, 2020; Tanimoto et al., 2024). These ventral regions of the subpallium were also where we have noted the most prominent differences in neuronal activity between *tsc2*$^{vu242/vu242}$ larvae and wild-type siblings, that were also clearly reversed by ANA-12 treatment.

In humans, various parts of the striatum are involved in decision making and motivation (Porter et al., 2015). Rodent studies have also shown that dopaminergic neurons in the nucleus accumbens (NAc) and the posterior tail of the striatum (TS) take part in threat learning (Duvarci, 2024). Notably, dopaminergic projections into the TS drive avoidant behaviors in response to novel stimuli, but do not encode outcome values (Menegas et al., 2018). Therefore, it is possible that the hyperactivity of striatal neurons in *tsc2*$^{vu242/vu242}$ fish is

similarly linked to exaggerated threat avoidance and "anticipatory" anxiety that is not ameliorated by a lack of actual negative outcomes.

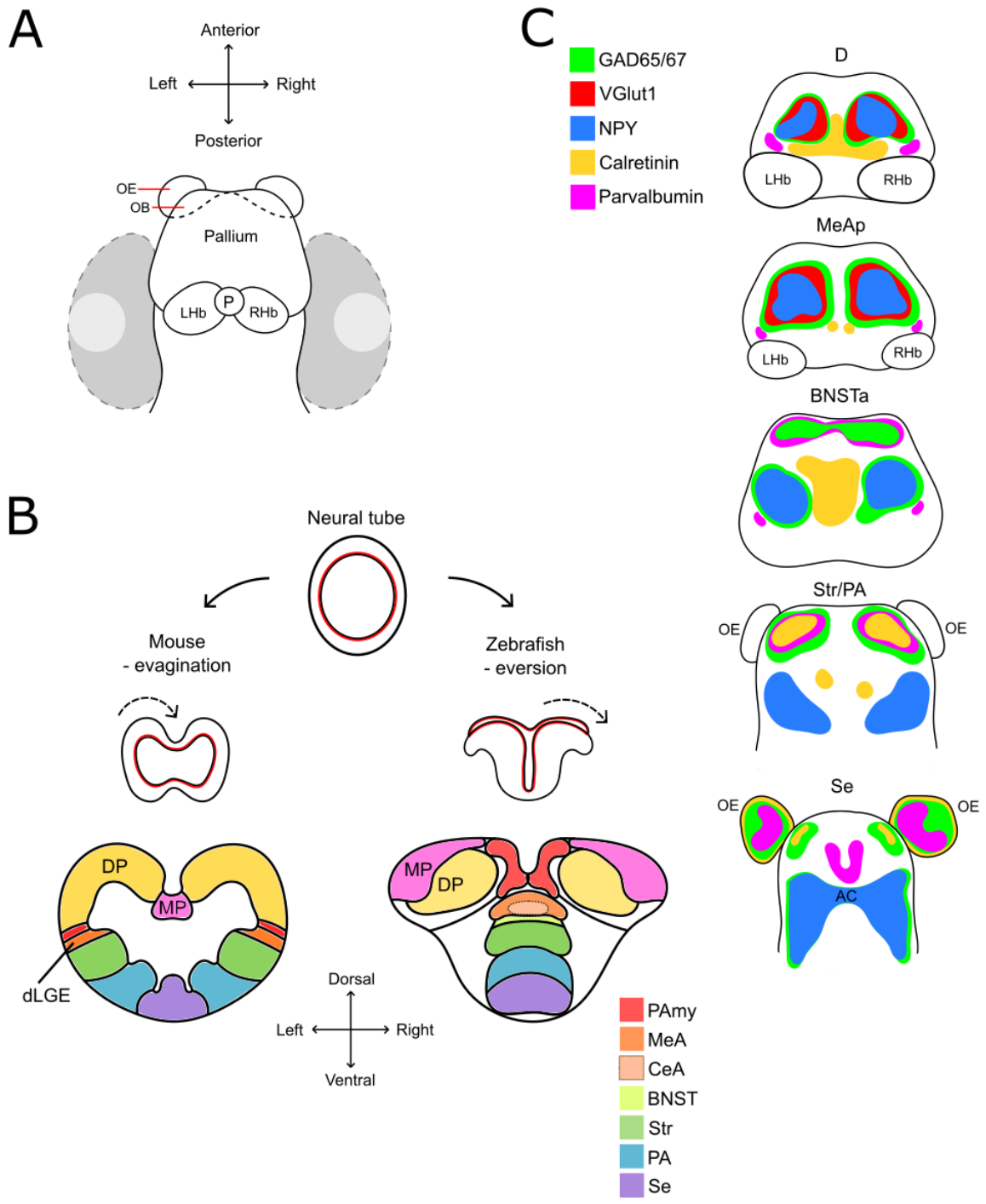

Figure 9. Graphical representations of the developing zebrafish brain. **(A)** Dorsal view of the forebrain at 5 dpf, showing the locations of the pallium, the olfactory bulbs (OB), olfactory epithelium (OE), pineal complex (P), and left and right habenulae (LHb, RHb), as well as the eyes, marked in grey. This orientation corresponds to the immunofluorescence images shown in the results section. **(B)** A simplified diagram showing the processes of evagination and eversion, comparing the development of mouse and zebrafish brain, and the location of

homologous structures. As seen here, eversion results in the components of the amygdaloid complex (pallial amygdala (PAmy), central and medial amygdala (CeA/MeA), bed nucleus stria terminalis (BNST), striatum (Str), pallidum (PA), and septum (Se)) being located along the midline, rather than laterally. **(C)** Schematic representations of the localization of GAD65/67, VGlut1, NPY, calretinin and parvalbumin at the level of dorsal telencephalon (D), posterior division of MeA (MeAp), anterior division of BNST (BNSTa), striatopallidum (Str/PA) and Se, based on our immunofluorescence data.

In mammals, the lateral septum (LS) is comprised of both anxiolytic and anxiogenic neuronal populations (Chen et al., 2021; Rizzi-Wise & Wang, 2021). The heterogeneity of LS function could also be related to its role in assessing changes in valence. It has been hypothesized that the LS might integrate motivation, mood and movement signals. Therefore, animals with dysregulated LS would respond incorrectly to various environmental cues, and could react with exaggerated motor responses (Wirtshafter & Wilson, 2021). The medial septum (MS) is also known to be involved in regulation of anxiety (Chang et al., 2025), as well as processing fear memory (Calandreau et al., 2007). Specifically, inhibiting the function of MS resulted in impaired extinction of fear memory (Knox & Keller, 2015; Tomaszewski et al., 2024; Tronson et al., 2009). While we have not delineated sub-regions of the septum, the lateral regions which were hyperactivated in *tsc2*$^{vu242/vu242}$ fish and downregulated by ANA-12 could correspond to the parts of mammalian LS that promote anxiety-like behavior. At the same time, we have observed an upregulation of the medial septum in fish treated with ANA-12. However, additional behavioral testing would be necessary to determine whether ANA-12 promotes boldness and exploratory behavior by increasing fear memory extinction.

In summary, we have found that multiple brain regions involved in anticipation of negative outcomes and processing anxiogenic stimuli are dysregulated in the *tsc2*$^{vu242/vu242}$ mutant. Treatment with ANA-12 rescued this impairment in multiple areas, particularly the habenula and ventral subpallium. We were also able to identify the latter as corresponding to the mammalian striatopallidum and septum. A further investigation into the neurotransmitters released by the affected neurons and their connectivity could resolve the precise mechanism of TrkB-regulated anxiety-like behavior in the *tsc2*$^{vu242/vu242}$ zebrafish model.

Limitations

In the larval zebrafish, such as were used in this study, the brain is smaller, and the processes of eversion and outgrowth are still in progress, which makes distinguishing between various brain regions more challenging than in adults. Additionally, some markers might not yet be expressed in early development, or be expressed differently because cells are not yet fully specified. Nevertheless, further studies including more brain markers should help in distinguishing regions that we were not able to identify. Other than by spatial inference, we were also not able to directly correlate neuronal activity with the expression of marker proteins, as the limited availability of zebrafish-specific antibodies did not allow for triple stainings with pERK/ERK. Therefore, for neurons with observed differences in activity, we were not able to fully classify them by neurotransmitter or molecular markers.

Resources availability

Lead contact

Further information and requests for resources and reagents should be directed to and will be fulfilled by the Lead Contact, Justyna Zmorzynska (j.zmorzynska@imol.institute).

Materials availability

This study did not generate new unique reagents. The fish mutant and transgenic lines are protected under material transfer agreement with the institutions that generated the lines. Upon appropriate agreement with these institutions, they can be requested from the lead contact.

Data and code availability

- Data: All data is included in the manuscript. Microscopy data reported in this paper will be shared by the lead contact upon reasonable request.
- Code: This paper does not report original code.
- Additional information: Any additional information required to reanalyze the data reported in this paper is available from the lead contact upon request.

Acknowledgements

We thank Kevin Ess (Vanderbilt University) for the *tsc2*$^{vu242/+}$ zebrafish line, the IIMCB Zebrafish Core Facility for assistance with the adult fish, and the IIMCB Microscopy Facility for sharing the Lightsheet Z.1. This work was supported by an OPUS grant no. 2020/37/B/NZ3/02345 (J.Z.) from National Science Centre, Poland.

Author contributions

O.D.: investigation, formal analysis, visualization, writing – original draft, writing – review & editing; J.Z.: conceptualization, investigation, formal analysis, writing – review & editing, supervision, project administration, funding acquisition.

Declaration of interests

The authors declare no competing interests.

References

Agetsuma M, Aizawa H, Aoki T, Nakayama R, Takahoko M, Goto M, Sassa T, Amo R, Shiraki T, Kawakami K, Hosoya T, Higashijima S, Okamoto H, 2010. ***The habenula is crucial for experience-dependent modification of fear responses in zebrafish.*** Nat Neurosci, 13(11):1354-6.

Amo R, Aizawa H, Takahoko M, Kobayashi M, Takahashi R, Aoki T, Okamoto H, 2010. ***Identification of the zebrafish ventral habenula as a homolog of the mammalian lateral habenula.*** J Neurosci, 30(4):1566-74.

Amo R, Fredes F, Kinoshita M, Aoki R, Aizawa H, Agetsuma M, Aoki T, Shiraki T, Kakinuma H, Matsuda M, Yamazaki M, Takahoko M, Tsuboi T, Higashijima S, Miyasaka N, Koide T, Yabuki Y, Yoshihara Y, Fukai T, Okamoto H, 2014. ***The habenulo-raphe serotonergic circuit encodes an aversive expectation value essential for adaptive active avoidance of danger.*** Neuron, 84(5):1034-48.

Aoki T, Kinoshita M, Aoki R, Agetsuma M, Aizawa H, Yamazaki M, Takahoko M, Amo R, Arata A, Higashijima S, Tsuboi T, Okamoto H, 2013. ***Imaging of neural ensemble for the retrieval of a learned behavioral program.*** Neuron, 78(5):881-94.

Bally-Cuif L, Vernier P, 2010. ***Organization and physiology of the zebrafish nervous system.*** In: Perry SF, Ekker M, Farrell AP, Brauner CJ, Zebrafish. Elsevier, 25-80.

Calandreau L, Jaffard R, Desmedt A, 2007. ***Dissociated roles for the lateral and medial septum in elemental and contextual fear conditioning.*** Learn Mem, 14(6):422-9.

Chang L, He Y, Li B, 2025. ***Role of the medial septum neurotensin receptor 1 in anxiety-like behaviors evoked by emotional stress.*** Psychoneuroendocrinology, 172:107275.

Chen YH, Wu JL, Hu NY, Zhuang JP, Li WP, Zhang SR, Li XW, Yang JM, Gao TM, 2021. ***Distinct projections from the infralimbic cortex exert opposing effects in modulating anxiety and fear.*** J Clin Invest, 131(14):e145692.

Chou MY, Amo R, Kinoshita M, Cherng BW, Shimazaki H, Agetsuma M, Shiraki T, Aoki T, Takahoko M, Yamazaki M, Higashijima S, Okamoto H, 2016. ***Social conflict resolution regulated by two dorsal habenular subregions in zebrafish.*** Science, 352(6281):87-90.

Crino PB, Nathanson KL, Henske EP, 2006. ***The tuberous sclerosis complex.*** N Engl J Med, 355(13):1345-56.

Doszyn O, Kedra M, Zmorzynska J, 2024. ***Hyperactive mTORC1 disrupts habenula function and light preference in zebrafish model of Tuberous sclerosis complex.*** iScience 27(6), 110149.

Doszyn O, Dulski T, Zmorzynska J, 2025. ***Protocol for the visualization of pRps6-positive cells in larval zebrafish brains using whole-mount immunofluorescence and light-sheet microscopy.*** STAR Protoc, 6(1):103587.

Duvarci S, 2024. ***Dopaminergic circuits controlling threat and safety learning.*** Trends Neurosci, 47(12):1014-1027.

Fore S, Palumbo F, Pelgrims R, Yaksi E, 2018. ***Information processing in the vertebrate habenula.*** Semin Cell Dev Biol, 78:130-139.

Gerlach G, Wullimann MF, 2021. ***Neural pathways of olfactory kin imprinting and kin recognition in zebrafish.*** Cell Tissue Res, 383(1):273-287.

Hendricks M, Jesuthasan S, 2007. ***Asymmetric innervation of the habenula in zebrafish.*** J Comp Neurol, 502(4):611-9.

Huang EJ, Reichardt LF, 2003. ***Trk receptors: roles in neuronal signal transduction.*** Annu Rev Biochem, 72:609-42.

Kedra M, Banasiak K, Kisielewska K, Wolinska-Niziol L, Jaworski J, Zmorzynska J, 2020. ***TrkB hyperactivity contributes to brain dysconnectivity, epileptogenesis, and anxiety in zebrafish model of Tuberous Sclerosis Complex.*** Proc Natl Acad Sci U S A, 117(4):2170-2179.

Kim SH, Speirs CK, Solnica-Krezel L, Ess KC, 2011. ***Zebrafish model of tuberous sclerosis complex reveals cell-autonomous and non-cell-autonomous functions of mutant tuberin.*** Dis Model Mech, 4(2):255-67.

Knox D, Keller SM, 2016. ***Cholinergic neuronal lesions in the medial septum and vertical limb of the diagonal bands of Broca induce contextual fear memory generalization and impair acquisition of fear extinction.*** Hippocampus, 26(6):718-26.

Lal P, Tanabe H, Suster ML, Ailani D, Kotani Y, Muto A, Itoh M, Iwasaki M, Wada H, Yaksi E, Kawakami K, 2018. ***Identification of a neuronal population in the telencephalon essential for fear conditioning in zebrafish.*** BMC Biol, 16(1):45.

Lecourtier L, Durieux L, Mathis V, 2023. ***Alteration of Lateral Habenula Function Prevents the Proper Exploration of a Novel Environment.*** Neuroscience, 514:56-66.

LeDoux JE, 2000. ***Emotion circuits in the brain.*** Annu Rev Neurosci, 23:155-84.

Lee A, Mathuru AS, Teh C, Kibat C, Korzh V, Penney TB, Jesuthasan S, 2010. ***The habenula prevents helpless behavior in larval zebrafish.*** Curr Biol, 20(24):2211-6.

Mathuru AS, Jesuthasan S, 2013. ***The medial habenula as a regulator of anxiety in adult zebrafish.*** Front Neural Circuits, 7:99.

Menegas W, Akiti K, Amo R, Uchida N, Watabe-Uchida M, 2018. ***Dopamine neurons projecting to the posterior striatum reinforce avoidance of threatening stimuli.*** Nat Neurosci, 21(10):1421-1430.

Pabba M, 2013. ***Evolutionary development of the amygdaloid complex.*** Front Neuroanat, 7:27.

Portavella M, Vargas JP, Torres B, Salas C, 2002. ***The effects of telencephalic pallial lesions on spatial, temporal, and emotional learning in goldfish.*** Brain Res Bull, 57(3-4):397-9.

Porter BA, Mueller T, 2020. ***The Zebrafish Amygdaloid Complex - Functional Ground Plan, Molecular Delineation, and Everted Topology.*** Front Neurosci, 14:608.

Porter JN, Roy AK, Benson B, Carlisi C, Collins PF, Leibenluft E, Pine DS, Luciana M, Ernst M, 2015. ***Age-related changes in the intrinsic functional connectivity of the human ventral vs. dorsal striatum from childhood to middle age.*** Dev Cogn Neurosci, 11:83-95.

Randlett O, Wee CL, Naumann EA, Nnaemeka O, Schoppik D, Fitzgerald JE, Portugues R, Lacoste AM, Riegler C, Engert F, Schier AF, 2015. ***Whole-brain activity mapping onto a zebrafish brain atlas.*** Nat Methods, 12(11):1039-46.

Rizzi-Wise CA, Wang DV, 2021. ***Putting Together Pieces of the Lateral Septum: Multifaceted Functions and Its Neural Pathways.*** eNeuro, 8(6):ENEURO.0315-21.2021.

Sah P, Faber ES, Lopez De Armentia M, Power J, 2003. ***The amygdaloid complex: anatomy and physiology.*** Physiol Rev, 83(3):803-34.

Salussolia CL, Klonowska K, Kwiatkowski DJ, Sahin M, 2019. ***Genetic Etiologies, Diagnosis, and Treatment of Tuberous Sclerosis Complex.*** Annu Rev Genomics Hum Genet, 20:217-240.

Schindelin J, Arganda-Carreras I, Frise E, Kaynig V, Longair M, Pietzsch T, Preibisch S, Rueden C, Saalfeld S, Schmid B, Tinevez JY, White DJ, Hartenstein V, Eliceiri K, Tomancak P, Cardona A, 2012. ***Fiji: an open-source platform for biological-image analysis.*** Nat Methods, 9(7):676-82.

Sengupta A, Yau JOY, Jean-Richard-Dit-Bressel P, Liu Y, Millan EZ, Power JM, McNally GP, 2018. ***Basolateral Amygdala Neurons Maintain Aversive Emotional Salience.*** J Neurosci, 38(12):3001-3012.

Switon K, Kotulska K, Janusz-Kaminska A, Zmorzynska J, Jaworski J, 2017. ***Molecular neurobiology of mTOR.*** Neuroscience, 341, 112–153.

Takei N, Inamura N, Kawamura M, Namba H, Hara K, Yonezawa K, Nawa H, 2004. ***Brain-derived neurotrophic factor induces mammalian target of rapamycin-dependent local activation of translation machinery and protein synthesis in neuronal dendrites.*** J Neurosci, 24(44):9760-9.

Tanimoto Y, Kakinuma H, Aoki R, Shiraki T, Higashijima SI, Okamoto H, 2024. ***Transgenic tools targeting the basal ganglia reveal both evolutionary conservation and specialization of neural circuits in zebrafish.*** Cell Rep, 43(3):113916.

Tomaszewski KF, Ziółkowska M, Łukasiewicz K, Cały A, Sotoudeh N, Puchalska M, Salamian A, Radwanska K, 2024. ***Projections from thalamic nucleus reuniens to medial septum enable extinction of remote fear memory.*** bioRxiv [Preprint], 2024.05.20.594930.

Tronson NC, Schrick C, Guzman YF, Huh KH, Srivastava DP, Penzes P, Guedea AL, Gao C, Radulovic J, 2009. ***Segregated populations of hippocampal principal CA1 neurons mediating conditioning and extinction of contextual fear.*** J Neurosci, 29(11):3387-94.

de Vries PJ, Whittemore VH, Leclezio L, Byars AW, Dunn D, Ess KC, Hook D, King BH, Sahin M, Jansen A, 2015. ***Tuberous sclerosis associated neuropsychiatric disorders (TAND) and the TAND Checklist.*** Pediatr Neurol, 52(1):25-35.

de Vries PJ, Heunis TM, Vanclooster S, Chambers N, Bissell S, Byars AW, Flinn J, Gipson TT, van Eeghen AM, Waltereit R, Capal JK, Cukier S, Davis PE, Smith C, Kingswood JC, Schoeters E, Srivastava S, Takei M, Gardner-Lubbe S, Kumm AJ, Krueger DA, Sahin M, De Waele L, Jansen AC, 2023. ***International consensus recommendations for the identification and treatment of tuberous sclerosis complex-associated neuropsychiatric disorders (TAND).*** J Neurodev Disord, 15(1):32.

Wirtshafter HS, Wilson MA, 2021. ***Lateral septum as a nexus for mood, motivation, and movement.*** Neurosci Biobehav Rev, 126:544-559.

Chapter 9. Conclusions, general discussion and future perspectives

TSC-associated neuropsychiatric disorders affect the majority of TSC patients; yet the mechanisms by which they arise have not yet been fully understood. This thesis aimed to elucidate the molecular pathways and patterns of brain activity underpinning anxiety-like behavior in the *tsc2*$^{vu242/vu242}$ zebrafish, as well as disturbances in light processing in the context of sensory processing alterations seen in ASD. My results have uncovered the mechanism by which mTorC1 hyperactivity in the left dorsal habenula disrupts the larval response to light, potentially recapitulating the sensory overstimulation observed in autistic patients. Additionally, I have made strides towards identifying the components of the amygdaloid complex, the region that governs fear and anxiety-related responses, in the developing zebrafish brain. I have also analyzed the role that TrkB signaling plays in modulating anxiety behavior and brain activity across the zebrafish telencephalon.

9.1 Aberrant light processing in the *tsc2* mutants

In a previous study conducted in our laboratory, Kedra et al. have demonstrated anxiety-like features in the *tsc2*$^{vu242/vu242}$ zebrafish (Kedra et al., 2020). However, in the light preference test, the mutant larvae spent less time in the light, which appeared to contradict the established paradigm, according to which in larval zebrafish, anxiety and environmental stressors lead to increased phototaxis (Bai et al., 2016). Additionally, ANA-12, the TrkB inhibitor which previously rescued anxiety symptoms (Kedra et al., 2020), did not correct the light preference deficit. Therefore, I explored the possible underlying causes of this effect. Together with DSc. habil. Zmorzyńska, I have identified a mechanism by which hyperactivation of mTorC1 in *tsc2*$^{vu242/vu242}$ zebrafish leads to aberrant neuronal activity in the left dorsal habenula, resulting in hypersensitivity to light, driving light avoidance. The same mechanism might potentially occur in TSC patients with ASD, as heightened sensitivity to sensory stimuli is a common feature of autism (Little et al., 2018). The initial contradiction between the typical anxiety phenotype and light avoidance that we have observed when interpreting our results could also be used to exemplify how in human patients, co-occurring disorders can interplay to produce atypical symptoms, and make accurate diagnosis more challenging.

The lack of light preference in *tsc2*$^{vu242/vu242}$ fish was rescued with mTorC1 inhibition. However, it is worth noting that the effect of rapamycin on behavior and brain activity was achieved with pretreatment – rather than being delivered acutely just before the experiment, rapamycin was introduced to the bathing medium from 2 days post fertilization (dpf) onwards, or injected directly into the habenula at 3 and 4 dpf; in fact, a single injection of rapamycin was not sufficient to produce a sustained effect on hyperactivated mTorC1 in the *tsc2*$^{vu242/vu242}$ mutant. This is consistent with rodent studies showing that there is an effective treatment window in early development (so called critical periods; Cox et al., 2018; Tsai et al., 2018), and the timing of rapamycin treatment is crucial for the rescue of TSC symptoms.

Currently, clinical trials evaluating the safety and efficacy of sirolimus treatment in infants under 4 to 6 months of age are underway (Capal et al., 2024; Driedger et al., 2025).

9.2 Mapping anxiety in the developing zebrafish

The BDNF-TrkB signaling pathway plays a significant role in synaptic plasticity and learning (Minichiello, 2009), as well as dendrite growth and maintenance through the activation of mTORC1 (Moya-Alvarado et al., 2023). Following previous results obtained in our laboratory (Kedra et al., 2020), I have also corroborated the involvement of TrkB in anxiety-like behavior of *tsc2*$^{vu242/vu242}$ zebrafish larvae. I have confirmed that TrkB is hyperactivated in the *tsc2*$^{vu242/vu242}$ mutant, and that ANA-12 rescues this hyperactivation, resulting in amelioration of anxiety, as seen in the open field and sudden light changes tests. Therefore, while TrkB signaling is not a 1:1 proxy for anxiety, I have used ANA-12 as a tool to track changes in anxiety-related brain activity and behavior.

Together with DSc. habil. Zmorzyńska, I have then analyzed the differences in neuronal activity in the habenula, pallium and subpallium, and whether activity of those regions is affected by ANA-12 treatment. As the zebrafish habenula is located dorsally, and morphologically distinct from neighboring structures, it is easy to identify and image. I have noted multiple clusters of hypo- and hyperactivated cells in both the left and right habenula of *tsc2*$^{vu242/vu242}$ fish, the majority of which were regulated by ANA-12, suggesting that the anxiogenic effect of TrkB signaling is exerted through habenular circuitry. However, I also aimed to explore the activity of the amygdaloid complex, which is much more challenging to identify due to the everted development of the zebrafish telencephalon (see Chapter 8, Fig. 9). Up to date, the most comprehensive work identifying the zebrafish amygdaloid territories, and their homology to the mammalian equivalent, was conducted in adult fish (Porter & Mueller, 2020). My goal was to delineate the same brain regions in larvae at 5 dpf, based on their localization in the dorsal-ventral axis and the expression of known marker proteins. The septum, identifiable as the most ventral layer of the telencephalon, showed significant differences in neuronal activity between *tsc2*$^{vu242/vu242}$ fish and wild-type siblings. In addition to reversing the pattern of activity, treatment with ANA-12 also regulated the expression of parvalbumin in this region. Interestingly, a dysregulation of parvalbumin-positive medial septum neurons was recently discovered in a mouse model of Dravet syndrome (DS), a neurodevelopmental disorder caused by pathogenic variants in the *SCN1A* gene (Zhu et al., 2024). DS and TSC share multiple symptoms, such as epilepsy, developmental delay, intellectual disability, and ASD features (Villas et al., 2017). While the study by Zhu et al. utilized primarily electrophysiological recordings, and therefore their results are not directly comparable with the findings of this thesis, it raises the possibility that dysfunction of septal neurons contributes to the shared features of DS and TSC.

In order to confidently identify the remaining telencephalic regions, a wider array of markers would be necessary. Delineating the borders between pallial amygdala (pAmy), medial and central amygdala (MeA and CeA) and the bed nucleus stria terminalis (BNST) was particularly challenging. Most of the amygdaloid nuclei are Isl1-negative, with the exception

of the medial division of BNST, determined to be an extension of the striatopallidal systems (Porter & Mueller, 2020). In adult zebrafish, the MeA, with its large numbers of calretinin-positive neurons, is distinct from the calretinin-negative CeA. While I have found layers with fewer calretinin-positive cells, they were not entirely absent. Therefore, another marker, such as substance P, also found in the MeA but not CeA, would help to confirm the identity of each region. Additionally, the posterior division of MeA is considered an eminentia thalami derivative, and therefore shows high levels of transcriptional regulator Lhx5 (Porter & Mueller, 2020). In terms of the most dorsal layer of the pallium, I have speculated that the calretinin-positive cell clusters could be a part of the pAmy. I have used VGlut1 as a marker of glutamatergic neurons; however, the expression of VGlut2 should confirm the location of pAmy, and whether it overlaps with the calretinin-positive area seen in my data (Porter & Mueller, 2020). In the ventral part of the subpallium, I have labelled the layer located dorsally of the septum as the striatopallidum. This region should be Isl1-positive, similarly to part of BNST (Porter & Mueller, 2020). The expression of Lhx6 and Nkx2.1 has been previously used to mark the pallidum (Mueller et al., 2008; Tanimoto et al., 2024). In turn, tyrosine hydroxylase (TH) could be used to mark the dopaminergic projections found in the striatum (Rink & Wulliman, 2001). It might also be worthwhile to analyze the expression of marker proteins in older larvae, in order to track the continuous development of amygdaloid territories in the zebrafish. A thorough understanding of zebrafish amygdala development will enhance the potential of the zebrafish as a model for translational research aimed at elucidating the mechanisms of anxiety, and investigating novel treatments of anxiety disorders.

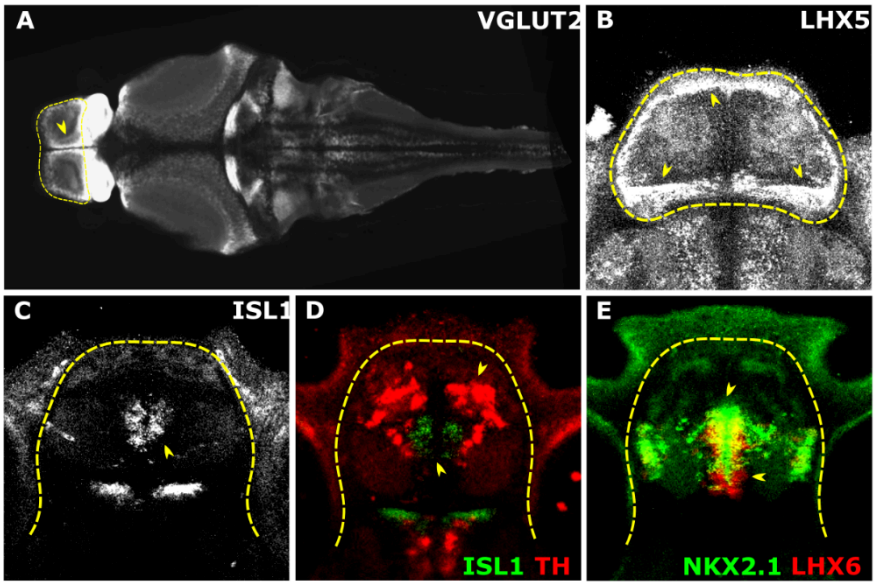

Figure 1. Expression of selected markers sourced from ZBrain atlas (https://zebrafishexplorer.zib.de/home/) – panel A and Mapzebrain (Kunst et al., 2019) – panels B-E. The expression of VGlut2 along the midline in the dorsal pallium (arrow, panel A) could mark the pallial amygdala. The expression of Lhx5 marks the posterior division of MeA (B). The expression of Isl1 extends dorsally to the BNST (C), but is also found in the

striatum, although it does not overlap with TH-positive cells (D). Overlapping expression of Nkx2.1 and Lhx6 is found medially in the pallidum (E).

9.3 TSC, anxiety and autism: future perspectives

Psychiatric comorbidity is common in children with ASD. According to one study, among the diagnosed concomitant disorders, anxiety disorders were reported in 56% of cases (Brookman-Frazee et al., 2018), while a meta-analysis by Lecavalier et al. calculated a total of 41.9% prevalence of various anxiety disorders found across several cohorts of children with ASD (Lecavalier et al., 2019). However, in a much broader meta-analysis, which also included adult patients, this value dropped to 20% (Lai et al., 2019). In general, reported rates of anxiety disorders in both children and adults with ASD vary greatly (Hollocks et al., 2019). These discrepancies are possibly caused to a large extent by shifting diagnostic criteria, particularly when it comes to overlapping symptoms. For example, social anxiety disorder can be difficult to distinguish from the lowered social preference typical for many autistic individuals, or compulsive behaviors characteristic of obsessive-compulsive disorder can be mistaken for the proclivity for repetitive behaviors as observed in ASD (Dulski et al., 2025; Hollocks et al., 2019). At the same time, co-occurring conditions can exacerbate each other. The distress caused by an anxiety disorder can worsen behavioral symptoms associated with ASD. In turn, various symptoms of autism, such as social difficulties or hypersensitivity to sensory stimuli, as well as common experiences of bullying, discrimination, and lack of adequate support, can all contribute to greater anxiety (Postorino et al., 2017). Similarly, increased rates of anxiety have been reported in people with various chronic physical illnesses (Lebel et al., 2020), including in children suffering from epilepsy (Cobham et al., 2020). Therefore, while at present a possible shared etiology between ASD and anxiety cannot be excluded, the mutual feedback of different symptoms, as well as the impact of non-psychiatric aspects of TSC on TANDs should be considered in future studies.

In our zebrafish model, we observe anxiety-like behavior at 5 dpf, while social preference is only fully developed at 3 weeks of age (Dreosti et al., 2015), in contrast to humans, who exhibit social behaviors from birth (Xiao et al., 2014) suggesting prenatal development of this behaviors. However, I have demonstrated that the *tsc2*$^{vu242/vu242}$ zebrafish at 5dpf display aberrant sensory processing, which is also an ASD-like symptom, alongside anxiety-like behavior. While the habenula plays a key role in both of those processes, they are not governed by the same mechanisms; as I have shown, anxiety in the *tsc2*$^{vu242/vu242}$ fish is regulated by the TrkB pathway, while the response to light is not. Additionally, I have also found areas in the subpallium, which I have identified as parts of the amygdaloid complex responsible for fear and threat avoidance learning, where inhibition of the TrkB pathway altered neuronal activity. While the picture of amygdaloid circuitry in larval zebrafish is not yet complete, my work can serve as a starting point for future studies aiming to elucidate how dysregulation of neuronal activity and connectivity formation in early development contributes to neuropsychiatric disorders later in life.

Moreover, while it was not the subject of this thesis, in our immunofluorescence staining data I have noticed high levels of P-Rps6 in the pineal complex of *tsc2*$^{vu242/vu242}$ mutant zebrafish compared to wild-type siblings. The function of the pineal complex, conserved across vertebrates, is to serve as a circadian clock, regulating the cycle of melatonin production and release to determine sleep patterns. It possesses a self-sustaining, intrinsic circadian oscillator, as well as a photoreceptive system allowing for entrainment by light exposure (Cahill, 1996; Falcón et al., 2009). The pineal organ is also very important for the formation of left vs. right habenula identity (Gamse et al., 2003). Crucially, dysregulation of the circadian patterns of melatonin and cortisol secretion has been correlated with many neuropsychiatric disorders (reviewed in Gianotta et al., 2024). Zebrafish possess a highly conserved biological clock, and secrete both cortisol and melatonin (Aranda-Martínez et al., 2022; Midttun et al., 2022). Additionally, they are diurnal (Zhdanova, 2006), which makes them potentially advantageous for modeling human sleep disorders, in comparison to nocturnal animals such as rodents.

Disturbances in the circadian rhythm, melatonin secretion and sleep patterns have been frequently reported in ASD patients, and mutations of multiple circadian clock genes have been linked to ASD (Carmassi et al., 2019; Lorsung et al., 2021; Yang et al., 2016). Among them, haploinsufficiency of *Bmal1*, an essential circadian clock gene, has resulted in an autism-like phenotype in mice, including behavioral changes such as aberrant vocalizations, deficits in sociability, repetitive behaviors, motor impairments and anxiety-like behavior. In addition to those behavioral changes, as well as decreased levels of clock proteins downstream of *Bmal1*, *Bmal1*+/− mouse mutants have also shown increased activity of mTORC1 in the cerebellum and forebrain, as measured by pRps6 levels, linking mTORC1 hyperactivation with aberrant circadian rhythms (Singla et al., 2022). While my results demonstrate the direct role of mTorC1 activity in the left dorsal habenula in light preference behavior, the observed mTorC1 hyperactivation in the pineal complex suggests that a further study might be needed to investigate the potential role of the pineal organ in the dysregulation of habenula development and regulation of light processing or circadian rhythm in TSC. Moreover, a recent study conducted in mice has found a link between circadian rhythm dysfunction, through either the loss of *Bmal1* or lesions of the suprachiasmatic nucleus, and depression and anxiety-like behaviors. Both the lesioned and knockout mice showed disrupted TrkB signaling in the striatum, and the injection of ANA-12 into the striatum rescued the behavioral symptoms, pointing to *Bmal1* as a potential target for treatment of not only sleep disturbances, but also mood disorders (Liang et al., 2025). Taken all together, this also underscores the complexity of how various TANDs can both share underlying causes, and interplay on a symptomatic level.

References

Aranda-Martínez P, Fernández-Martínez J, Ramírez-Casas Y, Guerra-Librero A, Rodríguez-Santana C, Escames G, Acuña-Castroviejo D, 2022. ***The Zebrafish, an Outstanding Model for Biomedical Research in the Field of Melatonin and Human Diseases.*** Int J Mol Sci, 23(13):7438.

Bai Y, Liu H, Huang B, Wagle M, Guo S, 2016. ***Identification of environmental stressors and validation of light preference as a measure of anxiety in larval zebrafish.*** BMC Neurosci, 17(1):63.

Brookman-Frazee L, Stadnick N, Chlebowski C, Baker-Ericzén M, Ganger W, 2018. ***Characterizing psychiatric comorbidity in children with autism spectrum disorder receiving publicly funded mental health services.*** Autism, 22(8):938-952.

Cahill GM, 1996. ***Circadian regulation of melatonin production in cultured zebrafish pineal and retina.*** Brain Res, 708(1-2):177-81.

Capal JK, Ritter DM, Franz DN, Griffith M, Currans K, Kent B, Bebin EM, Northrup H, Koenig MK, Mizuno T, Vinks AA, Galandi SL, Zhang W, Setchell KDR, Kremer KM, Prada CM, Greiner HM, Holland-Bouley K, Horn PS, Krueger DA, 2024. ***Preventative treatment of tuberous sclerosis complex with sirolimus: Phase I safety and efficacy results.*** Ann Child Neurol Soc, 2(2):106-119.

Carmassi C, Palagini L, Caruso D, Masci I, Nobili L, Vita A, Dell'Osso L, 2019. ***Systematic Review of Sleep Disturbances and Circadian Sleep Desynchronization in Autism Spectrum Disorder: Toward an Integrative Model of a Self-Reinforcing Loop.*** Front Psychiatry, 10:366.

Cobham VE, Hickling A, Kimball H, Thomas HJ, Scott JG, Middeldorp CM, 2020. ***Systematic Review: Anxiety in Children and Adolescents With Chronic Medical Conditions.*** J Am Acad Child Adolesc Psychiatry, 59(5):595-618.

Cox RL, Calderon de Anda F, Mangoubi T, Yoshii A, 2018. ***Multiple Critical Periods for Rapamycin Treatment to Correct Structural Defects in Tsc-1-Suppressed Brain.*** Front Mol Neurosci, 11:409.

Dreosti E, Lopes G, Kampff AR, Wilson SW, 2015. ***Development of social behavior in young zebrafish.*** Front Neural Circuits, 9:39.

Driedger JH, Schröter J; PROTECT-Study Group; Syrbe S, Saffari A, 2025. ***Long-term neuropsychologic outcome of pre-emptive mTOR inhibitor treatment in children with tuberous sclerosis complex (TSC) under 4 months of age (PROTECT), a two-arm, randomized, observer-blind, controlled phase IIb national multicentre clinical trial: study protocol.*** Orphanet J Rare Dis, 20(1):2.

Dulski T, Tolak S, Zmorzyńska J, 2025. ***Challenges and hopes for treatment of anxiety disorder in the autistic population.*** Brain Res, 1860:149675.

Falcón J, Besseau L, Fuentès M, Sauzet S, Magnanou E, Boeuf G, 2009. ***Structural and functional evolution of the pineal melatonin system in vertebrates.*** Ann N Y Acad Sci, 1163:101-11.

Gamse JT, Thisse C, Thisse B, Halpern ME, 2003. ***The parapineal mediates left-right asymmetry in the zebrafish diencephalon.*** Development, 130(6):1059-68.

Giannotta G, Ruggiero M, Trabacca A, 2024. ***Chronobiology in Paediatric Neurological and Neuropsychiatric Disorders: Harmonizing Care with Biological Clocks.*** J Clin Med, 13(24):7737.

Hollocks MJ, Lerh JW, Magiati I, Meiser-Stedman R, Brugha TS, 2019. ***Anxiety and depression in adults with autism spectrum disorder: a systematic review and meta-analysis.*** Psychol Med, 49(4):559-572.

Kedra M, Banasiak K, Kisielewska K, Wolinska-Niziol L, Jaworski J, Zmorzynska J, 2020. ***TrkB hyperactivity contributes to brain dysconnectivity, epileptogenesis, and anxiety in zebrafish model of Tuberous Sclerosis Complex.*** Proc Natl Acad Sci U S A, 117(4):2170-2179.

Kunst M, Laurell E, Mokayes N, Kramer A, Kubo F, Fernandes AM, Förster D, Dal Maschio M, Baier H, 2019. ***A Cellular-Resolution Atlas of the Larval Zebrafish Brain.*** Neuron, 103(1):21-38.e5.

Lai MC, Kassee C, Besney R, Bonato S, Hull L, Mandy W, Szatmari P, Ameis SH, 2019. ***Prevalence of co-occurring mental health diagnoses in the autism population: a systematic review and meta-analysis.*** Lancet Psychiatry, 6(10):819-829.

Lebel S, Mutsaers B, Tomei C, Leclair CS, Jones G, Petricone-Westwood D, Rutkowski N, Ta V, Trudel G, Laflamme SZ, Lavigne AA, Dinkel A, 2020. ***Health anxiety and illness-related fears across diverse chronic illnesses: A systematic review on conceptualization, measurement, prevalence, course, and correlates.*** PLoS One, 15(7):e0234124.

Lecavalier L, McCracken CE, Aman MG, McDougle CJ, McCracken JT, Tierney E, Smith T, Johnson C, King B, Handen B, Swiezy NB, Eugene Arnold L, Bearss K, Vitiello B, Scahill L, 2019. ***An exploration of concomitant psychiatric disorders in children with autism spectrum disorder.*** Compr Psychiatry, 88:57-64.

Liang X, Ding Y, Zhu X, Qiu J, Shen X, Xiong Y, Zhou J, Liang X, Xie W, 2025. ***Suprachiasmatic nucleus dysfunction induces anxiety- and depression-like behaviors via activating the BDNF-TrkB pathway of the striatum.*** Transl Psychiatry, 15(1):92.

Little LM, Dean E, Tomchek S, Dunn W, 2018. ***Sensory Processing Patterns in Autism, Attention Deficit Hyperactivity Disorder, and Typical Development.*** Phys Occup Ther Pediatr, 38(3):243-254.

Lorsung E, Karthikeyan R, Cao R, 2021. ***Biological Timing and Neurodevelopmental Disorders: A Role for Circadian Dysfunction in Autism Spectrum Disorders.*** Front Neurosci, 15:642745.

Midttun HLE, Øverli Ø, Tudorache C, Mayer I, Johansen IB, 2022. ***Non-invasive sampling of water-borne hormones demonstrates individual consistency of the cortisol response to stress in laboratory zebrafish (Danio rerio).*** Sci Rep, 12(1):6278.

Minichiello L, 2009. ***TrkB signalling pathways in LTP and learning.*** Nat Rev Neurosci, 10(12):850-60.

Moya-Alvarado G, Tiburcio-Felix R, Ibáñez MR, Aguirre-Soto AA, Guerra MV, Wu C, Mobley WC, Perlson E, Bronfman FC, 2023. ***BDNF/TrkB signaling endosomes in axons coordinate CREB/mTOR activation and protein synthesis in the cell body to induce dendritic growth in cortical neurons.*** Elife, 12:e77455.

Mueller T, Wullimann MF, Guo S, 2008. ***Early teleostean basal ganglia development visualized by zebrafish Dlx2a, Lhx6, Lhx7, Tbr2 (eomesa), and GAD67 gene expression.*** J Comp Neurol, 507(2):1245-57.

Porter BA & Mueller T, 2020. ***The Zebrafish Amygdaloid Complex - Functional Ground Plan, Molecular Delineation, and Everted Topology.*** Front Neurosci, 14:608.

Postorino V, Kerns CM, Vivanti G, Bradshaw J, Siracusano M, Mazzone L, 2017. ***Anxiety Disorders and Obsessive-Compulsive Disorder in Individuals with Autism Spectrum Disorder.*** Curr Psychiatry Rep, 19(12):92.

Rink E & Wullimann MF, 2001. ***The teleostean (zebrafish) dopaminergic system ascending to the subpallium (striatum) is located in the basal diencephalon (posterior tuberculum).*** Brain Res, 889(1-2):316-30.

Singla R, Mishra A, Lin H, Lorsung E, Le N, Tin S, Jin VX, Cao R, 2022. ***Haploinsufficiency of a Circadian Clock Gene Bmal1 (Arntl or Mop3) Causes Brain-Wide mTOR Hyperactivation and Autism-like Behavioral Phenotypes in Mice.*** Int J Mol Sci, 23(11):6317.

Tanimoto Y, Kakinuma H, Aoki R, Shiraki T, Higashijima SI, Okamoto H, 2024. ***Transgenic tools targeting the basal ganglia reveal both evolutionary conservation and specialization of neural circuits in zebrafish.*** Cell Rep, 43(3):113916.

Tsai PT, Rudolph S, Guo C, Ellegood J, Gibson JM, Schaeffer SM, Mogavero J, Lerch JP, Regehr W, Sahin M, 2018. ***Sensitive Periods for Cerebellar-Mediated Autistic-like Behaviors.*** Cell Rep, 25(2):357-367.e4.

Villas N, Meskis MA, Goodliffe S, 2017. ***Dravet syndrome: Characteristics, comorbidities, and caregiver concerns.*** Epilepsy Behav, 74:81-86.

Xiao NG, Perrotta S, Quinn PC, Wang Z, Sun YH, Lee K, 2014. ***On the facilitative effects of face motion on face recognition and its development.*** Front Psychol, 5:633.

Yang Z, Matsumoto A, Nakayama K, Jimbo EF, Kojima K, Nagata K, Iwamoto S, Yamagata T, 2016. ***Circadian-relevant genes are highly polymorphic in autism spectrum disorder patients.*** Brain Dev, 38(1):91-9.

Zhdanova IV, 2006. ***Sleep in zebrafish.*** Zebrafish, 3(2):215-26.

Zhu L, Demetriou Y, Barden J, Disla J, Mattis J, 2024. ***Medial septum parvalbumin-expressing inhibitory neurons are impaired in a mouse model of Dravet Syndrome.*** bioRxiv [Preprint], 2024.10.29.620933.

Acknowledgements

I would like to thank:

My supervisor Dsc habil. Justyna Zmorzyńska and Prof. Dsc habil. Jacek Jaworski for allowing me to work in their groups, and for all their expertise and guidance throughout this project;

The members of my Thesis Advisory Committee, Prof. Allan Kalueff and Dr. Cecilia Winata, for their valuable input into improving my work;

The Microscopy and Zebrafish Core Facilities of the IIMCB, for taking care of the equipment and animals without which this project would have been impossible, and for sharing their knowledge;

All colleagues from the Laboratory of Molecular and Cellular Neurobiology of the IIMCB and the Laboratory of Developmental Neurobiology of IMol for their help, support, and providing a wonderful work atmosphere.

This work was funded by the National Science Centre OPUS grant 2020/37/B/NZ3/02345.